3rd International Conference on Magnetic Resonance Microscopy

"Heidelberg Conference"

Division of Spatially Resolved Magnetic Resonance of the Groupement AMPERE

August 27 - 31, 1995
Würzburg, Germany

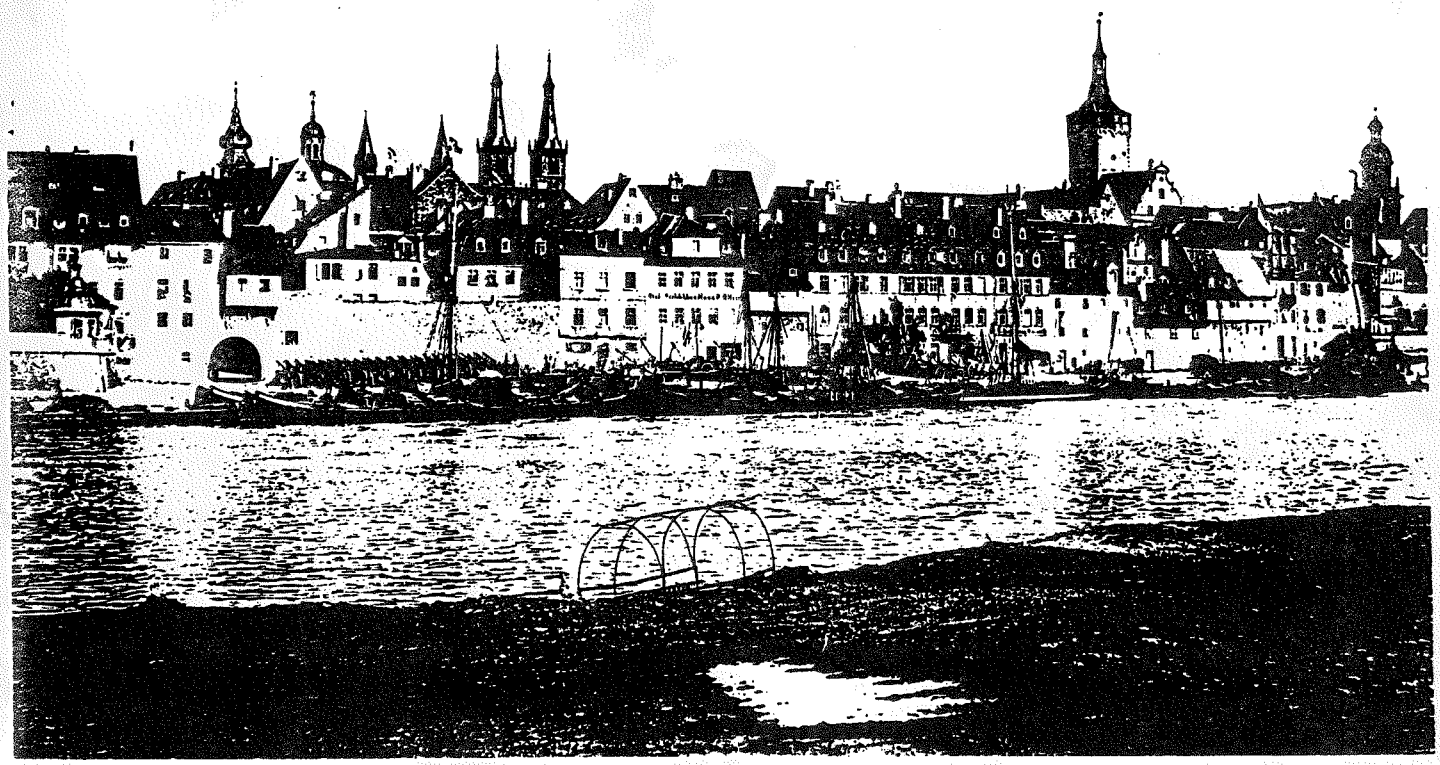

Würzburg at 1900: Photo by W.C.Röntgen

Book of Abstracts

INTRODUCTION

Welcome to the "3rd International Conference on Magnetic Resonance Microscopy - Heidelberg Conference -". After two conferences in Heidelberg, this event will take place for the first time in Würzburg, Germany. Here, one hundred years ago, Wilhelm Conrad Röntgen discovered the X-Rays at the Institute of Physics.
The conference was organized by the "Division of Spatially Resolved Magnetic Resonance" of the AMPERE Society.
The program includes invited lectures (30 minutes), contributed oral presentations (15 minutes), and poster sessions. There will be no parallel session and enough time to visit the posters and the industrial exhibits.

COMMITTEES

Groupement Ampere, Division of Spatially Resolved Magnetic Resonance
Chair: W. Kuhn
Vice Chair: L.J. Berliner
Secretary General: B. Blümich
Vice Secretary General: G.A. Johnson
Treasurer: A. Haase
Advisors: E.R. Andrew, L.D. Hall
Division Committee, Scientific Committee, and Program Committee:
J.L. Ackerman, R.L. Armstrong, P.T. Callaghan, A.N. Garroway, E. Fukushima, W.E. Hull, L.W. Jelinski, P. Jonsen, R. Kimmich, J.L. Koenig, R.A. Komoroski, P.C. Lauterbur, P. Mansfield, B. Maraviglia, G.D. Mateescu, G. Nesbitt, J.M. Pope, V. Sarafis, S.K. Sarkar, J.H. Strange, H.W. Spiess, S. Subramanian

LOCAL ORGANIZING COMMITTEE

A. Haase, W. Behr, M. Brandl, T. Breitling, T. Dorn, A. Eltze, C. Hillenbrand, K.H. Hiller, P. Jakob, E. Kahler, B. Kalusche, M. von Kienlin, F. Kober, E. Kuchenbrod, M. Landschütz, M. Meininger, F. Odoj, R. Pohmann, C. Preibisch, I. Ramoz, F. Roder, E. Rommel, J. Ruff, R. Schneider, C. Steinbauer, M. Szimtenings, S. Voll

CONFERENCE SITE

All conference activities will take place at the Biocenter of the University of Würzburg (University Campus "Am Hubland"). The lecture room, poster display, industrial exhibition and conference office are located at the Biocenter.

BADGES

Please wear your identification badges all the time. This will give you free access to the conference site, free conference bus transfer, free coffee, and free access to the poster reception.

POSTER DISPLAY

The posters are on display during the entire conference. There is an informal poster viewing on Monday evening, August 28, from 19:00 to 22:00 h. The poster viewing session will be on Tuesday, August 29, from 15:30 to 17:00 h. The authors are requested to be present at the poster during the poster viewing session.

SPEAKERS AND CHAIRS

Please arrive at least 10 minutes before your session to familiarize yourselves with the other speakers, and with the audiovisual system. A slide and video preview room is available to prepare your oral contribution. Please bring your slides and video to the lecture room at least 10 minutes before the session.

GENERAL INFORMATION

Local staff members can be identified by red colour name badges. The staff members will give you all necessary informations.

CONFERENCE OFFICE

The opening hours and registration hours are as follows:

Sunday, August 27,	12:00 - 18:00
Monday, August 28,	8:30 - 18:00
Tuesday, August 29,	8:30 - 18:00
Wednesday, August 30,	8:30 - 14:00
Thursday, August 31,	8:30 - 14:00

Informations about conference activities, social program, and transportation are available at the conference office.

Important phone and fax numbers of the conference office:

Phone:	0931-888-5867
	0931-888-5301
FAX:	0931-888-5851
	0931-888-5301

WELCOME RECEPTION

All participants are invited to attend the Welcome Reception on Sunday, August 27, 1995 at the Residenz (Röntgen Exhibit). The reception opens at 18:00 h. Drinks and snacks will be served.

LUNCH TICKETS

Lunch tickets can be purchased at the conference office. The price is DM 11,--. Lunch will be served at the University Mensa (walking distance of 2 minutes) from 12:00 to 14:00 h. There is also a cafeteria at the Mensa. Here sandwiches, sweet roles, drinks, etc. are available at low prices.

CONFERENCE REFRESHMENTS

Coffee and tea will be served during conference breaks. Refreshments are served free of charge. Additional soft drinks are available at the cafeteria and several machines at the biocenter.

CONFERENCE DINNER

The conference dinner will be given at the Gartensaal of the Residenz, Würzburg on Wednesday, August 30 at 19:30 h. Tickets are available for DM 50,-- at the conference office. Before the conference dinner, there will be the evening lecture. All participants are invited to come to this lecture. See program for details.

OTHER SOCIAL EVENTS

Several social events will be organized for the participants and accompanying persons. More informations are available on site.
A few of selected activities are:
- Guided City Tours
- Visit of the Residenz
- Visit of the Festung
- Boat Tours
- Tennis

TRANSPORTATION IN WÜRZBURG

There will be a free conference bus transfer. Three conference busses start at:
- Main Railway Station (at Bus Stop "Stadtrundfahrt")
- Residenz (Bus Stop at Car Parking)
- Hotel Mühlenhof (at Bus Stop "Steinlein", Versbacher Straße)

The busses start at 8:35 from Monday to Thursday. All busses will go directly to the University campus.
The busses leave the University campus 30 minutes after the last conference activity from Monday to Thursday.
In addition, Würzburg has an excellent and safe transportation system. A 24-hour ticket is available at the conference office (price: DM 6,50). The ticket is valid in all busses and trams in Würzburg.
The University campus can be reached with the following public busses:
- Bus line 10 (destination: Hubland (Uni-Zentrum)) leaves the bus stop "Sanderring" in the city, starting at: 8:05, 8:20, 8:35, 8:50, 9:05, etc.
- Bus line 14 (destination: Gerbrunn) leaves the main railway station, starting at: 8:15, 8:35, 8:55, 9:15, etc.

For more information, please contact the conference office.

MAIN SPONSORS OF THE MEETING

Bayerisches Staatsministerium für Unterricht, Kultus, Wissenschaft und Kunst, München, Germany
Deutsche Forschungsgemeinschaft, Bonn, Germany

INDUSTRIAL SPONSORS

The organizers would like to thank the following sponsors of this conference:

BRUKER Analytische Meßtechnik GmbH, Rheinstetten, Germany
BRUKER Medizintechnik GmbH, Ettlingen, Germany
CHAPMAN & HALL, New York, USA
CRYOPHYSICS GmbH, Darmstadt, Germany
DOTY Scientific Inc., Columbia, USA
HOECHST AG, Frankfurt, Germany
NYCOMED Arzneimittel GmbH, München, Germany
OXFORD Instruments GmbH, Wiesbaden, Germany
SCHERING AG, Berlin, Germany
SIEMENS AG, Unternehmensbereich Medizintechnik, Erlangen, Germany
SMIS Ltd., Guildford, UK
VARIAN GmbH, Darmstadt, Germany
VCH Verlagsgesellschaft mbH, Weinheim, Germany

Scientific Program

Monday, August 28, 1995

9.15 - 10.00	**Opening Session**	**(Chair: E.R. Andrew)**
9.15 - 9.30	Welcome Addresses	
9.30 - 10.00	Opening Lecture	G. Laukien
10.00 - 10.30	**Coffee Break**	
10.30 - 13.00	**NMR Instrumentation and Methods**	**(Chair: E. Fukushima)**
10.30 - 11.00	NMR Microscopy Coils	Peck T.L.
11.00 - 11.15	Novel Models and Designs for Small Bore RF Resonators	Crozier S., Forbes L., Doddrell D.M.
11.15 - 11.30	Design Considerations for a Scanning Microcoil DESIRE Microscope	Morris H.D., Gor'kov P., Lyding J., Adesida I., Lauterbur P.C.
11.30 - 11.45	High Temperature Superconducting Probe for NMR Microscopy	Yap M., Black R.D. Brey W.W.,Cole B.F., Hurlston S.E., Johansson M.E., Johnson G.A., Kotsubo V.Y., Nast R., Romo M., Withers R.S.
11.45 - 12.15	3-Dimensional Image Based Autoshim Procedures - Applications in High-Field, Narrow-Bore NMR Systems	Sukumar S.
12.15 - 12.30	A Compact Low Inductance Transverse Gradient System for Magnetic Resonance Microscopy: Application to the Human Spinal Cord	Andrew E.R., Inglis B.A., Kempka M., Mareci T.H., Szczesniak E.
12.30 - 12.45	A New Way of NMR Detection: Force Detection	Veeman W.S., Schaff A.
12.45 - 13.00	Hadamard NMR Imaging with Slice Selection	Nilgens H., Thelen M., Blümich B.
13.00 - 14.30	**Lunch**	
14.30 - 15.30	**Advanced Concepts**	**(Chair: J.H. Strange)**
14.30 - 15.00	NMR Force Microscopy	Vieth H.M.
15.00 - 15.30	NMR of Subsurface Earth Formations *in situ*	Kleinberg R.L.
15.30 - 16.00	**Coffee Break**	

16.00 - 17.15 EPR (Chair: W. Kuhn)

16.00 - 16.30	Free Radicals in Medicine: In Vivo ESR and EPR Imaging with Nitroxides, Metabolites and Spin Traps	Berliner L.J.
16.30 - 17.00	Dynamic Imaging of Diffusion and Fourier Transform ESR Imaging in the Study of Fluids, Membranes and Polymers	Xu D., Moscicki J.K., Shin Y.K., Freed J.H.
17.00 - 17.15	A Whole-Body Free Radical Imager	Lurie D.J., Yeung D., Foster M.A., Partridge R.S.

17.15 - 17.45 Break

17.45 - 19.00 NMR in Plant and Food Research (Chair: J.M. Pope)

17.45 - 18.15	NMR Imaging in Food Research: from the Laboratory to the Process Line	McCarthy M.J.
18.15 - 18.30	Whole Plant Functional NMR Imaging	Van As H., Van Dusschoten D., Nagarajan S., Vergeldt F., de Jager P.A.
18.30 - 18.45	In Vivo Measurement of Xylem Water Flow under Different Environmental Conditions Using Flow Sensitive NMR Imaging	Kuchenbrod E., Kahler E., Thürmer F., Haase A., Zimmermann U.
18.45 - 19.00	^{1}H NMR Imaging Studies of Scots Pine Needles Exposed to the Stress of Winter Desiccation	Lasarov H., Alvila L., Pakkanen T.T., Repo T., Sutinen M.-L.

19.00 - 22.00 Poster Reception

Tuesday, August 29, 1995

9.15 - 12.45 NMR in Materials Sciences (Chair: R.L. Armstrong)

9.15 - 9.45	MRM of Polymeric Solids and Microporous Materials	Cody G.D., Gerald II R.E., Botto R.E.
9.45 - 10.00	Simultaneous ^{1}H and ^{19}F Stray Field Imaging in Solids and Liquids	Randall E.W., Samoilenko A.A., Nunes T.
10.00 - 10.15	Investigations to the Influence of Radiation Induced Crosslinking On The Dynamic Processes In Cis-Polybutadiene As Seen By NMR Techniques	Denner P., Kuhn W., Walter B., Willing T.
10.15- 10.45	Solid State NMR Imaging of the Physical and Chemical Structure of Materials	Miller J.B., Hepp M.A.

10.45 - 11.15	**Coffee Break**	
11.15 - 11.45	NMR Imaging and Solvent Induced Changes in Materials	Gelan J., Adriaensens P., Vanderzande D., Ercken M.
11.45 - 12.00	NMR Imaging of 3D Foam Structures	Kose K.
12.00 - 12.15	A New Technique for Imaging Ultra-Short T_2 in Solids	Lurie D.J., McCallum S.J., Hutchison J.M.S., Alecci M.
12.15 - 12.30	Non-invasive Observation of Flow Profiles, Polarisation Layers and Fouling in Membrane Filtration Modules using NMR Micro-imaging	Yao S., Fane A.G., Pope J.M.
12.30 - 12.45	Multinuclear NMR Imaging of Controlled Drug Release from Hydrophilic Matrix Tablets	Fyfe C.A., Blazek A.
12.45 - 14.00	**Lunch**	
14.00 - 15.30	**Rare Isotopes and Contrast Media**	**(Chair: G.D. Mateescu)**
14.00 - 14.30	Oxygen-17 Nuclear Magnetic Resonance Spectroscopy and Imaging. Determination of the Rate of Cerebral Metabolism, of Oxygen and the Rate of Cerebral Blood Flow in the Human	Fiat D.
14.30 - 14.45	Recent Advances in ^{17}O MRI and MRS Detection Limits and Biomedical Applications	Mateescu G.D., Cabrera M.E.
14.45 - 15.00	Enhanced Spin Lattice Relaxation and Polymer Formation with Immobilized Paramagnetics	Balcom B.J., Kilfoil M.L., Sharp A.R.
15.00 - 15.30	Contrast Agents, Fundamentals	Muller R.N.
15.30 - 17.00	**Coffee Break and Poster Viewing**	
17.00 - 18.30	**NMR Imaging in Medicine - New Concepts -**	**(Chair: A. Haase)**
17.00 - 17.30	Dedicated MR Scanners	Bertora F., Biglieri E., Trequattrini A.
17.30 - 18.00	Medical NMR Imaging in Open Magnets	Hausmann R.
18.00 - 18.30	Interventional MR Imaging	Shaw D.

Wednesday, August 30, 1995

9.15 - 12.45 NMR in Biomedicine (Chair: W.E. Hull)

9.15 - 9.45	In Vivo Carbon-13 NMR Spectroscopy	Seelig J.
9.45 - 10.00	Three-Dimensional Measurements of Lung Properties during the Breathing Cycle	Shattuck M.D., Gewalt S.L., Glover G.H., Hedlund L.W., Johnson G.A.
10.00 - 10.15	Direct MR Imaging of the Guinea Pig Airways using Hyperpolarized ^{3}He	Hedlund L.W., Black R.D., Cates G.D., Cofer G.P., Guenther R., Happer W., Johnson G.A., Middleton H., Shattuck M.D., Swartz J.
10.15 - 10.30	Heteronuclear Spectroscopy and Imaging	Lutz O., Pfeffer M., Kull Th., Zutt A., Bunse M., Jung W.-J.
10.30 - 10.45	Radial Spectroscopic Imaging	Meininger M., Jakob P.M., v.Kienlin M., Haase A.

10.45 - 11.15 Coffee Break

11.15 - 11.45	The Role of NMR Imaging in Pharmaceutical Research and Development	Sarkar S.K.
11.45 - 12.00	^{1}H-NMR Microscopy at 7 T: 3D Visualization of Tumor Metastases in Mouse Organs Ex Vivo; Detection of Metastases and their Eradication by Immunotherapy In Vivo	Fichtner K.P., Hull W.E., Griesbach A., Schirrmacher V.
12.00 - 12.15	Quantitative NMR Microscopy on Multicellular Tumor Spheroids and Confrontation Cultures	Brandl M., Tonn J.C., Kotitschke K., Goldbrunner R., Kerkau S., Haase A.
12.15 - 12.30	Identification of Water Compartments in Developing Bird Embryos by NMR Microscopy	Ronen I., Ar A., Navon G.
12.30 - 12.45	Secrets of Beauty Care Products Studied by NMR Microscopy	Szayna M., Ilg M., Kuhn W.P.

12.45 - 14.00 Lunch

14.00 - 17.00 Guided Tours (NMR-Labs, Röntgen-Musem, City Tour, etc.)

18.00 - 22.00 Social Evening at Residenz

18.00 - 18.30	Reception at Residenz (all participants)	
18.30 - 19.15	Evening Lecture (all participants): An Illustrated Random Walk Through the Early History of X-Rays in Medicine (Chair: A. Haase)	Mould R.F.
19.15 - 19.30	Break	
19.30 - 22.00	Conference Dinner (Ticket required)	

Thursday, August 31, 1995

9.15 - 11.00 Diffusion NMR Imaging

(Chair: P.C. Lauterbur)

9.15 - 9.45	NMR Visualization of Diffusion and Flow Displacements	Kimmich R.
9.45 - 10.15	Diffusion MRI: From Tissue Micro-structure to Clinical Applications	Le Bihan D.
10.15 - 10.45	Microscopic MRI of Cartilage	Jelinski L.W.
10.45 - 11.00	NMR Microscopic Detection of Cartilage Stress Behaviour - An Approach to Dynamic NMR Microscopy	Gründer W., Hahn S., Keller T., Werner A.

11.00 - 11.30 Coffee Break

11.30 - 13.15 NMR in Porous Media

(Chair: P. Jonsen)

11.30 - 12.00	Porous Media NMR Imaging (Gels, Brains, Rocks, Soil)	Hall L.D.
12.00 - 12.30	NMR Imaging in Porous Media	Bowtell R., Peters A., Robyr P., Mansfield P.
12.30 - 13.00	Transport Processes in Porous Media	Nesbitt G.J.
13.00 - 13.15	Spatially Resolved NMR Study of Adsorption/Precipitation of Chemicals Inside Porous Media	Maddinelli G.

13.15 - 14.30 Lunch

14.30 - 15.30 Final Discussion

Adjournment

ORAL PRESENTATIONS

NMR MICROSCOPY COILS

T.L. Peck
Magnetic Resonance Engineering Laboratory, Beckman Institute,
Department of Electrical and Computer Engineering,
University of Illinois, Urbana IL 61801

NMR detection coils with diameters less than 1 mm (microcoils) provide an enhanced signal-to-noise ratio (SNR) for RF detection in NMR microscopy.[1,2] The development of microcoils has progressed from simple, hand-wound solenoids on glass capillary formers to more complicated planar designs fabricated using microlithography on glass, silicon, and gallium arsenide substrates.[3,4] Design optimization requires careful consideration of materials and geometry to maximize filling factor while minimizing linewidth. A recent extension of this effort involves the combination of planar microcoils and integrated pre-amplifiers on a single GaAs substrate.[5] This monolithic integrated NMR detector is the first step toward a "chip-based" NMR spectrometer.

The application of NMR techniques to medicine, biology, chemistry, and materials analysis has stimulated the rapid advancement of detection probe technology. For example, applications of solenoidal microcoils as on-line detectors for capillary electrophoresis and liquid chromatography have resulted in detection volumes of 5 nl and detection masses of less than 1 nanomole.[6-8] Recent advances in microimaging of the rat carotid artery[9] and of single neurons[10] demonstrate that new information is available in this size regime. This talk will outline current capabilities and limitations of microcoil technology to provide a basis for future developments in microspectroscopy and microimaging.

1. E.W. McFarland and A. Mortara, Magn. Reson. Imaging, **10**, 279, (1992).
2. T.L. Peck, R.L. Magin, and P.C. Lauterbur, *in press*, J. Magn. Reson.
3. T.L. Peck, R.L. Magin, J. Kruse, and M. Feng, IEEE Trans. Biomed. Eng. **41**:7 (1994).
4. T.L. Peck, L. LaValle, R.L. Magin, B.C. Wheeler, I. Adesida, and P.C. Lauterbur, Abstracts, 2nd Int. Conf. on Magn. Res. Microscopy, Heidelberg, Germany (1993).
5. T.L. Peck, S.J. Franke, M. Feng, J. Kruse, and R.L. Magin, Abstracts, 16th Int. Conf. of the IEEE Eng. in Med. and Bio. Society, Baltimore, MD (1994).
6. N. Wu, T.L. Peck, A.G. Webb, R.L. Magin, and J.V. Sweedler, J. .Am. Chem. Soc. **116**, 7929 (1994).
7. N. Wu, T.L. Peck, A.G. Webb, R.L. Magin, and J.V. Sweedler, Anal. Chem. **66**, 3849 (1994).
8. N. Wu, A.G. Webb, T.L. Peck, R.L. Magin, and J.V. Sweedler, Anal. Chem., submitted.
9. R.M. Summers, L.W. Hedlund, G.P. Cofer, M.B. Gottsman, J.F. Manibo, and G.A. Johnson, Magn. Reson. in Med. **33**, 785 (1995).
10. R.W. Bowtell, A. Peters, J.C. Sharp, P. Mansfield, E.W. Hsu, N. Aiken, A. Horsman, and S.J. Blackband, Magn. Reson. in Med. **33**, 790 (1995).

Novel Models and Designs for Small Bore RF Resonators

Stuart Crozier, Larry Forbes* and David M .Doddrell

Centre for Magnetic Resonance and Department of Mathematics, Qld. University, Brisbane, Qld. 4072. Australia*

Small bore, high field RF probes have, in the past, used mostly saddle coils or Alderman and Grant type resonators. While Birdcage and similar resonators have become the standard for whole-body and large bore horizontal systems, the progression of this technology to high resolution and micro-imaging magnet systems has been limited by a number of problems. One of the problems is that for small coil diameters and high frequency operation, sheet type conductors are often used and that the current density in these sheets is no longer uniform as can be reasonably assumed in large bore designs where the conductor cross-section is small relative to the diameter of the coil.

In this work we present a new method of deducing the real current density, and therefore, the generated fields in small bore high-pass birdcage type structures based on a fast Inverse Hilbert Transform technique (1) and show new hybrid resonator designs that are superior to conventional designs (2). The effects of RF shields can also be included in the calculations - a different methodology is presented in these cases (3). Results from 10 coils built to operate 200 - 600 MHz will be presented and comments made concerning the utility of these coils for improved signal-to-noise high resolution spectroscopy, microscopy and microspectroscopy. Figure 1 shows the current density in j_t (A/m) of a shielded high-pass birdcage (primary solid, shield dashed) and the resultant contour plot of the trasnverse field, the shield consisted of a slotted tube.

1. L.K. Forbes, S. Crozier and D.M. Doddrell, *Meas. Sci. Technol. 6, 284* (1995).
2. S. Crozier, K. Luescher, L.K. Forbes and D.M. Doddrell, *J. Magn. Reson.*, in press (1995).
3. L.K. Forbes, S. Crozier and D.M. Doddrell, *SIAM J. Appl. Maths.* , submitted.

Figure 1

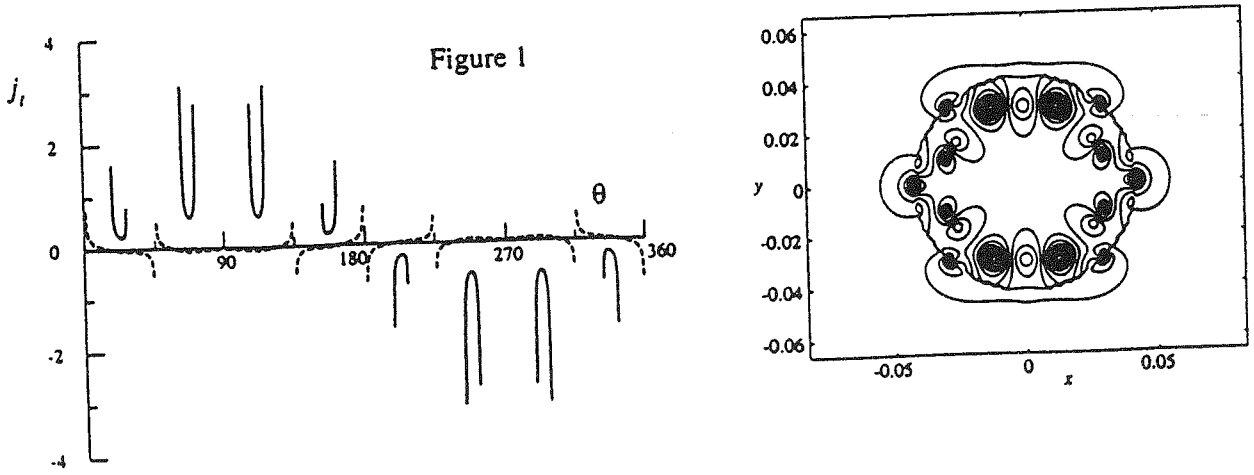

Design Considerations for a Scanning Microcoil DESIRE Microscope.

H. Douglas Morris *[1], Peter Gor'kov [1], Joseph Lyding [2,3], Ilesanmi Adesida [2,3] and Paul C. Lauterbur [1,3]

Biomedical Magnetic Resonance Laboratory [1] , Department of Electrical and Computer Engineering [2], and the Beckman Institute [3]
University of Illinois, Urbana IL 61801

The DESIRE (Diffusional Enhancement of Signal Intensity and REsolution) experiment[1] uses translational molecular diffusion to amplify spin saturation effects in a small volume (perhaps 1 μm or less across) to allow the observation of structures and small objects that would otherwise be invisible because of noise and diffusional blurring. One way to excite such a small volume is to use a tiny tagging RF coil. Unlike the somewhat larger microcoils that have been described [2-4], such very small coils need to function only as transmitters. The signal changes in the larger saturated region can be measured by larger microcoils.

The tagging coils can be used as the probe of a scanning NMR microscope. The diagram below shows our current design for this instrument. The tagging coil is supported from below and moved relative to the sample stage via piezoelectric bimorphs of the type used in scanning tunnelling microscopy (STM). The sample stage is approximately 0.5 micron thick Si_3N_4 and supports an aqueous sample. The microcoil is lithographically etched into a silicon wafer. The read out RF coil is constructed by conventional techniques.

We will show construction progress to date and a more complete description of the microscope design and operation.

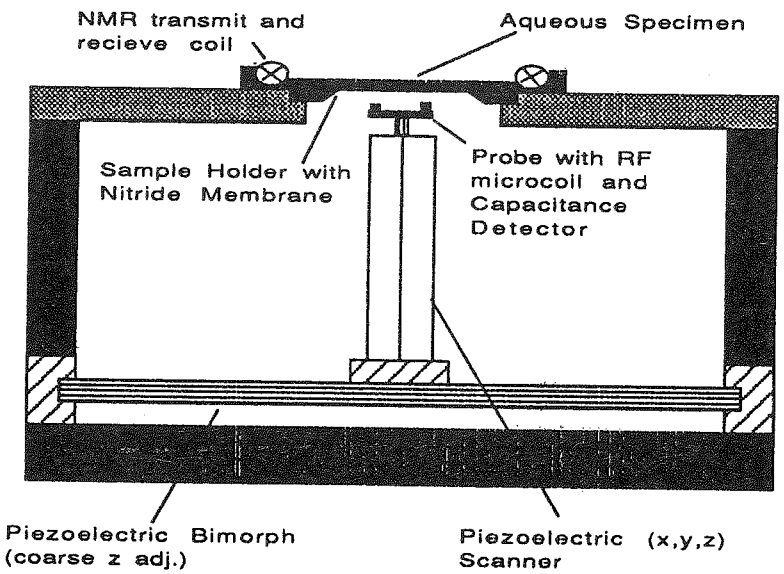

Diagram of scanning DESIRE microscope stage and RF coils

References:

1. P.C. Lauterbur, W.B. Hyslop, H.D. Morris,"NMR Microscopy: Old Resolutions and New Desires", XI International Society of Magnetic Resonance Conference, Vancouver, B.C. Canada, p. 124 (1992)
2. T.L.Peck, R.L. Magin, and P.C. Lauterbur, "Design and Analysis of Microcoils for NMR Microscopy", J. Mag. Res (in press).
3. T.L.Peck, L. LaValle, R.L.Magin , I. Adesida, and P.C.Lauterbur,"Planar Microcoils - Sensors for NMR Microscopy",Abstracts 2nd International Conference on Magnetic Resonance Microscopy, Heidelberg, Germany, 6-9 September, p.90 (1993).
4. T.L.Peck, R.L.Magin, J. Kruse, and M. Feng, "NMR Microspectroscopy using 100μm Planar RF Coils Fabricated on Gallium Arsenide Substrates", IEEE Trans. Biomed. Eng. 41:7 (1994).

High Temperature Superconducting Probe for NMR Microscopy

R.D. Black[2], W.W. Brey[1], B.F. Cole[1], S.E. Hurlston[2], M.E. Johansson[1], G.A. Johnson[2], V.Y. Kotsubo[1], R. Nast[1], M. Romo[1], R.S. Withers[1], M. Yap[1]
[1] Conductus Inc., 969 W. Maude Ave. , Sunnyvale CA 94086
[2] Center for *In Vivo* Microscopy, Duke University Medical Center, Durham NC 27710

Introduction

We report a High Temperature Superconducting (HTS) NMR microscopy (NMRM) probe with significant enhancement in performance and ease of use compared to previous design. The technology enabling these improvements is based on recently revealed NMR spectroscopy (NMRS) probe.

Background

A 7 T open-cycle NMRM system using a single $YBa_2Cu_3O_{7-\delta}$ (YBCO) on $LaAlO_3$ RF coil, in a quartz dewar operating at 10 K, has been reported with a 10-fold SNR improvement over a room temperature copper coil of comparable geometry.[1,2] The system recently has been adapted to function at 9.4 T. However the quartz probe system is difficult to use and not reliable. More recently an integrated open-cycle NMR spectroscopy (NMRS) probe in a 9.4 T field using a pair of YBCO coils has been reported with a 3 to 5 fold SNR improvement over a commercially available high resolution probe.[3] This robust probe has metal walls and is compatible with standard NMRS hardware, such as sample spinners and variable temperature controllers. In this study we present the NMRM version of the metal wall open-cycle system for clinical histopathology applications.

Methods and Results

7 T to 9.4 T To facilitate the transition from a 7 T quartz dewar to a 9.4 T metal wall probe, we fabricated a single 9.4 T YBCO on $LaAlO_3$ coil and imaged a rat kidney (TR 200 ms, TE 6.5 ms, FOV 60 x 60 x 160 μm) with the 9.4 T quartz dewar system. The 9.4 T YBCO coils are patterned into a split ring shape on each side of the substrate, similar to its 7 T predecessor. At zero field with the coil and the RF shield in liquid N_2, the coil resonates at 398.5 MHz and has a Q of 37,000. The relative SNR of comparable systems goes as square of its relative B_0 fields. A 9.4 T system has an 80 % SNR gain compared to a 7 T system.

NMRS to NMRM metal wall probe The NMRS probe uses rectangular YBCO RF coils with integrated interdigital fingers. The coils inner dimensions are compatible with standard 5 mm sample tube and the coils are arranged in a pair configuration. The pair resonates at 402.8 MHz with an unloaded Q of 44,000 at zero field and 4.2 K. An adaptation of this coil design for microscopy has been simulated and fabricated. The microscopy coil has inner dimensions of 20 x 16 mm. Simulation for S_{11} and S_{21} profiles was done with IE3D™, an integral-equation algorithm-based EM simulator from Zeland Software. The simulated resonant frequency is 400.62 MHz. The calculated effective capacitance and inductance are 3.1 pF and 51.6 nH respectively. Typical unloaded Q for these microscopy coils at zero-field and 4.2 K are in the 30,000 to 40,000 range. The room temperature sample is separated from the cold RF coils by a quartz vacuum barrier. A temperature controller regulates the helium flow to the probe. We use a cryogenically cooled GaAs MESFET amplifier with a noise temperature below 10 K and a power gain above 35 dB from 350 MHz to 550 MHz, when cooled to 77 K.

Discussion

Sample size The spectroscopy and microscopy probes share basic HTS coil technology as well as the basic cooling and vacuum packaging approach. The microscopy probe, however, accepts a 12 mm x 12 mm square cuvette rather than a standard 5 mm liquid NMR sample tube. The probe will fit in a 55 mm ID gradient set in an 89 mm magnet bore. The square cuvette provides a better filling factor due to the proximity of the pathology tissue sample to the planar coils. Moreover, the microscopy copper radiation shield and outer probe body must be consistent not only with the need for a low-loss RF shield and a low emissivity thermal shield, as in the spectroscopy probe, but also with the minimization of eddy currents to enable the gradient fields to penetrate.

Cold RF shield Black, *et al.*[3] have addressed the issue of copper thickness used for the cold RF shield. The copper should be thick enough to act as an RF shield, but should be thin enough to rapidly damp eddy currents. The skin depth of cold copper at 10 K and 300 MHz is about 0.4 μm. An 8-μm copper shield (20 x skin depth) was used to take 3-D spin warped images of fixed rat liver specimen (TR 400 ms, TE 10 ms) on the existing 7 T quartz dewar system. The obtained 30-fold SNR gain relative to a copper coil at room temperature made it possible to resolve fine features.

Applications One area of application for superconducting probe technology is in studying fixed tissue specimens. Most often, the increase in SNR provided by the probe is used to reduce the imaging time. We shall show images acquired using a fast spin echo sequence[4] to demonstrate the improvement in speed relative to studies performed with a copper coil held at room temperature. We note that other groups have used very small (~100 μm) solenoidal coils to make images of tissue[5]. Indeed, the improved SNR of the YBCO probe can be applied so as to give higher resolution and/or faster imaging times. We have chosen to maintain a relatively large field of view so as to maximize the utility of the probe to more standard histopathologic studies. In this way, the YBCO probe may be viewed as being capable of giving the resolution obtained with a small copper solenoid over a substantially larger volume. We shall show comparative studies that highlight this point.

Conclusion

An open-cycle, high-performance, and user friendly HTS NMRM probe is being developed based on recently developed HTS NMRS probe technology. Significant SNR improvement over the previous 7 T design can be achieved by increasing the B_0 field, cooling the RF shield, increasing filling factor through pair coil configuration, using a better preamp and improved cooling system.

Acknowledgments

This work was supported in part by NIH Grant # P41 RR05959, NSF Grant # CDR 8622201, NIH Grant # R43 RR09244 and NIH National Center for Research Resources.

References

1. Black, R.D., Early, T.A., Roemer, P.B., Mueller, O.M., Mogro-Campero, A., Turner, L.G. and Johnson, G.A., *Science*, 259, 793, 1993.
2. Black, R.D., Early, T.A. and Johnson, G.A., *J. Mag. Res., Series A*, 113, 74, 1995.
3. Anderson, W.A., Brey, W.W., Delin, K.A., Fuks, L.F., Hill, H.D.W., Johansson, M.E., Kotsubo, V. Y., Krivoruchko, M., Withers, R.S., Wong, W.H. and Yap, M., *36th ENC Abstracts*, 359, 1995.
4. Zhou, X., Cofer, G.P., Suddarth, S.A., Johnson, G.A., *Magn. Res. Med.*, 30, 60, 1993.
5. Peck, T.L., *Ph.D. dissertation, U. of Illinois*, 1992.

TITLE: 3-Dimensional Image Based Autoshim Procedures
- Applications in High-Field, Narrow-Bore NMR Systems

AUTHOR: Subramaniam Sukumar Ph.D.,
Bruker Instruments Inc.,
47697 Westinghouse Dr., Fremont, CA 94587, USA.

ABSTRACT:

Magnet shimming is critical for NMR spectroscopy and imaging applications. In most spectrometers the procedure is still done by monitoring the response of an NMR signal while manually adjusting the shim currents - a tedius and time consuming process. An ideal approach would be to measure the field seen by the sample and to calculate the shim currents that are needed to minimize the residual fields in the magnet. Imaging and spectroscopic imaging techniques offer a convenient means to measure the field and to monitor the progress of shimming. Eventhough there are some interesting experiments reported in the literature the technique has not been widely used in the NMR field because of instrumental or experimental limitations. For example, 3-axis shielded gradients were not available in commercial high-resolution spectrometers until recently. Image based shimming routines are elegant and work very well under certain circumstances but may not be practical for most NMR samples or applications. The method requires sufficient signal to noise ratio for accurate measurement of the field or frequency maps. Short T2 or T2*, and low spin density can result in low SNR. Other major limitations include the problems associated with accurate frequency measurement in the presence of multiple resonances or when the frequency offset due to inhomogeneities is greater than 2*PI radians. The image based methods use phase information in the image to calculate frequency therefore it will not be possible to directly obtain the frequency in the latter case. In the past the "phase wrap" problem was conveniently avoided by making sure the spins do not accrue a phase greater than 2*PI. 4D CSI shimming methods do not suffer from the above limitation but are associated with long acquisition times.

In this study a 3D gradient echo image based shimming procedure is shown to produce excellent results in a high resolution NMR spectrometer. The latter system was chosen for the study because homogeneity requirements for high resolution spectroscopy are very stringent and there are established standards that can be used to monitor the performance of the shimming techniques. Starting from zero room temperature shims it was possible to obtain excellent resolution in a 2mM sucrose solution in 90% water. The procedure took 5 iterations with each iteration taking about 4 minutes for data collection, calculation and loading of shims. In this experiment accurate frequency measurements were obtained by implementing a 3D phase unwrapping procedure. When samples with low SNR (e.g. Deuterated solvents) were involved 1D projections were used to improve the sensitivity.

Experiments designed to address the limitations associated with SNR, T2, T2*, frequency measurement and data acquisition times are essential if the image or spectroscopic image based methods are to be used routinely in NMR.

A compact low inductance transverse gradient system for magnetic resonance microscopy: Application to the human spinal cord

E. R. Andrew[1], B. A. Inglis[2], M. Kempka[1], T. H. Mareci[2] and E. Szczesniak[1]

[1] Departments of Physics and Radiology, [2]Center for Structural Biology, University of Florida, P. O. Box 118440, Gainesville, Florida 32611, USA

A new transverse gradient coil assembly for magnetic resonance microimaging is presented. It uses a compact coplanar coaxial arc geometry. The coil is symmetric, has the advantage of simplicity, generates a remarkably large volume of uniform transverse gradient field, features very low inductance, and can therefore be suitable for applications requiring fast switched gradients. The system can be used for large or intermediate sized MR imaging or for MR microscopy. We have constructed three practical systems. The largest with 13 cm internal diameter enabled a detailed check to be made of computer calculations which were found to be in excellent agreement with experiment. The other two practical systems, with inside diameter 22 mm, were constructed for MR microscopy in 7 Tesla 50 mm and 89 mm bore magnets. One of these has been used to obtain NMR transverse micrographs of the human spinal cord in vitro. Examples of these MR microimages, based on a 256 x 256 data matrix with 39 μm in plane resolution will be shown.

This transverse gradient system for MR microscopy features:

- extended field linearity
- simplicity and compactness
- low inductance
- reduced stray field
- minimal coupling with the r.f. coil
- absence of torque

This work was supported by NIH through grant P41 RR 02278.

A new way of NMR detection : force detection

W. S. Veeman, A. Schaff,
Physikalische Chemie, Gerhardt - Mercator Universität Duisburg, Lotharstr. 1, 47048 Duisburg

It was recently proposed by Sidles et al. that NMR imaging with single spin sensitivity and atomic resolution might be achievable with an alternative way of NMR detection, force detection. Rugar and co-workers at IBM have then shown that the force detection in principle works for both electron spin and nuclear spin detection. They achieved a resolution of 2.6 μm with nuclear spin detection. The sample (12 ng ammonium nitrate) was mounted on a very small cantilever which was excited by an oscillatory magnetic force between a rf modulated spin magnetization of the sample and a ferromagnetic particle.

It will be clear that if NMR imaging could be routinely performed with an atomic resolution, the impact of such a technique on various fields would be tremendous. On the other hand, if single spin detection proofs not to be feasible, an improvement of the sensitivity of the NMR experiment by one order of magnitude would already have great implications. Experiments with smaller amounts of sample (think of biochemical samples which are hard to isolate or of the detection of small amounts of impurities in water) or on for instance polymer films and surfaces would improve the only disadvantage NMR has as an analytical technique, the relative insensitivity in comparison to other spectroscopical or surface techniques.

In Duisburg we have built a probe that can detect cantilever motions using a beam deflection scheme, in contrast to the IBM group who used an interferometer. We want to show that it is also possible to detect nuclear spin signals with this kind of technique. At first we have made experiments at various pressures to determine the pressure dependence of the Q - factor of the cantilever. For this experiments we mounted a ferromagnetic particle at the end of the cantilever and excited the cantilever with a small modulated magnetic field, generated with a coil and a low frequency signal generator. A laser beam was deflected by the cantilever to a two segment photo diode. The motion of the cantilever caused a periodic change in the difference of both signals. This difference signal was detected in a lock - in amplifier.

After this we prepared the probe to detect nuclear spin signals. Our sample, a small crystalline piece of ammonium nitrate, was glued on the tip of the cantilever using a microscope. The ferromagnetic particle was mounted on a piezoelectric translator nearby.

In the near future we want to develop an imaging technique that allows us to reconstruct the spin density of a given sample using a two dimensional map of the cantilever signal (a "force map").

Hadamard NMR Imaging with Slice Selection

H. Nilgens,[1] M. Thelen,[2] B. Blümich[3]

[1] Max-Planck-Institut für Polymerforschung, Postfach 3148, D-55021 Mainz

[2] Klinik für Radiologie, Johannes-Gutenberg-Universität, Langenbeckstr. 1, D-55131 Mainz

[3] Institut für Makromolekulare Chemie, RWTH, Worringer Weg 1, D-52056 Aachen

Hadamard excitation has been used in combination with the filtered back-projection algorithm to measure NMR images of small objects on a Bruker MSL 300 spectrometer. The power of the stochastic excitation was 0.5 Watts. The spatial resolution is determined by the type of filter used for image reconstruction. For Hadamard excitation it is identical to the resolution obtained for pulsed excitation. The acquisition time is the same as for FLASH imaging methods.

Slice-selective pulses of the SPREAD type were optimized for low power and their performance was analyzed for pulsed and for Hadamard excitation. The rf power of SPREAD pulses is at least one order of magnitude lower than that of the DIGGER pulse. For pulsed excitation the perfomance of the SPREAD pulse was similar to that of the DIGGER pulse, and a slight image degradation was observed for the combination of HADAMARD excitation and SPREAD slice selection. A comparison of HADAMARD imaging with SPREAD slice selection and slice-selective 2D Fourier imaging by a multi-slice 3D reconstruction of an olive demonstrates that the low-power advantage of the Hadamard technique can indeed be capitalized on for practical use in NMR tomography.

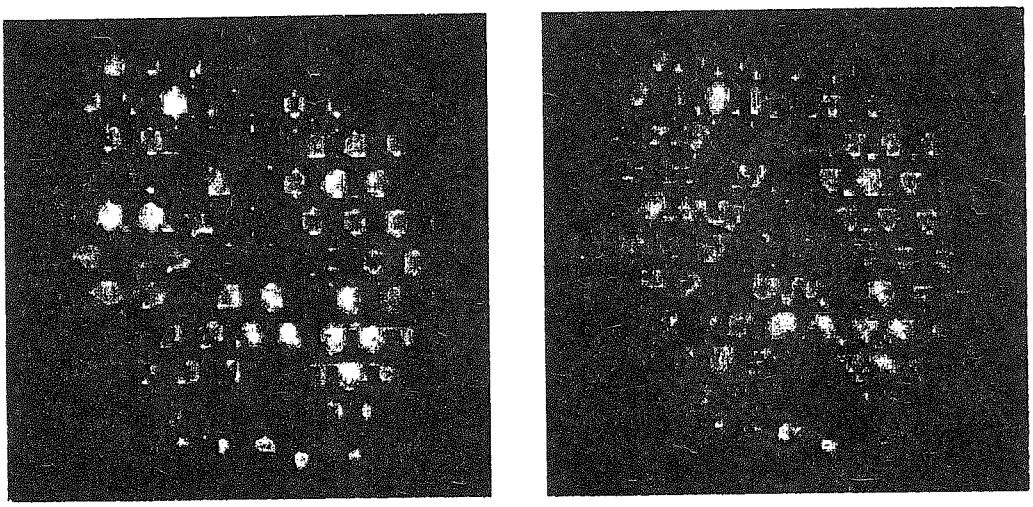

Fig.: NMR images of 50 water-filled capillaries with a diameter of 1 mm. Left: Spin-echo image, 64 phase encoding steps, 17 min acquisition time, 50 W rf power. Right: Hadamard image, 64 projections, 8 s acquisition time, 0.5 W rf power.

Reference:

H. Nilgens, B. Blümich, *Stochastic Spectroscopic Imaging*, in: D. N. Rutledge (Editor), *Signal Treatment and Signal Analysis*, Elsevier, Amsterdam, 1995.

NMR Force Microscopy

Hans-Martin Vieth, Freie Universität Berlin, Institut für Experimentalphysik

The spatial resolution achievable in NMR microscopy is mainly limited by the detection sensitivity, which for most experimental design scales with the number of spins per voxel. At present, in solid samples conventional inductive detection allows to observe about 10^{-16} protons corresponding to a minimum voxel size around $(50\mu m)^3$. In an alternative approach promising a more favorable scaling behavior ideas from scanning force microscopy have been combined with magnetic resonance methods. The technique is based on the measurement of the magnetic force acting between a tiny ferromagnetic tip and the spins in the sample. While Magnetic Force Microscopy (MFM) has become a routinely applied method for imaging of ferromagnetic structures, the detection of spins is much more demanding, because their magnetic moments are smaller by several orders of magnitude. To overcome the sensitivity problems long lasting coherent spin motion is generated by rf-irradiation and in a resonant way coupled to a vibrational mode of a high-Q micromechanical cantilever. In this way a displacement large enough for interferometric detection can be achieved and discriminated against effects caused by much larger non-magnetic forces. Images can be obtained by scanning the tip with respect to the sample while sensing the cantilever motion. The sensitivity achieved so far for single shot NMR force detection is of the order of 10^{13} spins, and the resolution for three-dimensional imaging is around 3μm x 15μm x 15μm. The ultimate goal is to detect magnetic resonance signals from individual nuclei; existing instruments, however, are far from having the sensitivity needed and considerable innovation in a number of areas, including improved sensors and new methods for manipulating spins is required. In the talk the present status of NMR force microscopy will be reviewed with particular attention to the basic physical principles involved, to the description of the apparatus used and to the prospects of further research and development in this field.

NMR of Subsurface Earth Formations *in situ*

R.L. Kleinberg
Schlumberger-Doll Research
Ridgefield, Connecticut, USA

Nuclear magnetic resonance measurements can provide a surprising amount of useful information about sedimentary geological formations. Sedimentary rocks are porous, and the pores can contain water, oil, or natural gas. Proton NMR is used to determine the amount of fluid in the pore space, the hydraulic permeability, and the distribution of pore sizes.

In order to make NMR measurements on earth formations *in situ*, borehole NMR apparatus has been constructed. Unlike the usual NMR apparatus, where a sample is placed inside a magnet and RF coil, the borehole instrument is contained in a cylindrical metallic sonde which is lowered as deep as 10 km into the earth. There are a number of unusual and interesting constraints on the construction and operation of the apparatus.

The nonexponential magnetization decays are analyzed in terms of a sum of exponentials. The data inversion is posed as a linear estimation problem, the solution of which is rendered unique by regularization. The resulting distributions of relaxation times have a one-to-one correspondence to the distribution of pore sizes, and form the basis of geological information displayed to petroleum engineers in the form of a "well log".

FREE RADICALS IN MEDICINE: IN-VIVO ESR AND EPR IMAGING WITH NITROXIDES, METABOLITES AND SPIN TRAPS

Lawrence J. Berliner, Department of Chemistry, Ohio State University, Columbus, Ohio 43210 U.S.A.

Developments in in-vivo ESR have grown significantly since their first reports in the early 1980's. This lecture intends to review the rapid progress in this area and to contrast the areas where it either complements or supersedes MRI. Work with nitroxide spin probes has been centered around imaging, oximetry and the stability of the nitroxyl moiety to metabolism (i.e., bioreduction) in living animals. Examples in the field of the imaging of an isolated heart through the direct detection on nitroxide metabolism in animals will be reported. The use of other, inert radical materials has been employed in oximetry measurements including the first report of in-vivo ESR on a human! The reactive oxygen species, ·OH and O_2^{-}· have been impossible due to their very short lifetimes and low levels. Direct spin-trapped adducts of ·OH-DMPO, ·OOH-DMPO are also very unstable and susceptible to in-vivo bioreduction and disproportionation. Hence, only the carbon based radical products of hydroxyl or superoxide lipid peroxidation are stable enough to accumulate (frequently as the PBN adduct). The most recent flurry of interest has been in nitric oxide, a critical metabolite of arginine involved in muscle and vasodilator, particularly as a defence in septic shock. Examples are shown for the direct detection of NO· in-vivo in laboratory animals. Lastly an example of the first demonstration of a bioradical metabolite of nitrosobenzene and related nitroaromatics is discussed.

DYNAMIC IMAGING OF DIFFUSION AND FOURIER TRANSFORM ESR IMAGING IN THE STUDY OF FLUIDS, MEMBRANES AND POLYMERS, D. Xu, J.K. Moscicki, Y.K. Shin, and J.H. Freed, Baker Laboratory of Chemistry, Cornell University, Ithaca, NY 14853

In recent years our laboratory has developed the method of dynamic imaging of diffusion (DID)-ESR for the study of translational diffusion of spin probes. It has proved to be a very reliable technique, and it is applicable to a range of problems, from the anisotropy of diffusion in liquid crystals to transverse (or lateral) diffusion in model membranes. The introduction of spectral-spatial ESR imaging of diffusion in model membranes combines both the Heisenberg exchange (HE) between colliding spin probes and DID-ESR methods to simultaneously measure micro (spectral) and macro (spatial) diffusion in the same system. We describe these methods and show how the results may be interpreted in terms of a free volume model which accounts for the effects of reduced free volume in the ordered phases on the molecular diffusion.

The DID-ESR (dynamic imaging of diffusion by ESR) technique has been developed for application to polydispersed polymer samples. Due to polydispersity the spin-labeled polymer molecules have a wide range of molecular weight, and this is also true for the matrix polymer molecules. A new theoretical analysis of the DID-ESR method in the presence of polydispersity is presented, plus its first application for measuring translational diffusion coefficients of liquid crystalline (LC) polymer melts. This includes a detailed analysis of the reliability of the method, the proper interpretation of average diffusion coefficients, and how the molecular weight dependence of the diffusion coefficient may be obtained from even a single experiment on a sample with wide polydispersity. The results obtained by our new method are consistent with those from the FRES (forward recoil spectroscopy) technique on the same model system. A comparison is made between these two techniques, and future experiments which combine them to further study LC polymer diffusion mechanisms are proposed.

Other technical developments have lead to the successful realization of FT-EPR Imaging. We have constructed a fast, high power pulsed magnetic field gradient driver and coil configuration that generates gradients of 80 Gauss/cm with rise and fall times of less than 50 nsec. We show that the spectral information obtained in either a single pulse FID, two pulse COSY, or a three pulse ELDOR sequence may then be displayed as a function of position. The ability to perform spatially resolved 2D-EPR is a unique capability of FT-EPR imaging. We demonstrate sensitivity and resolution comparable with conventional imaging and describe future plans to extend these capabilities.

A Whole-Body Free Radical Imager using Field-Cycled PEDRI

David J. Lurie, David Yeung, Margaret A. Foster and Richard S. Partridge

Dept. of Bio-Medical Physics, University of Aberdeen, Foresterhill, Aberdeen AB9 2ZD, U.K.

INTRODUCTION: There is currently considerable interest in the detection and imaging of free radicals in biological samples and in animals. Several research groups are developing instrumentation for EPR imaging, and samples as large as rats have been imaged[1]. Others are working on double-resonance NMR/ EPR methods using the Overhauser Effect, known variously as Proton-Electron Double-Resonance Imaging (PEDRI), Overhauser Imaging (OI), Overhauser MRI (OMRI) or Dynamic Nuclear Polarisation Imaging (DNPI). These Overhauser-based techniques involve the irradiation of the free radical's EPR line(s) and the subsequent detection of the proton NMR signal. If the free radicals are causing proton relaxation, EPR irradiation can result in an enhancement of the NMR signal and a corresponding increase in image intensity from those parts of the sample containing free radical. Since the power absorbed in a conducting sample is proportional to the square of the rf frequency, PEDRI is usually performed at field strengths of 10 mT or less in order to use EPR irradiation frequencies below 300 MHz. Operating at such low field strengths inevitably compromises the SNR of the imaging experiment. In Field-Cycled PEDRI (FC-PEDRI), the applied magnetic field is switched between two levels during the pulse sequence (Fig. 1), allowing the EPR irradiation to be applied at extremely low field (hence low frequency and low SAR) while the NMR excitation, gradient pulses and signal acquisition occur at a higher field, maximising the SNR[2]. We present here the details of a whole-body sized FC-PEDRI imager which we have constructed in our laboratory.

METHODS: The whole-body FC-PEDRI imager makes use of the field-compensation method of magnetic field cycling. The vertically-oriented detection magnetic field of 59 mT is provided by a whole-body permanent magnet (Field Effects, US), while the offset field is generated by an internal resistive coil (Magnex Scientific, UK) driven by a power supply amplifier (Copley Controls, US) (Fig. 2). The gradient coils are built into the structure of the permanent magnet, leaving a free bore of 52 cm inside the field-cycling (FC) coil. The FC coil has an inductance of 68 mH and a DC resistance of 0.66 Ω, yielding a time constant of 103 ms. The Copley amplifier is able to ramp the magnetic field between 0 and 59 mT in 40 ms. The ferrite permanent magnet is non-conducting, so no eddy currents are generated. Initial tests of the system have used a double-resonance rf coil assembly consisting of a 12.5 cm i/d split-solenoid (NMR T_x, R_x) tuned to 2.5 MHz and a 20 cm diameter coaxial birdcage resonator (EPR T_x) operating at 50 MHz. The imager is controlled by a commercial NMR console (SMIS, UK); as well as the standard imager functions, the console generates the field-cycling waveform from one of its DAC boards, and supplies the EPR irradiation signal from its internal synthesiser.

RESULTS: We have performed initial experiments using phantoms containing aqueous solutions of the nitroxide free radical proxyl carboxylic acid (PCA). The EPR irradiation was carried out at 50 MHz at an evolution field strength of 2.7 mT. These experiments confirm the expected reduced rf power deposition and improved SNR relative to our fixed-field PEDRI experiments performed at 10 mT. We plan to perform *in vivo* studies using the FC-PEDRI imager in the near future.

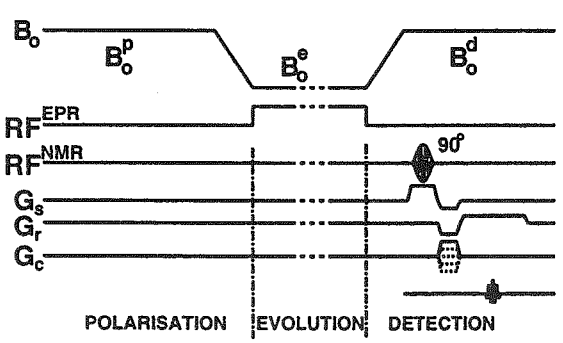

Figure 1: The FC-PEDRI pulse sequence.

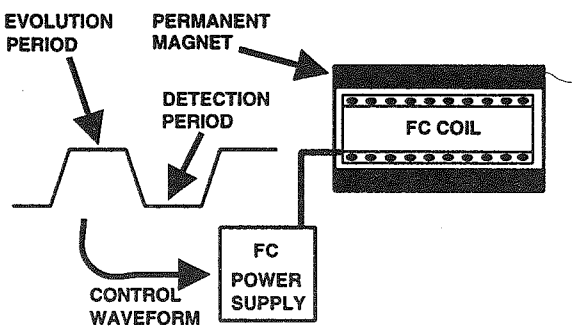

Figure 2: Arrangement of magnets.

1. M. Alecci *et al.* Biophys. J. **67**, 1274-1279 (1994).
2. D.J. Lurie *et al.* J. Magn. Reson. **84**, 431-437 (1989).

NMR Imaging in Food Research: from the laboratory to the process line

Michael J. McCarthy
Professor of Food Engineering
Department of Food Science and Technology
University of California
Davis, Ca USA 95616-8598

New food formulations, new food processes, the development of designed foods and emphasis on quality have resulted in the demand for new analytical methods. These analytical methods are needed to assist in understanding ingredient function, ingredient interactions, transport processes and in the assessment of food quality. NMR imaging has been shown to be a useful new experimental tool to examine the static and dynamic properties of food systems. This technique has proven to be most useful when combined with existing experimental methods and mathematical models of the physical/chemical processes being studied. Systems studied of importance for food manufacture include dehydration, extrusion, aseptic processing and baking. The development of NMRI test protocols for basic research studies of food stability and food physical properties may also be used to monitor processing systems.

Development of MRI as a process sensor has focused on the measurement of internal quality features which will complement existing sensor technologies. The major advantages of MRI are its ability to measure multiple internal quality features essentially in real time. The applications for MRI sensors include quality evaluation of fresh fruits and vegetables, food process control, in package quality assessment and storage stability testing. Initial quality assessment of fruit moving on a conveyor at commercial packing house speed have shown excellent agreement with standard destructive tests.

WHOLE PLANT FUNCTIONAL NMR IMAGING.

H. Van As, D. van Dusschoten, S. Nagarajan, F. Vergeldt and P.A. de Jager.
Wageningen Agricultural University
Dept. of Molecular Physics and Wageningen Agricultural NMR Centre
Dreijenlaan 3, 6703 HA Wageningen, The Netherlands.

The perspectives of functional plant imaging based on multi-echo sequences have been presented previously (1). Here whole plant functinal imaging is demonstrated using water culture plants in combination with an open access 0.5 T electro magnet and full environmental control of the leaf and root area.

As a first example, quantitative T_2 and flow imaging by a PFG-CPMG like imaging sequence (2) has been applied to an intact cucumber plant of about 1.2 m height. Water transport in separate xylem vessels has been measured. By combining the flow images with the T_2 images the relation between transport and water balance in the surrounding tissue can be studied.

A second example is functional NMR imaging based on quantitative T_1, T_2 and diffusion images (2) applied to study the effects of sudden osmotic stress in a tolerant (*Penniseutum americanum* L; cv. MH-179) and a susceptible (*Zea mays* L, cv. LG 11)) intact plant in time. Osmotic stress was induced by replacing the root medium by a - 0.9 MPa PEG-6.000 solution. Cross-sectional images of the stem showed that pearl millet adapted to the stress by shrinkage of the stem, increase of the tonoplast permeability and of the apparent diffusion coefficient in the central part of the stem. This plant survived a three days stress period. In contrast, hardly no changes were observed in the stem of the maize, which did not survive a one day stress period.

These results demonstrate the power of functional NMR imaging of whole plants. Further based on the results a mechanism can be proposed for drought adaptation in pearl millet by using cell water acting as a reservoir and maintaining movement of water to the leaves through diffusion which helped in the recovery of the plant once the stress was relieved.

This research was supported, in part, by the European Union, grant no. CI1-CT93-0187 and contract no. CHGE-CT94-0061.

References:

1. H. Van As. Functional NMR imaging of plants. Book of abstracts 2nd International Conf. on Magnetic Resonance Microscopy, Heidelberg, Germany, September 6-9, 1993, p. 70.

2. D. van Dusschoten, C.T.W. Moonen, P.A. de Jager and H. Van As, Book of Abstracts 11th SMRM, 1993, p.

3. H.T. Edzes, D. van Dusschoten, H. Van As. Quantitative imaging of NMR relaxation in plants. Book of abstracts 2nd International Conf. on Magnetic Resonance Microscopy, Heidelberg, Germany, September 6-9, 1993, p. 129.

In vivo measurement of xylem water flow under different environmental conditions using flow sensitive NMR imaging

E. Kuchenbrod, E. Kahler, F. Thürmer*, A. Haase, U. Zimmermann*

Physikalisches Institut, Lehrstuhl für Biophysik and *Lehrstuhl für Biotechnologie,
Am Hubland, 97074 Würzburg, Germany

Introduction: Quantification of xylem water flow is an important parameter for investigation of water transport in plants. We investigated water flow in an intact plant system using quantitive high resolution NMR imaging.

Materials and Methods: Young maize plants (*Zea mays*, 8-10 days old) were grown in hydroponics and kept in hydroponics for the experiments. NMR studies were performed on a Bruker AMX500 NMR microscope. The plants were placed in a climate chamber which allows simultaneous measurement of transpiration. Both flow and transpiration were measured while changing the environmental conditions by turning the light on and off. For flow quantitation we used a modified PGSTE [1, 2] magnetization-prepared NMR microimaging technique [3]. Eight flow weighted images were acquired and the flow velocity determined by a two parameter fit, assuming laminar flow in the vessels.

$$\text{fitting function [1]: } S(G) = S_0 \sin^2(\alpha v)/(\alpha v)$$

$\alpha = \gamma G \delta \tau$; v = average velocity, τ = distance of gradients; δ = duration of gradients

Further experimental parameters:
flow encoding: δ = 2 ms, τ = 50 ms, G: up to 150 mT/m
imaging: FOV = 5x5 mm^2 (128x64 or 128x32), Slice = 3mm; total acquisition time: 34 min

Results: Our measurements show that in the maize plant two different types of vascular bundles (v.b.) exist: a bundle system which is either very weakly or even not conducting, and a conducting system with flow velocities in the order of 1 mm/s. The active bundles in different leaves exhibit different flow velocities. Figure 1 shows a typical transpiration curve together with the total water flow (measured with NMR) under different illumination conditions. The total water flow was determined by summation of water flow of all v.b.. The good agreement between these two types of measurements is evident. The velocities in the single bundles show a similar dependence on illumination.

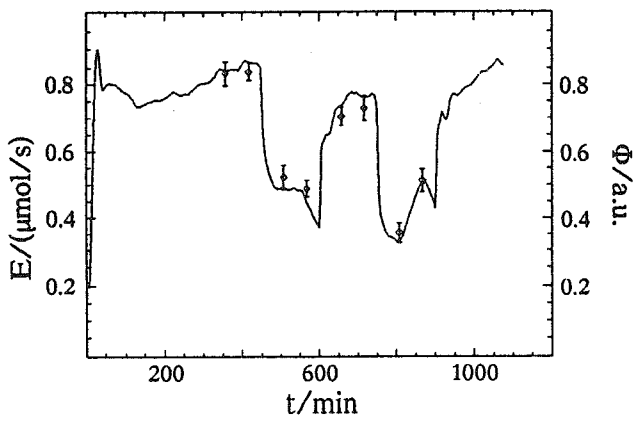

Fig. 1: A typical transpiration curve (solid line, E/(µmol/s)), when illumination changes (sharp edges), is shown. The squares indicate the total water flow Φ as measured with NMR. Φ is in a.u. since only relative changes were determined. The good relationship between change of transpiration and water flow and is evident.

Conclusions: Our measurements emphasize the potential role of NMR to study plant water flow. We demonstrate for the first time a spatially resolved *in vivo* measurement of plant water flow under changing environmental conditions. As compared to other methods NMR offers a unique opportunity to study this parameter in an intact plant system.

References:

1) Decorps, M., Bourgeois, D., *Magn. Reson. Med.* 19, 270 1991.
2) Kuchenbrod, E., Haase, A., *11th meeting of the ESMRMB*, Book of Abstracts, 391; 1994.
3) Haase, A., Brandl, M., Kuchenbrod, E., Link, A., *J. Mag. Reson.*, 105, 203; 1993.

^{1}H NMR IMAGING STUDIES OF SCOTS PINE NEEDLES EXPOSED TO THE STRESS OF WINTER DESICCATION

H. Lasarov[a], L. Alvila[a], T.T.Pakkanen[a], T. Repo[b] and M-L. Sutinen[c]

a) University of Joensuu, Department of Chemistry, P.O. Box 111, FIN-80101 Joensuu, Finland
b) University of Joensuu, Faculty of Forestry, P.O. Box 111, FIN-80101 Joensuu, Finland
c) The Finnish Forest Research Institute, Rovaniemi Research Station, P.O. Box 16, FIN-96301 Rovaniemi, Finland

Air pollutants may enhance winter desiccation by influencing water loss through the needles and by changing the water relations of tissues. NMR imaging is a non-invasive technique to diagnose damages of plants, e.g. declines of needles [1].

The objective of this study was to investigate water distribution in healthy and declined pine needles by NMR micro-imaging methods. For that purpose, green (healthy) and yellowish (declined) needles of Scots pine (*Pinus sylvestris* L.) were sampled in May 1995 from trees growing in the Rovaniemi district, in Lapland.

The experiments were performed on a Bruker AMX-400 spectrometer equipped with a microimaging accessory. The measurements were carried out using spin echo single slice pulse sequences. Two-dimensional images of pine needles were produced as cross-sectional slices. The distinction in distribution and in binding of water could be achieved between green and yellowish needle tissues by variation of the spin-echo time.

References:

1. Masuch, G., Franz, J-T., Marsmann, H., Gross, D. and Kettrup, A., Intern. J. Environ. Anal. Chem., 45, 1991, 179.

MRM of Polymeric Solids and Microporous Materials*

George D. Cody, Rex E. Gerald II and Robert E. Botto, Chemistry Division, Argonne National Laboratory, Argonne, IL 60439

Several aspects of magnetic resonance microscopy (MRM) are examined employing back-projection reconstruction techniques when used in combination with either simple Bloch-decay methods or MREV-8 multiple-pulse line narrowing techniques in the presence of static field gradients. Applications to the areas of ceramic processing, catalyst porosity measurements and the characterization of polymeric materials are presented. Two specific approaches employing MRM spin-echo techniques have also been utilized to study molecular transport of solvents and gases within microporous solids. Sequential imaging studies of solvent uptake in polymeric materials differentiates two different transport mechanisms. Exponential solvent concentration profiles observed for rubbery networks are consistent with Fickian behavior. In glassy systems, where solvent induces a phase transition of the network, a sharp solvent propagation front is observed which is typical of anomalous Case II transport. MR. analysis forms the basis of a model of anomalous transport in macromolecular solids which couples diffusion of solvent with kinetics of the 1st-order phase transition of the network and yields basic information about polymer architecture. Chemical-shift selective MRM of competitive gas diffusion experiments within porous media is being applied to monitor diffusivities of methane and other gases into materials designed for methane storage.

---

*Work performed under the auspices of the Office of Basic Energy Sciences, Division of Chemical Sciences, U. S. Department of Energy, under contract no. W-31-109-ENG-38.

Simultaneous ^{1}H and ^{19}F Stray Field Imaging in Solids and Liquids

E. W. Randall,[1] A.A. Samoilenko[2] and T. Nunes[3]

1 Chemistry Department, Queen Mary & Westfield College, London E1 4NS, England

2 Institute of Chemical Physics, Russian Academy of Sciences, 117977 Moscow, Russia

3 ICTPOL/IST, Av. Prof. Gama Pinto 2, 1699 Lisboa Codex, Portugal

The high field gradients (35 - 50 T/m) used in the stray field imaging technique (STRAFI)* ensure that both the ^{1}H and ^{19}F resonance regions are covered simultaneously by very short monochromatic pulses, and that separated images of these nucleides whether in solids or liquids or both, may be obtained; furthermore they may be discriminated with relaxation weighting.These facts will be demonstrated with different samples. The method may be extended to other combinations of nucleides.

---

* A.A. Samoilenko, D.Yu. Artemov, L.A.Sibeldina, *JETP Lett.*, 47, 417 (1988).

INVESTIGATIONS TO THE INFLUENCE OF RADIATION INDUCED CROSSLINKING ON THE DYNAMIC PROCESSES IN CIS-POLYBUTADIENE AS SEEN BY NMR TECHNIQUES

Denner, P., W. Kuhn*, B.Walter, Th.Willing
Institute of Physics, PH Erfurt/Muehlhausen,
99006 Erfurt, FRG
*Fraunhofer Institute for Biomedical Engineering,
66386 St. Ingbert,FRG

Crosslinked polymer chains are one of the most challenging problems in materials sciences. A major goal is to understand the connections between the bulk properties of polymeric materials and the influence of stabilizing crosslinks and conformational constraints on chain dynamic.
Important data for the construction of structure-property relationships come from the study of segment dynamics in the bulk. The dynamical properties of chain segments, i.e. mobile structural defects of a chain, in randomly crosslinked polymers depend on a variety of parameters, including the number of chemical crosslinks, the number of physical crosslinks, and the crosslinking procedure too. The number of crosslinks and the distribution of molecular mass between neighbouring chemical crosslinks determine the relaxational properties of the system. Physical crosslinks play an important role, particularly when the average length between chemical crosslinks is much longer than the entanglement length of the uncrosslinked polymer chains.

In this poster we report on ^{1}H-NMR measurements to the segmental dynamic in cis-1,4-polybutadiene crosslinked by radiation. The random displacements of structural defects along a polymer chain are described as a constrained diffusion process; the defect diffusion is limited to finite distances. In the diffusion model physical crosslinks, branches, chemical crosslinks and dynamical hindrances are acting as reflecting barriers. The restricted diffusion process between fixed and (or) fluctuating crosslinks has non-Markovian character. Correlation time and memory time for the local segment dynamic strongly depend on the crosslink density.

SOLID STATE NMR IMAGING OF THE PHYSICAL AND CHEMICAL STRUCTURE OF MATERIALS. J. B. Miller and M. A. Hepp, Chemistry Division, Code 6120, Naval Research Laboratory, Washington, D.C. 20375

Within the last several years methods for NMR imaging of solid materials have been developed which give very good spatial resolution in centimeter-sized samples. As important as spatial resolution is the ability to contrast regions of differing chemical and physical structure in materials. We will describe the use of chemical shift and relaxation to generate contrast in NMR imaging of solids. Examples of ^{1}H and ^{19}F imaging of polymers will be shown that illustrate contrast based on differences in chemical and physical structure of the materials. These may be related to chemical differences in the materials or to the stress history of the material.

NMR Imaging and Solvent Induced Changes in Materials.

Jan Gelan, Peter Adriaensens, Dirk Vanderzande and Monique Ercken
Limburg University, Instituut voor Materiaalonderzoek (IMO), Departement SBG
Universitaire Campus, Gebouw D, B-3590 Diepenbeek, Belgium.

It is well known that the properties of polymer systems can be dramatically influenced by interaction with solvents and vapors. A better understanding of these interactions, induced by solvent migration and polymer swelling, permit to improve the quality and the lifetime of polymer materials and to design polymer systems with controlled disclosure of components (such as drugs and other chemicals). Magnetic resonance imaging turns out to be a technique to monitor these solvent induced changes in an outmost non-invasive way.

In the introduction a few examples will be shown of the qualitative use of MRI-images to evaluate the influence of solvents on isolating materials, medical sponges and pharmaceutical rubbers.

In the main part of this contribution a more quantitative study will be shown on the kinetics of solvent ingress and polymer swelling as two separate phenomena which can be observed in a non disturbed way.

Typical case II (non Fickian) solvent migration combined with a clear case I swelling behavior will be illustrated on a PVC/dioxane system. For rubbery samples a case I solvent ingress together with a case I swelling is noticed. A gradual transition from case II to case I solvent migration will be illustrated in a PMMA/methanol system studied at variable temperature.

In order to understand these solvent diffusion processes a correlation will be made with the phase diagrams of the polymer/solvent systems.

One should however be aware of the fact that in many cases the classical case I and case II solvent diffusion laws are not followed at all, often being an indication of phase transitions in the materials. An interesting example of such solvent induced phase transition will be shown in the PC/acetone system where the cracking of the material will be explained by the crystallization of PC under the influence of acetone.

NMR Imaging of 3D Foam Structures

Katsumi Kose (kose@bukko.bk.tsukuba.ac.jp)
Institute of Applied Physics, University of Tsukuba, Japan

INTRODUCTION

How to divide 3D space into equal volume cells with minimum partitional area is a classical mathematical problem (1). Recently, a better solution than that by Lord Kelvin has been proposed (2), but this solution has not been verified experimentally. Since it is considered that a foam gives the solution for this problem, quantitative measurements of 3D foam structures are essential to this problem. The purpose of this study is thus to visualize 3D structures of foams using NMR imaging, to measure 3D geometrical quantities, and to evaluate the observed structures.

METHOD

Two specimens were prepared by immersing two kinds (different in cell sizes) of commercially available polyurethane foam into $CuSO_4$ doped water in 20 mmϕ NMR sample tubes. 3D microscopic MR images (FOV:$(19.2mm)^3$, matrix:128^3, voxel:$(150\mu)^3$) were obtained with a home built NMR imaging system using a 4.74T, 89mm vertical bore superconducting magnet and an actively shielded gradient coil. The pulse sequence used was a conventional spin-echo 3D imaging sequence (TR=200ms, TE=12ms) to avoid susceptibility artifacts (signal loss). Image distortion due to the gradient nonlinearity was checked using a phantom and that due to the static field inhomogeneity was evaluated using two images measured with positive and negative read-out gradients.

RESULTS AND DISCUSSIONS

Since only cross-sections of edges and vertices of bubble polyhedra were visualized in 2D slices of the 3D MR images, minimum intensity projection (mIP) images were computed to visualize network structure of the edges. Figures 1 and 2 are mIP images computed from 8 and 24 contiguous 2D slices, respectively, of the 3D image data.

A computer program to measure geometrical quantities of the bubble polyhedra was developed on the X window system running on a workstation and eight bubble polyhedra were extracted interactively on the CRT screen using three series of mIP images of which projection directions were x, y, and z directions. Some of them are shown in Fig.3.

Summary of the results is:

1. Only 12-, 13- 14-, and 15-sided polyhedra were observed. The average number of faces per polyhedron was 13.63. 2. Only quadrilateral, pentagonal, and hexagonal faces were observed. The ratio of the numbers of them was 9 : 70 : 21. 3. The cell size was nearly uniform. 4. The average value of isometric quotient for polyhedra was improved to 0.723 by contraction of the polyhedra along one direction. 5. There is a positive correlation between the surface area and the number of sides of the faces. 6. Intersection angles at vertices distributed around the tetrahedral angle of 109.47°.

The results agreed well with the study with soap bubbles (3) but did not agree with the solution recently proposed (1). The reason for the discrepancy is not clear at present, however, more systematic study using the method developed here may clarify the difference.

REFERENCES

(1) J. Gray, Nature 367, 598-599 (1994).
(2) D. Weaire and R. Phelan, Phil. Mag. Lett. 69, 107 (1994).
(3) E. Matzke, Am. J. Botany 32, 58 (1946).

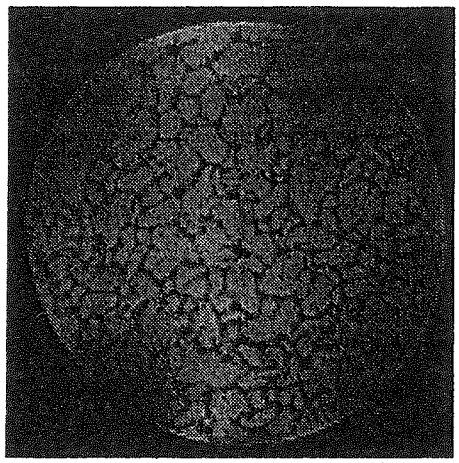

Fig.1 mIP image computed from 8 contiguous slices of the 3D image of the smaller cell-size foam

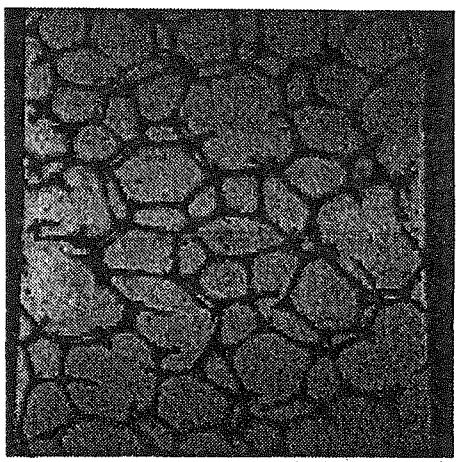

Fig.2 mIP image computed from 24 contiguous slices of the 3D image of the larger cell-size foam

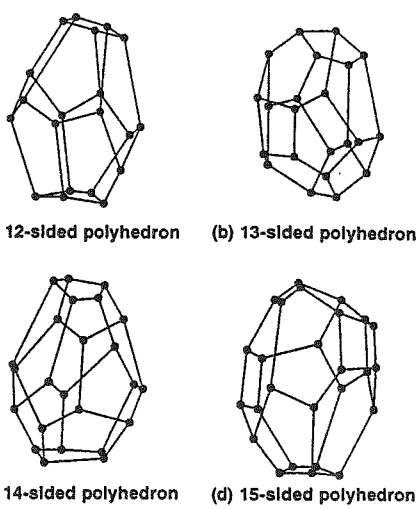

Fig.3 Foam polyhedra extracted from the 3D image data of the larger cell-size foam

A New Technique for Imaging Ultra-Short T_2 Solids

David J. Lurie, Stephen J. McCallum, James M.S. Hutchison and Marcello Alecci

Dept. of Bio-Medical Physics, University of Aberdeen, Foresterhill, Aberdeen AB9 2ZD, U.K.

INTRODUCTION: Several techniques for imaging solids have been developed in recent years, including multi-pulse line narrowing, magic angle spinning, oscillating gradient and STRAFI. While considerable progress has been made, most existing techniques suffer from restrictions, particularly in the size of sample which can be imaged, because of gradient strength and/or RF power limitations. In general, existing pulsed NMR techniques are limited to samples with T_2 values greater than about 10 μs[1].

In EPR, on the other hand, it is unusual to encounter samples with electron T_2 values *longer* than 1 μs. Most EPR spectroscopy and imaging is carried out using continuous-wave (CW) techniques in which the sample is bathed continuously with electromagnetic radiation and the applied magnetic field is swept past the resonances.

In this work we have combined modern CW detection technology with magnetic field gradients to demonstrate the feasibility of imaging ultra-short T_2 solids using swept-field NMR imaging.

METHODS: Experiments were carried out using an Oxford Instruments 7T magnet with a free bore of 125 mm inside the shim/gradient coils. The sample comprised two blocks of vulcanised rubber (1.5 × 3 × 2.5 cm and 1.5 × 3 × 4 cm) separated by 3.5 cm. It was placed inside a 300 MHz birdcage resonator (diam. 75 mm) around whose shield (diam. 120 mm) was wound a 20-turn split-solenoid used for magnetic field modulation. Field-sweep over a range of 1.76 mT was accomplished via the magnet's room temperature Z0 coil. The magnet's z-gradient coil was used to generate the required continuous gradient.

Detection of the NMR signal was achieved using a homodyne reflection bridge originally constructed by us for RF EPR spectroscopy[2]. It comprised a signal source (HP 8658B), 1W amplifier (Research Communications 9246), hybrid junction (Lorch Electronics JH-251E) and a diode detector. A lock-in amplifier (Stanford Research SR830) provided the audio signal to drive the field-modulation coil; the output of the diode detector was connected to the the lock-in, which detected the NMR absorption signal as a change in the reflected signal from the birdcage. On sweeping B_0, the resonance appeared at the lock-in's output as the first derivative of the lineshape. The sweep generator, RF source and lock-in amplifier were controlled via an IEEE 488 bus from a microcomputer (Acorn A5000), which also collected the data.

RESULTS: Fig. 1 shows spectra collected with different gradient values. As the gradient strength is increased, the separation of the two pieces of rubber is clearly evident. The spectrometer settings were: RF frequency 300.015 MHz, power 250 mW; field modulation frequency 881 Hz, amplitude 15 μT; sweep time 64 s; lock-in time constant 300 ms. Fig. 2 shows the spectrum of the empty resonator, arising from the Perspex former of the birdcage resonator, visible because B_1 was concentrated at the legs of the birdcage.

CONCLUSIONS: We have shown that it is possible to use swept-field CW NMR together with magnetic field gradients in order to image solids. The spectrometer was not optimised for the detection of the spectra shown here, so considerably better SNR is possible. The fact that Perspex was also detectable with good SNR suggests that it will be feasible to image samples with much shorter T_2s, possibly less than 1 μs.

Figure 1

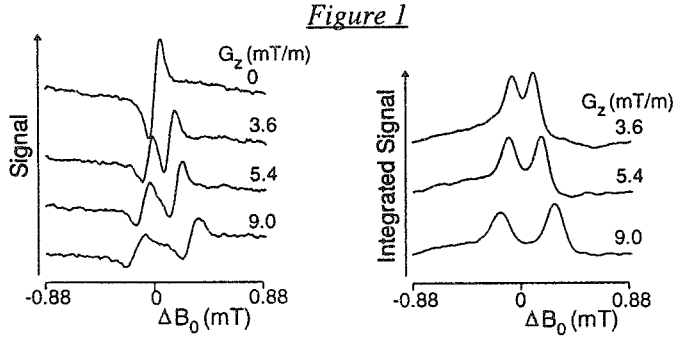

Figure 2

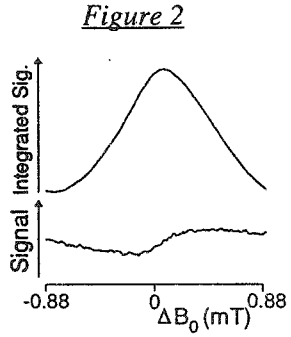

1. P. Jezzard, J.J. Attard, T.A. Carpenter and L.D. Hall Prog. NMR. Spectrosc. **23**, 1-41 (1991).
2. S.J. McCallum, M. Alecci and D.J. Lurie, SMR 3rd Annual Meeting, Nice, France (1995).

Non-invasive Observation of Flow Profiles, Polarisation Layers and Fouling in Membrane Filtration Modules using NMR Micro-imaging

S. Yao, A. G. Fane*, and J. M. Pope[#]

School of Physics and *UNESCO Centre for Membrane Science and Technology, The University of New South Wales, Sydney, N.S.W. 2052, Australia.

Nuclear magnetic resonance (NMR) micro-imaging techniques have been applied to the non-invasive study of flow and polarisation effects in hollow fibre and tubular membrane filtration modules. In multiple hollow fibre modules, flow distributions for both feedstock (shell side) and permeate (in the inner lumens of the hollow fibre membranes) have been mapped and the corresponding flow rates measured under different operating conditions. Measured flow velocities, when integrated over the cross section of the modules, yielded volume flow rates in good agreement with directly measured values, confirming the accuracy and reliability of the flow imaging methods employed. The results show evidence for 'channelling' of flow in regions of low membrane fibre packing density. Chemical shift selective imaging techniques have been used to visualise the development of oil 'polarisation layers' on the outer surfaces of the fibres during filtration of an oil/water emulsion. Formation of these concentration polarisation layers, which are sustained by the flux of permeate through the fibres, is reversible. They dissipate rapidly when the trans-membrane pressure gradient is removed. The results are consistent with previous, more invasive studies of gel polarisation phenomena in membrane filtration modules. They confirm that the hydraulic resistance of the oil layer is a major factor in controlling permeate flux.

A more detailed study of factors affecting the formation and build-up of oil polarisation layers during filtration of oil-water emulsions has been carried out using modules comprising a single tubular membrane (Enka polypropylene), with the feedstock supplied to the inner lumen. In this case it was possible to verify that, under steady state conditions, the thickness of the oil layer was determined by a dynamic equilibrium between the effects of the permeate flux and Brownian diffusion, which under our operating conditions was the main factor tending to remove oil droplets from the polarisation layer. Attempts to detect flow of the oil layers using chemical shift selective flow imaging indicated that within experimental error they were stationary. In the case of the tubular membranes it was also possible to observe the (irreversible) deposition of oil in the body of the membrane, which constituted the main fouling mechanism in this case.

[#] Current address: School of Physics, Queensland University of Technology, GPO Box 2434 Brisbane, Qld 4001, Australia.

Multinuclear NMR Imaging of Controlled Drug Release from Hydrophilic Matrix Tablets

C.A. Fyfe and A. Blazek
Department of Chemistry, University of British Columbia, 2036 Main Mall, Vancouver, B.C., Canada V6T 1Z1

Hydrophilic matrix tablets contain polymers that swell in water to form a gel layer which inhibits the immediate release of drug and provides a mechanism for its controlled release. NMR Imaging is an effective method for studying the swelling behavior of these matrices because it is a non-invasive technique that can provide both spatial and chemical information. The diffusion process of species entering or leaving the tablet can be monitored independently by imaging of different nuclei. Imaging of ^{1}H monitors the diffusion of water into the tablet and also diffusion of the hydrogel into the aqueous layer and, by choosing a substrate with a suitable nucleus such as ^{19}F, imaging can be used to study the diffusion of a model drug out of the tablet.

The tablet under study was prepared with 2-Hydroxypropylmethylcellulose (HPMC) and contained 5% w/w triflupromazine-HCl, a fluorinated tranquilizer. The tablet was flat-faced, 12.7 mm in diameter and about 1.2 mm thick. It was placed in a 15 mm NMR tube with its edges and one face sealed to limit diffusion and swelling to only one face of the tablet. Projections, i.e. one-dimensional images, of water and triflupromazine-HCl were acquired as the tablet swelled. These projections gave information about the rate of diffusion of water into the tablet and the rate of diffusion of drug into the bulk water. The variation of T_2 and T_1 with polymer concentration was quantified by preparing various mixtures of polymer, drug and distilled water and then measuring the T_1 and T_2 relaxation parameters of both ^{1}H (water) and ^{19}F (triflupromazine-HCl). All relaxation parameters were found to decrease as polymer concentration was increased.

For the drug, it was possible to obtain quantitative images that could be directly related to concentration. The direct imaging of the polymer was not trivial; thus its concentration was determined indirectly from its affect on the relaxation parameters of water and triflupromazine-HCl. As T_2 depended strongly on polymer concentration , T_2 weighting was used to determine quantitatively the distribution of HPMC during swelling. Projections for ^{1}H and ^{19}F were acquired with different times-to-echo (TE) at each acquisition time during the swelling process. From these projections, the T_2 relaxation time was calculated for various positions in the system and then converted to HPMC concentration using the experimentally determined relationship between T_2 and polymer concentration. From these experiments that diffusion characteristics of the polymer in the tablet can be studied and described quantitatively.

OXYGEN-17 NUCLEAR MAGNETIC RESONANCE SPECTROSCOPY AND IMAGING. DETERMINATION OF THE RATE OF CEREBRAL METABOLISM OF OXYGEN AND THE RATE OF CEREBRAL BLOOD FLOW IN THE HUMAN.

DANIEL FIAT
UNIVERSITY OF ILLINOIS AT CHICAGO
CHICAGO, ILLINOIS

The potential applications of ^{17}O magnetic resonance spectroscopy and imaging are protean. Determination of oxygen positions, concentrations, studying oxygen reaction paths and the thermodynamic and kinetic properties of chemical and biochemical reactions is essential for the understanding of some of the most important processes in nature.

We have used ^{17}O nuclear magnetic resonance to study and image phantoms and the human brain. The required modifications and accessories, and the required hardware and software for carrying out ^{17}O imaging of the human brain using a commercial clinical scanner will be described. The theory and methods used for the determination of the rate of cerebral metabolism of oxygen and the rate of cerebral blood flow in the human will be presented. The results will be analyzed in terms of signal to noise ratio, resolution and acquisition time. Methods based on acquisition of the echo will be compared with methods based on acquisition of the FID. ^{1}H and ^{17}O magnetic resonance imaging will be compared and the complimentary nature of information will be discussed.

The methodology has great potential for both physiological and pathophysiological studies in the man. This technology could significantly extend the already superb application of proton MRI for medical applications and improve our understanding of numerous disease processes including dementia, stroke, head trauma and epilepsy.

RECENT ADVANCES IN ^{17}O MRI AND MRS DETECTION LIMITS AND BIOMEDICAL APPLICATIONS

GD Mateescu and ME Cabrera
Department of Chemistry, Case Western Reserve University
Cleveland, Ohio 44106, USA

Since the reporting of the first ^{17}O images and localized spectra (1-3), significant progress has been recorded in applications on invertebrates and vertebrates. Water diffusion in gels and time release preparations was also reported (4). Of particular importance are the experiments leading to the determination, *in vivo*, of the rate of oxygen consumption (5-9). These investigations reached a new dimension with the introduction of interleave $^{17}O/^{31}P$ measurements which are yielding valuable information on the degree of uncoupling of the oxidative phosphorylation (OXPHOS) by various physical and chemical agents (10). The significance of such information derives from the fact that, recently, degenerative diseases (Alzheimer, Parkinson, ischemic heart, late onset diabetes, etc) are associated to OXPHOS perturbations induced by genetic mitochondrial and nuclear DNA mutations. We will report on the performance of a custom built double tuned $^{17}O/^{31}P$ probe for automatic interleave measurements designed to determine the rate of formation of *nascent mitochondrial water* and the corresponding time evolution of phosphate metabolites. We will also report the first direct observation of effects of temperature changes on the metabolic rate of larvae of *Tenebrio molitor*. Preliminary results indicate that there is a threefold increase in the rate of oxygen consumption at 30°C vs 20°C. This increase is 50% higher than that found, by extrapolation, in adult humans over the same temperature range. The advantage of ^{17}O MRS is that, unlike direct and indirect calorimetry, it can be applied in selected volumes of interest.

References

1. Mateescu GD, Butenhof KJ, Benedikt GM, Brescic I, High Resolution O-17 NMR and the Chemistry of Water Monomers, 9th ISMAR Meeting, Rio de Janeiro, June, 1986.
2. Mateescu GD, Yvars GM and Dular T, Oxygen-17 MRI, SMRM **6**, 929, 1987.
3. Mateescu GD, Yvars GM and Dular T, Water, Ions and ^{17}O MRI. In: Water and Ions in Biological Systems, Lauger, Packer and Vasilescu, Eds. Birkhauser: Basel-Boston, 1988, pp. 239-250.
4. Mateescu GD, Kinsey RA, Yvars GM, Oxygen-17 and Proton MR Microscopy in Materials Analysis, Mat. Res. Soc. Symp. Proc., Vol. **217**, 61-66, 1991.
5. Mateescu GD, Yvars GM,. Pazara DI, Alldridge NA., LaManna JC, Lust DW, Mattingly M and Kuhn W, ^{17}O-^{1}H MRI in Plants, Animals, and Materials. In: Synthesis and Applications of Isotopically Labelled Compounds, Baillie & Jones, Eds. Elsevier, Amsterdam, 1989, pp. 499-508.
6. Mateescu GD, From Materials Testing to Brain Function Testing, Spectroscopy International **3**, 14, 1991; Spectroscopy **6**, 18, 1991.
7. Mateescu GD, LaManna JC, Lust WD, Mars L and Tseng J, ^{17}O-MR: *In Vivo* Determination of Nascent Mitochondrial Water in Animals Breathing ^{17}O-enriched Air, SMRM **10**, 1031, 1991.
8. Pekar J, Ligeti L, Lyon R, Ruttner Z, Gelderen vP, Moonen C, Fiat D, McLaughlin AC, *In vivo* Mapping of Oxygen Consumption in the Cat Brain Using ^{17}O-MRI, SMRM **10**, 302, 1991.
9. Fiat D, Dolinsek J, Hankiewicz J, Dujovny M, Ausman J, Determination of RCMRO2 and RCBF by Noninvasive O-17 In Vivo NMR and MRI, Neurol. Res., 15, 237-248, 1993.
10. Mateescu GD and Fercu D, Interleave ^{17}O-^{31}P MRS: Novel Approach for *In Vivo* Determination of Defects in Oxidative Phosphorylation, Proc. Soc. Magn. Reson. Med. **12**, 110, 1993.

Enhanced Spin Lattice Relaxation and Polymer Formation with Immobilized Paramagnetics

Bruce J. Balcom, Maria L. Kilfoil, Allan R. Sharp, Department of Physics, The University of New Brunswick, P. O. Box 4400, Fredericton, N.B., Canada, E3B 5A3.

We have been studying acrylic polymerization resulting from light and X-ray exposure. Water based acrylic polymers initiated by either method yield pronounced changes in T_2 which may be observed by conventional T_2 weighted spin echo imaging (1,2). The spin lattice relaxation times are long (typically greater than one second) and do not change significantly in either case. This hinders a quantitative determination of the extent of polymer formation and makes traditional 3D imaging very time consuming. We have sought, and report here the discovery of a T_1 based method of observing polymer formation.

It is well known that increasing the rotational correlation time of paramagnetic contrast agents by attaching them to slowly tumbling macromolecules will significantly enhance their relaxivity (3). We have chemically attached the paramagnetic metals gadolinium, cobalt, and nickel to individual acrylic monomers. Formation of the acrylic polymer dramatically alters the rotational correlation time of acrylic monomers in the polymer network. By extension, paramagnetic metals in the labelled acrylic monomers will also increase their rotational correlation times upon polymer formation. Experimentally, with conventional chemical polymerization, we observe dramatic decreases in spin lattice relaxation times with polymers incorporating paramagnetic metals. The change in T_1 upon polymer formation depends on the paramagnetic employed, the extent of polymer cross linking and the concentration of polymer in solution. The T_1 change also depends on the strength of the polarizing B_0 field.

Similar changes in T_1 are observed when polymerization is initiated by UV/Vis light or X-ray radiation. The change in T_1 depends on the nature of the polymer and the paramagnetic employed, however, the initial T_1 may be manipulated over a large range by adjusting the concentration of labelled paramagnetic in the system. The use of these labelled paramagnetics in rapid 3D imaging of polymer formation will be discussed.

References:

(1) B. J. Balcom, T. J. Lees, Abstracts of the 36th ENC Conference, Boston, March 26-30, 1995.
(2) M. J. Maryanski et. al. *Mag. Res. Imag.* **11**, 253, (1993).
(3) R. B. Lauffer *Chem. Rev.* **87**, 901, (1987).

CONTRAST AGENTS
Fundamentals

Robert N. Muller
Department of Organic chemistry
and N.M.R. Laboratory
University of Mons -Hainaut - B-7000 Mons Belgium

In spite of the very large, although sometimes skill-demanding and time-consuming, flexibility of its *natural* contrast, MRI takes more and more advantage of the use of exogenous contrast media.
The design, the synthesis and the characterisation of such compounds - also called *magnetopharmaceuticals* - are highly sophisticated and require synergistic efforts of chemists, physicists, physicians and other specialists of life sciences.
Paramagnetic and superparamagnetic systems have attracted the interest of researchers because of their "catalytic" action on the relaxation of water protons.
In this respect, manganese and gadolinium ions exhibit attractive properties like large numbers of unpaired electrons : 5 for manganese and 7 for gadolinium as well as relatively long electronic relaxation times. They have thus been selected as the best catalytic centers for hydrogen relaxation in aqueous media : at a concentration of 1 millimole per liter they can induce a tenfold increase of the natural relaxation rate of water. Unfortunately these ions are toxic and, as such, cannot be used in vivo. The molecular complexes made of the active center, for instance a gadolinium ion, locked into an organic molecule is by far less toxic than the free ion or even the free organic ligand. Because of their reduced accessibility to water molecules these compounds show however a lower relaxivity than the bare paramagnetic ions. Nevertheless, the loss of relaxivity is not dramatic since a local concentration in the millimolar range is still more than enough to halve the relaxation time of the water in tissues. The stability of these supramolecular complexes is extremely high since only one molecule over about 1 billion is dissociated in aqueous solution.
Four compounds belonging to the class of *non-specific* injectable relaxation agents are currently available, their safety indexes are more than ten times higher than those of iodinated X-ray compounds. Among these MRI contrast media, two are called *non-ionic* since the paramagnetic complex has no net charge to be counterbalanced at the expense of an increase of viscosity and osmolarity.
The MRI contrast media of this first generation belong to the family of the non-specific agents. This means that, owing to their small size and their hydrophilic character, they freely diffuse to the interstitial space and as such are markers of the extravascular and extracellular domains.
The aims of the current research to shape the carrier of the magnetically active cores in order to achieve the proper pharmacokinetics and biodistributions while maintaining high efficiency and low toxicity.

DEDICATED MR SCANNERS

F. Bertora, E. Biglieri, A. Trequattrini
ESAOTE
via Siffredi 58
16153 GENOVA, Italy

Abstract:

Magnetic Resonance Imaging technology has always been associated with all-purpose, total body scanners, as it has been the case of early X-ray devices, due, at first, to the necessity of exactly defining the corporeal districts to which the technique was better suited for, and also due to the fact that available magnet technology lent itself more easily to the construction of large scale, simple magnets rather than small targeted units.

After the initial pioneering years the radiological community clearly defined the scope of eligibility of MRI procedures to almost coincide with the neurological and musculoskeletal districts, with an overwhelming predominance of the first, although a closer analysis shows that the actual needs, in terms of epidemiological data, should have not been so vastly different. This fact established the desirability of MR Imaging devices better suited to the specific needs of the individual districts.

The major obstacle toward such a goal has however been magnet technology. Magnet design had not yet advanced enough to allow the cost effective realization of the small scale, efficient magnets which would have been needed for dedicated applications.

The advent of the linear theory of permanent magnets represented the necessary breakthrough, allowing the design of the necessary devices.

Permanent magnet materials, as available today in the form of hard ferrites or of Rare Earth alloys, are remarkable materials, closely approaching the postulates on which the linear theory stands and can be exploited in may innovative ways to achieve results not else obtainable.

A brief review of the linear theory of permanent magnets conduces to a classification of the possible configurations in yokeless, yoked or hybrid designs, with further ramifications in one, two or three-dimensional structures.

Yokeless designs are the most elegant and intriguing, yielding structures which confine the field inside without making use of any high permeability material. They were among the first being investigated and can be utterly non conventional: in fact the first known example was immediately dubbed the "magic" ring.

Yoked structures are much more conventional in comparison but exhibit the unquestionable advantage of being potentially more efficient, in terms of use of the energy stored in the material.

The final category, that of hybrid structures, combines many of the merits of both and, although presenting the most delicate problems in manufacturing, could represent the optimal answer in many applications.

The above concepts have already found a practical applications in a commercial unit aimed at joint scanning and could be extended in the near future to other corporeal districts or to novel uses of MRI technology, like mammography or interventional imaging.

Medical NMR Imaging in Open Magnets

Richard Hausmann Ph.D.
Siemens Medical Engineering Group, Erlangen, Germany

Introduction:

In the last few years, new open magnet designs were introduced into the MR Imaging equipment market. Basically three different design criteria have been followed: Open multipurpose MR scanner like the MAGNETOM Open or the Picker Outlook, dedicated scanners for orthopedic applications only like the Esaote system and dedicated open MR scanner for interventional and intraoperative use like the GE MRT unit. In this paper I will focus on multipurpose open MR scanner and show the design and technical aspects, image quality and application possibilities of these new generation of scanners.

Technical considerations:

Open MR scanners are up to now limited to low field strength (typically < 0.3 Tesla).
The first really open MR scanner introduced is the MAGNETOM Open (Siemens Medical Engineering Group, Erlangen), as an example for a new generation of electromagnets. Special considerations were made for the gradient coil and the specific details of the stability and sensitivity of the magnet to external magnetic fields. These aspects will be described in detail.

Application aspects:

Although the MAGNETOM Open is a multipurpose scanner, which allows with different surface coils all anatomic regions of the body to be scanned, it is especially well suited for claustrophobic patients and children. This is simply due its extremely open design and the low noise gradient coil. It will be shown that image quality of this low field MR scanners is very competitive and diagnostically absolutely relevant. Using a two dimensional patient table allows isocenter scanning for all regions of the body. This makes orthopedic applications like shoulders, hips and elbows very easy even in extreme positions. The full access to the patient is also used for first attempts toward interventional techniques inside the MR unit.

Conclusion:

Open multipurpose MR scanner like the MAGNETOM Open allow easy patient handling, access and good image quality. New applications like kinematic motion studies and interventional MR can broaden the clinical use of MR as a modality far beyond pure diagnostic applications.

Interventional MR Imaging

Derek Shaw B.Sc. Ph.D.
GE Medical Systems Europe
Slough UK

In recent years the practice of medicine in nearly all countries has come under considerable financial pressure. One approach to reducing cost, and also improving patient comfort, has been to move towards minimally invasive surgery techniques. MRI has been a significant modality in diagnostic imaging since the late 80's, where it's excellent soft tissue differentiation has been especially useful, but to date it's potential to help in minimal invasive surgical procedures has not been extensively explored.

The major problems when considering MRI as a guidance technique for a surgical procedure are essentially poor patient access, slow/inappropriate imaging sequences and display hardware; plus the lack of MR compatible surgical tools.

The most demanding of the above limitations is patient access. This limitation has been reduced in the last few years by the availability of diagnostic systems which are more "open" in design, but this is only a partial solution. A 0.5T superconducting magnet specifically designed for interventional MRI has recently become available. The magnet uses new superconducting materials which, due to their higher transition temperature, do not need liquid helium to maintain their superconductivity (mechanical cooling is adequate). Removing the constraint of having to have a cryogen in the magnet enables radically new design approaches to be considered. For interventional MRI the concept which has been realized is to design a magnet which consists of 2 vertical "doughnuts" with 60cm holes standing 59cm apart. The gradients are contained within the magnet bore providing a large central volume free of any access limitations. Patient access is thus easily achieved with the physician standing between the "doughnuts". The patient either laying in a "conventional" position i.e. in the holes of the "doughnut" or head on to the physician.

In addition to the specificaly designed magnet the system, now being used in Brigham and Women's Hospital in Boston, has a 3D frameless stereotactic system which enables the surgical tools, e.g. a biopsy gun, to define the imaging plane. This, coupled with fast imaging techniques and image displays within the magnet, provide the physician with a unique environment in which to apply MRI as a guidance technique for minimally invasive therapy. Work is also proceeding to develop a range of patient support equipment and surgical tools which are compatible with the MR environment.

Results from this system will be presented which demonstrate the current state of the art when applying MRI to interventional surgical procedures.

IN VIVO CARBON-13 NMR SPECTROSCOPYY

Joachim Seelig, Biocenter of the University of Basel, Klingelbergstrasse 70, CH-4056 Basel, Switzerland

^{13}C NMR of selectively labeled substrates is similar to the classical ^{14}C radioactive isotope experiment. However, ^{13}C MR offers certain advantages. First, the kinetics of ^{13}C labeling of individual carbons from a variety of metabolites can be followed simultaneously and noninvasively. Secondly, the ^{13}C MR approach avoids chromatographic separations and chemical degradations. Finally, multiple ^{13}C labeling leads to ^{13}C-^{13}C homonuclear splittings, providing unique structural information on the integrity of the molecules involved [1]. The potential of ^{13}C MR will be demonstrated for the metabolism of

- multilabeled acetate and glucose in rat liver and rat brain [2,3]
- glucose metabolism in human brain and liver[4,5]

In particular, we have investigated the NMR visibility and quantitation of glucose in the human brain. Proton-decoupled ^{13}C-NMR spectra of the human head were obtained during hyperglycemic glucose clamping using intravenous infusions of [1-^{13}C]glucose in normal volunteers. At an enrichment level of 20%[1-^{13}C]glucose, the signals of α- and β-glucose could be detected in the human brain after an infusion period of 15 min. Increasing the enrichment level to 99 % [1-^{13}C]glucose improved the time resolution and allowed the detection of metabolic breakdown products of [1-^{13}C]glucose. The time course of ^{13}C label incorporation into the C2- C3- and C4- resonances of glutamate/glutamine and into lactate could be recorded in the human brain. Recently similar studies were performed on the human liver under two different conditions: i) intravenous infusion of [1-^{13}C]glucose, and (ii) oral intake of glucose in the form of a bolus. Comparison of the relative increase in the glycogen concentration demonstrated that oral intake led to a distinctly larger accumulation of glycogen in the liver than intravenous infusion.

[1] Cerdan, S., and Seelig, J. (1990) Ann. Rev. Biophys. Chem. 19, 43-67;

[2] Cerdan, S., Künnecke, B., and Seelig, J. (1990) J. Biol. Chem. 265, 12916-12926;

[3] Künnecke, B.,Cerdan, S., and Seelig, J.(1993) NMR Biomed. 6, 264-277

[4] Beckmann, N., Seelig, J., and Wick, H. (1990) Magn. Res. Med. 16, 150-160

[5] Beckmann, N., Turkalij, I., Seelig, J., and Keller, U.(1992) Biochemistry 30, 6362

Three-Dimensional Measurements of Lung Properties during the Breathing Cycle

M.D. Shattuck[1], S.L. Gewalt[1], G.H. Glover[2], L.W. Hedlund[1], G.A. Johnson[1]

[1]Center for *In Vivo* Microscopy, Duke University, Durham, NC 27710
[2]Richard M. Lucas Center for MRI, Stanford University, Stanford, CA 94305

A number of studies have demonstrated changes in T1, T2, and T2* in pathologic lung. The majority of these studies have focused on measurements at some "average" point in the breathing cycle. Recent efforts suggest that the MR properties of the lung may, in fact, change as a function of the degree of lung inflation [1]. We report here techniques and early results in measurement of T2* in the live guinea pig at multiple points of the breathing cycle.

We have improved upon our earlier projection technique [2] with a high speed (non-gated) sequence that uses the averaging inherent in projection encoding to limit artifacts from cardiac motion. We have enhanced this effect by shuffling the view order so that the effects of coherent motion are scattered throughout k-space. As a result, artifacts from cardiac motion and breathing are significantly reduced. We have compared scans taken *in vivo* and just after death to show the effects of cardiac motion and breathing.

The temporal averaging of radial acquisition allows measurements in the lung at various tidal volumes by maintaining the lung volume at a specific level for a large percentage of the scan. In Protocol 1, we examined the lungs of guinea pigs at end-expiratory volume using a 150 ms inspiration pulse every 1500 ms, leaving the lung at end expiration 90% of the time. The remaining 10% of the views are spread azimuthally throughout k-space so that their altered breathing state is effectively averaged away. In Protocol 2, the lung is expanded for 80% of the time. In this protocol, a specific pressure is applied to the lung for 100 ms, which is then maintained for 1100 ms and finally released. This sequence is then repeated every 1500 ms. This protocol is realized using a two-valve system—one valve controls inspiration, and the other controls expiration. The lung can be expanded to any tidal volume by a using different pressure or timing during the inspiration pulse.

For each lung volume, data were acquired at delay periods ranging from 200 μsec to 3200 μsec after the excitation pulse. Each scan produces a 128 x 128 x 128 volume with a field of view of 60 mm x 60 mm x 120 mm from 50640 radial views using a 10 ms repetition time. A 2D ventilation-synchronized sequence with and without cardiac gating has also been developed to compare the effects of the limited breathing and cardiac motion in the 3D sequence. T2* in the small animal lung range from 1–5 μsec.

1. C. J. Bergin, G. H. Glover, J. M. Pauly, Lung parenchyma: magnetic susceptibility in MR imaging. *Radiology* **180**, 845-848 (1991).

2. S. L. Gewalt, G. H. Glover, J. R. MacFall, L. W. Hedlund, G. A. Johnson, MR microscopy of the rat lung using projection reconstruction. *Magn Reson Med* **29**, 99-106 (1993).

Acknowledgments: This work is supported in part by NIH grant #P41 RR05959 and Schering-Plough Research Institute.

Direct MR Imaging of the Guinea Pig Airways using Hyperpolarized ^{3}He

LW Hedlund[1], RD Black[1], GD Cates[2], GP Cofer[1], R Guenther[3],
W Happer[2], GA Johnson[1], H Middleton[2], MD Shattuck[1], & J Swartz[3]

[1]Center for *In Vivo* Microscopy, Department of Radiology, Duke University, Durham, NC 27710
[2]Department of Physics, Princeton University, Princeton, NJ 08544
[3]Department of Physics, Duke University, Durham, NC 27708

Conventional proton imaging provides only indirect visualization of the gas spaces of the lung; it's based entirely on contrast between the signal deficient airways and adjacent signal rich water containing structures. We recently reported the first hyperpolarized helium (^{3}He) images of the lung airways [1]—a method for directly imaging airways. These first images were from a dead guinea pig. Here we report extension of ^{3}He imaging technique to the live animal.

The details of the laser polarization have been previously reported [1]. The current system uses a higher power (20 W) diode laser allowing polarization of 200 cc of gas to 30% in ~ 8 hrs. Gas is transferred from the polarization cell to the animal using a two-valve modification of a ventilator designed for MR microscopy of small animals [2]. One valve controls delivery of gas to the trachea and a second valve allows switching between two gas sources—breathing air-isoflurane and ^{3}He. Helium is delivered using normal breathing gas pressures and tidal volumes (3 to 6 cc/breath) and frequency (40–45 breaths/min).

Projection encoding (3D) was performed on 2.0 T system with a GE Signa 5.X console, shielded gradients (18 gauss/cm) and a 8 cm birdcage resonator adjustable to proton and He resonances. A series of rf pulses with TR of 3 ms follows each ventilator controlled breath of helium. Over-sampling of the center of k-space by radial trajectories averages out cardiac motion. Breaths of air-isoflurane alternate with the helium to keep physiological stability and anesthesia. Available gradients allow capture of the first point in the FID at 600 μsec and up to 400 views per breath. The view order can be either serial with increasing view angle or randomized to spread the view variations throughout k-space.

^{3}He images of lungs in live guinea pigs were acquired in less than 10 seconds. Signal was detected in all lung lobes. Pulmonary regions deficient of signal corresponded to major blood vessels, and thoracic regions without signal corresponded to chest wall, heart, and other mediastinal structures based on registered proton images from the same animal. Early indications suggest that hyperpolarized ^{3}He coupled with novel new imaging strategies will provide an effective method for overcoming the previous limitations in MR microscopy of the lung especially for imaging the air (gas) spaces.

1. Middleton, H, et al., MR imaging with hyperpolarized He-3 gas. *Magnetic Resonance in Medicine*, 1995. 33: p. 271-275.
2. Johnson, GA, et al., Histology by magnetic resonance microscopy. *Magnetic Resonance Quarterly*, 1993. 9(1): p. 1-30.

Acknowledgments: This work was supported by NIH (NCRR grant P41 05959)
AFOSR grant F49629, ARPA grant DAMD17 94 J 4469, ARO grant DAAH04-94-0204
and the Schering-Plough Research Institute.

Heteronuclear Spectroscopy and Imaging

O. Lutz, M. Pfeffer, Th. Kull, A. Zutt, M. Bunse, W.-J. Jung

Physikalisches Institut der Universität Tübingen und Forschergruppe Hypertonie und Diabetes, Max Grundig Klinik, Bühl

The stability and homogeneity of imagers are good enough to perform NMR experiments, e.g., at 1.5 T with whole body units using heteronuclei. With home made probes and large samples (500 ml) very weak NMR signals can be detected within reasonable measuring times.

Nuclei like ^{11}B, ^{13}C, ^{23}Na, ^{27}Al, ^{51}V, ^{81}Br and ^{129}Xe have been studied. Typical examples will be presented: e.g. ^{51}V in 1 micromolal aqueous solution, short longitudinal relaxation times of ^{81}Br at very low concentration, ^{11}B images of aqueous solutions and spectra of wine, and also noninvasive ^{13}C spectra of natural products. In gaseous xenon at atmospheric pressure, without and with added oxygen, relaxation times have been measured. T_1 of ^{129}Xe in pure xenon gas is very long: 13 200 s. Adding 0_2, a strong reduction is observed, allowing for ^{129}Xe gas imaging. By inverting xenon magnetization in a slice, the diffusion of ^{129}Xe in gas could be observed and the diffusion constant has been measured.

Adresse: Prof. Dr. O. Lutz
Physikalisches Institut
Morgenstelle 14
D-72076 Tübingen

Radial Spectroscopic Imaging

M. Meininger, P. M. Jakob, M. v. Kienlin, A. Haase,
Physikalisches Institut, Universität Würzburg, 97074 Würzburg, Germany

Spectroscopic imaging is most interesting for investigating the metabolism of biological systems, but suffers from its long acquisition time. By exploiting a given circular symmetry of the object, the number of spatial acquisition dimensions can be reduced by one, thus reducing the minimum acquisition time of spectroscopic imaging experiments dramatically. A new spectroscopic imaging technique is presented, combining one- or two-dimensional spectroscopic experiments with the previously described Radial Imaging. In the following we will call this Radial 1D-Spectroscopic Imaging and Radial 2D-Spectroscopic Imaging. As one application of our method we obtained metabolic maps of the plant *Ancistrocladus heyneanus.*

Radial resolved information of circular objects is obtained by inverse Abel transform of *one-dimensional spatial projections.* This results in pixels having the shape of concentric rings with uniform radial resolution. We combine conventional spectroscopic experiments with phase encoding in *one* spatial dimension. After spatial Fourier transform we get the desired projections for each spectroscopic point which can then be reconstructed, employing inverse Abel transform, to obtain Radial Spectroscopic Images.

The experiments were performed on a BRUKER Biospec 70/20 (7.0T) spectrometer. We used a spin-echo pulse sequence with additional CHESS water suppression for conventional and Radial 1D-Spectroscopic Imaging. Datasets had typically 512 spectroscopic points and 32 points per spatial direction. Radial 2D-Spectroscopic Images employed a COSY pulse sequence with pulsed field gradients and additional CHESS water suppression. Radial 2D-Spectroscopic Image datasets had 64 points in f1, 256 or 512 points in f2 and 32 spatial points. With a typical FOV of 10mm we obtained a spatial resolution of 500μm. For testing our method we used a phantom consisting of two concentric glass tubes, one filled with water, one with a 500mmol sucrose solution. As a suitable plant system for application we used *Ancistrocladus heyneanus*, a dicotyl indian liana plant. The condition of circular symmetry is well satisfied in the stem of this plant.

Conventional and Radial Spectroscopic Images of the phantom were compared, proving the ability of this method to measure the distribution of chemical compounds in cylindrical objects. The acquisition time could be reduced from 32 minutes for a 32x32 1D-Spectroscopic Image to 1 minutes for a Radial 1D-Spectroscopic Image (NA=2) with aquivalent radial resolution and comparable SNR due to the larger pixel sizes. The metabolic maps obtained with the radial technique correlate to those obtained by conventional spectroscopic imaging. Radial 2D-Spectroscopic Images of the phantom with a resolution of 512x64 spectroscopic and 32 spatial points were acquired in 25 min (NA=1). The radial resolved COSY spectra of *Ancistrocladus heyneanus* show the distribution of several spectral components in the plant. We now try to correlate this information to high resolution NMR spectra obtained from extracts of plant tissue in order to get information about the spatial distribution of specific alkaloids which are produced by *Ancistrocladus heyneanus.*

Our results demonstrate the feasibility of Radial Spectroscopic Imaging using one-dimensional projections. The time saving compared to conventional spectroscopic imaging is enormous. This technique will allow to reveal quantitative and dynamic metabolic information on cylindrical biological objects like dicotyl plants.

THE ROLE OF NMR IMAGING IN PHARMACEUTICAL RESEARCH AND DEVELOPMENT

Susanta K. Sarkar*, Sudeep Chandra and Rasesh D. Kapadia

SmithKline Beecham Pharmaceuticals
King of Prussia, PA 19406, USA

Abstract

Magnetic resonance imaging (MRI) is now an established technique in clinical medicine. Because of its non-invasive nature, MRI has significant applications to pharmaceutical research. The parallel between the requirement of pharmaceutical R&D and the suitability of MRI will be discussed. The utility of MRI and MR microscopy in developing novel therapeutics for diseases like Stroke, Renal Failure, Arthritis and Osteoporosis will be illustrated.

^{1}H-NMR Microscopy at 7 T: 3D Visualization of Tumor Metastases in Mouse Organs ex vivo; Detection of Metastases and their Eradication by Immunotherapy in vivo.

Klaus-Peter Fichtner[1], William E. Hull[1], Andreas Griesbach[2], Volker Schirrmacher[2]
Central Spectroscopy Dept. [1] and Dept. of Cellular Immunology[2], German Cancer Research Center
Im Neuenheimer Feld 280, D-69120 Heidelberg, FRG

Introduction: Adoptive immunotherapy (ADI) is a novel strategy for cancer treatment for which a highly effective mouse model has been developed over the last ten years. The murine ESb-MP lymphoma cell line of the DBA/2 mouse [1] inoculated intradermally in the flank of female DBA/2 mice results in a localized primary tumor, followed by focal metastases in liver, kidney, and other organs (fatal within ca. 35 days). ADI therapy between Days 21 and 25 (5 Gy irradiation followed by systemic injection of 3×10^7 immune spleen cells taken from allogeneic B10.D2 mice which develop immunity to ESb-MP) results in complete remission of primary tumor and metastases in DBA/2 mice. We have investigated the possibilities for using ^{1}H-NMR micro-imaging to monitor noninvasively tumor growth, the development of metastases and the results of ADI therapy in individual mice. Furthermore, we are using 3D ^{1}H-NMR microscopy as a pathology tool to examine metastases in internal organs ex vivo in formaldehyde fixative at resolutions $\leq$ 50 µm.

Methods: All imaging experiments were performed on a Bruker AM-300 super-wide-bore spectrometer: 7.0-T, 15-cm vertical magnet, Aspect 3000, standard micro-imaging hardware with a wide-bore microscopy probehead and actively shielded gradient system. **3D micro-imaging:** tumor-bearing DBA/2 mice were sacrificed between Days 24 and 35 and organs were excised and preserved in 10% formaldehyde/PBS. In some cases organs were given an arterial flush with fixative in order to determine (and minimize) the effect of blood on relaxation parameters (e.g. T_2^* effects) and resolution. Two rf inserts (slotted-tube resonator, ∅ = 15-mm, Z-axis length h_z = 23 mm, 90° hard pulse $PW_{90°}$ = 24 µs (100 V_{pp}); and a 4-turn Helmholtz coil, ∅ = 10-mm, h_z = 18 mm, $PW_{90°}$ = 11.4 µs) were tested. Measurements were made at 30°C, and detailed image analysis was performed with an Aspect X32 workstation using UXNMR. Mouse kidneys (ca. 10 mm long) were placed upright in the upper conical portion of a Pasteur pipette which was placed in an 8-mm or 10-mm NMR tube containing the formaldehyde fixative. Liver lobes were examined in 12-mm or 15-mm sample tubes. The desired angular orientation of the sample relative to the ZX-plane was precisely adjusted by rotating the upper bore tube and the attached spinner turbine holding the sample. Spin-echo (SE) imaging sequences were used with various *TR* (0.25 - 2.0 s) and *TE* (8 - 30 ms, single echo), and the FOVs in both the read and phase-encoding dimensions were optimized (zoomed) using various combinations of slice-selective presaturation pulses to minimize signal from the solution outside the FOV. Typical 3D data matrices for ZXY images with 256×256×32 voxels (41×41×250 µm in the kidney) or 128^3 voxels (without zero-filling) were acquired in ca. 8 h. **In vivo imaging:** ^{1}H-resonator: ∅ = 27 mm, h_z = 36 mm, $PW_{90°}$ = 60 µs. **Anesthesia:** 80 -120 µl *i.p.* injection of 4% chloralhydrate/ 0.4% Rompun in PBS (for max. 2 - 3 h) or inhalation of N_2O + O_2 (0.6 + 0.2 ml/min) plus 1.0-1.8% isoflurane (for 3 - 4 h). **Respiratory gating:** an adaptation of the fiber optic sensor designed by Doddrell *et al.* [2] was used with a Bruker Physiogard 785. The mice were positioned head-up in a home-built holder (ca. 24-mm diam.) made from a plastic centrifuge tube. The temperature within the resonator was maintained at 30-35°C with the spectrometer's variable temperature controller. Four coronal (ZX) and 8 transversal (XY) slices (1-mm) were acquired with a multislice spin-echo (SE) sequence using fat presaturation. T_2 -weighting was obtained by varying *TE*.

Results & Discussion: **Isolated kidneys.** Spin-density (ρ) images had little morphological contrast; metastases with diam. > 50 µm were best discriminated as hyperintense lesions in the cortex in T_1-weighted images (*TR* = 400 ms). Details of kidney morphology were best visualized with T_2 weighting, particularly when organs were *not* flushed before fixation. Average ROI relaxation times: metastases T_1 = ca. 1.2 s, T_2 = 17-18 ms; cortex T_1 = ca. 1.8 s (flushed) and ca. 1.7 s (not flushed), T_2 = 18 ms. Diffusion weighting did not improve the detection of metastases. **Isolated liver.** Small metastases and the rim of large metastases exhibited increased ρ, T_1, and T_2 (T_1/T_2 = 550/16 ms) relative to normal liver tissue (T_1/T_2 = 470/13 ms); the necrotic center in large metastases had even larger ρ, T_1, and T_2 . **In vivo studies.** With the aid of coronal and transverse views, comparable slices were obtained for different animals on different days (2 - 3 day intervals). On Days 22-24 (within the therapy window), focal metastases (0.8 - 1.5 mm diam.) could be observed as hyperintense bright foci in the liver and kidney cortex in T_2-weighted images (*TE* = 30 ms). On Days 28 - 30 days untreated animals exhibited numerous metastases (1-3 mm diam.) in liver and kidney and in some cases a focal metastasis in the spleen. We were able to demonstrate noninvasively for individual mice that successful ADI treatment applied as late as Day 28 led to remission of primary tumor and complete eradication of macroscopic metastases that were visualized on Days 22 - 24 and were absent ca. 3 weeks later. Detailed studies concerning the time course of metastasis and therapy optimization are now possible.

[1] Schirrmacher, V.; *et al.*, *Int. J. Oncol.* 6:505-521 (1995).
[2] Doddrell, D.M.; *et al.*, *Magn. Reson. Imag.* 32:1027-1032 (1993).

QUANTITATIVE NMR MICROSCOPY ON MULTICELLULAR TUMOR SPHEROIDS AND CONFRONTATION CULTURES

M. Brandl, J.C. Tonn*, K. Kotitschke, R. Goldbrunner*, S. Kerkau*, and A. Haase
Physikalisches Institut, Universität Würzburg, Am Hubland, 97074 Würzburg, Germany
*Neurochirurgische Klinik, Universität Würzburg, Josef-Schneider Str. 11, 97080 Würzburg, Germany

INTRODUCTION

In basic cancer research, tumor spheroids are by now a well established method to study tumor metabolism. As a model it mimics physiological tumor metabolism closer than cell monolayers (1). We have investigated tumor spheroids of high viability essential for cancer research. Quantitative, highly resolved relaxation (T_1 and T_2) and diffusion parameter images are obtained. Furthermore, we followed the invasion process of tumor cells into rat brain aggregates by NMR microscopy. The NMR results are correlated to histological observations.

MATERIALS AND METHODS

Malignant melanoma cells from the MV3 cell line were cultured as spheroids employing the standard liquid overlay technique (1). After 7-14 days spheroids with diameter of 400 μm to 1000 μm, providing high viability, were selected for NMR microscopy experiments. For confrontation cultures the multicellular MV3 spheroids were co-cultured with fetal rat brain aggregates.

The spheroids were immobillized with 1% PBS agar and transferred into capillaries of 1 mm inner diameter. Quantitative imaging was performed with a BRUKER AMX-500 widebore system working at 11.75 T field strength (89 mm inner diameter). We used a homebuilt microimaging probehead including gradientsystem (G_{max} = 1.6 T/m) and 2 mm solenoid coil. Quantitative relaxation times (T_1,T_2) and diffusion parameter images were acquired within 3 hours using Magnetization Preparation (2) in combination with asymmetrical echo sampling (3). The maximal inplane resolution was 14x14 μm^2 and the slice thickness varied between 100 μm and 200 μm.

RESULTS AND DISCUSSIONS

The calculated highly resolved T_1,T_2 and diffusion maps of the investigated spheroids reflect a morphological structure which correlates to cross-sectional images derived by light microscopy. They exhibit a necrobiotic core surrounded by a viable rim of cells. The contrast was manifested mainly in relaxation maps, where average relaxation times T_1 = 1.94 ± 0.17 s and T_2 = 42.8 ± 6.3 ms were obtained for proliferating cells, whereas T_1 = 2.49± 0.31 s and T_2 = 104.3 ± 29.4 ms were measured for the necrobiotic center. The mean diffusion coefficients of these two areas were 0.59 ± 0.12 μm^2/ms and 0.85 ± 0.14 μm^2/ms, respectively. The obtained parameter maps seemed to reflect clearly biophysical alterations within the spheroid. In addition, we could follow the dynamic process of tumor cell invasion in co-culture systems of tumor spheroid and fetal rat brain aggregate.

CONCLUSION

In the present study we were able to demonstrate that the morphology of spheroids and especially the proliferation gradient can be visualized by quantitative NMR relaxation (T_1, T_2) and diffusion maps. We found T_2 relaxation to be the most sensitive parameter for achieving optimal contrast within spheroids reflecting clearly biophysical alterations. Furthermore, we could visualize and map confrontation cultures of spheroids. Therefore, we think that quantitative NMR microscopy will be a sensitive tool for investigating biophysical properties of tumor spheroids and for studying their invasion processes which is of utmost interest in tumor biology.

Literature

1 M. Lund-Johansen, R. Bjerkvig, G.J. Rucklidge, *Spheroid Culture in Cancer Research*, ed. Al. Bjerkvig, 2-18, CRC Press, Boca Raton (1992).
2. A. Haase, M. Brandl, E. Kuchenbrod, and A. Link, *J. Magn. Reson.*, A **105**, 230-233 (1993).
3. M. Brandl, A. Haase, *2nd SMR Meeting*, Abstract 1054, SMR (1994).

Acknowledgements

We thank P.D. Dr. E.Klein, Dermatologische Klinik Würzburg for kindly providing malignant melanoma cell line (MV3). We acknowledge financial support under Grant HA 1232/3-2 by the Deutsche Forschungsgemeinschaft (DFG).

Identification of Water Compartments in Developing Bird Embryos by NMR Microscopy

Itamar Ronen, Amos Ar§ and Gil Navon

School of Chemistry, Faculty of Exact Sciences Tel Aviv University, and
§ Department of Zoology, Faculty of Life Sciences, Tel Aviv University

During their development, bird embryos mobilize water, whether initially present in the egg yolk and in the albumen, or metabolically produced by the embryo itself, in order to create temporary and permanent water compartments. These compartments can be formed either in the embryo body itself or in its surroundings. Large quantities of water accumulate first in the subgerminal liquid, then are transferred to the allantoic and chorionic sacs, and are finally absorbed by the embryo. This process takes place in parallel to the depletion of water present in the albumen. The water accumulated in the embryo undergoes compartmentalization to intracellular and extracellular water, of which an important fraction is present in the embryonic blood.

The scope of the present work is to establish a method that will enable to follow the mobilization of the embryonic water and to distinguish between the various water compartments using NMR microscopy, relying on the different transverse and longitudinal relaxation times and the different self-diffusion rates of the water protons in the different environments. NMR microscopy, being a non-invasive method, can provide a tool for correlating events occuring during the development of the embryo and the status of the chick and the adult fowl.

A number of quail eggs were put in refrigeration, where the development of the embryo was arrested. Each day during the following week , a group of eggs was transferred to an incubator operating at 37.4°C. The eggs were incubated for different periods ranging between 3-9 days. MRI images of the eggs at various stages development were performed on a Bruker 360 AMX spectrometer, using an ^1H microimaging probe.

Fig. 1 is a diffusion-weighted spin-echo image of a 9 days old egg. The fast-diffusing watery content of the embryo's eyes and that of the albumen is seen in evident contrast to the slowly-diffusing water in the egg yolk.

Fig. 2 is a T_2 - weighed image of a 3 days old egg, showing clearly on the upper part the water compartment which surrounds the embryo (non visible in the image), the albumen at the lower part, and the egg yolk in the middle.

NMR microscopy can thus provide a valuable tool for detecting the presence of water compartments in bird eggs, and for investigating the physical properties of the water in the various compartments.

Reference: A. Ar, in: Avian Incubation, S. G. Tullett, ed., Butterworth, London (1991).

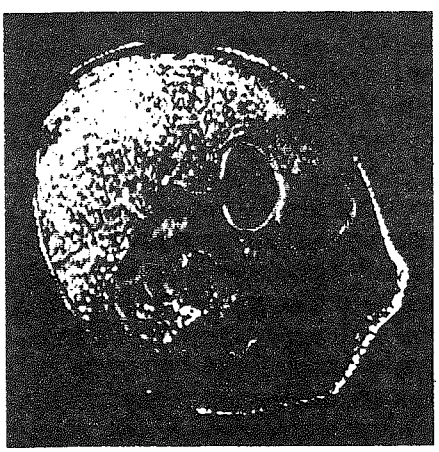

Fig. 1

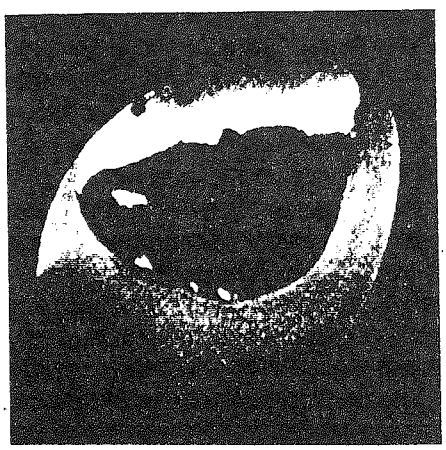

Fig. 2

Secrets of Beauty Care Products Studied by NMR Microscopy

M. Szayna, M. Ilg°, W.P. Kuhn**

*Fraunhofer Institut für Biomedizinische Technik (IBMT), St. Ingbert, Germany;

°Bruker Medizintechnik GMBH, Ettlingen, Germany.

In the last years *in vivo* and *in vitro* investigations of human skin structure and its functions were of growing interest. Magnetic Resonance Imaging (MRI) and Spectroscopy (MRS) have been found as a very successful tool in this field. In particular Nuclear Magnetic Resonance Microscopy, with a spatial resolution matching the size of the structures being under investigation, seems to be the turning point, because of not only a possibility to present the anatomical structures, but also to correlate them with the metabolic functions.

The *in vivo* studies were performed using a 4.7 Tesla Biospec and 3 Tesla Whole Body Bruker Systems. The in plane resolution was about 80 μm with slice thickness of 500 μm. Total measure time for 2 averages was less then 2 minutes.

All *in vitro* experiments on the skin samples were carried out on a 9.4 Tesla Bruker NMR System equipped with home made 3 mm and 10 mm rf coils. Data processing was done using the parameter selective SUNRISE image processing software.

Performed *in vitro* measurements have included both the parameter selective (T_1 and T_2) and chemical shift selective imaging (water and fat). Obtained resolution in *in vitro* experiments was in the range of 5 to 10 μm, regarding the type of experiment with a slice thickness from 150 to 500 μm.

Presented results are from *in vivo* and *in vitro* measurements using standard ointments (W/O and O/W) and different skin-care products selected from the market.

Our investigations were focused on the following subjects:

- *in vivo* investigations of skin abnormalities,
- *in vivo* studies of skin hydration due to the applied ointment,
- *in vitro* study of skin epidermis layers,
- influence of Stratum Corneum on the process of uptake the ointment from the skin surface.

Physico-chemical characterization of the investigated ointment have preceded most of *in vivo* experiment. The ointment was applied on a volunteer and afterwards the increase of skin moisture was calculated based on the proton density images.

Observed increase of the hydration in the outermost part of epidermis reflects two processes taking place after applying the ointment; penetration of the water from the ointment into the skin and retaining of the water in the outer parts of the skin caused by skin occlusion due to the presence of fatty molecules, which slow the process of water evaporation from the body.

There is also possible a comparison between the effectiveness of skin hydration by different creams taken from the market. Quoted results were in agreement with calculated T_2 relaxation maps, which show an increase of about 40% in T_2 values for the epidermis layers.

Performed separate water and fat images revealed the same trends. We could observe penetration of water molecules through the skin (increased signal intensity), but fatty molecules seem to remain outside the skin or penetrate the skin in a negligible amount.

Additionally to *in vivo* experiments, a comprehensive study were undertaken using human skin samples. After applying the ointment on the skin a characteristic increase of the signal intensity, just below the skin surface, caused by the uptake of water during the sample preparation, could be observed. For more detailed study of this process, chemical shift selective imaging was employed. Water and fat images were done from the same slice, and they clearly present the water distribution from the surface of the skin via subsequent epidermis layers. Increased proton signal on the water images in a thin layer (thickness about 50 μm) shows the hydration of the outer epidermis layers, caused by the applied ointment.

This effect is not observed on the fat images, which reveal almost no penetration of the fat components to the skin. A reason might be either the much shorter T_2 values for the lipid signal, which cause a decay of transverse magnetization before detection of the NMR signal, or simply a very low lipid content.

ABSTRACT
for the
3rd. International Conference on Magnetic Resonance Microscopy
Würzburg
August 1995

AN ILLUSTRATED RANDOM WALK THROUGH THE EARLY HISTORY OF X-RAYS IN MEDICINE

Richard F. Mould

41, Ewhurst Avenue,
Sanderstead,
South Croydon,
Surrey CR2 0DH,
United Kingdom.

The very early contributors to the medical applications of X-rays following Röntgen's discovery of X-rays in Würzburg, November 1895, were largely physicists, engineers, and because of their interest in images, also photographers. The 'medical men' as they were then called, limited their contributions to such as the localisation of foreign bodies and radiography of the chest (for tuberculosis was then very common) and of the skeleton (for anatomical deformities and fractures).

This presentation will commence with the early days of 1895-1905 and show some of the major developments of this period in diagnosis and therapy (not always for cancer, but also for benign diseases----and cosmetic purposes!). The illustrations have been drawn from the early textbooks and from journals such as the Archives of Skiagraphy and the Archives of the Roentgen Ray.

Many aspects will be included, such as early quality control of X-ray tubes (visual inspection of the colour of the tube!), case histories of interest to an after dinner speech (radiograph of a man who swallowed his false teeth!), apparatus known as X-ray cannons (with perhaps a radium bomb also included), Boer War radiography in South Africa where the only protection was a photograph of Queen Victoria and mobile diagnostic equipment on cars, aeroplanes and tricycles. Unusual (for today) test objects will be demonstrated, including snakes and frogs, as well as the first imaging phantoms: the Osteoscope and the Chiroscope.

Non-medical applications will also not be forgotten, for the early X-ray textbooks always included a chapter on this topic. X-rays for 'infernal machines' (terrorist bombs) in 1896 customs sheds, detection of fake diamonds and other items of interest to an audience which is relaxing after a Conference Dinner, will conclude this celebratory random walk through 100 years of X-rays.

22 December 1994

NMR visualization of diffusion and flow displacements

Rainer Kimmich

Universität Ulm, Sektion Kernresonanz, 89069 Ulm, Germany.

NMR imaging of parameter fields characterizing displacements by diffusion or flow refers to situations where transport is inhomogeneous. Such circumstances can arise in structured as well as in structureless systems. A series of applications of NMR imaging techniques to both cases will be reported.

Percolation of fluids in pore networks, diffusion of metal ions into alginate, and coherent or incoherent flow in fertilized bird eggs in the incubation phase are examples for transport in structured samples. Modern theories of percolation clusters predict fractal properties of the so-called "backbone" of the cluster. Ion transport in gels shows features which cannot be understood in terms of conventional diffusion equations. Bird eggs in the incubation phase are living, moderately structured systems. The question is what mechanism provides the transport required for metabolism.

Typical situations where transport in bulk fluids becomes inhomogeneous, occur with turbulent flow or thermal convection. The latter can lead to stationary coherent-flow patterns (Rayleigh/Bénard instability). This phenomenon is a textbook example for the generation of "order" in a "disordered" medium by heat transport.

Different NMR techniques have been employed for the examination of the problems mentioned so far. Displacements by coherent flow can be visualized by time-resolved three-dimensional multi-plane tagging imaging. Fading of the tagging planes qualitatively indicates incoherent flow. Movies of the flow processes can be produced based on a series of images recorded while incrementing the time of flight. In this way even complicated flow patterns can be rendered in the form of images.

Quantitative velocity fields in the frame of the achievable voxel resolution can be obtained with aid of six-dimensional *Fourier encoding velocity imaging* (FEVI). That is, the velocity vector of each voxel is recorded, so that images of the velocity magnitude or of any velocity component can be rendered.

NMR imaging studies of concentration fields of (paramagnetic) ions can be based on relaxation contrasts. However, the quantitative evaluation requires detailed knowledge of the underlying relaxation mechanism. With nuclear species, which can directly be detected, spin density images are feasible. Another way to record the spatial distribution of solutes or adsorbates is magnetic-susceptibility imaging. If the diffusing particles perceptibly change the local susceptibility - this is the case with paramagnetic species in particular - the local concentration can be derived from the local susceptibility after calibration of the linear relationship.

A further tool which favorably supplements NMR techniques for transport studies is provided by field-gradient experiments for the characterization of self-diffusion. It will be shown that the combined application of diverse NMR techniques to the problems listed above provides a detailed insight into the physics of the underlying transport mechanisms.

DIFFUSION MRI: FROM TISSUE MICROSTRUCTURE TO CLINICAL APPLICATIONS

Denis Le Bihan, M.D., Ph.D.
Service Hospitalier Frederic Joliot, Commissariat a l'Energie Atomique
Orsay, France

Diffusion NMR is the only available method to measure diffusion displacements in vivo. However, as biological tissues are not infinite, homogeneous media, care must be given to the interpretation of diffusion NMR data. First, one must remember that NMR is sensitive only to molecular displacement. Only when the statistical distribution of the displacement is known can we relate the NMR signal to a diffusion coefficient. Otherwise the term of 'Apparent Diffusion Coefficient' (ADC) must be preferred. With this respect, q-space methods should give better information in terms of molecular displacements. Second, diffusion is a tensor, that is an array of theoretically 9 (6 in practice) numbers which can be determined by NMR. As diffusion is sometimes anisotropic (brain, muscle) and the principal directions of diffusivity do not necessarily coincide with the gradient axes, accurate measurements require the complete determination of the diffusion tensor. Third, diffusion in vivo can be restricted to compartments. The demonstration of restriction can be made by showing that the diffusion distance reaches a plateau when the diffusion time increases. In fact, other factor, such as membrane permeability or macromolecular, fiber,organelle obstacles (characterized by a tortuosity factor) could also reduce the diffusion coefficient without the plateau pattern. In this case, the use of very short diffusion times (requiring very powerful gradients) should reveal a free diffusion behavior oppositely to hindered or impeded diffusion. Finally, because of these problems, it remains difficult to ascribe multiple diffusion measurements to specific compartments. It remains that diffusion NMR is a very powerful tool that will help us to better characterize anatomically and functionally tissues at cellular level. Very promising clinical applications, such as brain ischemia and temperature imaging are already under evaluation. Water diffusion is decreased at a very early stage in brain ischemia, in relation to cytotoxic edema, allowing detection at the acute phase. Diffusion MRI may soon become the method of choice to successfully manage stroke patients, helping to predict the outcome, to evaluate therapies and to monitor recovery. Diffusion is also an important parameter to monitor temperature changes in real time during interventional procedures involving tissue heating (hyperthermia, laser surgery, focused ultrasounds) or cooling (cryotherapy). Such therapeutic modalities can now be performed within the MR magnet (interventional MRI). Other applications, such as evaluation of kidney and cardiac function, are also evaluated.

Microscopic MRI of Cartilage

Lynn W. Jelinski
Professor, Engineering
Cornell Center for Advanced Technology - Biotechnology
Cornell University
Ithaca, New York 14853 USA

A non-invasive marker for cartilage degradation would be invaluable for evaluating the efficacy of potential antiarthritis drugs. To this end we have been investigating the sensitivity of microscopic MRI parameters, including T_1, T_2, and diffusion (D) to osteoarthritic lesions and to biochemically- and mechanically-induced cartilage degradation.

The water self-diffusion coefficient for lesion canine cartilage due to osteoarthritis shows an increase of about 25% over that of surrounding cartilage. This increase in D can be mimicked by enzymatic degradation of cartilage with trypsin, hyaluronidase, and collagenase, or by mechanical means. However, we have established using excised disks of living cartilage whose proteoglycan and collagen contents were manipulated by biochemical intervention in tissue culture, that the diffusion measurement is not sensitive to the proteoglycan content of cartilage. Instead, self-diffusion appears to monitor mesoscopic tissue damage. These results show that D, measured in a spatially-resolved manner by pulsed field gradient nuclear magnetic resonance imaging (PGSE - MRI), can localize regions of cartilage degradation.

NMR Microscopic Detection of Cartilage Stress Behaviour An Approach to Dynamic NMR Microscopy

W. Gründer, S. Hahn, T. Keller, A. Werner
Institut für Medizinische Physik und Biophysik, Universität Leipzig
Liebigstr.27, D-04103 Leipzig, Germany

Introduction
Investigations of joint cartilage have shown that, in dependence on the angle of cartilage surface to static magnetic field, internal matrix structures can be observed as zones of different intensity in the T_2 weighted microimages[1]. Water T_2 relaxation in orientated (collageneous) zones inside of hyaline cartilage is strongly influenced by anisotropic dipolar coupling in these cases. Under magic angle conditions dipolar coupling is minimized in these regions and the multilaminar structure of the articular cartilage disappears. We have shown, that the existence of such orientated regions of collagen fibres are essentially determined by calcium ions[2]. Removement of calcium ions (by EDTA incubation) obviously leads to an isotropic arrangement of matrix collagen in these zones and to a homogeneous appearence of the cartilage. In this paper we show, that the existence and the extension of such zones of orientated matrix structures are strongly influenced by mechanical stress. We demonstrate that by application of magic angle technique stress behaviour of joint cartilage can be depicted.

Material and Methods
Full depth cartilage plugs (Ø 20 mm, Ø 3 mm) of human, pig and sheep femoral condyles, resp., were used in our experiments. The measurements were performed on a 300 MHz spectrometer (Bruker AMX300 WB) equipped with a microimaging unit. To perform angular dependent measurements under different loading conditions a special probe head was developed. Two cartilage plugs (Ø 3 mm) with cartilage surface against each other were used inside of a silicon tube to simulate joint situation. MR images were taken using GE and SE sequences (TE= 4-100 ms, TR= 500-200 ms) with 20-70 µm in-plane resolution and 500 µm slice thickness. Histological and scanning electron microscopic reference investigations were performed.

Results
The presentation of cartilage structure in NMR microimages depends on mechanical loading. Our experiments demonstrate, that cartilage collagen orientation is strongly influenced by mechanical stress. We found, that the collagene network arrangement and the resulting mechanical properties of cartilage are determined essentially by calcium ion concentration. By means of time dependent measurements of cartilage changes following mechanical loading viscoelastic properties of the joint cartilage can be recorded.

Conclusions
Using angular dependent dipolar coupling of orientated cartilage matrix structures, especially of the different zones of orientated collagen fibres, stress behaviour of joint cartilage can be depicted in different stages of arthrosis. We have found, that dynamic MRI measurements under different mechanical loading can give informations with respect to viscoelastic properties of joint cartilage and can improve the assessment of early arthrotic changes.

References
1. Rubenstein, J.D. et al., Radiology **188**, 211, 1993
2. Gründer,W. et al. Proc. SMR, Nice 1995

Porous Media NMR Imaging
(Gels, Brains, Rocks, Soil)

Laurie D Hall
Herchel Smith Laboratory for Medicinal Chemistry,
University of Cambridge School of Clinical Medicine,
Robinson Way, Cambridge, UK, CB2 2PZ

It is well known that Magnetic Resonance Imaging (MRI) and Microscopy can be used to visualise the diffusion and perfusion dynamics of the liquidus components of porous media including hydrogels, human tissues, soil and rocks. This talk will illustrate the scope of such measurements using practical examples from all of the above areas. Emphasis will be directed to the features which these seemingly diverse materials have in common, and on the modelling of the resultant data.

NMR Imaging in Porous Media

R. Bowtell, A. Peters, P. Robyr and P. Mansfield

Magnetic Resonance Centre, University of Nottingham, Nottingham, UK, NG7 2RD.

Introduction For many years, NMR techniques have been used in the investigation of porous media. Measurements of NMR relaxation times and of the diffusive behaviour of fluids in the porous microstructure have proved particularly useful. In heterogeneous samples a greater amount of information can of course be gathered by combining these measurements with imaging. Adding a spatial dimension to the measurement process normally, however, leads to increased measuring times. To date, the resolution in most imaging experiments carried out on porous media, has been considerably coarser than the pore scale. NMR Microscopy potentially offers the possibility of making NMR measurements at a resolution approaching the pore size[1]. However, the strong magnetic fields which are usually employed in high resolution NMR microscopy can lead to the presence of large magnetic field inhomogeneities, whose effects must be overcome if this potential is to be realised. Building on work carried out at 0.5 T, we have applied NMR microscopy at 11.7 T to the investigation of porous rock samples. Techniques which allow the generation of images that are relatively insensitive to field inhomogeneity, whilst having reasonable image acquisition times, have been implemented and measurements of T_1 and fluid flow have been made.

Techniques and Results For rapid imaging, a modified version of the echo-planar imaging sequence, which uses a series of 180° RF pulses instead of gradient reversals, has been employed. The PEPI[2] sequence allows the generation of a two dimensional image from a single echo train, but is much less sensitive to magnetic field inhomogeneities than standard EPI, and therefore better suited to the imaging of porous media. Images with a 64^2 matrix size and voxel dimensions of up to 50 x 50 x 100 μm have been generated in less than 100 ms using this technique. Microscopic resolution flow maps have been generated by preceding the imaging module with a flow encoding sequence designed to be relatively insensitive to the effects of magnetic field inhomogeneity[2] and to diffusion in the applied field gradients. The high speed of the sequence allows the monitoring of flow variation in transient processes. By adding a phase encoding gradient to the PEPI sequence it is also possible to generate three dimensional images in a relatively rapid fashion. Using this sequence in an inversion recovery experiment, volumar T_1 maps with a 64^3 matrix size and isotropic resolution of 80 μm have been generated in under three hours. The equivalent 3DFT experiment would have had a six day acquisition time.

References

1) G.J. Nesbitt *et al*, in "Magnetic Resonance Microscopy" (B. Blümich, W. Kuhn Eds.) p287, VCH Weinheim, 1992.

2) D.N. Guilfoyle *et al*, *J. Magn. Reson.* **97** 342, 1992.

3) B. Issa and P. Mansfield, Proc. 12th Meeting SMRM, p1236, 1993.

ABSTRACT

3rd International Conference on Magnetic Resonance Imaging

August 27-31, 1995, Würzburg, Germany

TRANSPORT PROCESSES IN POROUS MEDIA

G.J.Nesbitt

Koninklijke/Shell Laboratorium, Amsterdam
(Shell Research B.V.)

Babhuisweg 3, 1031 CM, Amsterdam, The Netherlands

It is well known that classical hydrodynamic equations can be used to describe the behaviour of ideal fluids within well defined limits. In this manner numerical simulations can be used to verify and predict macroscopic(measurable) properties. Unfortunately many systems, porous media in particular, are comprised of less than ideal fluids constrained within complex boundary conditions. These properties have frustrated the development of analytical techniques which have a direct relationship with a microscopic measurable property, such as the molecular distribution, viscosity, diffusion, or flow behaviour, of a fluid in a porous material.This has also confined most modelling to using statistical methods or concentrating on phenomenological descriptions.

This paper shows examples where a correlation between NMR-measured parameters and macroscopic behavior has been possible. Specifically, the structural [chemical-shift] and dynamic [spin-lattice (T_1), spin-spin (T_2) relaxation, diffusion or flow characteristics of a system can be spatially determined on a microscopic scale, while being inherently sensitive to interactions which occur on a molecular scale. This relationship is significant where local morphology determines macrosopic properties.

Models describing the transport of fluids through porous beds incorporate certain assumptions with respect to mass transfer at a particle interface. The nature of the adsorption/desorption profile drives the intraparticle mass transfer which in turn can be controlled by local conditions to be surface or pore diffusion sensitive. Validation of the models in this respect has been limited, however it is known that drying conditions influence the deposition of adsorbate onto support material, for example.

For this reason NMR gradient techniques have been used to investigate drying and wetting processes in silica extrudate. The results show conclusively that deviations from theory can be detected and investigated. The quantitative determination of the local transport coefficients allows the interpretation of bulk processes.

Spatially Resolved NMR Study of Adsorption/Precipitation of Chemicals Inside Porous Media

G. Maddinelli
Eniricerche S.p.A, via F. Maritano 27, S. Donato, 20097 - Milano, Italy.

Abstract

Precipitation inhibitors are generally injected into hydrocarbon formations to prevent crystal nucleation of undesirable salts, i.e. $CaCO_3$ or $CaSO_4$, which would cause serious problems of scale formation during oil production[1]. Phosphine-polyacrylic acids (PPAA) belong to a widely used class of threshold inhibitors. This kind of technical application is mainly based on a complex mechanism of adsorption/precipitation within the well which allows a slow release (solubilization) of the inhibitor molecules in the fluids during oil production.

NMR imaging methods provide a unique tool to follow these kind of phenomena occurring directly inside the porous media of interest. In our study we have investigated the phase behaviour of 0.5 % PPAA solutions containing Ca^{++} ions and placed in a column packed with quartz sand. Solutions were prepared using deuterated water (99.9%) as a solvent. Replacing water with deuterated water clearly affects relaxation times of protons because of isotopic dilution, making the NMR method very sensitive to spin dynamics even inside rock cores[2]. T_1 -weighted spin-echo images gave profiles of the distribution of PPAA during flow of the solutions inside the sandpack, while spatially resolved T_2 estimation (by nonlinear least-square fitting of several images acquired by varying the echo time[3]) allowed precipitation phenomenon to be probed. In fact, spin-spin relaxation, which is particularly sensitive to slow motions, was affected by precipitation process which caused a relevant T_2 decrease in the area interested. No adsorption was found to occur under the conditions adopted, while precipitation was visualized at the interface area between the different solutions. The phenomenon occurred very slowly and was mainly governed by diffusion of the chemicals, and precipitation of PPAA was not extensive. In conclusion, MRI methods revealed a good potential for investigating chemical and physical processes distribution inside these kind of materials.

References

[1] J.E. Oddo and M.B. Tomson, Applied Geochemistry, **5**, 527-532, 1990;
[2] J.L.A. Williams, G.Maddinelli, D.G.Taylor, J. Magn. Reson., Series A **109**, 124-128, 1994;
[3] J.L. Antti, O.K. Nieminen and J.L. Koenig, J.Magn. Reson., **85**, 95-110, 1989.

POSTER PRESENTATIONS

The NON-CON transverse gradient coil for NMR microscopy

E.R. Andrew and M. Kempka

Departments of Physics and Radiology, University of Florida, P.O. Box 118440, Gainesville, Florida 32611, U.S.A.

A new type of transverse gradient coil of great simplicity is presented, built of units consisting of two identical non-concentric coils. It is called the NON-CON coil. Use of full circle current paths instead of arcs simplifies coil construction and manufacture. The number of current elements in each unit is reduced significantly. The main features of the coil are a compact symmetric and quiet design, improved volume of uniform field gradient, low inductance, short time constant, absence of torque, reduced stray field. The coil design uses a number of symmetrically disposed units, whose location is optimized by the gradient descent technique. Details of design, analysis and manufacture of the NON-CON coils will be shown. Although developed initially for NMR microscopy, this transverse gradient coil system can be equally well used for larger systems of MR imaging.

This work is supported through grant P41 RR02278.

A Three Dimensional NMR Imaging Scheme utilising doubly-resonate gradient coils

S. L. Codd, M. J. D. Mallett, M. R. Halse and J. H. Strange.
Physics Laboratory, University of Kent, Canterbury, CT2 7NR, UK.

A 3DFT gradient echo technique has been developed which uses series resonant gradient coils to produce three dimensional NMR images with an echo time of 40-80 μs. The method utilizes a multi-resonant circuit developed by Mansfield et al and is an improvement on imaging sequences which use simple sinusoidal gradient waveforms. If the gradient coils are only able to resonate at a single frequency, then it is impractical for an imaging scheme to sample all of *k*-space. Previous schemes using a single resonant frequency for each gradient coil only sample half of *k*-space and the second half of *k*-space must be predicted using conjugate symmetry. The inaccuracies involved in the necessary "cut and paste" of *k*-space inevitably lead to artifacts in the final image. The essential features of the new method, which uses a read gradient coil with two resonant frequencies, is that: 1) all of *k*-space is sampled; 2) the RF pulse is applied when the gradients are all zero; and 3) the echo forms when the gradient is at a maximum (and hence fairly constant) value. Large field gradients are used in NMR imaging to dominate the homogeneous dipolar broadening present in solid materials. By resonating the gradient coils, this imaging method helps overcomes the risetime problems associated with large gradients, and the use of a doubly resonate gradient coil has allowed an imaging scheme which samples all of k-space, drastically reducing the artifacts normally observed in other oscillating gradient schemes. Three dimesional images have been obtained of in-vivo finger joints with a resolution of 0.2 mm and echo times of 40-80 μs.

A compensation method for image acquisition in presence of time-varying gradients

M. Staemmler
Fraunhofer Institute IBMT, D 66386 St. Ingbert, Germany

Introduction

Imaging of samples with short T_2 relaxation times is impaired by either signal loss due to gradient switching times or by pulse bandwith limitations induced by the gradients. This paper describes a method to compensate for the adverse effects of acquiring data during gradient ramp up.

Methods

Using a 2D or 3D FID based projection reconstruction imaging sequence (fig.1) the acquisition starts already during the gradient ramp up. The $\int g(t)dt$ results in:

$$\begin{array}{lll} 1/2\, g_0 t & \text{for} & 0 \le t < t_0 \\ g_0 t & \text{for} & t \ge t_0 \end{array}$$

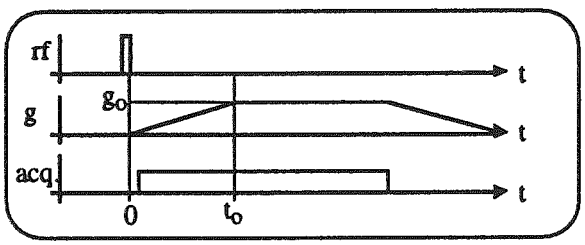

Fig.1: FID based pulse sequence

Compared to the ideal situation where the dephasing is constant with $g_0 t$ the signal in the "slow" dephasing period $0 \le t < t_0$ can be numerically resampled to obey $g_0 t$ by using an algorithm similar to histogram equilization [1].

Since the resampling is based on the comparision between the ideal situation and the real situation using integrals it is applicable for any arbitrary gradient ramp shape.

Results

For verification two projection data sets were obtained on a UNITY™ 400 with a switched and a slowly ramped up gradient. The later data set was subjected to the compensation algorithm described above. Comparing the individual projection traces showed a strong correlation between the two sets. After reconstruction of both data sets using a standard projection reconstruction algorithm the resulting images exhibited the same structures, the typical blurring due to acquisition in presence of a ramped up gradient could not be observed.

Conclusion

This compensation method allows to acquire data in the presence of a time varying gradient. Projection reconstruction imaging can be performed on samples with short T_2 relaxation times using FID or half-echo based acquisition schemes.

References

1 Pavlidis, T., "Algorithms for Graphics and Image Processing", Springer Verlag,1981

Single Point Imaging. A Method to Measure Gradient Rise and Stabilization

Mircea Bogdan[1], Bruce J. Balcom[1], Robin L. Armstrong[1], Theodore W. Bremner[2], Department of Physics[1] and Department of Civil Engineering[2], The University of New Brunswick, P. O. Box 4400, Fredericton, N.B., Canada , E3B 5A3.

NMR Imaging and localized spectroscopy rely on switched magnetic field gradients. These time varying magnetic fields induce eddy currents in neighbouring conductors in the magnet, probe or gradient set. These secondary magnetic fields cause a variety of undesirable distortions and artifacts in NMR Imaging and localized spectroscopy. A variety of methods of been proposed to minimize the effects of eddy currents and decrease gradient switching times(1). NMR methods which attempt to measure the effects of eddy currents generally rely on distortion of the NMR signal, following a pulsed gradient, observed by a series of low flip angle RF pulses (2). We wish to introduce Single Point Imaging (SPI) as a method of observing gradient rise and stabilization as a pulsed field gradient is switched on. The method may be employed to characterize gradient performance for a wide variety of spectrometers.

SPI relies on the application of a broad band RF pulse in the presence of variable amplitude phase encoding gradient(s) with sampling of a single point on the resulting free induction decays a fixed period of time after excitation. In our method we employ one phase encoding gradient to generate one dimensional longitudinal profiles of a uniform cylindrical phantom. In the generic SPI experiment one typically waits until the phase encoding gradient has stabilized before applying the RF pulse. One may in principle, however, apply the RF pulse at any point after switching the gradient. If the phase encoding time after the pulse is brief, typically between 50 and 100 usec, and the time dependent gradient may be considered quasi static in this time period, the real k space trajectory of the imaging sequence will systematically differ from the ideal. Fourier transformation of the k space data yields one dimensional profiles of the uniform cylinder which are contracted from the ideal case. The effective gradient relative to the ideal case may be extracted from the contracted profiles. Experiments characterizing the gradient performance of a Nalorac 32 cm horizontal bore 2.4 Tesla magnet with a 20 cm i.d. self shielded, water cooled, gradient set will be presented. No effort has been made to optimize the pre-emphasis network.

The method relies on linear behaviour of the induced eddy currents and yields the most quantitative results for gradients which are close to stabilizing or with very long time constants. The method does not, in its present form, permit compensation of B_o shifts which frequently accompany switched gradients.

References:

(1) J. Van Vaals, A. Bergman *J. Magn. Reson.* **90**, 52, (1990).
(2) R. E. Wysong and I. J. Lowe *SMRM Abstracts,* 10th Annual Meeting, San Francisco, California, 1991.
(3) S. Gravina and D. G. Cory *J. Magn. Reson. B* **104**, 53, (1994).

Automatic compensation of eddy currents for localized NMR spectroscopy and NMR microscopy.

K. Bartušek, B. Jílek

Academy of Sciences of Czech Republic,
Institute of Scientific Instruments
Královopolská 147, 612 64 Brno, Czech Republic

A precise compensation of eddy currents, which arise after application of the gradient magnetic field, is important first of all in localized NMR spectroscopy and NMR microscopy, where it decreases the number of undesirable spin echoes and shortens the measuring time. The principle of the digital generation of gradients, the circuit design of the preemphasis based on digital signal processors (DSP), and the simple NMR measuring method are the basis of the automatic, precise pre-emphasis adjustment. It is possible to reduce the preemphasis adjustment errors by using optimization techniques.

The method of the gradient magnetic field measuring consists in the selective excitation of nuclei in a thin layer and in determining the instantaneous frequency of the FID. From this function, the pre-emphasis constants are determined. The iterative optimization of a pre-emphasis filter was used for increasing the measuring precision and it makes the high precision determination of the long time constants possible.

Generally, the field generated by eddy currents induced by pulsing a magnetic field gradient coil has not the same spatial variation as the field generated by the gradient coil. By the presented method an effect of the main field shift and the gradient term were eliminated. A reduction in the gradient magnetic field (50 mT/m) to the level of the static magnetic field in 100μs was achieved. It is possible to calculate the pre-emphasis constants for eliminating the effect of eddy currents of the other field components from the matrix of constants measured in some selective defined layers. The method was verified on the homebuilt NMR spectrometer.

Novel Designs for High Purity, Shielded Z^n Coils

Stuart Crozier, Stephen Dodd and David M .Doddrell

Centre for Magnetic Resonance, Qld. University, Brisbane, Qld. 4072. Australia

An NMR shim set is usually used to correct imperfections in the homogeneity of the main magnet. These coils are typically designed by arranging conductors to attempt to annul two or more of the major harmonic impurities prediction by the coil symmetry. Recently (1), a novel use for longitudinal or zonal shim coils has been found whereby by pulsing these coils localized spectroscopy or localized imaging may be facilitated. The "shim" type coils used in this work were not suitable for fast pulsing, however.

Here we present a new methodology for designing both pure shim coils and shielded higher order coils suitable for rapid pulsing. The methodology is the Simulated Annealing (2,3) of spherical harmonic errors. This design can also incorporate minimum inductance and power constraints, is very flexible and as it operates in real space the implementation of dimensional constraints is trivial. Results will be presented for shielded longitudinal coils of various order. By incorporating the spherical harmonics of the field produced by the coil in the error function, very "pure" coils result.

1. C.H. Oh, K. Hilal, Z.H. Cho and I. K. Mun, *Magn. Reson. Med.* **18**, 63 (1991).
2. S. Crozier and D. M. Doddrell, *J. Magn. Reson.* **103**, 354 (1993).
3. S. Crozier, L. K. Forbes and D. M. Doddrell, *J. Magn. Reson.* **107**, 126 (1994).

High resolution NMR with picomole sensitivity

A.G.Webb, D.Olson, T.L.Peck, R.L.Magin and J.V.Sweedler
Beckman Institute for Advanced Science and Technology
University of Illinois, Urbana IL 61801

In many biomedical applications, samples for NMR analysis are often mass-limited to less than 1μg. Examples include structural determination of pharmaceutical contaminatnts and the contents of single cells. Even when using commercially available 3 mm diameter probes, the excessively long data acquisition times that result from poor sensitivity become prohibitive. We report here on the application of solenoidal RF microcoils (100-400 μm diameter and an active volume of 5-50 nl (1)) to NMR microspectroscopy at 7.05 T. In this size regime the sensitivity of the coil (B_1/i) is inversely proportional to the diameter of the coil (2). Therefore the decrease in SNR resulting from the smaller sample volume is partially offset by the increase in coil sensitivity.

Microcoils were constructed using insulated copper wire (50 μm diameter) wound directly onto 360 μm o.d. (75-245 μm i.d.) fused silica capillaries. The coils were 17 turns for a total length of 1 mm. The coil assembly was immersed in a susceptibility-matched liquid perfluorocarbon. Approximately 3 hours shimming is required on a new coil.

One-dimensional proton spectra have been obtained using ethylbenzene as a standard for sensitivity and linewidth. For a mass of 4.3 μg (41 nmol), the linewidth of the central peak of the triplet was 0.6 Hz, and the SNR greater than 100:1 for a single scan. The figure below shows a COSY spectrum of a model compound 2,3 dibromopropionic acid (1.0 μg, 4.5 nmol) acquired in 2.2. hours. The proton scalar coupling is clearly resolved. We have also obtained high resolution 1-D spectra of 250 pmoles of cholic acid in less than 30 minutes.

As a sensitivity comparison between our solenoidal coils and a standard commercial probe, using sucrose and arginine as standards, we have determined that microcoil-detection improves the mass sensitivity by approximately two orders of magnitude, corresponding to four orders of magnitude decrease in the total data acquisition time.

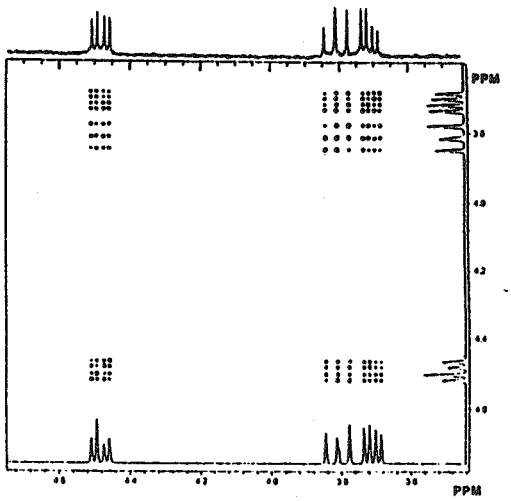

1. N.Wu, T.L.Peck, A.G.Webb, R.L.Magin and J.V.Sweedler, J.A.C.S., 116, 7929 1994.
N.Wu, T.L.Peck, A.G.Webb, R.L.Magin and J.V.Sweedler, Anal.Chem., 66, 3849 1994.
2. T.L.Peck, R.L.Magin and P.C.Lauterbur, J.Magn.Reson., in press.

A circular polarized surface receiver coil for quantitative relaxation studies at rat hearts *in vivo* at 7 T

Eberhard Rommel and Axel Haase
Physikalisches Institut der Universität Würzburg, Am Hubland, D 97074 Würzburg, Germany

Purpose: An actively decoupled circular polarized surface coil for rat heart applications is presented which is designed as sensitive receiver coil in combination with a homogeneous transmitter coil.

Introduction: The advantage of surface coils compared to whole body coils is the higher sensitivity in the desired field of view. On the other hand the B_1 homogeneity is poor, so that for relaxation studies like Snapshot-Flash IR-imaging where exact inversion pulses are required, it is necessary to use them in combination with a homogeneous whole-body transmitter probehead. This is a field where lab-design of coils is not only useful, but essential for the work.

Coil Design: The quadrature coil consists of a circular and a butterfly surface coil. The coils were etched out of copper plated foil material. For rat heart studies this flexible arrangement is wound half circular around the chest of the rat. Electric RF fields are reduced by distributing the tune capacitance on four capacitors per turn, i.e four capacitors for the cirular coil and eight capacitors for the butterfly coil. At the cable connecting points, a network of three ceramic chip capacitors (ATC) is used for fixed asymmetric parallel matching to 50 Ohm. Fine tuning is possible with a small saphire trim capacitor (Tronser) at each coil part.

Decoupling: The butterfly coil is oriented perpendicular to the transmitter coil, so it is already decoupled under ideal conditions, but these are not generally fulfilled.The circular coil is oriented parallel to the transmitter coil and needs active decoupling.
So both quadrature parts of the coil are actively decoupled during transmitter operation using PIN diodes (Unitrode) which in combination with an inductor and one of the tune capactitors form high impedance circuits. To avoid ' hot spots' due to the RF field of the decoupling circuits they are built up with SMD inductors (Siemens). Additionally the loops formed by capacitor, inductor and PIN diode are oriented perpendicular to the transmitter coil. Two switching circuits per coil were used, and the other capacatitors were bypassed by SMD inductors for the dc control current of the PIN diodes. In this way the loaded quality factor was not affected, and the PIN diode switches improved the decoupling by 21 db.

Results: In off mode the quadrature surface coil has no visible influence on the RF field homogeneity of a homogeneous transmitter coil.
The PIN diode switches improve the decoupling by 21 db.
The sensitivity gain compared to a whole-body rat coil is about 3.

References:
1) E. Rommel, T. Harth, A. Haase, A Crossed Coil Probehead for Snapshot Flash Relaxation Studies, in "Proc. SMRM 12th Annual Meeting, New York, 1993", p. 1338
2) H. Merkle, M. Garwood, and K. Ugurbil, Dedicated Circularly Polarized Surface Coil Assemblies for Brain Studies at 4 T, in "Proc. SMRM 12th Annual Meeting, New York, 1993" p. 1358

A METHOD OF SUSCEPTIBILITY "COMPENSATING" RF COILS

F.O. Zelaya, S. Crozier, S. Dodd and D.M. Doddrell.

Centre for Magnetic Resonance, University of Queensland, St.Lucia, Queensland 4072, Australia.

The perturbation imposed on the homogeneity of a constant magnetic field B_0, by the presence of media of different magnetic susceptibilities is well known *(1,2,3)*. This situation is encountered in most NMR Spectroscopy and Imaging applications, either by the existence of different material and component boundaries in the gradient and RF coils and probes; or by multiple susceptibility differences within the sample itself. Although most of these perturbations can be corrected by shimming, residual effects give rise to artefacts and loss of spatial resolution in imaging experiments; as well as imposing a limit on the spectral resolution that can be achieved in spectroscopic investigations.

In the work presented herein, we propose and demonstrate a simple strategy that can be used to compensate for susceptibility induced artefacts caused by the presence of metallic conductors in the vicinity of the sample (4). The method relies on the appropriate layering of para-magnetic and dia-magnetic materials. We also demonstrate how Magnetic Resonance Imaging may be used to monitor susceptibility compensation methods.

1. P.T. Callaghan, *J. Magn. Reson.* **87**, 304 (1990).
2. D.T. Edmonds and M.R. Wormald, *J. Magn. Reson.* **77**, 223 (1988).
3. P.T. Callaghan, "Principles of Nuclear Magnetic Resonance Microscopy", Clarendon Press, Oxford, 1991.
4. F.Zelaya, S.Crozier, S.Dodd, R.McKenna and D.M. Doddrell, *J. Magn. Reson.* , in press.

An automatic shimming tool for arbitrary volumes at 7T

Tobias Dorn, Eberhard Rommel, Peter Jakob and Axel Haase

Physikalisches Institut der Universität Würzburg, Am Hubland, D 97074 Würzburg, Germany

Introduction: Many imaging methods, e. g. CSI, EPI or spectroscopic imaging require a b0-homogeneity of fractions of ppm within the ROI while outside the homogeneity is not of interest. With conventional manual shimming methods, only simple-shaped SROI (shimming region of interest) like a slice or the whole sample can be treated. If two or more strong frequencies are present, e. g. fat and water, shimming becomes more difficult. Spatial separation of the components may lead to the supressing of one peak. The presented program enables the user to optimize the b0-field considering the mentioned problems in dialog with a graphical interface. It is implemented at a Bruker 7T-21cm magnet. The FOV can be set from 3x3x3cm to 7x7x15cm, the resolution up to 64x64x64.

Methods: To get information about the magnetic fields the shims coils produce per unit current a *reference-set* must be measured using a large water phantom. This can be done by simply selecting the desired FOV and resolution. The measuring method is the same as described in the following.
A map of the inhomogeneity of the sample is built from the difference of two phase-reconstructed fast gradient-echo experiments with a different echo time. In present of two frequencies the first echo time and the time difference between the echoes is set to a integer multiple of the reciprocal of the frequence offset. Therefore the two peaks are acquired in-phase and the following algorithms may not distinguish between the two substances. A fast reliable 3D-phase-unwrapping algorithm is applied on the phase-difference image.
To select the SROI the user can determine a simple geometric object in 3D-space or use the mouse to cut a region from a magnitude-reconstructed image of the sample. Additional all voxels of this image with a value below a given treshold are eliminated in the segmentation.
The optimal shim currents within the limits given by the shim-unit are then computed by a constraint least square algorithm. To reduce self-compensating fields the dimension of the problem is reduced by deleting columns with small influence on the SROI from the *reference-set* matrix.
Two or sometimes three iterations lead to the best possible result, whereby the first shim should be computed for a larger region and the desired SROI selected in the following steps.

Results: We obtained good results with shimming on a perfused rat-heart and phantoms of fat or bacon and water. In the illustrated example we shimmed two times on a phantom with 25ml cyclohexane enclosed in 100ml water. The resolution was 64x64x32, the FOV 6x6x6cm and the SROI a slice of 10mm. The b0-field in the central slice of thickness 1.8mm is shown: First the zero-shim without and with in-phase detection, then the field after two autoshim iterations, last the spectra of the whole SROI. The left 2D-plot is skaled to 1000Hz, the next to 500Hz.

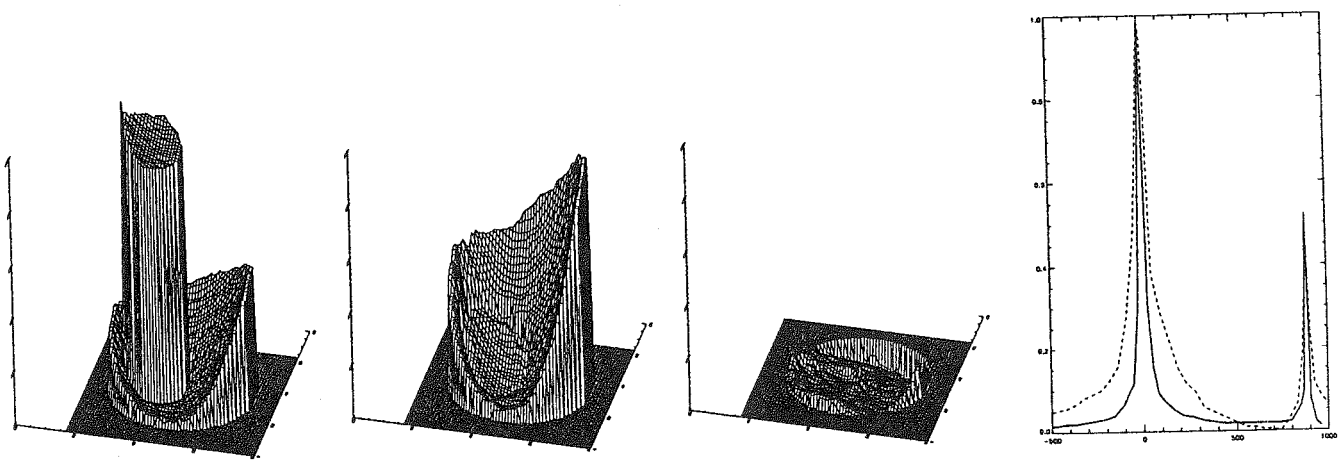

References:
1. E. Schneider, G. Glover, Magn. Reson. Med. 18, 335 (1991)
2. P.Webb, A.Macovski, Magn. Reson. Med. 20, 113 (1991)

ASSESSMENT OF THE MICROSCOPIC DISTRIBUTION OF THE MAGNETIC FIELD BY MR IMAGING AND SPECTROSCOPY

F. Schick[1,2], S.H. Duda[2], O. Lutz[1], C.D. Claussen[2]

Institute of Physics,[1] Department of Diagnostic Radiology,[2]
University of Tübingen, 72076 Tübingen, Germany

The distribution of the susceptibility inside a sample influences the field homogeneity. Some field mapping techniques allow to assess the macroscopic field in a slice: The mean magnetic field strength inside each picture element is correlated with the greyscale in the image.

The intensities of gradient echo signals depend on the microscopic field distributionand T_2, whereas spin echo images are only T_2-sensitive. Thus, information on the microscopic field inhomogeneity can be derived from spin echo and gradient echo images of the same slices with matching parameters.

To overcome the common procedure of T_2- and T_2^*-measurements for evaluation of the microscopic field distribution, a new method (MAGSUS) was developed showing microscopic field inhomogeneities due to susceptibility effects in one image without further data processing. MAGSUS uses the frequency-dependent phase of a two pulse excitation to obtain a signal pattern in the images which is very sensitive to the field distribution in each pixel. MAGSUS images showed clear differences of regions inside the epiphysis (high trabecular density) and the diaphysis (pure bone marrow) of the femur or tibia due to the different microscopic field distributions.

Methods sensitive to the microscopic field distribution are described and compared. Applications of gradient echo imaging, MAGSUS imaging and localized spectroscopy leading to clinically relevant information are presented.

Address: Fritz Schick; Physikalisches Institut; Auf der Morgenstelle 14;
72076 Tübingen; Germany.

Experiments with gradient-localized DESIRE microscopy

H. Douglas Morris*, Nian Yang, Carl Gregory and Paul C. Lauterbur

Biomedical Magnetic Resonance Laboratory, University of Illinois, Urbana IL 61801

Microscopic NMR imaging experiments inherently produce less signal due to the smaller number of spins in each voxel and diffusion further decreases signal intensity and resolution.[1] Several calculations [2-6] have placed a practical volume resolution limit for MRI at hundreds of $(\mu m)^3$. These calculations are based upon optimized versions of contemporary standard MRI techniques.We have proposed a way to use diffusion to amplify the signals from the spins in microscopic volumes[7], possibly decreasing that limit by several orders of magnitude. This so-called DESIRE (Diffusion Enhanced Signal Intensity and REsolution) effect operates by the saturation of spins as they diffuse through a microscopic region and spread the saturation through a much larger volume.

The heart of the DESIRE experiment is the separation of the localization and observation steps. Standard techniques use spatially and temporally varying magnetic field gradients to encode spatial information in the frequency and/or phase of an NMR signal. In the microscopic domain, this relationship becomes muddled due to the short residency time of the nuclear spins within a particular voxel. For example, the 1-dimensional self-diffusion distance for water can be about 20 μm in 100 ms.

A microscopic region within which the longitudinal nuclear magnetization is excited can be established. For a sufficiently small volume the excited nuclear spins exchange with their external counterparts while still remaining in an excited state. The time constant of this excited state, T_1, is of the order of seconds in simple liquids and some tissues, and provides a signal memory for the spins that were once within the excitation region that increases for a time of the order of T_1. It can be shown that for irradiation regions of 1 μm^3 enhancements of many orders of magnitude are possible. The observation step of the DESIRE experiment then provides the difference NMR signal generated by the entire excited region.

Experiments.

We have carried out 1 and 2D DESIRE gradient localized experiments on structured phantoms. 1D experiments requires only a constant gradient and simple RF waveforms. Higher dimensional experiments requires shaped RF and gradient waveforms to excite 2 or 3D spatial regions. Quantitative comparisons with theory are being made.

References.

1. Paul T. Callaghan, "Principles of Nuclear Magnetic Resonance Microscopy", p. 201 - 206 , Clarendon Press (1991).
2. E. W. McFarland,"Time-independent Point-spread Function for NMR Microscopy", Magn. Reson. Imaging 10, 269 (1992).
3. S. Gravina and D.G. Cory, "Sensitivity and Resolution of Constant Time Imaging", J. Mag. Res. B 104, 53 (1994).
4. C.B. Ahn and Z.H. Cho, "Theoretical and Experimental MRI at 4 μm resolution", Med. Phys. 15,815 (1988).
5. X. Zhou and P.C. Lauterbur ,"Diffusion Limited Resolution for Different Pulse Sequences in NMR Microscopy", Abstracts, International Conference on NMR Microscopy, Heidelberg, Germany, p. 88 (1991).
6. X. Zhou and P.C. Lauterbur in Magnetic Resonance Microscopy,pp. 3-27, VCH Publ. (1992).
7. H. D. Morris, W. B.Hyslop, and P. C. Lauterbur, "Diffusion- Enhanced MRI Microscopy ",Proceedings of the Society of Magnetic Resonance 1,376 (1994) San Francisco USA.

Mechanically Detected NMR without Mechanical Springs

THOMAS GEILKE, SILKE WILLAMOWSKI, GÜNTHER NEUE

Physikalische Chemie, Universität Dortmund
44221 Dortmund

Mechanically detected Magnetic Resonance is an interesting technique which can be used for studying microscopic samples of solids. The basic idea is to detect small forces experienced by nutating spins in an inhomogeneous magnetic field. If the spins are irradiated on-resonance by constant rf, periodic nutation leads to small periodic forces which are able to excite mechanical resonance in a suitable tiny spring which holds either the sample or some magnetic material that interacts with the sample. Usually, for detecting vibrations laser interferometry is used as amplitudes of the oscillations are very small.

The disadvantages of the above procedure are the smallness of the spring and the interferometric detection of oscillations. The first makes it very difficult to handle the spring which is usually of the type that is also used in Atomic Force Microscopy. The second point leads to a fairly large extension of the apparatus and stability problems.

It is presented how these disadvantages can be avoided by using a magnetically suspended sample with a feedback loop which has the property of representing an electronic simulation of a spring. The design is drastically simplified and allows for a simple adjustment of resonance frequency and damping of the "spring".

Fast *q-space* imaging using line scan techniques.

D. van Dusschoten, J. van Noort and H. Van As
Wageningen Agricultural University
Dept. of Molecular Physics and Wageningen NMR Centre
Dreijenlaan 3, 6703 HA Wageningen, The Netherlands

One of the unique properties of NMR is its capability to quantitatively image fluid motion. This not only concerns the average movement of fluids per measuring unit, a voxel, but also the dispersion of the movement superimposed on the average motion. This can be achieved by *flow velocity imaging* and *q-space imaging* which, in fact are experimentally identical and are based on Pulsed Field Gradients techniques. *Q-space imaging* requires that the number of scans is a power of 2, the echo amplitude near the edges of the *q-space* is reduced to 0 and the maximum phase shift for the pfg-steps is less than π, in order to obey the Nyquist sampling theorem. These requirements lead to a very long experimental time when combined with *k-space imaging*. Therefore *q-space* has often been combined with projection imaging, but heterogeneity of the sample regurlarly complicates the interpretation of the results.

The combination of line scan imaging, where the slice selection direction of the 90 ° pulse is perpendicular to the slice selection of the 180 ° pulse, with pulsed field gradients, is a good solution to this problem. A line scan, with a resolution of 2x2x0.2 mm and a flow resolution of app. 50 μm/s, can be achieved within a few minutes even when measuring at 0.5 T.

In order to ensure phase coherence within the sequence and phase stability during the few minutes of the scan two precautions are necessary: 1. The frequency offsets of the rf pulses is always a multiple of 1 kHz. 2. The duration of these frequency offsets is always a multiple of 1 or 2 ms for both the 90° and the 180 ° pulses. When only one set of flow encoding gradients is used flow velocity can be quantitatively measured in real time with a time resolution down to 15 ms.

TECHNIQUES FOR SPATIALLY RESOLVED NMR OF MACROMOLECULAR MATERIALS

M. Klinkenberg, D. Hauck, G. Eidmann, P. Blümler, B. Blümich

Institute for Macromolecular Chemistry and Magnetic Resonance Center, RWTH, 52056 Aachen

Magnetic resonance can be exploited in different ways for the analysis of macromolecular materials. In materials research it is less the molecular structures which are of interest but more the correlation of macroscopic properties with molecular parameters and the spatial distribution of these properties.

At Aachen University of Technology (RWTH) a Magnetic Resonance Center *MARC* has been founded, which is devoted to the characterization of materials and catalytic processes by the whole spectrum of magnetic resonance methods, including liquid-state NMR, solid-state NMR, solid- and liquid-state NMR imaging, NQR, and EPR. The center is administered by the Department of Macromolecular Chemistry and operated jointly by the four departments of applied chemistry of the RWTH.

Currently three projects are being pursued for spatially resolved NMR of solid and soft matter. These are:

1) The characterization of spatial variations in molecular orientation and mechanical modulus in the vicinity of inhomogeneities and defects in strained elastomer bands. Spectroscopic 2D deuteron NMR imaging is used for mapping the direction of order and the degree of molecular orientation of deuterated butadiene oligomers incorporated in elastomers as spy molecules.

2) Imaging of time-dependent temperature gradients which develop in cylindrical, carbon-black filled SBR samples under dynamic-mechanical shear and compression.

3) A surface scanner is constructed for analysis of surface areas of large objects like airplane tires and liquids in swollen and porous materials. The principles of inside-out-NMR used in oil prospecting and of stray-field imaging are combined for localized relaxation analysis and subsequent parameterization of the echo decay.

Progress and perspectives in each of these projects will be reported.

Investigation of the dispersion in chromatographic columns by pulsed field gradient NMR

Ulrich Tallarek, Klaus Albert and Ernst Bayer
Institut für Organische Chemie, Universität Tübingen, Auf der Morgenstelle 18, D-72076 Tübingen

Georges Guiochon
Department of Chemistry, University of Tennessee, Knoxville, TN, 37996-1600 and Division of Chemical and Analytical Sciences, Oak Ridge National Laboratory, Oak Ridge, TN, 37831-6120

1. The structure of a chromatographic bed (the matrix being porous silica or a chemically modified one in a cylindrical column made of PEEK, 4.4 mm i.d.) is very complex. The particle size distribution has a finite width and consequently the formation of a homogeneous, regularly structured bed is impossible to achieve. The distance between particles varies widely across the bed and so does the average diameter of the channels which form between and around the particles. These channels are tortuous and constricted causing the distribution of linear velocities of the mobile phase across a column section to be chaotic, both in space and time. So what can we learn and extract from the solvent molecules' diffusive behaviour regarding structural features, how do they see and feel the barriers, geometrical arrangements of the porous silica matrix ? Pulsed field gradient (spin echo or stimulated echo) NMR (PFGNMR) allows the diffusive observation time to be varied very easily (independently from the gradient strength), thereby being the crucial experimental test for the presence and dimension of diffusive barriers. It could be shown that diffusion consists of inhomogeneous or anisotropic self diffusion with the echo attenuation being uniquely determined in the space of "dynamic displacements" (q space). The anisotropy most probably arises from restricted diffusion which is caused by barriers that are (locally at least) of a low dimensionality.

2. In a simplified version the column may be considered as being made up of a series of individual plates. The number of plates in a column of length L is N (also frequently called the efficiency of the column), so the height equivalent to a theoretical plate (HETP or H) is L/N and the ratio of H to d_p (average particle diameter) is called the reduced plate height h. The higher N is, the better will be the column for doing any separation. The plate heights defined in chromatography are related to the corresponding axial and radial apparent dispersion coefficients by the classical relationships :

$$D_{ap,a} = H_a\, u/2 = h_a\, \nu\, D_m/2 \qquad \text{and} \qquad D_{ap,r} = H_r\, u/2 = h_r\, \nu\, D_m/2$$

They permit the conversion of the apparent dispersion coefficients measured by PFGNMR (using the stimulated echo version) at different flow rates into reduced plate heights or conversely. ν is the reduced velocity or particle Peclet number $Pe = \nu = u\, d_p/D_m$, where u is the cross sectional average velocity and D_m the diffusion coefficient in the bulk mobile phase or diffusivity. The relationship between the axial and radial reduced plate heights and the mobile phase velocity is given by :

$$h_a = B/\nu + A\, \nu^n + C\, \nu \qquad \text{and} \qquad h_r = B/\nu + D$$

where A, B and C are numerical coefficients, function of the nature of the packing material used, of the analyte studied and of the homogeneity of the packed bed. D is a coefficient accounting for the contribution of eddy diffusion to radial dispersion. Axial and radial dispersion coefficients were measured independently as a function of the flow velocity of the mobile phase. The results are reported and compared to similar ones obtained by using conventional chromatographic techniques.

The Effects of Ultrasonic Cavitation on NMR Imaging

Derrick P. Green, Bruce J. Balcom, Department of Physics, The University of New Brunswick, P.O. Box 4400, Fredericton, New Brunswick, Canada, E3B 5A3.

Ultrasonic cavitation is well known to have pronounced chemical and physical effects in solution (1). The recent discovery of single bubble sonoluminescence has rekindled interest in the cavitation phenomena (2). We have recently shown that ultrasonic cavitation in a water phantom causes signal attenuation in a standard spin echo image (3). We have also shown that ultrasonic cavitation causes acoustic streaming in a water phantom which may be observed and quantified with a DANTE flow imaging sequence (4). In this work, we systematically examine the parameters which determine the signal attenuation and streaming.

Ultrasound experiments are performed using a 50 Watt piezoelectric transducer resonating at 31kHz. The transducer is directly coupled to a 5 cm I.D., 22 cm long, plexiglass tube filled with distilled water. The power and duration of sonication is electronically controlled using a Macintosh Centris 650 computer running the software program LabView. The NMR imaging hardware consists of a Nalorac 2.4 Tesla 32 cm horizontal bore superconducting magnet, a 20 cm self shielded gradient, a Tecmag S-16 console, and a Macintosh Quadra 950 running MacNMR.

In a standard experiment, we examine the signal intensity within a slice of the phantom as a function of time. With echo times of approximately 100 msec, the signal decreased by more than 75% with the ultrasound at full power. Upon cessation of ultrasound, signal recovered almost immediately. At very short echo times, the signal observed is independent of ultrasound treatment. The identical experiment performed at low field (8 MHz) with the same water phantom and ultrasound apparatus requires very long echo times (greater than 200 msec) in order to observe any change in signal intensity.

Acoustic streaming was examined using the DANTE flow detection sequence (5). Echo times in the imaging sequence were kept short so that no signal attenuation occurred. The delay following the application of the DANTE tag lines was varied to highlight flow. Using the DANTE sequence, acoustic streaming can be quantified and mapped out in three dimensions. Operation of the ultrasound transducer in the magnet did not diminish the S/N of the phantom image.

(1) K.S. Suslick (Ed.), *Ultrasound, Its Chemical, Physical, and Biological Effects*, VCH: New York, 1988

(2) L.A. Crum, *Physics Today*, September, 22 (1994)

(3) B.J. Balcom, and D.P. Green, Abstracts of the 36th ENC Conference, March 26-30, 1995

(4) D.P. Green, B.J. Balcom, Abstracts of the 3rd SMR Conference, August 19-25, 1995

(5) T.J. Mosher, and M.B. Smith, *Magn. Res. Med.*, **15**, 334 (1990)

Measuring the Progression of Foreign Body Reaction to Silicon Implants using *in vivo* MR Microscopy

LW Hedlund[1], M Neuman[2], CR Edwards[2], R Black[1], GP Cofer[1], and GA Johnson[1]

[1]Center for *In Vivo* Microscopy, Department of Radiology, Duke University, Durham, NC 27710
[2]Case Western Reserve University, Cleveland, OH

Implantable imaging coils offer two unique capabilities: 1) high resolution for imaging internal structures [1, 2], and 2) evaluating foreign body responses for testing of coating materials for biocompatibility and *in vivo* durability. In this study in rats, we coated imaging coils with sheet silicone and placed them in the neck to evaluate 1) the foreign body reaction *in vivo*, and 2) the coating's *in vivo* durability as a fluid barrier.

Coils were a bilayer of copper foil on a 6 μm Teflon substrate sandwiched between two 10 mil silicone sheets fused together using a silicone RTV adhesive. The coils outer diameter was 10 mm and the inner was 5 mm. The silicone extended beyond the copper foil. The coils were dimensioned to yield a resonant frequency in air of 4–6 MHz higher than the required 300 MHz for 7 T imaging. Under anesthesia, the common carotid artery (CCA) was exposed and the coil was inserted between the CCA and muscle and sutured in place. Rats were imaged 1, 7, 14, and 28 days after surgery using an external pick-up coil inductively coupled to the implanted coil [3]. *In vivo* imaging was done under isoflurane anesthesia and with cardiac gating. Scan-synchronous ventilation was used. Acquisitions (3DFT) were obtained with a TR of 400–600 ms, TE of 9 msec, and in-plane resolution was 32 μm. On the 28th day, animals were sacrificed by anesthetic overdose. The coil and adjacent tissues were removed enblock and formalin fixed. The fixed specimens were then reimaged. *Ex vivo* imaging was similar to *in vivo* imaging except in-plane resolution was 15 μm. Linear measurements were made using NIH Image software.

At 24 hrs after surgery, there was a diffuse, elevated signal intensity band between the silicone of the coil and adjacent subcutaneous tissue (SC side) and between silicone of the coil and rectus muscle (RM side). On the SC side, the boundary between the hyperintense band and adjacent tissue was thin and did not have a well-defined border. From 7 to 28 days, this hyperintense band developed a discrete border on the SC side. On both sides of the coil, this band was relatively homogeneous in signal intensity, and its thickness over this time tended to increase. By comparison to Day 1, the thickness of the SC band increased 146%, by Day 28, and the RM band increased 51%. The thickness of the coil's silicone barrier changed no more than ±3% over 28 days. Its thickness was about 510 μm. The integrity of the silicone barrier in half of the animals was maintained for the full 28 days. In the others, the silicone barrier failed for unknown reasons, as indicated by the presence of copper corrosion products, and so the coils could not be used for imaging.

The band of hyperintensity immediately adjacent to the silicone on Day 1 may represent a transitory inflammatory reaction. On subsequent days, the more discrete and well-defined hyperintense band becomes, we believe, the tough, fibrous capsule found four weeks later. The internal architecture of this band on the later days was relatively uniform and no clear structural detail could be detected. We conclude that MR microscopy with implanted coils is a useful tool for evaluating the deposition of the foreign body fibrous capsule and for determining the degree of bio-stability of the capsule and the "foreign body" reaction.

1. T. H. R. Farmer, G. P. Cofer, G. A. Johnson, Maximizing contrast to noise with inductively coupled implanted coils. *Invest. Radiol.* **25**, 552-558 (1990).

2. L. Arnder, X. Zhou, G. Cofer, G. Mills, L. Hedlund, G. Johnson, Magnetic resonance microscopy of the rat carotid artery at 300 MHz. *Invest. Radiol.* **29**, 822-826 (1994).

3. R. M. Summers, L. W. Hedlund, G. P. Cofer, M. B. Gottsman, J. F. Manibo, G. A. Johnson, MR microscopy of the rat carotid artery after balloon injury using an implanted coil. *Magn. Reson. Med.* 33, 785–789 (1995).

Acknowledgments: This work supported in part by NIH grant #P41 RR05959 and ERC grant #CDR-8622201.

In-Vivo Application of NMR Microscopy on the Human Body Using a SQUID-Based Amplifier

J. Constantin Széles[1,2], Sándor Mészáros[3], Udo Losert[4], Peter Polterauer[1] and Ernst Wolner[2]

1) Surgical Clinic of the University of Vienna, Department of Vascular Surgery; A-1090 Vienna, Austria.
2) Surgical Clinic of the University of Vienna, Department of Heart and Thorax Surgery; A-1090 Vienna, Austria.
3) Institute of Nuclear Research, PO Box 51; H-4001 Debrecen, Hungary.
4) Center for Biomedical Research at the University of Vienna; A-1090 Vienna, Austria.

ABSTRACT

NMR Microscopy has been used in initial experiments towards viewing microscopic structures on the extremities of the human body. For the initial experiments, a spatial resolution of about 100μm was obtained (*in-vivo*) on the finger which was placed into the bore of a high-field magnet. Detailed images of the layers of the skin and anatomical structures were obtained, and explanations of the findings are presented. The results suggest that NMR Microscopy (NMRM) is a viable approach towards the *in-vivo*, non-destructive examination of micro-anatomical structures of the human body, hence opening a wide area of potential clinical applications.

The task following the initial results has been to manipulate the equipment in order to obtain the best results possible. Conventionally, the sensitivity (spatial resolution) of NMR Microscopy is improved by using high bias fields and strong gradients. Nevertheless, a detection method with frequency independent sensitivity high resolution is also expected using low fields. The principle of this alternative method is the detection of the static magnetic moment change with a Superconducting Quantum Interference Device (SQUID)-based sensor for biomagnetic measurements. The SQUID is not restricted by a bore, which creates a larger field of view as well as freedom of movement to access various parts of the body when combined with NMRM. The simultaneous presence of active biomagnetic and resonance signals and their separation needs to be taken into consideration when using this method. Furthermore, the presence of noise, and the problem of selective detection of resonance signals will be discussed. Results obtained using an experimental arrangement are presented.

Imaging Paramagnetic Solids by STRAFI

E. W. Randall,[1] A.A. Samoilenko[2] and T. Nunes[3]

1 Chemistry Department, Queen Mary & Westfield College, London E1 4NS, England
2 Institute of Chemical Physics, Russian Academy of Sciences, 117977 Moscow, Russia
3 ICTPOL/IST, Av. Prof. Gama Pinto 2, 1699 Lisboa Codex, Portugal

In the limit of **the high field gradient approximation**, which pertains in the Stray Field Imaging (STRAFI) method,* we show that imaging of materials with very small values for T2 is not a problem. Examples included here are: crystalline inorganic, diamagnetic and paramagnetic hydrates and acetylacetonate complexes; and the crstalline organic free radical, diphenyl picryl hydrazyl mono-hydrate. Relaxation weighting allows discrimination between different parts of the phantom, and one may envisage the production of localised diffusion maps, at even extremely slow diffusion rates.

---

* A.A. Samoilenko, D.Yu. Artemov, L.A.Sibeldina, *JETP Lett.*, 47, 417 (1988).

Stray Field Imaging (STRAFI) Studies of the Ingress of Polymer Treatment Coatings into Porous Building Materials

S. Black[a], D.M. Lane[a], P.J. MacDonald[a], D.J. Hannant[b], M. Mulheron[b], G. Hunter[c], and M.R. Jones[d]

Departments of Physics[a] and Civil Engineering[b],
University of Surrey,
Guildford, Surrey GU2 5XH, UK

Departments of Chemistry[c] and Civil Engineering[d],
University of Dundee,
Dundee DD1 4HN, UK

Nearly all environmental degradation of cementitious and porous ceramic bulding materials, whether physical as in freeze-thaw, chemical as in sulphate attack, or diffusive as in ion-diffusion, is ultimately traceable to water transport within the pore structure of the material. Control of water tansport into and out of building materials is therefore of major economic significance and much emphasis is now placed on treatments which involve the application of hydrophobic or other surface polymer coatings. Indeed, many regulatory authorities require such treatments as a matter of course, despite the current lack of understanding of the dynamics of either the application procedures or the movement of water within the treated material.

In principle, liquid MRI can spatially and separately map unbound water and organic liquids absorbed by cementitious materials; in practice, very broad spectral lines ($T_2 \geq 10\ \mu s$) are observed as the result of incompletely-averaged internuclear dipole-dipole interactions, of large variations in magnetic susceptibilty across pore surfaces, and (particularly) from very rapid relaxation caused by high concentrations of paramagnetic metal ion impurities. Stray Field Imaging (STRAFI) can overcome broad resonance lines, permitting high resolution imaging of solids and of confined, and paramagnetic, liquids[1,2,3]. This paper descibes the application of STRAFI to map not only the spatial distribution of a surface treatment (alkyltriaryloxysilane) of a mortar sample (sand and Ordinary Portland Cement), but also to follow by time-course experiments the diffusion dynamics of the treatment solution entering the mortar surface.

Acknowledgement.- We thank the UK Engineering and Physical Sciences Research Council for financial support.

[1]A.A. Samoilenko, D.Yu. Artemov, and L.A. Sibel'Dina, *JETP Lett.*, **47**, 1988, 417.
[2]K.L. Perry, P.J. MacDonald, E.W. Randall, and K. Zick, *Polymer*, **35**, 1994, 2744.
[3]T.B. Benson and P.J. MacDonald, *J. Magn. Reson., A*, **112**, 1995, 17.

The use of High Power RF Excitation Pulses for Slice Selection in Solids Imaging

K. Carlton
Science Dept, Canterbury Christ Church College, Canterbury, CT1 1QU, UK

M.R.Halse and J.H.Strange
Physics Laboratory, University of Kent, Canterbury, CT2 7NR, UK

High power RF excitation transmitter pulses are required in the imaging of solids. Class A amplifiers are conventionally used for slice selection to effect the necessary sinc function modulation of the RF envelope. Not only are these amplifiers expensive but at high powers shaped pulses can suffer from distortion due to non linearity of transmission to the sample coil. The existence of non-linear crossed diodes in the transmitter/receiver coils, for example, make accurate representation of shaped pulses difficult. On the other hand class C amplifiers are simpler and cheaper but are they are not able to modulate the signal. We are seeking to produce a slice selection technique for the imaging of solids using a class C amplifier. Early attempts to reproduce the effects of the sinc function envelope using pulse density modulation of short, powerful pulses of uniform amplitude produced a good profile in the selected region but unfortunately suffered from serious problems due to sidebands. We have recently improved the technique, however, and have produced much better results with very much weaker sidebands. The latest results produce significant improvements over the use of a single hard 90 degree pulse. In addition this technique does not require any refocussing which means that it can be used for slice selection with sinusoidal gradient methods. In essence one of the techniques involves collecting a data set using a 180 pulse in the presence of a slice select gradient and following this with a non selective 90 pulse. A second data set is obtained using a 180 without a gradient followed, once again, by a non selective 90. The two sets of data are subsequently subtracted to form a single set from which an image is obtained.

PLANE SELECTION IN THE INDIRECT MARF SOLID STATE IMAGING

F. DE LUCA, N, LUGERI, S. MOTTA, G. CAMMISA and B. MARAVIGLIA
Dipartimento di Fisica, Università "La Sapienza", 00185 ROMA, Italy

In the past few years, we have been performing an Indirect Magic Angle in the Rotating Frame (*I-MARF*) solid state imaging technique based on the Lee-Goldburg line narrowing sequence [1], recently extended to a T_2 weighted image analysis, entirely based on post-processing of the acquired experimental data [2].The main characteristic of the method is the rather easy experimental set-up, and in the new application that we now propose, slice selection becomes feasible, by the simple insertion of a DC gradient.

In the MARF imaging method, the dipolar contribution to the linewidth is drastically reduced by the transformation to the Tilted Rotating Frame (TRCF), with the "magic" tilt angle given by $\theta_M = 54°44'$. When the magic angle condition $\frac{B_1}{\Delta\omega} = \frac{1}{\sqrt{2}}$ is "broken" in the Y direction, by a selection gradient $G_S = \frac{\partial B_0}{\partial Y} \neq 0$, the full line-narrowing effect can survive just in the neighborhood of a certain Y_0 which represents the position of the selected plane, that can be imaged by the usual projective procedure by the "Magic Angle conserving" effective field gradient in a direction perpendicular to Y.

The effects of this selected mismatching can be estimated by the espression of the second moment of the narrowed line [1]

$$\left[\Delta\omega_{TRCF}(Y)^2\right]^{1/2} = \left|\frac{1}{2}(3\cos^2\vartheta(Y)-1)\right|\left[\Delta\omega(Y)^2_{LAB}\right]^{1/2} \qquad (1)$$

where $(\Delta\omega)^2_{LAB}$ is the second moment in the Laboratory Frame.

Assuming a gaussian shape for the NMR line of the solid, each plane at *Y* ideally contributes to the overall spectrum with a gaussian, that is "amplitude and width modulated" by both the nuclear magnetization in the plane and the narrowing efficency, as determined by the value of ϑ *(Y)* in that plane.

We have tested the validity of this idea by the numerical evaluation of the effect of a linear gradient along Y, and superimposing each plane's contributions along the whole sample, so as to obtain a straightforward "image" of the selectivity of the method. The calculations have shown that the contribution of the desired slice is completely retained, and well distinguishable from the "baseline" generated by the rather rapidly falling-off of the "out-of-magic" planes.

One-dimensional profiles of different slices on test phantoms made of intermediate bandwidth solids and rigid polymers (Adamantane and Polyethylene) have proven the feasibility of the method, which then may represent a valuable tool for a more detailed investigation of solid systems of practical interest.

Bibliography

[1]- M. Lee, W.I. Goldburg, Phys. Rev., 1965, **140**, 1261

[2]- F De Luca, N. Lugeri, S. Motta, G. Cammisa and B. Maraviglia, J. Magn. Reson. Series A, in press

Primary Echoes in High Field Gradients

E. W. Randall,[1] A.A. Samoilenko[2] and T. Nunes[3]

1 Chemistry Department, Queen Mary & Westfield College, London E1 4NS, England

2 Institute of Chemical Physics, Russian Academy of Sciences, 117977 Moscow, Russia

3 ICTPOL, Av. Prof. Gama Pinto 2, 1699 Lisboa Codex, Portugal

High order primary Hahn echoes where reported first for the case of solid ^{3}He for which about forty echoes were recovered.[1,2] We will show that multiple primary echoes can be observed from either solids, including paramagnetic solids for which T_2 values are particularly short, on the one hand, or from liquids for which diffusion is very fast on the other, by use of high static gradients in the fringe field of a superconducting solenoid. These experiments provide a new and convenient tool to mesure the self-diffusion constant, especially the very small ones in solids, if the spin-spin relaxation time is already known.

References

1. M.Bernier and J.M. Delrieu in Magnetic Resonance and Related Phenomena, *Proc. XIXth Congress Ampere* Heidelberg (ed. H.Brunner, K.H. Hausser, D. Schweitzer), Groupement Ampere, Heidelberg (1976).
2. G. Deville, M. Bernier and J.M. Delrieu, *Phys. Rev. B*, 19, 5666 (1979).

Determination of the Spatial Distribution of Water in Textile Materials

Karl.-F. Elgert

DITF, Institut für Textilchemie, Körschtalstr. 26, D-73770 Denkendorf,

Introduction

Many processes in manufacturing textiles (e.g. washing and dyeing) are performed in heterogenous systems. Porosity plays an important role and even minor deviations from preset process parameters might cause unusable products. Deviations from a homogenous distribution of the polymer in textile materials as fabrics, cops, yarns, knittings etc. are believed to cause anomalous dyeing and washing effects. The result of mass transfer in heterogenous systems like textile materials depends in patricular wether fast or slow exchange conditions prevail. One special problem which arises is to characterize the construction, structure and porosity of the material before and after processing without its destruction.

Materials and Methods

A possible way to overcome theses problems and to understand the effects of porosity and fluid flow in porous textiles is to apply NMR imaging to the determination of the spatial distribution of polymer and water. We used a typical coil of cotton yarn of 160 mm diameter, 150 mm length and an inner tubing of 50 mm diameter. The dimensions of interest are ranging from 20 to 200 µm. This assambly has been used as an example for the uptake of a dyeing fluid as well as for the characterisation of the construction and porosity in a partly dried state. We placed samples of different geometry and wetting state in an Bruker 0.5T TOMICON and observed the fluid uptake over periods up to 20 min. Gradient echo techniques as well as spin echo sequences have been applied. The edge length of the detected voxels were 300 µm. The following reconstrustion to a 3-dimensional view of the data set was done by image processing.

Results and Discussion

The method enabled us for the first time to describe the spatial distribution of water and polymer in the textile samples under study. Especially important views into the inside of the coil of cotton yarn could be reached. Parts of different polymer density as well as the inner contours of the coil and the canal system were found to give new important views. Segmentation allows the identification of all relevant coil parameters, its dimensions, the local density of the polymer and the dimensions and outlets of the tubing. The spatial extent as well as deviations from the random structure and the density distribution of the coil windings of different density can be minutely described and visualized.

Additionally, the behavior of the coil under flooding by water has been analyzed. From the results of these experiments it can be concluded that the water invades first the parts of high permeability and remains longer under drying in the parts of high polymer density by capillarity. These preliminary results show that the great advantage of this method is the opportunity to a non invasive and accurate measurement of the inner structure of textile materials.

Conclusions

We demonstrate a general application of nmr imaging to textile materials. The study demonstrates that nmr microimaging aided by image processing with the possibility of generating sections in every plane of interest can be widely used in textile research.

Typical images and section planes will be presented.

Single Point Imaging of Partially Dried, Hydrated White Portland Cement

Mircea Bogdan[1], Bruce J. Balcom[1], Robin L. Armstrong[1], Theodore W. Bremner[2], Department of Physics[1] and Department of Civil Engineering[2], The University of New Brunswick, P. O. Box 4400, Fredericton, N.B., Canada, E3B 5A3.

Moisture content in concrete has a major influence on the durability and mechanical properties of the material during its service life (1). Knowledge of the moisture distribution in drying concrete is of paramount importance given the ubiquitous use of concrete as a construction material. We are studying the drying of hydrated white Portland cement as a model for the more complicated concrete system.

Traditional spin echo imaging methods are ill suited to examining water content in hydrated white portland cement because of the short spin-spin (T_2^* = 170 μsec, T_2 = 320 μsec) and spin lattice relaxation times of this system (T_1 = 1.2 msec). Single Point Imaging (SPI) relies on the application of a broad band RF pulse in the presence of a variable amplitude phase encoding gradient(s) with sampling of a single point on the resulting free induction decays a fixed period of time after excitation. SPI was recently shown to be more sensitive than conventional spin echo imaging if the gradient ramp time is longer than spin-spin relaxation (2). This is the case for the cement specimens. Because of the short T_1 of the cement samples, the SPI sequence may be run with a short repetition time to sample k space and signal average in a relatively short time period. We sample k space only in the z direction to acquire longitudinal profiles of the drying cement cylinders. The phase encoding time was 290 μsec with a repetition time of 50 msec; the pulse flip angle was 13°. Resolution was 0.7 mm. 3D imaging is possible but does not provide additional information for these samples.

White Portland cement cylinders (5 cm in length and diameter), open to the atmosphere at one end, were dried under ambient conditions for a period of one month. Over this time period water content decreased by 35% but the measured relaxation times did not change. A short T_2 component associated with water chemically bound to calcium in the cement is present (3) but unobservable in our experiments. The time series of SPI profiles represent true maps of relative proton density and clearly show capillary flow in the early stages of drying followed by a slower diffusion controlled process.

References:

(1) J. A. Hanson *ACI Journal* **65**, 535, (1968).
(2) S. Gravina and D. G. Cory *J. Magn. Reson. B* **104**, 53, (1994).
(3) W. P. Halperin et. al. *Magn. Reson. Imaging* **12**, 169, (1994).

Evaluation of the Drying Process of the Finnish Milled Peat Using NMR Microscopy

J. Taivainen[a], J. Timonen[a], L. Alvila[a], T.T. Pakkanen[a] and K. Hänninen[b]

[a]Department of Chemistry, University of Joensuu, P.O. Box 111, FIN-80101 Joensuu, Finland
[b]Technical Research Centre of Finland, VTT Energy, FIN-40101 Jyväskylä, Finland

Peat is a complex mixture of organic material formed under a specific natural humus formation. Economically the most essential usage of peat is combustion in heating and power plants. For optimal drying procedure the state and amount of adsorbed water is important, but not yet specifically known. In the typical chemical analysis the peat is extracted to several fractions [1], and these fractions are investigated with different nondestructive spectroscopical and degradative chemical methods [2].

For these studies the milled peat was fractionated in four operational fractions: bitumen, fulvic acid, humic acid and humin [3]. The characteristics of drying of milled peat and its two subfractions, humic acid and humin, were investigated by means of ^{1}H-NMR microscopy. Experiments were performed on a Bruker AMX-400 spectrometer equipped with a standard microimaging accessory. Imaging was executed using a single slice spin echo method on pelletized, moistened samples under continuous air flow. The amount of water was estimated from the total intensity of ^{1}H-signal.

Spatially drying proceeds from the outer borders of the pellet leaving a uniform distribution of water in the moist area of the sample. Some of the peat fractions, especially humic acid, contain large amounts of paramagnetic species, which have an strong effect on both imaging and the estimation of the amount of water. The loss of moisture during drying follows a logaritmic model, and differences between the drying rates of the peat and the subfractions are noticed.

References:

1. Fuchsman, C. H. *Peat Industrial Chemistry and Tecnology*, Academic Press, New York, 1980
2. Stevenson, F. J. *Humus Chemistry*, John Wiley, New York, 1982
3. Hänninen, K. Phenolic Acids in Humus Chemistry, *Ann. Acad. Scient. Fennicae A II.Chemica*, 213, 1987

Visualization of Non-Viscometric Behaviour of a Compressible Paste in Couette Flow with MRI

J. Götz[#], W. Kreibich[&], M. Gelbert[#], M. Peciar[%], J. Zachmann[#]

[#] Institut für Mechanische Verfahrenstechnik und Mechanik, University of Karlsruhe, Germany
[&] BRUKER Medizintechnik GmbH, Ettlingen, Germany
[%] Strojnicka fakulta, Slovenska Technicka Univerzita Bratislava, Slovak Republik

Introduction:

In addition to those for medical applications, the advantages of Magnetic Resonance Imaging (MRI) for non-invasive investigations in materials, resolved in space and time, are becoming more and more apparent (1). The importance of obtaining a temporal series of images (movie) can be seen in the case of a Couette flow (flow between concentric cylinders, the inner of which is rotating).
"NMR imaging (can be) used to measure the concentration and velocity profiles during the demixing of initially well-mixed suspensions" (2). In their article (2), Abbot et al. describe an irreversible radial particle migration in (viscous) Newtonian suspensions, caused by non-uniform shear rates. When the rotational speed of the inner cylinder is increased, Kose (3) found a transition from circular to vortex flow, which can even become wave-like. Our MRI study of a flowing compressible paste shows a different kind of chaotic and non-viscometric behaviour within a Couette experiment. Viscometric flows are flows with a known distribution of strain independent of the material. Common experiments in rheology are pipe flow, flow between two plates and Couette flow.

Materials and Methods:

The experiments were performed on a BRUKER Biospec BMT 24/40 with a 40 cm bore and a proton resonance frequency of 100 MHz. The system was fitted with a gradient insert possessing an inner diameter of 120 mm and a maximum gradient strength of 188 mT/m. The RF resonator had an inner diameter of 72 mm.
NMR parameters of the spin echo experiments were matrix 256^2, FOV 5 cm, ST 2 mm, TE 10 ms. The recovery time of 100 ms and two averages resulted in imaging times of 2 min 36 sec.
The concentric Couette cylinders, with a hollow space between diameters of 20 and 40 mm, were constructed entirely of PVC (length 450 mm). This gap was filled with a Teflon (Hostaflon® TF 1750, Hoechst AG) paste with a particle size of 20 μm.

The relative moisture was 70% at the start of the experiments which comprised manual rotation of the inner cylinder with the outer cylinder at rest. In order to establish good contact between the inner cylinder and the paste, the surface of the inner cylinder had a saw-tooth profile.

Results:

After a certain number of rotations, the images clearly show the occurrence of spherical agglomerations between the inner cylinder and the main part of the paste. This is accompanied by a decrease in the thickness of the paste filling. In the paste filling, no shear deformation can be observed. The thickness of the shear zone is probably less than the actual image resolution.

Conclusion:

Compressible Teflon pastes are characteristic of many industrially relevant materials. MRI experiments can provide important contributions towards a deeper understanding of the structural changes and flow processes of such materials. The experiments presented clearly show the possibility that, in certain cases, flowing pastes in a Couette flow cannot be described with help of „simple" continuum mechanics. The latter is a prerequisite for evaluating traditional Couette experiments, where only the torque necessary to turn the inner cylinder is measured. The experiments show that the prerequisite homogeneity and wall adhesion may not be achieved in the case of pastes.

References:

(1) Gladden, L. F.:Industrial Applications of NMR Imaging, *Proc. ECAPT'94*, 466 (1994)
(2) Abbot, J. R., et al.: Experimental observations of particle migration in concentrated suspensions: Couette flow, *J. Rheol.* 35, 773 (1991)
(3) Kose, K.: Spatial mapping of Velocity Power spectra in Taylor-Couette Flow Using Ultrafast NMR Imaging, *Phys. Rev. Letters* 72, 1467 (1994)

Determination of Local Fluid and Solid Concentrations of a Compressible Paste flowing in a Ram Extruder with ^{1}H- and ^{19}F- MRI

W. Kreibich[&], J. Götz[#], M. Gelbert[#], M. Peciar[%], H. Buggisch[#]

[&] BRUKER Medizintechnik GmbH, Ettlingen, Germany

[#] Institut für Mechanische Verfahrenstechnik und Mechanik, University of Karlsruhe, Germany

[%] Strojnicka fakulta, Slovenska Technicka Univerzita Bratislava, Slovak Republik

Introduction:

Magnetic Resonance Imaging (MRI) enables non-invasively and time-dependently the detection and quantification of structure and structural changes of products. Thus MR imaging can be used for the optimization of product properties and processing operations (1). One example of such processes is the extrusion of non - compressible pastes (2). In the case of a three phase system (compressible paste) containing fluid, solids and air simple proton density imaging does not provide sufficient information. A decrease in proton density can result either from an increase in the local porosity (i.e. solid particles pushing water molecules away) or from an decrease in the degree of saturation (i.e. air replacing water). These quantities can be calculated if the local concentration of the solid is also known.

The goal of our study was to determine during the extrusion of a compressible paste

- the local concentration of the fluid
- the local concentration of the solid
- •• calculated local porosity values and
- •• calculated local saturation values.

Materials:

The experiments were performed on a BRUKER Biospec BMT 24/40 with a 40 cm bore and 2.4 T field strength. The system was fitted with a gradient insert (inner diameter 120 mm, maximum gradient strength 188 mT/m). The RF volume coil (inner diameter 72 mm) was double tuned to resonate with ^{1}H and ^{19}F nuclei.

A Teflon (particle size 20 µm) - water paste (70% relative moisture) was extruded in a ram extruder (length 400 mm, inner diameter 40 mm; constructed entirely of PVC) through a die of 23.3 mm diameter.

Methods:

- Determination of the local concentration (c_F) of the fluid (water) by acquiring proton density spin echo images
- Determination of the local concentration (c_S) of the solid (Teflon) by acquiring ^{19}F images using the Single Point Imaging (SPI) method (3) implemented recently.
- •• Calculation of the local porosity $\varepsilon = 1 - c_S$ and
- •• the local saturation $S = c_F/(1-c_S)$.

Experimental Discussion:

- **^{1}H-MRI:** The spin echo imaging experiments were performed with two sets of parameters (matrix 256^2, FOV 6 cm, TE 10 ms) and (matrix 64^2, FOV 10 cm, TE 4 ms), respectively.
- **^{19}F-MRI:** It is not practical to measure independently the concentration of a proton-containing solid (short T_2) and the concentration of a proton-containing fluid (long T_2), especially when there is the possibility of a part of bound water (short T_2).

Teflon pastes were selected because such solids contain fluorine and no hydrogen, while the opposite is true for the fluid (water), thus enabling one to measure solid and liquid concentrations independently. Teflon pastes are characteristic for many industrially relevant materials and are themselves used for extrudates and coatings.

^{19}F nuclei in solid Teflon have a T_2^* of about 80 µs, which is far too short to be detected with standard imaging techniques. The SPI technique (3), also called Constant Time Imaging (4), does not require gradient switching between excitation and signal detection. Therefore this detection time (which corresponds to the echo time of spin echo experiments) can be set as short as 40 µs for acquiring ^{19}F images of the solid Teflon. Performing 240 averages of a 45^3 acquisition matrix (reconstructed as 64^3) resulted in a total imaging time of about 12 hours.

Results and Discussion:

When starting the extrusion, one firstly observe water pressed out of the paste and flowing out of the die. In conjunction, the solid's content is increased and relative dry regions form in the dead zones. In the extrudate, bright lines appear, which represent fissures (water filled cracks). Also dark cavities can be seen (air filled cracks), which are known as "shark skin". The existence of these cracks is a significant problem, since such extrudates are worthless. Directly before the die, both the water and the solids concentration is decreased in comparison to the interior. This fact must be interpreted as expanded air.

- •• Quantitative results with calculated local saturation and
- •• porosity values will be published.

References:

(1) Gladden, L. F.:Industrial Applications of NMR Imaging, *Proc. ECAPT'94*, 466 (1994)

(2) Götz, J., Buggisch, H., and Peciar, M.:NMR imaging of pastes in a ram extruder, *J. Non-Newtonian Fluid Mechanics* 49, 251 (1993)

(3) Nauerth A. and Gewiese B.: SPI - Single Point FID Imaging, MRI with echo times < 50 µs, *Proc. SMRM 12th meeting*, 1215 (1993)

(4) Gravina, S. and Cory, D. G.: Sensitivity and Resolution of Constant-Time Imaging, *J. Magn. Reson. B* **104**,53 (1994)

A Simple Method for Reducing Diffusion Effects in MR Microscopy

V. Mlynárik, A. Degrassi and R. Toffanin
POLY-biós Research Centre and POLY-tech Coop. r.l., Area Science Park,
Padriciano 99, I-34012 Trieste, Italy

Molecular diffusion in the presence of imaging gradients strongly attenuates the transverse magnetization in MR microscopy (1,2). Resulting images have then a diffusion-weighted contrast. Using the common spin echo imaging sequences with the read refocusing and the phase encoding gradients in the first half of the echo time, the degree of attenuation due to molecular diffusion depends on the echo time. Evaluation of the T_2 values and T_2 maps from a series of images measured with different echo times is thus impossible.

Haase and co-workers (3) suggested a method for eliminating the diffusion effects which utilises a magnetization-preparing pulse sequence prior to the imaging sequence. We have developed a simple alternative to this method. In the standard spin echo sequence, the read refocusing and the phase encoding gradients are applied immediately before the acquisition. The effects of diffusion are then minimal and independent of the echo time (4). The proposed sequence can be also combined with the Carr-Purcell-Meiboom-Gill pulse train.

The straightforward testing of our method is complicated by the fact that the magnetization preparation method and the proposed method use 90° and 180° pulses, respectively, for slice selection. We therefore carefully adjusted parameters for the slice selection to obtain exactly the same slice thickness with the both methods.

Examples of T_2 weighted images and T_2 maps demonstrate that the T_2 values measured by the proposed technique are similar to those obtained with the magnetization-preparing pulse sequence. In addition, there is a slight gain in sensitivity which is in accordance with the theoretical calculations.

References

1. M. Brandl, A. Haase, *J. Magn. Reson. B* **103**, 162-167 (1994).
2. P. T. Callaghan, L. C. Forde, C. J. Rofe, *J. Magn. Reson. B* **104**, 34-52 (1994).
3. A. Haase, M. Brandl, E. Kuchenbrod, A. Link, *J. Magn. Reson. A* **105**, 230-233 (1993).
4. V. Mlynárik, A. Degrassi, R. Toffanin, O. Jarh, F. Vittur, *Magn. Reson. Med.*, submitted for publication.

THE NARROW-PULSE CRITERION IN PGSE DIFFUSION MEASUREMENTS

A. Caprihan, E. Fukushima, and L. Z. Wang
The Lovelace Institutes
2425 Ridgecrest Dr., SE
Albuquerque, NM 87108 USA

We derive a criterion for the applicability of the commonly used narrow-pulse expressions for the signal attenuation in PGSE diffusion experiments from two different approaches. In the first, we start from a general expression, for example, by Stepisnik, for the attenuation caused by diffusion in the presence of magnetic field gradients. We calculate the fractional contribution F to the attenuation from that part of the PGSE sequence with the gradients on; we then plot contour lines of constant F in the parameter space defined by $\delta D/a^2$ and $\Delta D/a^2$ which are durations of the gradient and of the interval between the gradient pulses, respectively, in units of the average time a^2/D for a molecule to diffuse across a restricted space of dimension a. The narrow-pulse approximation will hold wherever F is small. In the second approach, we begin from the computer simulations by Blees who calculated attenuation as a function of the gradient amplitude g and plotted it against $qa=\gamma\delta ga/2\pi$. Because the successive minima of attenuation as a function of qa will occur at multiples of unity only for truly narrow pulses, we use the deviation from the narrow pulse values for qa as a measure of the departure from the narrow pulse limit. The contour lines of constant fractional deviation of signal minima from their narrow pulse values as a function of $\delta D/a^2$ and $\Delta D/a^2$ are geometrically similar to those of F. In both cases, sufficient conditions for the applicability of narrow-pulse expressions are more stringent than is usually supposed. For example, an arbitrary requirement that $F<<0.1$ is equivalent to a 5% shift in the second minimum position in qa. Although neither of these conditions seems very strict, they lead to the conclusion that gradient pulse duration δ must be much shorter than $0.02D/a^2$ in order for the narrow pulse expressions to be valid.

Abstract for Würzburg meeting; 8/95.

Aspects of Diffusional Enhancement in NMR Microscopy

Paul C. Lauterbur, W. Brian Hyslop, H. Douglas Morris,
John J. Lee, Nian Yang and Carl D. Gregory
Biomedical Magnetic Resonance Laboratory
University of Illinois at Urbana-Champaign
1307 West Park Street
Urbana, Illinois 61801 U.S.A.

Diffusion can be used to enhance signal intensity effects from small structures in microscopic magnetic resonance imaging by recruiting new spins into a perturbed region and then measuring the total effect, such as saturation, over a larger volume. We call this general scheme DESIRE, for Diffusional Enhancement of Signal Intensity and REsolution. Simulations and analytic calculations of enhancement factors, which can reach many orders of magnitude, have been carried out and are being compared with experimental results, using several methods. We anticipate that, in favorable circumstances, it will be possible to obtain useful 3D image resolution comparable to that of visible light microscopy. Current experimental and theoretical results will be presented. The figure below shows an experimental test of the consistency of 1D amplification in a static gradient and a comparison with theory.

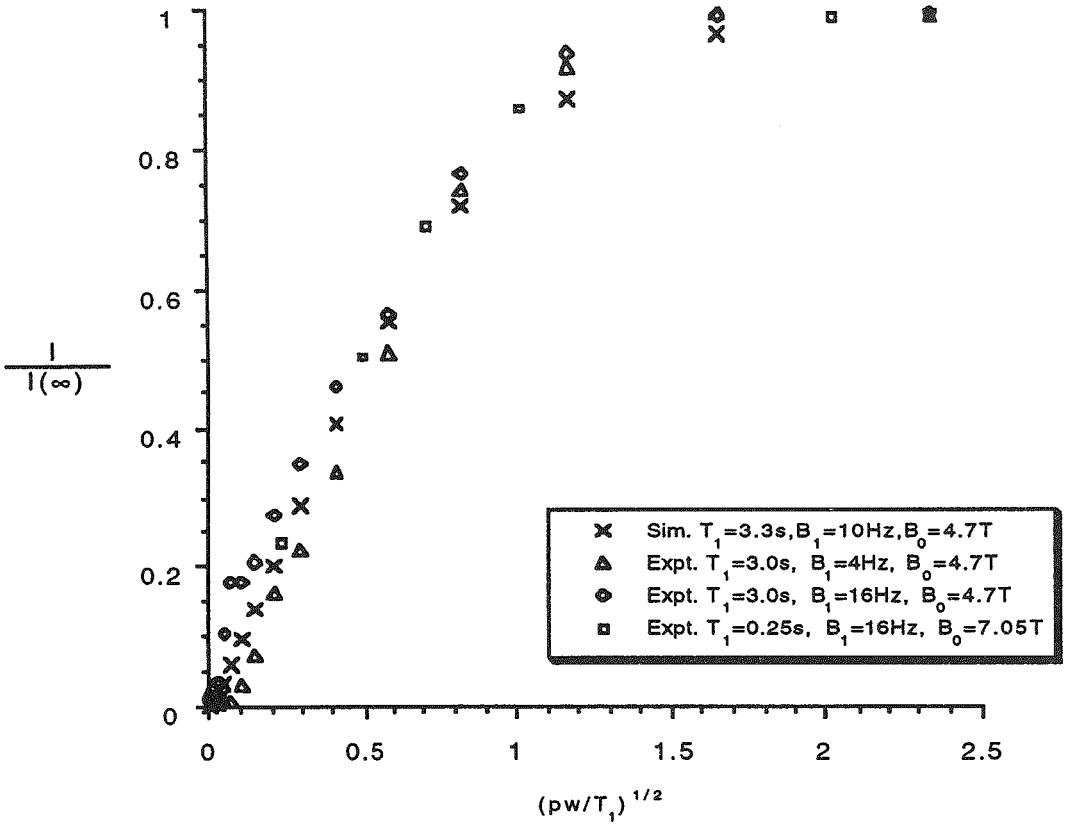

The normalized one-dimension gradient-localized DESIRE amplification function. Pulse width (pw) is the length of time the saturating pulse is applied. Note that experiments and simulations agree over a range of more than an order of magnitude in T_1 and for several values of other variables.

A Pulse Sequence for Rapid Determination of the Anisotropic Diffusion Tensor

V. Gulani*, J. S. Shimony*, G. A. Iwamoto #, P. C. Lauterbur*
* Biomedical Magnetic Resonance Laboratory, # Department of Veterinary Biosciences, University of Illinois at Urbana-Champaign, Urbana, IL 61801

Introduction

Diffusion tensor mapping has been accomplished on phantoms, *ex vivo* animal brains and tissue, and *in vivo* human brains (1). Current sequences used to map the diffusion tensor all require the collection of separate diffusion weighted images for each direction, and thus also long experiment times (1,2). To decrease the time required to make diffusion tensor measurements, we have developed the pulse sequence diagrammed below. For samples exhibiting axial symmetry, the sequence utilizes a single 90 degree pulse followed by four 180 degree pulses to obtain four echoes, each contributing to a different image, each with diffusion weighting in a different direction. This sequence allows a four-fold reduction in the time required for diffusion measurements over conventional methods. For general samples the sequence has been expanded to obtain the six measurements needed to fully characterize the anisotropic diffusion tensor. In addition, a $1/T_2$ map can be obtained from the same data set. We have tested this sequence on water phantoms, on celery, and on excised rat spinal cords.

Methods

All diffusion coefficient measurements were performed on a Varian MR-500 Spectrometer (11.7 T, 51 mm bore) equipped with a DOTY Scientific micro-imaging probe (5 mm maximum sample size). The sequence depicted below was implemented and extensively tested. Each of the four echoes shown contributes to a different image. The gradient pulses are applied in the following four orientations: $(G_{dx}, G_{dy}, G_{dz}) = G_0$ {(1, 0, 0), (0, 1, 0), (0, 0, 1), (1, 1, 0)}. Echoes from each orientation are collected sequentially as depicted and the diffusion gradients are then updated. This process is repeated until all diffusion weighted echoes have been collected (for a given phase encoding step). The phase encoding gradient is then updated, and the above process is repeated until all phase encoding steps have been collected. This method interleaves the echoes, and therefore does not emphasize in any one diffusion map the physiological changes that may occur during acquisition. If all diffusion gradients are set to zero, one can also obtain from the data a $1/T_2$ map.

A set of four diffusion weighted images was acquired for each of the orientations of diffusion gradients described above. The duration of each diffusion gradient pulse, δ, was 2 ms, and the separation between diffusion pulses, Δ, was 10.4 ms. The calculated b-factors ranged from 0 s/mm^2 to 211 s/mm^2. The collected data were used to obtain maps of D_{zz}, D_{yy}, D_{xx}, and D_{xy} (3).

To establish the accuracy of the measurements, the experiment was first performed on pure water, which is expected to yield an isotropic diffusion coefficient. The experiment was then repeated on celery, whose vascular bundles are known to exhibit anisotropic diffusion. Finally, preliminary diffusion maps were obtained of excised rat spinal cords, and the diffusion anisotropy of spinal white matter was determined.

Results and Discussion

Results obtained for water and spinal cord are summarized in the table below. All experiments were carried out at 297 K.

Self diffusion coefficients of water in pure water and excised rat spinal cord

All diffusion coefficients are given in mm^2/s

Sample	$D_{zz} \pm sd$	$D_{yy} \pm sd$	$D_{xx} \pm sd$
Pure water (n=100 pixels)	2.3 ± 0.1	2.3 ± 0.1	2.3 ± 0.1
Celery			
parenchyma (n=100 pixels)	2.1 ± 0.2	2.0 ± 0.4	2.0 ± 0.3
bundle (n=9 pixels)	1.8 ± 0.2	0.5 ± 0.3	0.6 ± 0.3

The diffusion coefficient of pure water was found to be isotropic within experimental precision, and to agree with the literature and our own previous measurements (2). The $1/T_2$ measurements also agreed with measurements using other sequences. The parenchyma of celery showed isotropic diffusion within experimental precision, and the vascular bundles exhibited anisotropic diffusion, as expected. The values of the diffusion coefficients agreed with our previous measurements. The D_{xy} maps were obtained, but the small off-diagonal terms are not completely understood. Isotropic diffusion was seen in the spinal gray matter, while diffusion anisotropy was seen in white matter. This is in qualitative agreement with data obtained elsewhere (4) on rat spinal cords. Our results show that the use of multiple echoes can significantly reduce the time required to determine the anisotropic diffusion tensor.

References

1. Basser, P. J., Mattiello, J., LeBihan, D., *Biophys. J.*, 66, 259, 1994.
2. Gulani, V., Yang, Y., Shimony, J., Chandra, S., Lauterbur, P. *Proc. 2nd Meet. SMR, San Francisco*, 1040, 1994.
3. Shimony, J., Gulani, V., Lauterbur, P., *Proc. 1st Meet., SMR*, Dallas, 1994.
4. Marcci, T., Inglis, B., Yang, L., Wilken, D., Plant., D., Wirth III, E., *36th ENC*, Boston, 265, 1995.

Acknowledgements

V. Gulani is supported by a NIMH MD/PhD predoctoral fellowship. This work was partially supported by NSF Science and Technology Center Award, NSF DIR 89-20133, NIH Biomedical Research Technology grant, PHS 5P41RR056964, NIH Shared Instrumentation Grant, PHS 1S10RR06243-01, Illinois Department of Community Affairs, Grant No. 91-82128, National Center for Supercomputing Applications, and the Servants United Foundation. The authors thank Dr. S. Chandra for helpful discussions.

Pulse Sequence for Rapid Measurement of the Anisotropic Diffusion Tensor in Axially Symmetric Samples

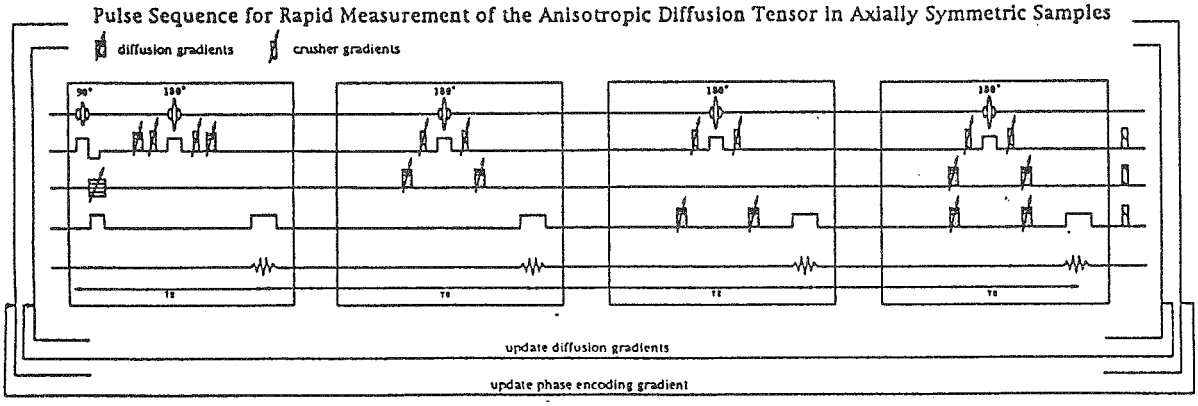

Time Course Changes of Apparent Diffusion Coefficients Following MCA Occlusion in Mouse Brain as Function of the Time of Flight.

Yaniv Assaf, Adi Mayk+, Yoram Cohen

School of Chemistry, Tel Aviv University, Ramat Aviv, Tel Aviv 69978, Israel
+TEVA Pharmaceutical Industries, Sackler School of Medicine , Tel Aviv University, Tel Aviv 69978, Israel

Introduction: Cerebral ischemia is a major causes of death and disability in the industrial world. Since our demonstration of the utility of diffusion-weighted MRI (DW-MRI) for early detection of stroke (1) DW-MRI has become the method of choice for studying early events following stroke in experimental models. Although the potential of DW imaging (DWI) has been demonstrated largely in animal models it is currently gaining importance also in clinical studies now that several solutions have been proposed to solve motion artifacts in DWI (2, 3).
Here we report the time course of the changes in the apparent diffusion coefficients (ADCs) following middle cerebral artery (MCA) occlusion in mouse brain at 8.4 T as a function of the diffusion time of flight (TOF).
Method: Male ICR mice were subjected to left MCA occlusion (4). Imaging was started 30 minutes after the induction of ischemia and was followed also at 24 hours, one week and two weeks after the ischemic event. Imaging has been performed on a 8.4 T AMX Bruker spectrometer equipped with a BGU 2 mini-imaging accessory. In each imaging session we acquired a multislices T1 image and three sets of multislices stimulated echo (STE) images with and without diffusion sensitizing gradients but with different TOF. The STE images were collected with the following parameters: Field of view 25X25mm, slice thickness 1.5mm, TR/TE/δ = 4000/40/10 ms and g was 0 or 3.5 gauss/cm. TM was set to 11.3, 66.3 or 166.3 msec resulting in TOFs of 21.67, 76.67 and 176.67 msec , respectively.
Results and discussion: The Table and Figure 1 show the ADCs values obtained at 30-60 minutes and two weeks following the ischemic event. Figure 2 shows the ratios between the ADCs of the ischemic zone and the respective contralateral normal area as a function of the TOF and age of the ischemic event.

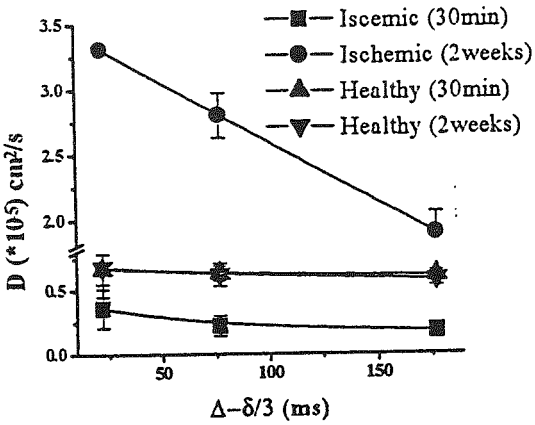

Figure 1

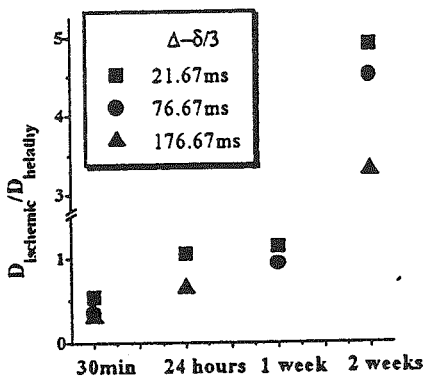

Figure 2

Δ–δ/3 (ms)	30 min		2 weeks	
	Ischemic	Healthy	Ischemic	Healthy
21.67	0.36±0.15	0.67±0.12	3.31±0.01	0.68±0.23
76.67	0.22±0.08	0.63±0.06	2.8±0.17	0.62±0.09
176.67	0.18±0.06	0.61±0.04	1.9±0.16	0.58±0.05

At early time points the ADCs of the ischemic area are smaller than that of the non-ischemic area, then at one day to one week they level out giving ratios close to unity. Two weeks after the ischemic event the diffusion coefficient of the injured area is much larger than that of normal brain. The dependency of the ratios of the ADCs on the TOF is interesting. We find that at least at early time points (up to several days) increasing the diffusion TOF increases the sensitivity toward detection of ischemia and result in a better contrast in the images. This is due to the larger decrease in the ADCs of ischemic area with increasing the TOF as compared to normal brain. The physiological meaning of the observed changes in the ADCs at different time points will be discussed.

References

1. M. E. Moseley, Y. Cohen, *Magn. Reson. Med.*, 14, 330, 1990. 2. S. Warach, D. Chien, et al., *Neurology*, 42, 1717, 1992. 3. A. de Crespigny, M. Yenari, et al., *SMR*, p. 137, 1994 4. B. Gotti, et al. *Brain research*, 1990, 522, 290.

Assessment of the Diffusion of Iron in Gel Samples using Fast T_1 Imaging

Tomas Kron[1], David Jonas[2] and James M. Pope[2#]

[1]Department of Radiation Oncology, Newcastle Mater Misericordiae Hospital, Locked Bag 7, Hunter Region Mail Centre, NSW 2310, Australia.
[2]School of Physics, The University of New South Wales, Sydney NSW 2052, Australia.

One dimensional diffusion of paramagnetic (Fe^{3+}) ions in aqueous gels has been studied by measuring changes in water proton spin lattice (T_1) relaxation due to the presence of the ion, as a function of time. This has been achieved with high spatial resolution using a fast, T_1 sensitive, NMR micro-imaging method. The aim of the study was to investigate the diffusion of ferric iron in gels containing Fricke solution, which can be used for radiation dosimetry. Fricke solution contains ammonium ferrous sulphate which, in the presence of sulphuric acid and oxygen, is converted to ferric sulphate by ionising radiation. When incorporated in a tissue-equivalent gel it can, in principle, be moulded to form phantoms in the shape of any part of the anatomy and employed to assess different radiotherapy protocols, yielding a three dimensional 'image' of the radiation dose which can be 'read out' either optically or using Magnetic Resonance Imaging (MRI) methods. However the results are adversely affected by diffusion of the Fe^{3+} ions through the gel matrix.

In this study, diffusion of Fe^{3+} was investigated using a fast Look-Locker type T1 imaging sequence and two differently doped gels which were brought into contact at time zero. In this way the effects of diffusion were observed in subsequent images obtained as a function of time over a period of several hours. An inverse square root function of the form:

$$\frac{1}{T_1} = \frac{1}{T_1^A} + \frac{1}{2}\left(\frac{1}{T_1^B} - \frac{1}{T_1^A}\right)\left[1 - \frac{x}{\sqrt{x^2 + n(t)}}\right]$$

was employed to fit the change in $1/T_1$ across the junction between the two gel phases. Here x is the distance from the boundary between the gels (x=0), T_1^A and T_1^B are the relaxation times of the starting gels and $n(t) \propto Dt$ is a fittting parameter, the time dependence of which is used to extract a diffusion constant D for the Fe^{3+} ions. A diffusion constant of 0.025 ± 0.005 cm^2/hr was determined in this way for Fe^{3+} in a 1.5% agarose gel matrix. This is in agreement with data in the literature. It was found that diffusion could be decreased by reducing the concentration of sulphuric acid and by adding a chelating agent such as xylenol orange to the gels. Diffusion was slower in gelatine gels, but these gels tended not to set properly when 0.05M H_2SO_4 was added, as required for dosimetry.

From the results we conclude that a gel consisting of 1.5% agarose (for stability), 3% gelatine and 0.1mM xylenol orange, (to combat diffusion and allow a visual evaluation of the effects of radiation), forms a suitable base for NMR dosimetry.

Current address: School of Physics, Queensland University of Technology, GPO Box 2434, Brisbane Queensland 4001, Australia.

Articular Cartilage Degradation as Measured by Self-Diffusion Using NMR

Y. Xia*, T. Farquhar‡, N. Burton-Wurster‡, George Lust‡, and L. W. Jelinski§

* Department of Physics, Oakland University, Rochester, MI 48309, USA
‡James A. Baker Institute, Cornell University, Ithaca, NY 14853, USA
§Center for Advanced Technology - Biotechnology, Cornell University, Ithaca, NY 14853, USA

Cartilage is an avascular connective tissue coating the ends of bone or joints and it provides a smooth surface for joint motion and cushions the joint against shock impact. Early signs of articular cartilage degradation include a number of biochemical and physical changes, including reduced proteoglycan content, increased water content, reduced mechanical stiffness, and increased fibronectin content. NMR has the potential as non-invasive means of assessing cartilage degradation in the earliest stages of the disease (osteoarthritis), and possibly, for evaluating the efficacy of chondroprotective treatments.

It has previously been suggested that the water self-diffusion coefficient (D), measured by pulsed-gradient spin-echo nuclear magnetic resonance, is a marker for proteoglycan loss in articular cartilage. However, it is established here using excised disks of cartilage whose proteoglycan and collagen contents were manipulated by biochemical intervention, that the self-diffusion measurement is *not* directly sensitive to the proteoglycan content of cartilage. Instead, self-diffusion appears to monitor mechanical damage at micron scale that manifests itself in increased porosity and water content. It is further shown that NMR microscopic imaging can be used to produce two-dimensional diffusion maps, which vary with the degree of cartilage degradation. Diffusion imaging experiments were also carried out on cartilage disks that were damaged by repeated mechanical loading prior to imaging, and on diseased tissue collected from the site of a natural cartilage lesion, and the results are qualitatively consistent with the findings from the biochemically treated tissues.

DIFFUSION CHANGES IN BRAIN WATER AND METABOLITES

A. Van der Toorn[1*], R.M. Dijkhuizen[1,2], E. Sykova[3], T. Reese[1], K. Nicolay[1]

[1]Dept. of in vivo NMR, Bijvoet Center for Biomolecular Research, Utrecht University, The Netherlands
[2]Dept. of Neurosurgery, University Hospital Utrecht, The Netherlands
[3]Lab. Cell. Neurophys., Inst. Exp. Medicine ASCR, Prague, Czech Republic
*Present address : Dept. Molecular Physics, Agricultural University Wageningen, Dreyenlaan 3, 6703 HA Wageningen, The Netherlands

A significant decrease in the apparent diffusion coefficient (ADC) of brain tissue water has been found in cerebral ischemia and anoxia [1]. Although cytotoxic cell swelling has been suggested to be the main cause of these ADC changes [2], there is still debate about the underlying mechanisms. Changes may be caused by changes in the relative volumes of the extracellular and intracellular space, by changes in the diffusion behaviour of one or both water fractions and by changes in the rate of water exchange across the cell membrane [1, 3, 4].

To learn more about the relationship between water ADC changes and cell volume changes in brain tissue, we decided to study these parameters in neonatal rat brain. Diffusion weighted U-FLARE images were used to obtain ADC maps of the brain of 8 to 9 days neonatal rats after terminal anoxia. These maps showed a time-dependent ADC decrease after induction of anoxia which differed for grey and white matter; the ADC decrease started later in white matter. Parallel to these studies time-dependent changes in the diffusion of tetramethylammonium (TMA^+) through the extracellular space were measured in grey and white matter of neonatal rat brain after induction of anoxia using ion-sensitive micro-electrodes. These measurements provide information about the tortuosity and the volume of specifically the extracellular space. The measurements of the TMA^+ diffusion showed decreases in the extracellular space volume and increases in the tortuosity, which occurred later in white matter than in grey matter. The time-dependence of the observed changes parallelled that observed for the ADC changes. Cell swelling is apparent from changes in the extracellular space volume fraction and probably causes the ADC changes. Furthermore, the experiments suggest that the observed ADC changes may be partly caused by changes in the tortuosity of the extracellular water fraction after cell swelling.

In another study, changes in the intracellular environment associated with cell swelling were investigated by measuring changes in the ADC of the metabolites *N*-Acetyl-Aspartate (NAA) and Creatine (Cre) in adult rat brain after induction of focal cerebral ischemia. The experiments showed a significant decrease in the ADC's of NAA and Cre within four hours after induction of ischemia. Therefore, changes in the intracellular environment may also play a role in the overall decrease of the water ADC after induction of ischemia.

1) Moseley, M.E., *et al.*, Magn. Reson. Med., 1990. **14**: p. 330-346. 2) Verheul, H.B., *et al.*, NMR in Biomed., 1994. **7**: p. 96-100. 3) Helpern, J.A., R.J. Ordidge, and R.A. Knight.*SMRM, 11th Annual Meeting*. 1992. Berlin, p. 1201 4) Norris, D.G., T. Niendorf, and D. Leibfritz. *SMRM, 12th Annual Meeting*. 1993. New York, p. 579

Chemical Shift Selective Flow Imaging: Applications in Membrane Filtration of Oil-water Emulsions

S. Yao, J.M. Pope#, and A.G. Fane*

School of Physics and *UNESCO Centre for Membrane Science and Technology, The University of New South Wales, Sydney, NSW 2052, Australia

Quantitative NMR flow imaging is increasingly used in both medical and non-medical applications for non-invasive measurement of flow velocities and flow profiles. Most non-medical studies to-date have been focused on pure liquids and simple solutions, despite the widespread technological importance of flow in complex fluids such as macromolecular solutions, suspensions and emulsions, where flow measurements of chemically distinct nuclear species may be particularly interesting. For example in membrane-based filtration and separation processes, 'concentration polarisation', (the process by which the dissolved or suspended species becomes concentrated at the surface of the membrane by the process of filtration), can play a very important role in determining the efficiency of the filtration process. However, in many instances the factors influencing the distribution and fluidity of the concentration polarisation layers are not yet clear due to lack of convincing non-invasive experimental results. In this poster, a chemical shift selective flow imaging sequence using stimulated echos for data acquisition is reported. The pulse sequence is applied to the membrane filtration of an oil-water emulsion for the experimental determination of the fluidity of the concentration polarisation layers formed from the oil droplets. Our results show an axial flow <7.5mm/s (half digital resolution in the velocity dimension) for the concentration polarisation oil layer in the present study with a 5 vol. % oil-water emulsion being fed through a tubular membarne module at a trans-membrane pressure difference ~70KPa and crossflow Renolds number, Re in the range 100-1000.

Current address: School of Physics, Queensland University of Technology, GPO Box 2434, Brisbane Queensland 4001, Australia.

NMR IMAGING OF CONVECTION PATTERNS

J. Weis, R. Kimmich, H.-P. Müller
Sektion Kernresonanzspektroskopie, Universität Ulm, D-89069 Ulm, Germany

Two special magnetic resonance imaging techniques were applied to the Rayleigh/Bénard problem of thermal convection (1). The methods were tested using a water cell with horizontal bottom and top covers kept at different temperatures with a downward gradient.

Using Fourier Encoding Velocity Imaging (FEVI) a five-dimensional image data set was recorded referring to two space dimensions of slice-selective images and all three components of the local velocity vector. On this basis, the fields of the velocity components or of the velocity magnitude were evaluated quantitatively and rendered as grey shade images.

Furthermore the convection rolls were visualized with the aid of two- or three-dimensional multi-stripe/multi-plane tagging imaging pulse sequences based on two or three DANTE combs for the space directions to be probed. Subsequent images illustrating the fluid motions by convection in all three space dimensions were produced (2).

It is demonstrated that the full spatial information of the convection rolls is accessible with microscopic resolution of typically $100 \times 100 \times 100\ \mu m^3$. This resolution is effectively limited by flow displacements in the echo time, which should be well within the voxel dimension.

The main perspective of this contribution is that the combined application of FEVI and multi-stripe/multi-plane tagging imaging permits quantitative examinations of thermal convection for arbitrary boundary conditions and with imposed through-flow apart from the direct visualization of convective flow in the form of subsequent images.

(1) H. Benard, *Rev. Gen. Sci. Pure Appl.* **11**, 1261 (1900). (2) J. Weis, R. Kimmich and H.-P. Müller, submitted for publication

Porous Media Convection: Using Fast Spin Echo Velocity Encoding for Visualization

M.D. Shattuck[1], R.P. Behringer[2], J.G. Georgiadis[3], and G.A. Johnson[1]

[1]Center for *In Vivo* Microscopy, Department of Radiology, Duke University, Durham, NC 27710
[2]Department of Physics, Duke University, Durham, NC 27708
[3]Department of Mechanical Engineering, Univesity of Illinois, Urbana-Champaign, IL 61801

We studied Porous Media Convection (PMC) using magnetic resonance imaging (MRI). The primary control parameter for PMC is the Rayleigh number which we varied from onset ($Ra=Ra_c$) to $8Ra_c$. We use fast spin echo velocity encoding scheme, which produces the velocity distribution at each point in a two-dimensional slice. From this data we can calculate the mean velocity on a 256 x 256 grid. The spatial resolution of each scan was .390 mm with a velocity resolution of .02 mm/s.

We analyzed both ordered and disordered packings of mono-disperse spheres, in circular, rectangular, and hexagonal planforms. The disordered media were characterized by large ordered regions of close packing with grain boundaries and isolated defects. The defects created regions of larger permeability, and thus spatial variations in the Rayleigh Number, Ra. We define the critical Ra, Ra_c, as Ra at the onset of convection in the ordered regions. We find that stable localized convective regions exist around grain-boundaries and defects at $Ra < Ra_c$ and remain as pinning sites for the convection patterns in the ordered regions as Ra is increased above Ra_c. In ordered media, defects only occurred within a thin region near the vertical walls. Stable localized convection began at $0.5\ Ra_c$ in the wall regions, and did not seem to affect the pattern in the interior regions. We observed roll-like structures that decayed rapidly to stable patterns between 1 and $5Ra_c$, which is consistent with theory. However, we found a wavenumber which is 0.7π compared to π derived from linear stability theory. We found an asymmetry between the size of up-flowing and down-flowing regions, with their ratio decreasing as Ra is increased, and a time-dependent state beginning at $6Ra_c$ and continuing through $8Ra_c$, the largest Ra that we studied. The slope of the Nusselt curve was determined to be 0.70 ± 0.05 which does not agree with the predicted value of 2 .

This work supported by the DOE through grant No. DE-FG05-90R14141,
NIH through grant No. P41 RR05959, NSF through grant No. CDR-8622201.

COMPUTER SIMULATION AND SIX-DIMENSIONAL SPIN DENSITY/VELOCITY NMR MICROIMAGING OF LACUNAR SYSTEMS. A COMPARATIVE ANALYSIS OF PERCOLATION PROPERTIES

H.-P. Müller, J. Weis, R. Kimmich
Sektion Kernresonanzspektroskopie, Universität Ulm, D-89069 Ulm, Germany

Using computer-simulated random site-percolation networks (1) as template, phantoms of lacunar systems were fabricated. The pore space was filled with water and experimentally investigated with the aid of nuclear magnetic resonance (NMR) microimaging.

For the combined record of the three-dimensional spin-density distribution and the three-dimensional velocity vector field of water percolating through the pore networks a four-dimensional FEVI (Fourier Encoding Velocity Imaging) was employed for each velocity component. Voxel sizes of $0.10 \times 0.10 \times 0.10$ mm^3 and $0.25 \times 0.25 \times 0.25$ mm^3 were achieved using two phase encoding and one read out gradient. From these six-dimensional data sets, three-dimensional velocity magnitude images and velocity histograms for each velocity component were derived (2).

Exclusion of all voxels of the spin density images with velocities below the noise level provides an experimental means to directly image the percolation backbone.

The combination of structural characteristic parameters (fractal dimensionality, fractal dimensionality of the backbone, correlation length) of the percolation cluster, velocity histograms and power laws for the flow distribution allow a characterization of the percolation properties of percolation networks.

The results obtained for these ideal percolation networks can thus be compared directly with experiments. The water-filled pore spaces of other, less random lacunar objects such as glass-bead agglomerates and a natural sponge were also examined with respect to percolation properties. Parameters analogous to those of the random percolation clusters are suggested for the characterization of the percolation properties.

(1) R. Orbach, *Science* **231**, 814 (1986). (2) H.-P. Müller, J. Weis, and R. Kimmich, submitted for publication

RELAXATION-DIFFUSION PROCESSES IN NATURAL POROUS MEDIA

M. Martín-Landrove, A. Benavides and G. Jaimes

Centro de Resonancia Magnética, Facultad de Ciencias, Universidad Central de Venezuela,

Apartado Postal 47586, Caracas 1041A, Venezuela.

In heterogeneous systems, it is well known that the transversal relaxation rate is dependent on the π–π pulse frequency in a CPMG experiment [1,2], due to the quenching of different relaxation channels. In sedimentary rocks there has been some evidence of relaxation rate dispersion [3] possibly associated to restricted diffusion through the porous material. In this work we present a very simple approach to the problem by the careful measurement of the spin-echo shape to obtain information about the internal local fields average at different pulse frequencies. The spin-echo signal was registered at a fixed echo time and each experiment was performed with a different r.f. pulse frequency in a range depending on the transversal relaxation of the sample. The measurements were carried out on a wide variety of sedimentary rocks including Berea sandstone and local rock samples. The experiments reveal that due to the diffusional process there is a diminution of the spectral second moment as the delay time between pulses is increased. Pulsed Field Gradient (PFG) measurements were also performed to determine the self diffusion coefficient under the same r.f. pulsation rate conditions.

1. Zimmerman, J.R. and Brittin, W.E.; 1957, J. Phys. Chem., **61**, 1328.

2. Hills, B.P. et al.; 1989, Molecular Physics, **67**, 903.

3. Kleinberg, R.L. et al.; 1993, SPE 26470, 553.

TRANSVERSAL RELAXATION RATE DISTRIBUTION ANALYSIS IN POROUS MEDIA

M. Martín-Landrove, R. Martín and A. Benavides
Centro de Resonancia Magnética, Facultad de Ciencias, Universidad Central de Venezuela,
Apartado Postal 47586, Caracas 1041A, Venezuela.

A common result in the analysis of relaxation measurements for natural porous systems is a stretched-exponential relaxation behavior, mainly due to the disordered geometry of the porous system. In the case of transversal relaxation, a dependence on the r.f. pulsation frequency is additionally observed for the stretched-exponential parameters, which means that the transversal relaxation rate distribution is modified as different relaxation channels participate in the global relaxation process. Even though there are very efficient non linear regression methods to extract the stretched-exponential parameters from the experimental data, all of them rely on assumptions related to the functional dependence on these parameters and their initial values. Besides this difficulty, the stretched-exponential parameters by themselves do not give enough information about the relaxation rate distribution, since they represent averaged properties of the particular distribution that depend in a non well-established way on the microscopic properties of the porous material. Therefore what has to be done is to determine carefully the actual relaxation rate distribution. In the present work, we carried out Carr-Purcell-Meiboom-Gill experiments at different r.f. pulsation frequencies upon a wide variety of samples including glass beads, sand and sedimentary rocks. To obtain the transversal relaxation rate distribution, we used a specially designed simulated annealing algorithm, which in general gives the inverse Laplace transform. In model systems such as glass beads or packed sand, the distributions were not dependent on the r.f. pulsation rate. On the other hand, for sedimentary rocks, a very complex behavior was observed suggesting the possibility of different diffusion domains and scales in the porous system. Further studies are pursued to establish some correlation between distribution parameters and rock properties.

SPATIALLY RESOLVED NMR OF AGING AND VULCANIZATION IN SBR

C. Fülber[+*], B. Blümich[*], K. Unseld[#], V. Herrmann[#]
[*]Institut für Makromolekulare Chemie, RWTH, 52056 Aachen
[+]Max-Planck-Institut für Polymerforschung, 55021 Mainz
[#]Dunlop, SP Reifenwerke, 63450 Hanau

Thermal oxydative aging of carbon-black filled SBR was investigated by NMR spectroscopy and imaging. Areas of aged material were localized by parameter-selective ^{1}H-NMR imaging. The image contrast obtained by NMR relaxation parameters correlates with mechanical relaxation spectra of aged and unaged materials. The time dependence of the aging process was monitored by filtered NMR projections for samples with and without aging protectant. The action of the aging protectant can be understood on a molecular level in terms of local inhibition of the aging process for a fraction of chain segements as opposed to a slow down of the characteristic aging time. Furthermore, the change in cross-link density as a function of space was derived for an aged sample from ^{1}H spin-echo decays. The NMR cross-link density shows a linear correlation with the torques measured on a vulcameter for a series of differently cross-linked, unfilled SBR samples.

The interfacial contact layer between two covulcanized rubber sheets was studied by NMR imaging. This interface significantly influences the mechanical properties of the whole system. Depending on the compounding receipes of the sheets an interfacial layer could be detected by T_{2e}-weighted imaging. In unfilled systems this layer is also visible through optical microscopy, where it appears darker, which indicates a higher density of cross links. Its diameter is of the order of 250 µm. This proves, that NMR imaging can indeed be used for process optimization in the fabrication of elastomer products.

A vulcanization chamber has been constructed to fit a commercial microimaging probe. With it the vulcanization process of cylindrical SBR samples was investigated *in situ* by observing the time constant T_2^* of the free induction decay. The NMR data for a small sample were calibrated by rheological measurements with the same heating curve. For larger samples the vulcanization becomes spatially inhomgeneous, because the sample was heated from one side, where the vulcanization front started and moved through the sample with time. The time dependence of the inhomogeneous vulcanization was investigated by NMR imaging. From a series of phase-encoded axial projections the time dependence of the vulcanization process has been obtained for different positions along the sample axis. The speed of vulcanization decreased for sample regions further away from the hot plate.

C. Fülber, B. Blümich, K. Unseld, V. Herrmann, Kautschuk, Gummi, Kunststoffe 48 (1995) 254 - 259.

Investigation of network parameter alteration of natural rubber by thermal aging observed by nmr-microscopy

U. Heuert, M. Knörgen, H. Schneider
Universität Halle, FB Physik, Friedemann-Bach-Pl. 6, D-06108 Halle
P. Barth, W. Kuhn
Fraunhofer-Inst. für Biomed.Technik, Ensheimer Str. 48, D-66386 St. Ingbert

We have prepared some rubber samples under different aging conditions (air or nitrogen atmosphere, several aging times and temperatures) to get a more or less strong surface layer and to get a series of definitly aged rubber pieces. The aging effects on the material (for example the thickness of the surface layer if there is one) were measured by nmr-microscopy (T_2-contrast). The interpretation was done by a special relaxation function based on the Andersson-Weiss- and BPP-formula, which gives information about the essential network parameters and dynamics. The aim of the work is to get some knowledge about the influence of the aged regions in the rubber of physical properties like diffusion. This was also observed by nmr-microscopy in one dimension (profile). On the other hand we will discuss the relationship between these physical properties alterated by aging and the network parameters.

NMR IMAGING OF MORPHOLOGICAL CHANGES IN POLYETHYLENE CABLE INSULATION MATERIAL

F. Weigand[+], D. Demco[+], H. W. Spiess[+], B. Blümich[*], G. Salge[#], K. Möller[#]

[+]Max-Planck-Institut für Polymerforschung, 55021 Mainz

[*]Institut für Makromolekulare Chemie, RWTH, 52056 Aachen

[#]Institut für Allgemeine Elektrotechnik und Hochspannungstechnik, RWTH, 52056 Aachen

One of the earliest uses of synthetic polymers is for insulation of power cables. For underground high-voltage cables lightly cross-linked polyethylenes are used. The issues of material degradation in high electric fields and under partial discharges are topics of technological importance. Before break-through some 200,000 discharges are observed, leading to small cavities in the material. From light microscopy it is known, that the cavities form a tree like structure. On the other hand it is also known, that polyethylene is a semicristalline material consisting of crystalline lamellae separated by amorphous material. The amorphous material in the core is mobile, the one interfacing to the crystalline lamellae is more rigid. Small angle x-ray scattering of virgin and affected material indicates no change in the long period, which is the repetition period of the crystalline lamellae. By spatially-resolved investigation of ^1H spin diffusion from the mobile amorphous regions into the magnetization depleted interfacial and crystalline regions, the characteristic domain sizes of mobile amorphous, rigid amorphous, and crystalline layers were determined across the affected sample region (Fig. 1). In the discharge region the size of the mobile amorphous regions increased on the expense of the size of the crystalline domains. The rigid amorphous domains essentially disappeared. Further systematic investigations are in progress.

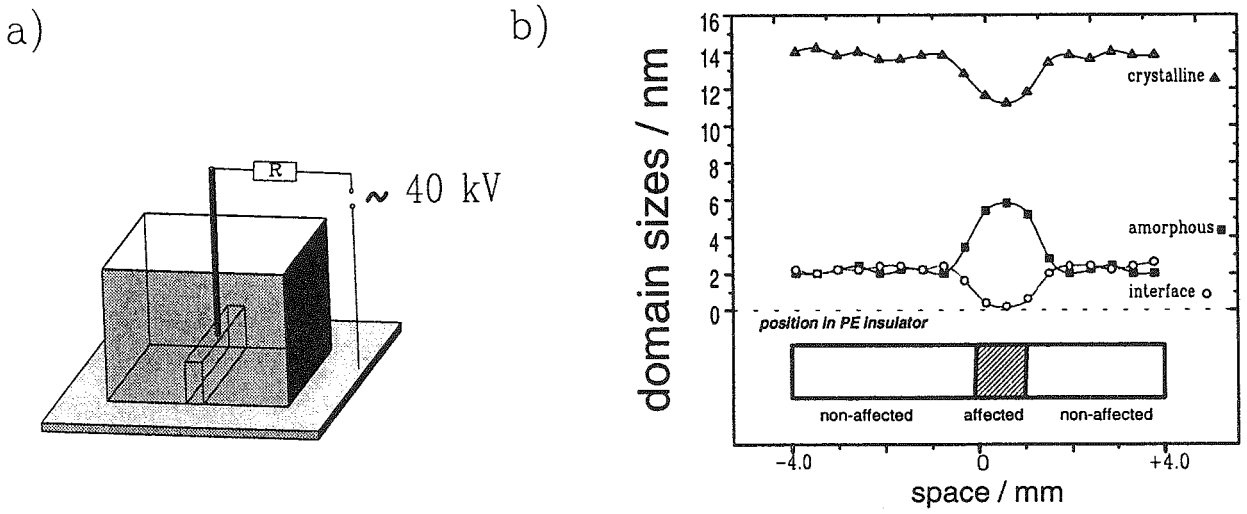

Fig. 1: a) Polyethylene sample used for high-voltage discharge testing. The region cut out from the sample for NMR imaging of spin diffusion is indicated. b) Sizes of crystalline, mobile amorphous and interfacial domains derived from analysis of spin diffusion curves as a function of space across the discharge region.

Time Resolved T_2 Mapping of the Photopolymerization of Acrylamide

Thomas J. Lees, Bruce J. Balcom, Department of Physics, The University of New Brunswick, P.O. Box 4400, Fredericton, NB, Canada, E3B 5A3.

Light induced polymer formation, spatially resolved, is amenable to study by NMR imaging (1). In the present work we consider the quantitative determination of T_2 as a function of time and space during polymerization of acrylamide. Photopolymerization of polyacrylamide, a water based gel, occurs when flavin is illuminated by a UV light source in the presence of a precursor acrylamide monomer/bis acrylamide cross linker mixture (2).

In these experiments the UV light source is a 1 kWatt Hg(Xe) arc lamp. Imaging is performed on a Nalorac 32 cm horizontal bore 2.4 Tesla superconducting magnet with a water cooled 20 cm self shielded gradient set. The spectrometer is a Tecmag Libra S-16 running MacNMR and the RF probe is a homebuilt birdcage coil (length 7 cm, i.d. 6.4 cm). A cuvette containing the flavin/acrylamide mixture is placed at the centre of the birdcage coil and held fixed for the length of the experiment. The coil is centred in the magnet and the arc lamp is positioned collinear with the bore of the magnet so that its collimated beam of light, filtered in the infrared, illuminates the cuvette. The upper half of the cuvette is obscured by an opaque mask so that only the bottom half is polymerized. A one dimensional T_2 map of the sample is produced by a set of 12 profiles with an initial CPMG train of varying length followed by a standard spin echo sequence (3,4). The length of the CPMG train will be equal to the effective echo time for each profile. The T_2 of any position can then be fitted through the series of CPMG weighted profiles.

A time resolved series of T_2 maps reveals the time course of the polymerization. T_2 values change from 340ms to 180ms in the illuminated region. A plot of $1/T_2$ vs illumination time is initially level and uniform along the profile during a short induction period, and then starts to increase with constant slope in the illuminated region. The slope of the plot is the same throughout the illuminated region although the induction period is slightly shorter at the base of the cuvette. After approximately 60 minutes the slope levels off indicating completion of polymerization. Blocking the light source midway through the illumination stops polymerization. Reillumination restores the original slope of the $1/T_2$ vs time plot. There was little temperature change ($< 3^\circ$) over the course of the polymerization. The kinetics of the polymerization do not show a significant magnetic field effect.

(1) B. J. Balcom, and T. J. Lees, Abstracts of the 36th ENC Conference, 323, 1995

(2) H. R. Maurer, "Disc Electrophoresis and Related Techniques of Polyacrylamide Gel Electrophoresis", Walter de Gruyter, Berlin, 1971

(3) A. Haase, M. Brandl, E. Kuchenbrad, and A. Link, *J. Magn. Reson. A*, **105**, 230 (1993)

(4) S. J. Doran, PhD Thesis, Cambridge University (1993)

THE ANALYSIS OF NMR FREE INDUCTION DECAY IN PARTIALLY CRYSTALLIZED POLYMERS

T.P. Kulagina,G.E.Karnaukh

Institute of Chemical Physics, Russian Academy of Sciences, Chernogolovka,Moscow region 142432, Russia

In this work, the theory of the NMR spectra based on the polarization of layers developed for solids [1,2], has been appllied for the discription of NMR spectra in partially crystallized polymers. With due regard for spin dephasing and spectral diffusion, the system of linear kinetic equations for the density polarization was obtained [1,2].In the case of partially crystallized polymers, the typically observed free induction decay (FID) can be represented as a combination of those for crystalline and amorphous portions of a polymer,$G_{cr}(t)$ and $G_a(t)$,respectively:

$$G(t)= (1- p)G_a(t) + p\, G_{cr}(t).$$

The function $G_a(t)$ was reported in [3] at $T>T_g$,where T_g is the glass-transition temperature.Within the temperature range under study,it can be represented in terms of Bloembergen correlation function within the Anderson-Wiess model and has a Gaussian or exponentional form.

$G_{cr}(t)$ manifests in two different types of FID [4].The most typical partially crystallized polymers are poly(ethylene oxide) (PEO) and poly(vinylidene fluoride) (PVF).In PEO, the FID is similar to that in crystalline solids,whereas in PVF,the oscillations are proportional to cos(bt).The reasons for differnt behavior of FID in these subctances were not clear so far.

Therefore two forms of FID can be explained by the difference in the transfer of spin-spin polarization: for PEO, a structure similar to that of CaF_2 forms in the polymer bulk.This structure is described by the system [2].For PVF,the dipole-dipole interaction of a separate CH_2-group provides the main contribution into the spin-spin interaction.

The suggested theory showed to good agreement with the experimental results [4].

1.A.V.Ivanova,B.N.Provotorov,Zh.Eksp.Teor.Fiz.,108,1(1995).

2.G.E.Karnaukh,T.P.Kulagina,B.N.Provotorov,XXVII AMPERE Congress,Kazan,1,40(1994).

3.T.P.Kulagina,XXVII AMPERE Congress,Kazan,2,620(1994).

4.V.D.Fedotov,V.M.Chernov,Vysocomol.Soedin.,Ser.A,19,1501(1977).

Magnetic Resonance Imaging of Solvent Diffusion in Glassy Polymers.

Monique Ercken, Peter Adriaensens, Dirk Vanderzande and Jan Gelan
Limburg University, Instituut voor Materiaalonderzoek (IMO), Departement SBG,
Universitaire Campus, Gebouw D, B-3590 Diepenbeek, Belgium

MRI (magnetic resonance imaging) is a rather new technique in the field of polymer science. Standard MRI experiments easily detect protons of mobile solvent molecules, providing a method to image the diffusion kinetics, the spatial distribution and other effects (e.g. cracking) of solvents in the polymer matrix in a non-destructive and non-invasive way.

Polymer-solvent systems exhibit a wide range of diffusion phenomena, going from common Fickian diffusion to Case II diffusion. These diffusion characteristics represent the extreme responses of polymers to the solvent and have substantially different characteristics. Fickian (or Case I) diffusion is characterized by an increase in solvent concentration going from the inside of the polymer to the fully swollen regions at the outside of the sample, for which the rate of diffusion is much less than that of the segmental polymer relaxation rates. The distance diffused by a species is proportional to the square root of time and the T_2 relaxation rate is constant throughout the swollen part. This commonly applies to rubbery polymers. Case II behavior on the other hand has the following characteristics : (1) A sharp concentration boundary between the polymer core and the swollen region of the sample is present. (2) The concentration throughout the swollen region is constant. (3) The front advances through the glass at constant velocity and (4) the T_2 relaxation rate decreases towards the polymer core. This behavior is also being called relaxation-controlled, because the diffusion is much faster than that of polymer segmental relaxation. This commonly applies to polymers in the glassy state.

In this contribution, the diffusion of 1,4-dioxane in polyvinyl chloride (PVC) will be described as a first classical case. As a second system, the diffusion of acetone and mixtures of acetone/methanol in a low molecular weight bisphenol-A polycarbonate (PC) will be investigated. Since these polymers are in the glassy state, one would expect transport characteristics obeying the laws of Case II transport. We want however to point out that those classical laws are only valid if no other phase transitions of the polymer than from the glassy to the rubbery state (e.g., solvent-induced crystallization) occur during the diffusion process. As an example, the diffusion of acetone into PC is considered.

Influence of Temperature on Solvent Diffusion Kinetics using Magnetic Resonance Imaging.

Monique Ercken, Peter Adriaensens, Dirk Vanderzande and Jan Gelan
Limburg University, Instituut voor Materiaalonderzoek (IMO), Departement SBG,
Universitaire Campus, Gebouw D, B-3590 Diepenbeek, Belgium

Solvent diffusion in rubbery polymers can generally be described by Fick's law of diffusion. Glassy polymers, however, because of their time-dependent responses exhibit 'non-Fickian' or 'anomalous' diffusion kinetics. Case I (Fickian) and Case II can be viewed as the two limiting types of transport process, with 'anomalous' behaviour lying between them. The type of diffusional behaviour observed for any polymer-penetrant system will vary with temperature and penetrant activity. Indeed, over a sufficiently wide range of temperature and/or penetrant activity, a given system should exhibit all the types of behaviour mentioned above.

The amount of penetrant absorbed per unit area at time t is often represented by :

$$M_t = Kt^n$$

where K and n are constants. Phenomenologically, the penetration process may thus be described by the relation :

$$d_t = Kt^n$$

where d is the diffusion distance, K is a constant and n is the exponent of time (t). For Fickian systems n=1/2, for Case II transport n=1 and for 'anomalous' diffusion $1/2 < n < 1$. Also, Super Case II diffusion (n>1) can occur. During this kind of process, an induction period at the start and an acceleration in front traverse rate at the end are observed.

In this contribution, some of the results concerning the study of the diffusion of methanol into polymethylmethacrylate and of some solvents in natural rubber as a function of temperature are presented. Time-resolved MRI images of the diffusion process in the polymer matrix have been generated at 9.4 Tesla using a Unity 400 Varian spectrometer equipped with a micro-imaging probe of 25 mm in diameter. All the images have a slice thickness of 4 mm and an inplane resolution of about 70 μm pixel^{-1} in a field of view of 25 × 25 mm. They were recorded using a multislice spin-warp sequence.

Skin Layer Effects on the Diffusion of Organic Solvents into Injection Moulded Polypropylene Studied by NMR Microimaging

R. J. Abbott[a] , G. Hunter[a], J. A. Chudek[a], and L. Squires[b]

[a]Department of Chemistry, University of Dundee, Dundee DD1 4HN, UK

[b]Non-wovens Division, Don and Low PLC, Glamis Road, Forfar DD8 1EY, UK

Most previous NMR microimaging studies of liquid imbibition into polymers have been on the imbibed liquids which generally have a T_2 of the order of milliseconds and relatively short T_1's making them suitable for study by liquid imaging techniques. The imbibition of an organic solvent is known to cause varying degrees of swelling in polypropylene, this is likely to affect the segmental mobility of the polymer chain with consequent effects on T_1 and T_2. The present work describes the imbibition of carbon tetrachloride which requires that the imaging is of the polymer itself. Even above the glass transistion temperature, T_g, polypropylene does not normally give a sufficiently narrow NMR line to allow imaging by liquid techniques. However, the swelling caused by solvent imbibition causes sufficient increase in polymer backbone mobility to effectively move from a glassy state to a more rubber like state. The consequent increase in T_2 is sufficient to allow a detectable echo at about TE = 2ms.

The images of injection moulded cylinders of polypropylene indicate that an anisotropic imbibition of solvent occurs with ingress only from the cut ends. It is considered that this results from the high degree of molecular orientation, induced by the injection moulding process, which occurs at the skin layer.

QUASI-FREE ELECTRONS AND EXCHANGE INTERACTIONS IN THE SHORT-RANGE ORDER STRUCTURE OF MATERIALS

Nguyen Van Tri, Institute of Technical Physics,
Hanoi National University of Technology, Hanoi Vietnam
Karl - Heinz Gothe, Institut für Physik, Technische Universität Ilmemau, Germany.

From experimental results with ESR in combination with other methods, numerous exchange complexes of odd electrons and the concerning effects in many different disordered materials have been revealed. The behaviour of these complex centers shows some unusual or special characteristics. It is especially notable that these new effects stand in close connection with the fundamental properties (such as the peculiar conductivity, the fastness, the torsional module, the catalytic activity, etc.) of the disordered material, and with details of a technological nature arising mainly from distinctions in the mode of preparation. These phenomena only can be adequately explained through a new consideration on the grounds of the Short-Range Order Structure (SROS). On the basis of the experimental results, a model for Quasi-Free Electrons (QFE) in the Resonant Cavity (RC) constituted by valence bond planes of the short-range order network and a model for the Super-Exchange Interaction in the SROS of the materials have been elaborated : The sole quantum state of the QFE in the RC only can be a Standing Wave. In the ground wave states, there are only two allowed energy bands. The states of negative effective mass and states of greater-becoming effective mass of the QFE can persist near the lower band-edge. This peculiarity springs from the natural reaction of the RC to the broadcloth of energy level to band. This effect can give rise to some unusual phenomena such as ESR emission and sudden conductivity changes. Because of the infiltration of the natural stratistical fluctuation of the RC-paramenter in the SROS, the population distribution course of QFEs into the band levels shows a "compression" form with a pitch that plays a decisive role in the spectral intensity concentration. This effect occurs especially distinctly in the case of an excellent short-range ordering or an ideal amorphism in the material. Because of the standing wave nature of the respective QFEs, the pair coupling probability depends resonantly on the exchange path length between two Spins. The SROS deformation can produce in the RC a relatively strong local electric field of low symmetry, under which the QFE can be strongly "polarized" and therefore obtain a considerable energy splitting term. This effect gives rise to the regular displacements of the ESR line groups.

On the basis of these models there is the possibility of a more profound understanding about the apperrance and the role of exchange complexes in disordered materials, and therefore of the molecular electronic micromechanisms concerning the specific features and technological factors of these materials.

As illustration examples, under numerous application cases, two types of the super - exchange couple pairs [Cu - Y - Cu] and the superconducting mechanism in $YBa_2Cu_3O_x$ compounds, and the phenomena of sudden conductivity changes in amorphous silicon are discussed.

ABILITY OF SOME SPECIFIC NATURAL STRUCTURES TO INTERACT CONCURENTLY CONTRARY TO DIOXIN. ESR STUDY.

Nguyen Van Tri, Pham The Vung, Dinh Pham Thai
Hanoi National University of Technology
Ha Vàn Mao, Dinh Ngoc Lam - Cancer Research Center.
Hanoi, Vietnam

On the basis of the ESR experimental results, some new active natural complexes (symbolized XD*) present in special vegetable produces have been revealed. The nucleus structure of these complexes can show a electron Spin combination almost similar to the one of Dioxin (2, 3, 7, 8 - TCDD). However, it is especially remarkable that the Spin combination of XD* occupies a quintuplet ground state with a deeply negative exchange energy $J < 0$. This behaviour opposes entirely to the one of Dioxin possessing a combination of four π electron Spins with a singlet ground state ($S = 0$) and a positive exchange energy $J > 0$.

Special binding complexes of Dioxin to XD* structures have been also observed with a negative exchange energy $J < 0$. These [XD* - Dioxin] complexes appear with a very high probability, about 10^3 times of the one of the [Hemoglobin - Dioxin] complex in human blood and of the [Mn - Porphyrinoprotein - Dioxin] complex in human liver. The properties of these interaction complexes corresponding with the results achieved in some respective experimental clinical studies over a long period of time suggest that the specific natural XD* structures are able to conquer and arrest potently Dioxin molecules, i.e. to interact concurently contrary to the toxicity of Dioxin, namely to its carcinogenous activity. This ability depends on many factors such as the concentration and the lifetime of the XD* state, the kinetic conditions of the surrounding and the interaction.

TWO-DIMENSIONAL PURE NQR POSITIONAL SPECTROSCOPY WITH SLICE SELECTION

H. Robert and D. J. Pusiol

Facultad de Matemática, Astronomía y Física, Universidad Nacional de Córdoba, Ciudad Universitaria, 5000 Córdoba, Argentina

The first steps towards a 3D Nuclear Quadrupole Resonance (NQR) positional spectroscopy method is reported. The image plane, or slice, is defined by the application of a spatial-dependent magnetic field and the distribution of quadrupole nuclei in this slice is mapped-out by using a two-dimensional NQR rotating frame technique (2D-ρNQRI).

It has been previously demonstrated [1] that one-dimensional profiles of powdered solid samples, containing quadrupole nuclei, can be recorded using a NQR version of Hoult's rotating frame technique [2]. One-dimensional spatial encoding is based on gradients of the RF amplitude of a single variable excitation pulse. A spin density one-dimensional profile is reconstructed from a 2D data matrix $S(t, t_x)$, which is on turn created by recording the intensity of the FID signal as a function of the evolution time t and incrementing the rf pulse length t_x parametrically from experiment to experiment.

The 2D-ρNQRI achieves resolution in the second dimension by arranging the transmitter coils in a cross-coil probe [3] to generate a second RF gradient in the y-direction. The 2D rotating frame zeugmatography technique involves a preparation period of the observed magnetization, which consists of two consecutive pulses of duration t_x and t_y. The time intervals (t_x,t_y) being varied in step wise linear fashion to give a set of FIDs from which the two-dimensional spin density can be extracted together with the spectroscopic information contained in the selected image plane.

It is desirable or even necessary to control the slice thickness, or third dimension, when producing a two-dimensional image of an object. With this purpose a static zero-crossing field gradient is applied to the quadrupole resonance sample [4], so that the NQR spectrum is a superposition of a single line (corresponding to the zero-field plane) and a powder pattern arising from nuclei located far away from the zero-field plane. The field gradient is applied in a direction normal to the desired image plane or slice. For practical purposes, the contribution of the Zeeman perturbed nuclei to the on-resonance spectrum is negligible. As the selected plane of the sample experiences a zero magnetic field, the complete spectroscopic information is still preserved.

The application to this scheme of the recently developed fast imaging technique [4] is also discussed.

References

[1] E. Rommel, P. Nickel, R. Kimmich and D. Pusiol, J. Magn. Reson., **91** 630 (1990).

[2] D.I. Hoult, J. Magn. Reson., **33**, 183 (1979).

[3] H. Robert and D. Pusiol. to be published.

[4] H. Robert and D. Pusiol, to be published.

High-Resolution, High-Speed in-vivo Proton Spectroscopic Micro Imaging

J.Weis, U.Görke, R.Kimmich
Sektion Kernresonanzspektroskopie, Universität Ulm, 89069 Ulm, Germany

Although ^{1}H Magnetic Resonance Spectroscopic Imaging (MRSI) is to provide high spatial and high spectral resolution reasonable *in vivo* application requires acquisition time of 15 minutes or less. The standard MRSI methods, such as the multidimensional Fourier transform techniques [1] phase-encoding two- or three-dimensional spatial information into the FID, need extremely long measurement time to achieve sufficient spectral resolution. Instead, we used a faster technique [2] which reduces the number of dimensions to be measured by one compared to the method suggested by Maudsley [1]. This pulse sequence uses readout gradient during acquistion to encode 2d information simultaneously - spectroscopic and spatial [3, 4]. Significant improvement of the signal to noise ratio was achieved by using low readout gradient in a high magnetic field (4.7 T). In this case, large chemical shift offset need to be taken into account. Additionally, the line-broadening by static magnetic field inhomogeneity in the sample reduces spectral resolution. Both kinds of artifact, chemical shift offset and shifts caused by B_0 variations, can be corrected by appropriate post detection processing. Therefore, presaturation pulses and extremely good shimming are not necessary. The purpose of our work is the combination of a fast measurement method and suitable data processing techniques to obtain high quality images of spectral information *in vivo*. Spectroscopic information is used to correct for imaging artifacts, on the one hand, and to display structures according to their chemical shifts, on the other hand. In addition to spatial information well resolved spectra are comparable with those obtained by ususal single voxel spectroscopy. This is demonstrated on the ^{1}H MRSI data set of a human finger.

References

[1] Maudsley, A.A., Hilal, S.K., Perman, W.H. and Simon, H., J.Magn.Reson. 51, 147, 1983.
[2] Weis, J., Frollo, I., Budinsky, L., Zeitschrift für Naturforschung 44a, 1151-1154, 1989.
[3] Mansfield, P., Mag.Res.Med. 1, 370-386, 1984.
[4] Matsui, S., Sekihara, K., and Kohno, H., J.Mag.Reson. 67, 476-490, 1986.

Microscopic MR Imaging of Lactate Using SLIM and GSLIM

J.A. Kmiecik, D.E. Hrad, C.D. Gregory, Z.-P. Liang, and M.J. Dawson
Biomedical Magnetic Resonance Laboratory, University of Illinois at Urbana-Champaign, 61801 USA

INTRODUCTION

As an indicator of the energetic and oxygenation status of tissues, lactate has become one of the most studied metabolites in the ^1H spectrum. Its concentration has been shown to increase in various pathologies in brain and muscle, and physiological rises of lactate levels in fatiguing muscle have also been demonstrated with spectroscopic techniques. However, because of the low concentration of lactate and the resulting problems concerning poor sensitivity and required water and lipid suppression, imaging of lactate, even at conventional resolution, has not been common. To address these issues, a lactate imaging protocol, combining highly effective lactate selectivity and processing with the efficient non-Fourier reconstruction techniques, SLIM (spectral localization by imaging; 1) and GSLIM (generalized SLIM; 2), has been devised and shown to provide quantitative images of physiological concentrations of lactate in test phantoms and in fatigued frog skeletal muscle at microscopic resolution.

METHODS

Phantoms consisted of a 1200μm inner diameter glass capillary within which were 700μm and 300μm capillaries of 10mM and 100mM lactic acid, respectively. In studies of fatigued muscle, paired 5th toe flexors (approximately 500μm diameter by 7mm long) were dissected from the frog *Rana pipiens* and bathed in oxygenated ice-cold Ringer's solution (105mM NaCl, 2.5mM KCl, 2mM $CaCl_2$, 1mM $MgCl_2$, 15mM PIPES buffer, pH 7.2). After a period to allow the muscles to return to a resting state, one muscle was placed in 2mM NaCN in Ringer's to maximize lactate concentration, and the other in 0.5mM iodoacetic acid (IAA) in Ringer's to serve as a negative control for lactate. The muscle in NaCN was electrically stimulated (one 1-second tetanic contraction per minute for 120 minutes) and then both muscles were placed within a single 1200μm capillary of Ringer's solution along with a 300μm capillary of 100mM lactic acid which served as a concentration standard.

Microscopic lactate imaging was performed at 7T on a GE GN-300 wide-bore imaging spectrometer using a home-built imaging system with a Tecmag acquisition controller. A 6-turn solenoidal RF coil 2mm in diameter and 6mm long was used. A home-built gradient coil set, of 2.9cm inner diameter and 3cm functional length, provided field gradients up to 45G/cm. The imaging sequence incorporated lactate editing based on a double-quantum coherence filter with inclusion of zero-quantum signal as devised by Trimble *et al.* (3) The effective lactate editing enabled frequency-encoding of one spatial dimension, with phase-encoding of the remaining two (generally, 16x16x8). Quantitation of lactate concentrations in arbitrarily shaped compartments was made possible by the use of SLIM, while image reconstruction was performed by GSLIM. "Image masks" as required by SLIM and GSLIM were created from high-resolution water images (256x128x8).

Imaging parameters for the muscle lactate datasets were: receiver bandwidth, ±2500Hz; FOV, 2.5mm x 2.5mm x 10mm; TE, 102ms; TR, 1.1s; signal averages, 80; total imaging time, 3.1hrs. Lactate phantom images were acquired with 408 averages in 15hrs. Water images were acquired with TE, 68ms; TR, 1.1s; total imaging time, 17min.

RESULTS

Images of the phantom illustrate the improvement in resolution using GSLIM vs. Fourier transformation for the phantom studies. While the resolution of the images processed by Fourier transformation is poor, the pixel size of the GSLIM image is 10μm x 10μm in-plane with 970μm slice thickness. Compartmental values determined by SLIM, which relate lactate concentrations in the desired volumes of interest, were 0.05 for the area outside the phantom, and 1.1, 10.2, and 100 for the water, 10mM lactic acid, and 100mM lactic acid capillaries, respectively.

GSLIM images of muscle, of similar resolution, clearly illustrate lactate in the fatigued, NaCN-poisoned muscle, while very little is visible in the IAA-treated muscle. Lactate concentrations were determined by SLIM to be 12mM in the fatigued muscle and 2mM in the control.

DISCUSSION

By combining effective lactate selectivity, 3D imaging with frequency encoding of one dimension, and efficient image reconstruction techniques, images of physiological concentrations of lactate at microscopic resolution were obtained within a practical acquisition time. Accurate quantitation of lactate concentrations within volumes of interest was shown by phantom experiments.

This technique can be applied to a variety of applications requiring microscopic lactate imaging. The descrimination of fast-twitch glycolytic muscle fibers from slow-twitch oxidative fibers is one example under study.

REFERENCES

1. Liang, Z.-P., and Lauterbur, P.C., *J. Mag. Reson.*, B102, 54, 1993.
2. Liang, Z.-P., and Lauterbur, P.C., *IEEE Trans. Med. Imag.*, 10, 132, 1991.
3. Trimble, L.A., Shen, J.F., Wilman, A.H. and Allen, P.S., *J. Mag. Reson.*, 86, 191, 1990.

ACKNOWLEDGMENTS

This work was supported by the following grants:
NIH 5 T32 CA 09067, 1 F31 MH 10742-01, and
PHS 1 R01 CA 51430.

In vivo Imaging of Uniformly Labeled ^{13}C Glucose in Tumors

D. Artemov, Z.M. Bhujwalla, and J.D. Glickson
Division of NMR Research, Department of Radiology, Johns Hopkins University School of Medicine, Baltimore, MD 21205

Introduction

The search for more sensitive methods to detect metabolic and physiological heterogeneity is important as such methods allow further understanding of tumor pathophysiology. In these studies,
Carbon-13 NMR spectroscopic imaging with broadband proton decoupling and NOE signal enhancement was used to obtain the spatial distribution of uniformly labelled 13C (UL) glucose in solid tumors.

Method

The low sensitivity of ^{13}C NMR requires the use of labeled compounds and efficient methods for signal enhancement. Spectroscopic studies of glucose metabolism are usually performed with the substrate singly labeled in the first position. UL glucose has 6 labeled carbons, but carbon-carbon spin coupling leads to a significant increase in the complexity of the resonance patttern. To a first approximation glucose can be considered as a linear molecule in which only the neighboring atoms are coupled. In this case the number of resonances is (3N-2), where N is the number of carbon atoms. Detection of all of these signals provides an improvement in signal to noise over the detection of a single labeled atom by a factor of $N/\sqrt{(3N-2)}$. For glucose (N=6) this ratio is 1.5, which reduces the accumulation time more than two-fold. The broad range of chemical shifts of uniformly labeled glucose does not permit use of standard 2D imaging techniques; therefore, 2D spectroscopic imaging was implemented and 2D images of glucose distribution were obtained by integration of spectral lines for each voxel. Very high slice selective gradients required because of the short slice selective pulse introduced loss of signal. Therefore the projection presaturation method was employed for slice selection, and a hard excitation pulse followed by a 500 μs phase encoding period was used. Signal enhancement was achieved by generating an NOE during the relaxation delay; broadband decoupling was applied during data acquisition. To compensate for off-center positioning of the sample, the receiver phase was incremented with every phase encoding step.

A GE Omega 400 spectrometer equipped with shielded gradients, and a homebuilt double tuned $\{^{13}C/^{1}H\}$ probe was employed. Studies were performed on RIF-1 tumors grown in the flanks of C3H/HeN mice. Anesthetized animals with a cather implanted in the tail vein, were placed in a thermostabilized probe. Blood glucose concentrations were initially increased by a bolus of labeled glucose and then maintained constant at about 300mg/dL by intravenous infusion of an exponentially decaying volume of a 0.3 M solution of 99%-UL-Glucose (Cambrige Isotopes) in saline. The total volume of glucose solution infused over a period of 3 hours did not exceed 0.8 ml .

Results

A representative ^{13}C glucose image obtained from a RIF-1 tumor is shown in Figure 1. The image was acquired within 50 minutes, with an in-plane resolution of 2x2mm, slice thickness of 5mm, 8x8 phase encoding steps, and 64 scans per step.

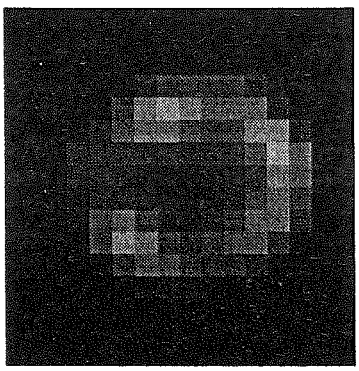

Fig. 1

Detection of the total signal of UL-glucose provides a significant increase in sensitivity. High quality 2D images with pixel volumes of $20mm^3$ were obtained within 30-40 minutes for an average concentration of about 7-8 mM of glucose. The spectroscopic imaging technique does not produce chemical shift artefacts, and, in principle, provides additional information about the distribution of other metabolites such as lactate, and lipids. Consistent with previous reports (D.Artemov et al., SMR abstracts, 1995), the distribution of glucose in RIF-1 tumors was heterogeneous.

Acknowledgments

This research was supported by NIH Grants CA51935 and CA51950. We thank Dr. V.P. Chacko for technical assistance, Dr. D.C. Shungu for the design of software for processing of spectrosopical imaging data, and Mr. G. Cromwell for transplanting the tumors.

Abnormal Energy Metabolism In Patients with Dilated Cardiomyopathy Detected Invasively (Endomyocardial Biopsy) and Non-Invasively (^{31}P-MR Spectroscopy)

S. Neubauer, M. Horn, M. Goedde, K. Harre, A. Laser, W. Bauer, T. Pabst+, D. Hahn+, G. Ertl, K. Kochsiek.
Departments of Medicine and Radiology+, Würzburg University, FRG

Introduction

In patients with dilated cardiomyopathy (DCM) reductions of both creatine phosphate and creatine, substrates comprising the guanidino pool size of the heart, have been reported. The non-invasive technique of ^{31}P-MR spectroscopy allows the estimation of creatine phosphate content (CP/ATP ratio) (1,2), while analysis of endomyocardial biopsy specimen using conventional biochemical techniques allows measurement of total creatine content (3).

Hypothesis

Reductions of the myocardial guanidino pool size can be detected invasively (endomyocardial biopsy) and non-invasively (^{31}P-MR spectroscopy) in the same group of patients with dilated cardiomyopathy. ^{31}P-MR spectroscopy measurements can thus be validated against the gold standard of endomyocardial biopsy.

Methods

5 patients with severe dilated cardiomyopathy and 6 patients with chest pain but normal left ventricular function and coronary arteries (Control) underwent cardiac catheterization and endomyocardial biopsy (1-3 mg) ± 3 days before/after a MR-spectroscopy study. Left ventricular (LV) ejection fraction (EF) was determined from LV angiography. ^{31}P-MR spectra from the anteroseptal myocardium were acquired at rest on a 1.5 T Philips MR system using ISIS localization. Total acquisition time per spectrum was 30 min. Peak areas were determined by Lorentzian line fits. From the ^{31}P-MR spectra, the myocardial creatine phosphate (CP)/ATP ratio was determined. In endomyocardial biopsies, total creatine content (Crea; nmol/mg protein) was measured by reversed phase high-pressure liquid chromatography; in addition, total creatine kinase (CK) activity (IU/mg protein) was measured spectrophotometrically and lactate dehydrogenase (LDH) isoenzymes (%1-5) by agar gel electrophoresis.

Typical ^{31}P-MR spectra of a control patient and of a patient with dilated cardiomyopathy are shown in the figure.

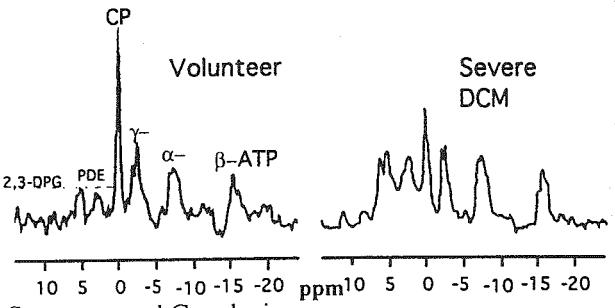

Summary and Conclusions

Patients with dilated cardiomyopathy had severely reduced left ventricular function (EF 31%). ^{31}P-MR spectra (Figure and Table) showed substantially reduced CP/ATP ratios. In 1-3 mg endomyocardial biopsies of control patients, total creatine kinase activity and total creatine content were lower than previously reported for explanted donor hearts, probably since such biopsies contain more connective tissue than subepicardially sampled larger tissue pieces. However, in dilated cardiomyopathy, reductions in the guanidino pool size and alterations in CK and LDH systems could clearly be detected. Thus, reductions in guanidino pool size can be detected by both ^{31}P-MR and endomyocardial biopsy in the same group of patients. The results indicate that when validated against the gold standard of endomyocardial biopsy, the non-invasive technique of ^{31}P-MR spectroscopy is well suited for clinical studies of cardiac energy metabolism in heart failure.

References

(1) Neubauer S, Krahe T, Schindler R, Horn M, Hillenbrand H, Entzeroth C, Kromer EP, Riegger GAJ, Lackner K, Ertl G: *Circulation* 1992; 86: 1810-1818
(2) Hardy CJ, Weiss RG, Bottomley PA, Gerstenblith G: *Am Heart J* 1991; 122: 795-801
(3) Nascimben L, Pauletto P, Pessina AC, Reis I, Ingwall JS: *Circulation* 1991; 84, 4: II-563

Results	LV EF (%)	CP/ATP [a]	Total creatine [b] (nmol/mg protein)	Total CK [b] (IU/mg protein)	LDH 5/1 [b]
Control	72±1	2.10±0.14	41.2±4.4	6.4±0.9	0.023±0.005
DCM	31±6*	1.32±0.08*	32.0±4.8*	3.8±0.2*	0.063±0.026*

Data are mean ± SE; *p<0.05 Control vs. DCM
[a] = determined non-invasively by ^{31}P-MR spectroscopy, [b] = determined invasively from endomyocardial biopsies

Hearts with chronic myocardial infarction show increased susceptibility to high-workload but not to low-workload metabolic stress

Michael Horn, Christiane Pauli-Magnus, Melanie Schroeder, Peter Bureik, Kai Hu, Klaus Schnackerz§ and Stefan Neubauer, Medizinische Universitätsklinik and Physiologisch-Chemisches Institut§, Würzburg, FRG

Introduction: The surviving myocardium post-myocardial infarction (MI) undergoes structural and functional remodeling: left ventricular (LV) dilatation and dysfunction. In parallel, energy reserve via creatine kinase (CK) is reduced[1]: Total CK activity, total creatine, creatine phosphate and the CK reaction velocity decrease by up to 50 %. It was recently shown that hearts of transgenic mice[2] with a null-mutation of CK-M (knock-out) show unaltered susceptibility to ischemia/reperfusion injury but increased susceptibility to ß-adrenergic stimula-tion. Thus, we hypothesized that hearts with impaired energy reserve via CK show increased susceptibility to high-workload but not to low-workload metabolic stress.

Methods: Male Wistar rats were subjected to ligation of the left anterior descending coronary artery (LAD) or sham operation. 8 weeks later, in-vivo LV end-diastolic pressure was measured. Hearts were isolated and perfused in the Langendorff mode with Glucose (11 mM)-containing Krebs-Henseleit buffer. LV pressure and heart rate were measured by a Latex-balloon. End-diastolic pressure was set to values measured in-vivo by adjusting LV balloon volume. ^{31}P-NMR spectra were recorded at 5 min intervals to define creatine phosphate (CP) and ATP contents. Absolute ATP concentration was measured by an external ^{31}P standard.

Protocol 1: 15 min of total global ischemia followed by reperfusion (Sham: n=11, MI: n=5)

Protocol 2: Inotropic stimulation by increasing (10, 100, 250 ng/min) dosages of Isoproterenol (Sham: n=6, MI: n=6)

Results: Mechanical performance (end-diastolic pressure (EDP), rate-pressure product (RPP), coronary flow (CF)) and high-energy phosphate content of sham and MI hearts during control perfusion (Table 1).

	EDP	RPP	CF	CP	ATP
	[mmHg]	[10^3 mmHg/min]	[ml/min]	[mM]	[mM]
Sham	10±0	28.6±8.5	22.4±3.8	15.1±1.8	10.8±0.5
MI	17±5**	23.8±6.9	25.6±5.4	10.0±1.2**	10.6±1.2

** p<0.005 sham vs MI; unpaired, two-tailed t-test

During ischemia/reperfusion injury no significant differences in mechanical recovery and ATP and CP content could be detected between sham and MI .

	end of ischemia	end of reperfusion	
	ATP	RPP	CP
	[mM]	[10^3 mmHg/min]	[mM]
Sham	3.6±0.3	10.2±3.0	11.1±0.3
MI	3.7±0.4	12.9±3.9	11.3±1.2

Figure 1 shows typical ^{31}P-NMR-spectra of a MI heart at control and during high-workload metabolic stress

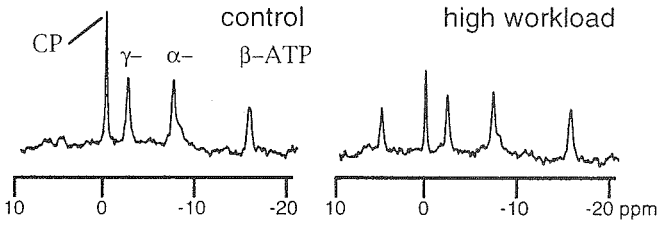

During high-workload metabolic stress RPP and CF increased by the same extent in both groups.

	250 ng/min Isoproterenol	
	RPP	CF
	[% of control]	[% of control]
Sham	200±11	147±20
MI	236±20	133±19

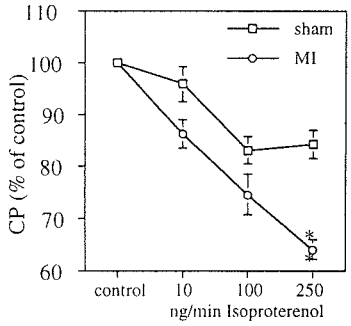

Conclusions: Chronically infarcted hearts with reduced energy reserve via CK do not show changes in the susceptibility to ischemia/reperfusion, i.e. metabolic stress associated with low workload. However, susceptibility is markedly increased during metabolic stress associated with high metabolic turnover due to ß-adrenergic stimulation by Isoproterenol, similar to findings in CK-M deficient mice[2]. In chronically infarcted hearts, maximum workload can be achieved only at increased energetic costs.

References

1) S. Neubauer, M. Horn, et al. J. Clin. Invest 1995; 95:1092-1100

2) H.D. Weinberger, J.J.A. Huntley, et al.. Circulation 1994; 90(4): I-209

Morphology and myelination of a human fetal and adult medulla oblongata

Linda Vanormelingen MD[1]
Marjan Vandersteen MD-PhD[1]
Jan Gelan PhD[2]
Peter Adriaensens PhD[2]
Emile Beuls MD[1,3]
Yvan Palmers MD[1,4]

1 Department of Anatomy at the Limburg University , B-3590 Diepenbeek, Belgium.
2 Institute for Materials Research at the Limburg University, B-3590 Diepenbeek, Belgium.
3. Department of Neurosurgery, University Hospital, Maastricht, The Netherlands.
4. Department of Radiology, St. Jansziekenhuis, B-3600 Genk, Belgium.

The lower brain stem (medulla oblongata) of a normal human fetus, 21 weeks gestational age, was fixed in 10% formalin and subsequently investigated in the three orthogonal planes in a 9,4 T MR device (TR=2500 msec/TE=20msec/ 1mm. slice thickness/ inplane pixel resolution 40 by 40 micron).

The high resolution of the images allow a detailed micromorphologic analysis of the lower brain stem as isolated fibre tracts and several important brain stem nuclei are clearly depicted as well in the transverse as in the longitudinal images. Confrontation of the MR images of this fetal medulla oblongata with those of a formalin fixed adult medulla oblongata shows a remarcable inversion of MR contrast of several structures: fibre tracts of the fetal specimen have higher signal intsensities, the grey matter nuclei have lower signal.

Myelination in the central nervous system starts in the spinal cord between the 11th and 14th week of fetal development. In the brain, no myelin if formed before the end of the fifth fetal month. Although different fibre tracts start myelination at slightly different time and have different rates of myelination rate, it is generally accepted that myelin accumulates slowly in the third trimester followed by a sudden and marked increase in deposition towards birth.

Histologic control of the above mentioned specimen confirms the identification of all microstructures. The very high water content of unmyeliniated or poorly myelinated fetal fibre systems might explain the high signal intensities of these structures in MR images.

Myelination is an important indicator of fibre system maturation, as it accompagnies synaptic development. Hence high field MRI can be used as a tool in the study of human central nervous system maturation.

The Morphology of Teeth using Magnetic Resonance Microimaging

J A Chudek[1], G Hunter[1], C H Lloyd[2], R L Mackay[1] and S N Scrimgeour[1,2]
Departments of [1]Chemistry and [2]Dental Prosthetics and Gerontology, University of Dundee, Dundee DD1 4HN, Scotland, UK

Although traditional radiology still remains the imaging technique of choice for oral and maxillofacial diagnosis and treatment, magnetic resonance imaging has been shown to have significant value (eg Monahan *et al.*, 1994, J. Amer. Dent. Assoc., **125,** 998-1002). However, for diseases of the mineralised tooth tissue (eg caries) the detection of the early changes in this tissue are of considerable importance to a conservative approach to treatment. In 1988 Chudek and Kuhn (unpublished) showed that it was possible to obtain a microimage of the pulp chamber and a composite material filling in a tooth, though not the mineralised tissue, using the spin echo technique. More recently the mineralised tooth structures have been imaged using stray field imaging, STRAFI (Baumann *et al.*, 1993, Oral Surg. Oral Med. Oral Pathol., **75**, 517-522).

Several early caries detection techniques, which may have general clinical application, are to be validated using MRM. To date, such validation has been possible only by invasive (destructive) techniques. However, before diseased tissue can be studied acceptable images of healthy teeth must be acquired. The three dimensional structure of the soft tissue and the external morphology of four healthy teeth and of one with a minor suspected carious lesion has been determined using MRM. Two first premolars (maxillary and mandibular) had been extracted during orthodontic treatment: two upper centrals were extracted after periodontal involvement. The fifth tooth was an impacted right third molar, removed surgically and subsequently found to have a suspect lesion. All five showed the expected dental morphologies (external and pulpal). The carious region of the impacted wisdom tooth gave an intense image. All images are of a quality which has allowed the research to be extended to validate other caries detection techniques.

"Biophysical Basis for the Appearance of Articular Cartilage in MRI"

L. Wachsmuth, R.X. Raiss, E.J. Schneider, H.P. Juretschke, U. Belz, K. Metternich

Adress: L. Wachsmuth, Hoechst AG Werk Kalle-Albert, TD Rheumatologie, Rheingaustr. 190-196, 65203 Wiesbaden

Articular cartilage is mainly composed of collagen fibrils, which provide for stiffness and structure, and proteoglycans, responsible for a high water binding capacity and the required osmotic resiliance. In various reports the appearance of articular cartilage in Magnetresonance-Imaging (MRI) has been reported differently. Up to now, no single explanation is currently accepted. Lehner, *et al*[1], who studied bovine cartilage *in vitro* observed a superficial layer with low signal and a deep layer with higher signal intensity in T_1-weighted sequences. They attributed the differences in zonal signal intensity to variation in water content. Modl, *et al*[2], noted the presence of three layers on heavily T_2-weighted sequences: a thin , low signal superficial layer, a high signal intermediate zone, and a low signal deep zone. They concluded that these layers correspond to the different histologic zones, namely the superficial, the transitional, and the radial zone. They postulated that the differences might be attributed to changes in static magnetic susceptibility according to the different orientation of the collagen fibrils in the extracellular matrix. Paul, *et al*[3], proposed that the signal intensity of cartilage was primarily determined by variations in proteoglycan content across the thickness of matrix. Rubenstein, *et al*[4], attributed the laminar appereance of articular cartilage to dipole-dipole interactions ("Magic-Angle-Phenomenon") between the protons of water molecules diffusing preferentially along the spatially orientated collagen fibrils and the direction of the magnetic field B_0.
During preparatory studies for animal models of osteoarthritis we tried to elucidate some of these issues working with sesamoid bones and cartilage explants from bovine metacarpophalangeal joints.

Experiments were performed on a Bruker Biospec 4.7 T magnet with a mini-imaging gradient-set and a home-built solenoid-coil. We used a spin-echo imaging method, TE=13ms, TR=332ms, 256^2, pixel size 60µm. To avoid susceptibility artifacts explants and intact bones were immersed in physiological saline solution.

Magic-angle-experiments: Explants were fixed in the magnet allowing free rotation along an axis perpendicular to B_0. The explant shows completely different appearance of the cartilage in images obtained with just the same parameters depending on the rotation angle. In one case the thickness of the high signal layer is about 0.1mm. After turning the explant by 55° the thickness of the apparently homogeneous high-signal layer increases tenfold to about 1mm. This last value coincides with the histologically determined thickness of the cartilage layer.

Contrast media experiments: Sesamoid bones of the same joints as above were imaged with identical parameters and set-up, except that an activated surface-coil was positioned parallel to the cartilage surface and in the Magic-angle relative to B_0 for signal detection. As contrast agent Mn^{2+}-solutions of varying molarity were used. The bones were soaked in these solutions for various periods of time. In some instances proteoglycan content was reduced by pretreating the sesamoid bones with papain-solution. In healthy cartilage Mn^{2+}-treatment leads to a nonhomogeneous appearance of the cartilage layer with higher intensity in the radial zone. Increasing Mn^{2+}-concentration causes signal void in the same area. In papain-treated samples the appearance of the cartilage layer is homogeneous after Mn^{2+}-treatment, and no changes occur with increasing concentration.

Conclusions: The appearance of articular cartilage on MR-images depends on both:(1) The collagen fibrils with their unique anisotropic organisation ("arcade-structure"), which explain the angle-dependent effects, and (2) the uneven distribution of proteoglycans across the cartilage layers. With the technique of angle-dependent MRI variations in the structure of collagen can be monitored, while with the application of contrast agents changes in the concentration and distribution of proteoglycans can be assessed.

Literature: 1. Lehner KB, Rechle HP, Gmeinwieser JK, et al: Structure, function, and degeneration of bovine hyaline cartilage: Assessment with MR imaging in vitro. *Radiology* 1989;170:495-9 2. Modl JM, Sether LA, Haughton VM, Kneeland JB: Articular cartilage: correlation of histologic zones with signal intensity at MR imaging. *Radiology* 1991;181:853-5 3. Paul PK, Jasani MK, Sebok D, et al: Variation in MR signal intensity across normal human knee cartilage. *J Magnet Reson Imag* 1993;3:569-74 4. Rubenstein JD, Kim JK, Morava-Protzner I: Effects of collagen orientation on MR imaging characteristics of bovine articular cartilage. *Radiology* 1993;188:219-26

$T_{1\rho}$: An Alternative Contrast Parameter in Magnetic Resonance Histology

Robert Thomas Engelhardt, Ph.D. and G. Allan Johnson, Ph.D

The Center for *In Vivo* Microscopy, Department of Radiology,
Duke University Medical Center, Durham, NC 27710, USA

Magnetic resonance histology (MRH) has shown considerable promise in the evaluation of fixed tissue specimens [1] As the field strength is increased to increase the SNR and resolution in the MR microscope, conventional contrast parameters, T_1 and T_2, may prove to be less viable contrast mechanisms.

We have explored the use of $T_{1\rho}$ as an alternative contrast parameter in high-field MRH, through MR microscopy experiments on a 2.0 T and 9.4 T Bruker CSI systems. Phantoms were characterized and related to the literature using spectroscopy experiments at 9.4 T (5.75% agar gel, 1.0 mM $MnCl_2$, 7.3% and 20% gelatin). Imaging experiments were performed at both 2.0 and 9.4 T on two, 17.5 day old, perfusion fixed, mouse embryos, embedded in gelatin to minimize drying and susceptibility differences. T_1, T_2, and $T_{1\rho}$ have been measured for several types of tissues at four locking field strengths (0.7, 0.9, 1.3 and 1.7 G).

T_1 and T_2 imaging experiments were performed using a conventional spin warp imaging sequence. $T_{1\rho}$ imaging experiments were performed using a presaturating spin locking pulse, followed by a conventional spin warp imaging sequence. Muscle, diencephalon, lung and liver were chosen for the relaxation time measurements as they offered both good tissue specificity and size.

Both static and locking field dispersion of $T_{1\rho}$ were observed in the selected mouse embryo tissues. The observed $T_{1\rho}$ relaxation times were generally significantly longer than the T_2 relaxation times, increased with locking field strength, and were consistently shorter at 9.4 T than at 2.0 T. Mono-exponential $T_{1\rho}$ decays indicate that a free water/bound water exchange mechanism is important in the locking field dispersion. The static field dispersion of $T_{1\rho}$ and T_2 are both believed to be due, in part, to diffusion losses through susceptibility induced gradients (paper in preparation for submission to Magnetic Resonance in Medicine). The losses are much smaller in the $T_{1\rho}$ images, and decrease as the locking field is increased. Under commonly used circumstances, $T_{1\rho}$-weighting produces similar or improved contrast over T_2-weighting, but without significant susceptibility artifacts.

1. Johnson, GA, et al., Histology by magnetic resonance microscopy, *Magnetic Resonance Quarterly*, 1993. 9(1): p. 1-30.

Acknowledgments: This work is supported in part by NIH grant # P41 RR05959.

NMR microimaging of relaxation enhancement and magnetic susceptibility changes due to heavy metal loading of an alginate biosorbent

N.Nestle, R. Kimmich
Universität Ulm, Sektion Kernresonanzspektroskopie,
Albert-Einstein-Allee 11, D-89069 Ulm, FRG

In recent years, heavy metal uptake by alginate and other biopolymers has been studied by various methods. Such materials are of interest especially of two reasons:
1) they offer an alternative to synthetical ion exchange resins in the treatment of industrial waste waters.
2) alginates and similiar gelling polysaccharides are very popular agents for cell immobilization in biotechnology; absorption of heavy metal ions in such immobilization matrices might change the behaviour of the entrapped cells.

Most of the work done on heavy metal biosorption processes was concerned with the sorption equilibria of different heavy metal ions in dependence of various experimental parameters. In some publications, the kinetics of absorption were studied, too (*e.g. 1*). However, despite a controversy on the appropriate description of ion uptake behaviour in alginate gels, no experiments on the temporal evolution of the ions' spatial distribution during the absorption process are known to us.

NMR microscopy is an excellent tool to perform such studies:
As many heavy metal ions (e.g. Cu^{2+}, rare earth and actinoid ions) are paramagnetic, NMR relaxation behaviour and magnetic susceptibility distribution of the gel samples changes upon absorption of such ions. There is also an observable - albeit smaller - change in relaxation rates upon loading with certain diamagnetic ions such as Th^{4+} and UO_2^{2+}.

These changes can be exploited as contrast mechanisms in NMR microimaging. Relaxation weighted images are straightforwardly acquired using standard imaging sequences (e.g. *2*). Another approach for image contrast is susceptibility: while differences in susceptibility are also observable as a source of artifacts in conventional images (due to the simple geometry of our tube-shape samples, they even allow estimates of ion concentration), a quantitative mapping of this parameter is possible by means of resonance offset imaging (*3*).

In our contribution, we shall present results of our different imaging approaches along with a theoretical interpretation of what can be learned from the images about the kinetics of the absorption processes.

1. Kuyucak N, Volesky B (1989) *Biotechnology & Bioengineering* **33** 809-814
2. Nestle N, Kimmich R (1995) *Applied Biochemistry and Biotechnology*, in press
3. Weis J, Frollo I, Budinsý L 1989 *Zeitschrift für Naturforschung* **44a** 1151-1154

Microimaging of microcarrier cultured cancer cells

Ulrich Pilatus, Dmitri Artemov and Jerry D. Glickson

Division of NMR Research, Department of Radiology,
The Johns Hopkins University School of Medicine, Baltimore, MD, 21205

NMR spectroscopy of cultured cell lines under physiological conditions requires high cell densities (> 10^7 cells/ml) and continuous perfusion. For adherent cell lines this can be achieved by growing the cells on microscopic spherical carriers (Ø > 100µm) which provide a large surface area in small volumes. The cell-covered microcarriers can be immobilized in the NMR tube enabling perfusion of the sample. In this setup viable cells are maintained during NMR experiments for more than 48h. Cell growth can be monitored by recording increase in phosphate metabolites with ^{31}P NMR. Alternatively, diffusion weighted ^{1}H NMR spectroscopy can be used to monitor other intracellular metabolites (e. g. choline, creatine, lactate) [1]. In addition, by analyzing the attenuation of the water signal as function of the gradient strength, the total intracellular volume, cell size and the apparent intracellular water diffusion constant can be determined [2]. All these methods provide a gross sample average and the data can only be interpreted assuming a sample with homogeneous distribution of cells and microcarriers. Formation of channels and areas, where the perfusion is blocked by high cell density might lead to a heterogeneous cell population with cells in poorly perfused areas having different metabolite concentrations. Here we demonstrate that homogeneous sample composition and cell growth can be monitored by NMR microscopy.

Cells, grown on spherical solid polystyrene carriers (150 -300µm ø), were transferred into a 10mm screw cap NMR tube and immobilized by tightly fitting them between two filters fixed to a central capillary which is used to guide the perfusate to the bottom of the tube. A spin density NMR image was obtained with gradient echo, with in plane resolution of 40µm x 40µm, slice thickness of 150µm, 6ms echo time, and a repetition time of 100ms (Fig. 1a). It shows the central capillary in the middle of tube and a homogeneous distribution of the beads (dark areas). No significant change of this pattern was observed after 40h of cell growth in the perfusion system. A diffusion weighted image obtained under conditions of full suppression of the extracellular water signal [2] of the same region is shown in Fig. 1b. The size and intensity of the bright spots which represent intracellular water grew continuously during the experiment. No preferential areas could be detected which indicates homogeneous cell growth.

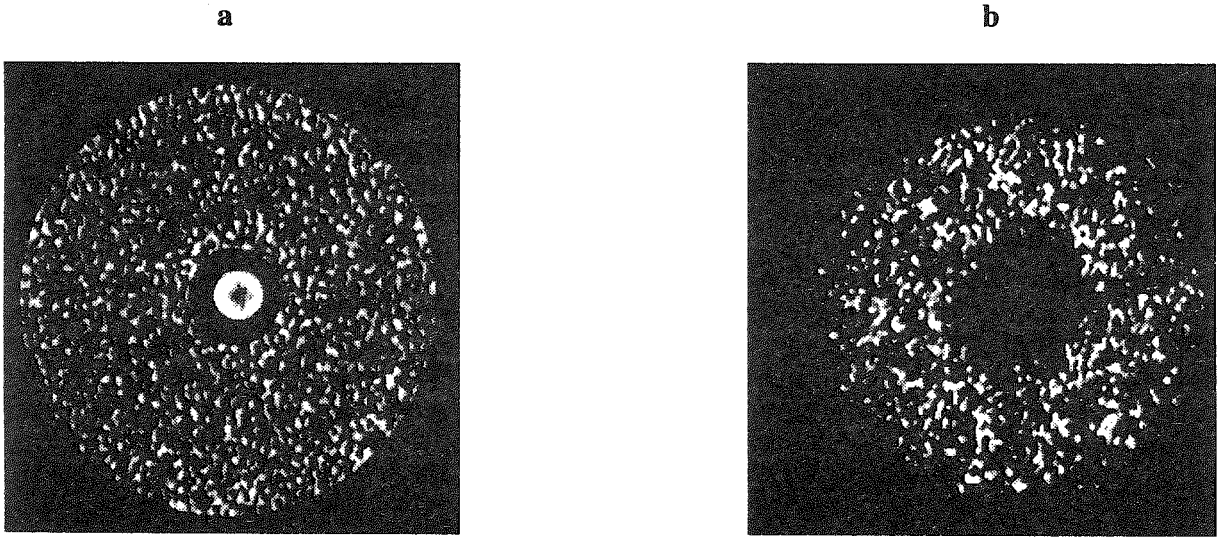

Fig.1: NMR images of cells on polystyrene beads, perfused in a 10mm NMR tube. a: Spin density image showing beads and water. b: Diffusion weighted image showing cell distribution.

References
1. P.C.M. van Zijl, C.T.W. Moonen, P. Faustino, et al., *Proc. Natl. Acad. Sci.* 88, 3228 (1992)
2. U. Pilatus, H. Shim, P.C.M. van Zijl, J.D. Glickson, Proc. Soc. Magn. Res. (1995) (in press)

Acknowledgment: This study was supported by NCI CA51950 and CA58235.

NMR-Microscopy of Transport in Fertilized Bird Eggs

U.Görke, J.Weis, R.Kimmich
Sektion Kernresonanzspektroskopie, Universität Ulm, 89069 Ulm, Germany

In all stages of incubation incoherent transport phenomena in fertilized bird eggs have been observed. In a previous paper we have already examined incoherent transport in fertilized hen eggs (1^{st} till 4^{th} day of incubation) by single voxel spectroscopically resolved diffusion measurements [1]. The apparent diffusion coefficient of water in egg white and yolk was larger than the diffusion coefficient of free water indicating macroscopically incoherent flows. In this work NMR micro imaging has been used for visualization of coherent and incoherent flow in fertilized bantam and quail eggs from the 4^{th} till 10^{th} day of incubation. The eggs were kept under hatching conditions in a saddle-coil implemented in the standard Bruker microimaging-probehead. Measurements were performed at 4.7 T with a Bruker BIOSPEC magnet and a PC-controlled RF and field gradient unit. The images were recorded using a gradient recalled echo sequence (FLASH). Transport was detected by a time-of-flight method imaging a DANTE multistripe tagging pattern or by encoding velocity with a bipolar magnetic field gradient (FEVI [2]). Both methods consistently show areas with and without movements of water. Distortions of the DANTE multistripe tagging grid clearly distinguish between coherent and incoherent flows with displacements up to 1mm/s. In addition, measurements with FEVI indicate that the movements are pulsating. The aim of this work is to demonstrate a method for characterization of biological macroscopically incoherent flows (perfusion) with NMR. This information may allow conclusion about the underlying mechanism which induce flow of the liquids inside the egg. Studying transport phenomena *in vivo* at this length and time scales can provide insight into the pathways of transport relevant for metabolism.

References

[1] F.Klammler and R.Kimmich, *Phys.Med.Biol.* **35**, 67 (1990)
[2] Bittoun, J., Bourroul, E., Jolivet, O., Idy-Peretti, I., Mousseaux, E, Tardivon, A., Peronneau, P., *Mag.Res.Med.* **29**, 674 (1993)

^{19}F NMR Imaging of 2-Deoxy-2-fluoro-D-glucose and Its Metabolites in Tumor Bearing Mice

Yoko Kanazawa, Keiko Umayahara, Toshiyuki Shimmura, and Tsuneo Yamashita*
Facutly of Pharmaceutical Sciences, Kyushu University, Fukuoka 812-82, Japan and Daikin Industries*, Settsu 566, Japan.

Introduction

2-Deoxy-2-fluoro-D-glucose (^{18}FDG) is known as a clinical radio-pharmaceutical for tumor diagnosis. In the previous NMR study of FDG in mice, we showed the metabolism beyond FDG-6-phosphate as follows. FDG-6-P is converted to its epimer, 2-deoxy-2-fluoro-D-mannose-6-P (FDM-6-P), followed by a further metabolism to its nucleotide bound form. In tumors, UDP-FDM is the dominant metabolite of FDG after 1 day, when the F compounds in other organs except for heart have almost been washed out. In the present work, the usefulness of ^{19}F NMR spectrum and images of FDG for tumor diagnosis in small animals was evaluated.

Methods

C3H mouse (8 - 9 weeks, female) transplanted with MH134 cells either as ascite or into subepidermal tissue on the back 8 days prior to the experiment was used after 16 h fasting. FDG was injected (200 mg/kg) through a tail vein. The mouse was fixed in the NMR sample holder under ether anesthesia. During the NMR experiments, anesthesia was mainteined with 0.5 % halothane/(air + O_2, 4:1). Varian Unity 400plus (9.4 T) equipped with 40 mm F/H body coils and shielded gradients was used for both spectrum and images. The ^{19}F images were obtained at 376 MHz with spin echo: Tr = 1 s, Te = 4 ms, 64 x 16 points, FOV 6 cm x 4 cm no slice, chemical shift selection of 1 kHz, data accumuration time of 40 - 160 min. The tumor cells and organs were excised immediately after ^{19}F imaging for the metabolite quantification by high resolution NMR.

Results

The ^{19}F image (Fig. 1) obtained (1) 1 h after the FDG injection, where the FDG-6-phosphate, the dominant metabolite in tumor cells, was selected as image object, and (2) 1 day later where UDP-FDM, the dominant species in tumor, was selected.
The concentration of UDP-FDM in the tumor determined after ^{19}F image (Fig. 1c) was 0.2 mmol/kg. That of FDG-6-P used for the 1 h image was estimated as ca. 1 mmol/kg. The method of FDG-NMR image was shown to have a potential for the tumor detection in small animals.

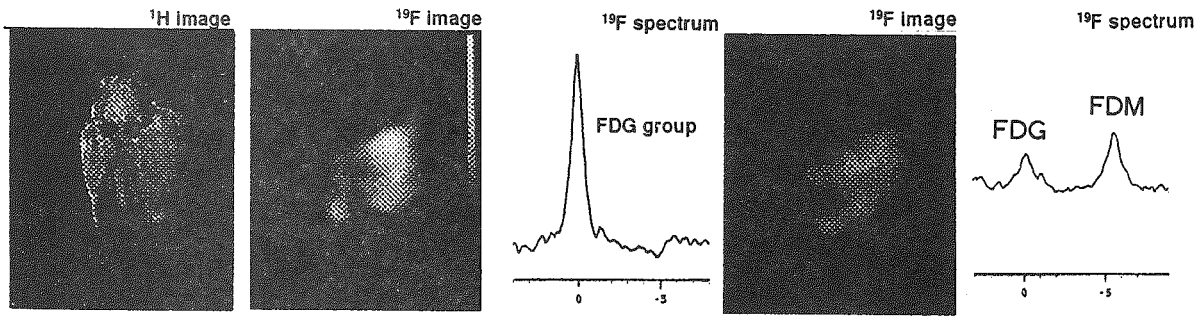

^{1}H coronal. ^{19}F,(1 h) FDG selected. 107 min data acquisiton. ^{19}F,(25 h) FDM selected. 160 min data acquisition.

Fig.1. Images of FDG injected mouse with subepidermal tumor on back.

Diffusion of Water in Rat Sciatic Nerve Measured by ^1H PFG NMR Spectroscopy and Microimaging: Compartmentation and Anisotropy

Y. Seo, Y. Morita*, Y. Kusaka* and M. Murakami

Lab. MRI&S, Dept. of Molec. Physiol., Natl. Inst. for Physiol. Sci., 38 Myodaiji, Okazaki, 444 Japan (E-mail: yseo@nips.ac.jp)
*Dept. of Orthop. Surg., Kyoto Pref. Univ. of Med., Kyoto, 602 Japan

Diffusion of water was measured in rat Sciatic nerve at 22.5 ± 0.5°C using spin-echo pulsed field gradient (SE-PFG) NMR spectroscopy and stimulated-echo pulsed field gradient (STE-PFG) imaging.

SE-PFG NMR spectra were observed at 2.34 T at 22.5 ± 1°C using an MSL-100 spectrometer with a gradient control unit (IRGU) and a diffusion probe (Diff25: actively shielded gradient coil up to 6 T/m) with a 10 mm diameter RF-coil (Bruker, Karlsruhe). Three diffusion coefficients (ca. 1, 0.3 and $0.02 \cdot 10^{-9}$ m²/sec at a diffusion time of 10 msec) were obtained, and the fraction of the three components changed by orientation of nerve fibers against gradient direction.

The extracellular water signal was quenched by $MnCl_2$ saline solution. Two diffusion coefficients of water was observed. The faster diffusion coefficient was $0.9 \cdot 10^{-9}$ m²/sec when the axis of the nerve fiber was set in parallel to the gradient field (D_0), and was $0.3 \cdot 10^{-9}$ m²/sec when the axis of the nerve fiber was set in perpendicular to the gradient field (D_{90}) at a diffusion time of 10 msec. Values of D_{90} and D_0 decreased when diffusion time was changed from 3 msec to 50 msec. A diameter of cylinder (5 μm) was obtained on an assumption of restricted diffusion in cylinders, which agree with a range of diameter of axon fibers in the rat sciatic nerve. The slower diffusion component did not show any orientation or diffusion time dependency, which might be assign intracellular water of myelin cells.

From these diffusion parameters, we can get diffusion weighted microimages for extracellular, intra-axonal and intra-myelin cellular water by using an AMX-300wb spectrometer with a gradient control unit (BGU-II) and a micro-imaging probe (Micro5.0: actively shielded gradient coil up to 2 T/m) with a 2 mm diameter RF-coil (Bruker, Karlsruhe).

3D Flow Measurement in the Coronary Arteries of the Perfused Beating Rat Heart

F. Roder*, K.-H. Hiller*, W.R. Bauer+, G. Ertl+, A. Haase*
*Physikalisches Institut, EP5, Universität Würzburg, Am Hubland, 97074 Würzburg
+Universitätsklinik Mannheim, 68135 Mannheim, Germany

Introduction:

The measurement of flow in the coronary arteries is of great importance for the understanding of heart failure and heart regulation mechanisms. We present a new technique to measure flow in the complete arterial vessel tree of the perfused beating rat heart.

Materials and Methods:

Heart Preparation: Hearts of male wistar rats were prepared according to the Langendorff mode. Retrograde perfusion was done with Krebs-Henseleit-buffer equilibrated with Carbogen (95% O_2 , 5% CO_2). The hearts were constantly perfused with a total coronary flow rate of 18 ml per minute. A water filled Latex-balloon was inserted into the left ventricle to measure left ventricular pressure. The pressure curve was registered in a Personal Computer, which performs trigger pulses to synchronize the MR-pulse-sequence to the heart cycle. The hearts were beating with rates of about 270 beats per minute.

MR-Imaging: The Imaging was done with a 11.7 Tesla Bruker AMX500 wide bore system, which is equiped for micro-imaging. The data were acquired with a thick slab 3D gradient echo sequence, which acquires 8 successive echos with different flow encodings. The pulse sequence (see fig.1) was synchronized to the heart cycle (TR≈220ms), while the echotimes were TE= 1.4/2.8/6.8/8.2/12.2/13.6/18.4/19.8 ms. The total imaging for 64x64 phase encoding steps is about 15 min.

Data-analysis: For it is well known that the signal phase is sensitive to flow in magnetic resonance, we reconstructed the phase by Fourier-transformation. From the phases in each voxel we can calculate the velocity in each voxel.

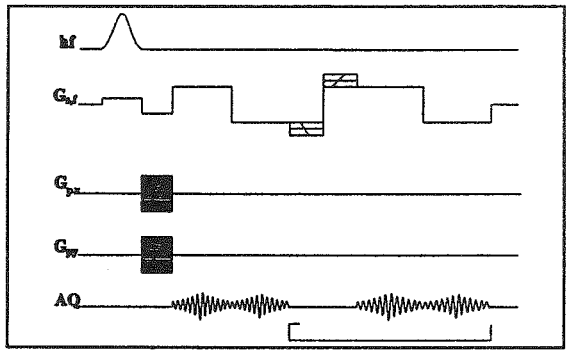

Fig 1:*3D-MR-Imaging sequence, with multi echos for flow encoding.*

Results:

Figure 2 shows the calculated flow-profile (v_z) in one vessel in 6 subsequent slices, while the vessel is orientated in z-direction as well. The total flow measured in this vessel is 2.3±0.8 ml/min. Greater flow is measured in slice 5 and 6, although no bifurcation is seen in this segment of the vessel.

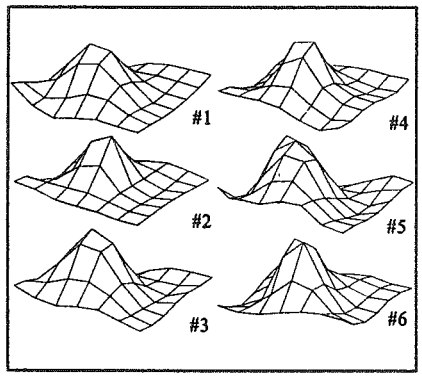

Figure 2

Discussion:

The method offers the possibility to measure the flow in all three directions (v_x,v_y,v_z). But it is limited to encode the flow in read direction. So it is necessary to do three readouts to measure flow in all three directions.

The measured flow in the one vessel seems to be in the correct range compared to the total coronary flow, while the variation is not satisfying. The exact flow measurement is disturbed by T_2^*-effects, which influences especially the measured phase in the higher echos. This disturbance might be avoided by the use of spin-echos instead of gradient-echos.

Nevertheless this technique will offer new information, while the magnitude images can be processed as normal angiograms of the coronary vessels [1].

Acknowledgements:

This work was supported by grant of the "Deutsche Forschungsgemeinschaft" (DFG) (DFG-Ha 1232 /8-1,DFG-SFB355).

We thank S.Voll for her help.

References:

1. Roder F, Bauer WR, Haase A, et.al. Visualization of coronary arteries of the perfused rat heart with 3D-MR-Microscopy. Proc.of the SMRM 1993,1,#300

NMR Microimaging of Mouse Tail Tendon Collagen: A Non-Destructive Approach For Studying Aging Associated Changes In Collagen Structure

Fernando Commodari, and Richard G. S. Spencer
National Institutes of Health, National Institute on Aging, Gerontology Research Center, 4940 Eastern Avenue, Baltimore, MD USA, 21224

Magnetic resonance microscopy is non-invasive and non-destructive and may be used *in vivo* to probe dynamics and structure. *In vitro* age related changes in collagen on excised rat tail tendon have been demonstrated in the literature using physical-chemical techniques. In the present work, NMR microimaging is used in the study of hydration in mouse tail collagen. The main goal is to obtain information on water mobility and binding characteristics, and on macromolecular structure and dynamics at the water-tendon interface in normal, aged, and diseased states. The availability of transgenic mice with known collagen defects, provides a model for comparison of intrinsic NMR relaxation and diffusion parameters to aging mouse tail tendon *in vivo* using NMR. This work complements high resolution liquid and solid-state NMR studies of structure and dynamics at the molecular level *ie.* water-polypeptide interface.

In developing a methodology for these studies, preliminary data analysis of NMR microimages obtained at 9.4 T (FOV 8mm x 8mm; NA=2, 2mm slices, 256 x 256 MTX, TR=1.5 s, TE= 8 to 60ms) for nude mouse tails shows that for a tendon region of interest (ROI), the T_2 is (13 ± 2) ms and for a muscle ROI the T_2 is (41 ± 23) ms. These values are based on repeated measurements on the same ROIs for the same tail. The limitations and problems encountered with this protocol will be discussed as will possible solutions to these problems and future directions.

Strain and Water Kinetics in the Compressed Intervertebral Disc Analyzed by High Resolution MRI

O. Uyemura*,, Y. Kusaka*, S. Nakajima*, H. Hase*,**
Y. Hirasawa*, T. Morimoto, Y. Seo*****
*Dept. of Orthop. Surg. & **Dept.of Physiol., Kyoto Pref. Univ. of Med., Kyoto 602 Japan
***Dept. of Molecular Physiol., National Inst. for Physiol. Sci.

INTRODUCTION : The intervertebral disc has a water-rich region at its center called nucleus pulposus, which is surrounded by a water-tight fibrous tissue called annulus fibrosus. A load applied to the disc makes the disc height decrease and the disc matrix expand horizontally. At the same time, the intradiscal water moves within the disc and the applied energy is transformed into the kinetic energy of the water. This mechanism is very important for absorbing mechanical stress applied to the disc. The aim of this study is to clarify the strain and water kinetics within the compressed disc.

MATERIALS AND METHODS : Six bovine coccygeal intervertebral discs were obtained with adjacent vertebral bodies. Markers of monofilament nylon threads (0.3mm in diameter) were inserted into the disc in the anterior-posterior direction to visualize the matrix strain on MR coronal images. The specimen was fixed in a non-magnetic compression device which was set at the center of the magnet (Biospec47/40, Bruker). A 700kPa static load was applied toward the major axis of the spine for 240minutes. Mid-coronal MR images (gradient echo images and T_1 calculated images) were taken before and during compression. The water content of the nucleus pulposus can be estimated from the T_1 calculated image, since the T_1 relaxation time has positive correlation with the water content in the nucleus pulposus(Spine,2271-75,1993). The disc height, width and the position of nylon threads were measured on gradient echo images. We also calculated the volume of the nucleus pulposus with its height (h) and the diameter (2r) as $\pi r^2 h$.

RESULTS : The diameter of the nucleus pulposus expanded more rapidly than that of the intervertebral disc in the early phase of loading. The calculated volume of the nucleus pulposus increased and reached at the maximum value at about 40 minutes after the beginning of compression. The water content at the center of the nucleus pulposus changed similarly to the volume of the nucleus pulposus.

DISCUSSION : The volume of the nucleus pulposus increases temporarily because the effect of increase in the diameter of the nucleus pulposus is greater than its decrease in height. This means, there is a concentric water movement in the compressed disc. The concentric water movement might come from the following reasons. The diameter of the nucleus pulposus increases more rapidly than that of annulus fibrosus in the early phase of loading. During this phase, the density of solid matrix at the nucleus pulposus decreases, while the one around the nucleus pulposus increases. This unequal strain in the disc generates pressure gradient within the disc which causes concentric water movement.

Functional MRI of the somatosensory cortex in rats during stimulation of the forepaw: Dependence of signal intensity on stimulation frequency

M. L. Gyngell, C. Bock, B. Schmitz, M. Hoehn-Berlage, K.-A. Hossmann

Max-Planck-Institut für neurologische Forschung, Gleuelerstr 50, D-50931 Köln, Germany.

Introduction

Functional MRI based on T_2^* weighted sequences has been used to startling effect in the mapping of brain function in humans (1) and has been demonstrated by Hyder (2) to be applicable to animal models. The purpose of this study was to investigate the behaviour of the fMRI signal enhancement during stimulation as a function of the stimulation frequency in α-chloralose anaesthetised rats, using a model described by Ueki (3).

Methods

Male Sprague-Dawley rats (n=4, body weight=390-450g) were used. The surgical preparation was performed with the animals anaesthetised by 1.2% halothane in a 7:3 mixture of N_2O and O_2 delivered via a face mask. Following tracheotomy and paralysis with pancuronium bromide (0.2 $mg.kg^{-1}.h^{-1}$) the animals were artificially ventilated to keep arterial pCO_2 at about 40mmHg and then placed prone in a plexiglass stereotactic headholder for accurate positioning within the NMR spectrometer. Halothane anaesthesia was discontinued 45 to 60 minutes prior to the NMR measurements and substituted by an intravenous administration of α-chloralose ($80mg.kg^{-1}$) and replacing N_2O by N_2. Chloralose was supplemented ($40mg.kg^{-1}$) at 90 minute intervals. A pair of small needle-electrodes were inserted into the skin of each forepaw so that they could be independently electrically stimulated. The stimulation consisted of rectangular pulses of 0.3ms duration and 0.5mA current applied with frequencies of 1.5, 3, 4.5, 6, 7.5 or 9Hz.

Multi-slice FLASH pilot scans were used to define an imaging plane for the functional studies slicing coronally through the somatosensory cortex at 1.25mm anterior to the bregma. Functional imaging was performed using a FLASH sequence with a heavy T_2^* weighting (TE=60ms, TR=70ms, $\alpha=22.5°$). The scan time was 4.5 seconds per image for 64^2 pixel matrix. A field-of-view of 24mm and a slice thickness of 1.5mm were employed. Typically 8 images were acquired prior to stimulation and 8 during stimulation. Electrical stimulation was applied for 40s. These sets of 16 images were obtained with stimulation of one paw. This was carried out for each of the stimulation frequencies given above. The procedure was then repeated for the other paw.

Results and Discussion

Subtraction of images acquired without stimulation led to perfect cancellation within the brain and in outlying structures. Subtraction of control images from stimulation images revealed hyperintense areas in either the right or left somatosensory cortex as a result of left or right forepaw stimulation respectively. The fMRI signal was, in all animals, most pronounced for stimulation at 1.5 and 3Hz. The hyperintensity reduced continuously from 4.5Hz to 9Hz. No signal was seen at 9Hz stimulation frequency. At 7.5 Hz the hyperintensity was just detectable in averaged datasets. This is consistent with laser-Doppler measurements of cerebral blood flow made outside the magnet using the same stimulation protocol which showed a similar response. The frequency response of the neurons may be a predictor of recovery following a pathological state. This study suggests that it is possible to use fMRI techniques to investigate the integrative central nervous system function in longitudinal studies of disease models.

References

(1) J.W. Belliveau et al, Science, **254**, 716-719 (1991)

(2) F. Hyder et al, J. Cereb. Blood Flow Metab., **14**, 649-655 (1994)

(3) M. Ueki et al, J. Cereb. Blood Flow Metab. **8**, 486-494 (1988)

Ultrafast perfusion measurement for the observation of functional activation of rat brain during forepaw stimulation: comparison with functional MRI

M. Hoehn-Berlage, C.M. Kerskens, E. Busch, B. Schmitz,
C. Bock, M.L. Gyngell, K.-A. Hossmann
Max-Planck-Institut für neurologische Forschung, Köln

Introduction: Functional activation in α-chloralose-anaesthetized rats was described by Ueki et al.(1). This animal model was used by Hyder et al. (2) to show that fMRI will detect functional activation. Williams et al. (3) demonstrated that the spin tagging method monitors blood perfusion in rat brain as a function of arterial pCO_2 variation. Their technique, however, was based on a slow spin-echo sequence, thus excluding the recording of fast perfusion changes.
Here, we show an ultrafast version of the spin tagging perfusion technique, based on snapshot FLASH, with a measurement time of only 3s. Sensitivity of the technique is demonstrated by application to perfusion changes during functional activation of rat brain during forepaw stimulation. Finally, comparison with the activated area as observed by regular T_2*-fMRI is shown.
Methods: Sprague-Dawley rats were anaesthetized with α-chloralose (80mg/kg). For electrical stimulation, small needle electrodes were inserted into the skin of both forepaws. Rectangular pulses (0.3 ms; 0.5mA) were applied at 3Hz for 1 min. NMR measurements were performed on a 4.7T BIOSPEC system (Bruker), equipped with actively shielded gradients. A 12cm Helmholtz configuration was used for excitation, a 16 mm surface coil for signal detection. Both coils were decoupled. The perfusion sequence consisted of two similar image acquisitions, separated by 10s, with a magnetisation preparation step of 3s followed by snapshot FLASH imaging. In the first (inversion) acquisition, blood flowing into the brain was inverted adiabatically in the neck through a combination of a magnetic field gradient (1G/cm) in the z-axis and a B_1-field of 50mG, set off-resonance to excite a slice through the neck, approximately 2cm upstream from the imaging plane. In the second (control) acquisition, the field gradient was reversed to leave flowing spins undisturbed. A perfusion-weighted image was obtained by subtraction of both acquisitions which suffered the same signal loss due to magnetisation transfer but differed in magnetisation of inflowing spins. Snapshot FLASH was recorded with centric phase encoding, TR=3.5ms, TE=2.0ms resulting in 224 ms imaging time for a 128x64 matrix. Field-of-view was 4cm, slice thickness 2mm. The T_2*-weighted sequence for fMRI used FLASH with TE/TR of 60/70ms, and a flip angle of 22.5°.
Results: Switching anaesthesia from halothane to α-chloralose resulted in a loss of signal intensity in perfusion-weighted images as a consequence of blood flow reduction. Stimulation of forepaw caused a well circumscribed increase in signal intensity in the somatosensory cortex. To show specificity of the localized hyperintensity, stimulation was alternated between left and right forepaw, thus resulting in hemispheric exchange of the activated cortex region. Subtraction of two inversion images, recorded during rest and stimulation, respectively, also depicted the hyperintense region of the activated somatosensory cortex area. Thus, a temporal resolution of 3s could be achieved. The area of increased perfusion was in excellent spatial agreement with the territory observed in T_2*-weighted fMRI upon stimulation.
Conclusion: We have introduced a fast perfusion-sensitive technique. Influence of different anaesthetics on cerebral perfusion can be observed. For the first time, it has been shown that spin tagging can detect localized blood flow changes during functional activation in anaesthetized animals. The high temporal resolution makes this technique an important complementary experiment for fMRI. Apart from a wide range of future applications to study cerebral blood flow under pathological conditions, this technique may also help answer the question of the relative contribution of inflow versus BOLD effects in T_2* functional imaging.

1) M. Ueki, F. Linn, K.-A. Hossmann, J. Cereb. Blood Flow Metab. 8:486-494 (1988)
2) F. Hyder, K.L. Behar, M.A. Martin, A. M. Blamire, R.G. Shulman, J. Cereb. Blood Flow Metab. 14: 649-655 (1994)
3) D.S. Williams, J.A. Detre, J.S. Leigh, A.P. Koretsky, PNAS 89: 212-216 (1992)

What Can We Learn From Spiders?

Y. Xia* and L. W. Jelinski§

* Department of Physics, Oakland University, Rochester, MI 48309, USA

§Center for Advanced Technology - Biotechnology, Cornell University, Ithaca, NY 14853, USA

The dragline silk fiber from the golden orb-weaving spider, *Nephila clavipes*, has some unique features. For example, the silk fiber is stronger per unit weight than steel, it is more elastic than nylon, and it is almost perfectly optimized between high tensile strength and high elasticity. Even more remarkably, the spiders spin the silk fiber at room temperature, atmospheric pressure, and using water as a solvent. By comparison, steel and synthetic polymer manufactures require high pressures, high temperatures, solvents, and catalysts. The following table compares the natural silk fiber with several man-made materials.

Material	Tensile Strength (GPa)	Energy to break (10^3 J kg^{-1})
dragline silk	1	100
high tensile steel	2	1
KEVLAR	4	30
rubber	0.001	80

There are a number of fundamental questions that one can ask about the spider silk. Two of them are:

- Why is the (dragline) silk fiber so strong?
- How does the (dragline) silk fiber become so strong?

The first question addresses the molecular structure of the silk fiber, which consists almost entirely of protein. The second question probes into the processing that takes place inside the major ampullate glands, which produce the dragline silk. Note that the silk is in liquid state inside the glands and it is solid when the silk is released from the spinneret at the end of the spider body.

We have used multislice NMR Microscopy to image live spiders at a transverse resolution of 45 μm per pixel and with a 300 μm slice thickness. Results from the preliminary studies indicate that it is possible to spatially resolve the major ampullate glands inside the spider body *in vivo*, and that the features in the NMR images of spider match the anatomic pictures acquired using optical microscopy. Three-dimensional image reconstruction of the spider is in progress.

NUCLEAR MAGNETIC RESONANCE MICROSCOPY OF THE DEVELOPMENT OF THE PARASITOID WASP *VENTURIA CANESCENS* WITHIN ITS HOST MOTH *PLODIA INTERPUNCTELLA*

JOHN A. CHUDEK*, ALISON M.E.CROOK*, STEPHEN F. HUBBARD#, and GEOFFREY HUNTER*

Departments of Chemistry* and Biological Sciences#
University of Dundee
Dundee DD1 4HN,
Scotland

Nuclear magnetic resonance microscopy was used to image the parasitoid wasp *Venturia canescens* (Hymenoptera: Ichneumonidae) within larval and pupal instars of its host, the Indian Meal Moth, *Plodia interpunctella* (Lepidoptera: Pyralidae). The images were obtained using gradient echo and chemical shift selective pulse sequences and clearly showed the location and shapes of the parasitoid as it developed from a L_1 larva to a pupal stage within the host. The digestive, nervous and tracheal systems of the host were identified and changes were observed as the host underwent metamorphosis. Destruction of the host tissues by the parasitoid was visible. It was found that the parasitoid first ate the fat body and digestive system of the host, allowing the host to continue to grow, and only progressed to the vital organs when its own development neared pupation.

Magnetic Resonance Microscopy of Internal Structure of the Honey Bee Drone and Queen

B TOMANEK, A JASIŃSKI, Z SUŁEK, P KULINOWSKI, S KWIECIŃSKI, A KRZYŻAK,

T SKÓRKA, J KIBIŃSKI, J MUSZYŃSKA*

H. Niewodniczański Institute of Nuclear Physics, MRI Laboratory, 31-342 Kraków, Poland

*Institute of Pomology and Floriculture, Division of Apiculture, 24-100 Puławy, Poland

Non-invasive investigation of insects internal structure is a nontrivial problem. All the work reported so far was done post mortem after killing an insect. In most cases internal organs are studied after extraction from the insect body. Optical microscope images of anatomical cross sections of thin slices are very rare in the literature because hard hityne outer shell of insect makes cutting very difficult. In this work we applied Magnetic Resonance (MR) microscopy to image honey bees of all casts to see whether physiologically useful information can be obtained from MR images.

Magnetic Resonance microscopy was used to record MR images of internal structure of honey bee *Apis mellifera carnica* drone and queen *in vivo*. Honey bees were immobilized by placing them inside a glass tube and cooling down to around 10°C. A home built MR microscope operating at 270 MHz capable of producing images of honey bees with in plane resolution of 30 μm × 30 μm from a slice of 440 μm was used.

MR images of saggital and transverse cross-sections through head, thorax and abdomen of the drone, and a saggital image through abdomen of the queen are presented. A number of internal organs of the drone such as: brain, oesophagus, thoracic ganglion, aorta, testis, spermatic ducts and mucus gland were identified. In the queen image ovary, midgut, spermatheca, vagina, sting cavity, rectum and air sacs are clearly visible.

Financial support from the Committee for Scientific Research grant No 2 2442 91 02 is gratefully acknowledged.

One-dimensional profile of restricted diffusion of cell-associated water in plant tissues

N. Ishida*, H. Ogawa** and H. Kano***

* National Food Research Institute, Tsukuba, Ibaraki 305, Japan
** JEOL Datum Ltd., Akishima, Tokyo 196, Japan
*** National Institute of Agrobiological Resources, Tsukuba, Ibaraki 305, Japan

Restricted diffusion of cell-associated water in cherry fruits during ripening was examined by NMR microscopy to know properties of individual tissues in the fruits. Intracellular compartment size (a), permeability of membrane partitions consisting of the compartments (P) and diffusion coefficient (D_0) which characterize cell conditions, were attempted to be estimated.

An NMR spectrometer (JEOL GSX-270 WB) and its micro-imaging system (JEOL GIM-270) were used for measurements. Diffusion weighted images were measured by a pulse-gradient stimulated-echo method with a 90°(X)-90°(Y)-90°(Y) pulse sequence. The data were transferred to a microcomputer and treated according to Meerwall and Ferguson's modification (1981) of the model of Tanner (1978). Since measurement of images took a long time and it required many images measured by changing diffusion time to calculate above parameters, a, P and D_0, one-dimensional profiles of restricted diffusion with various diffusion times were measured in a short time by selectively exciting narrow areas along with a line paralleling the X-axis of NMR images.

Large amount of water was detected in the seed while water in the pericarp was small in early stages of fruit growth. Water decreased in the seed but increased in the pericarp with progression of the growth stages. Intracellular transport rate of water (D_0) was high in the early growth stages and grew low with ripening in the seed, while it showed a contradictory trend in the pericarp. Size of the compartments (a), in which water was freely transported, slightly increased in the young but permeability of the membrane partitions (P) gradually decreased with the growth stages.

Quantification of xylem water flow under different environmental conditions as measured by Gd-DTPA induced signal enhancement in NMR imaging.

E. Kuchenbrod, E. Kahler, A. Haase

Physikalisches Institut, Lehrstuhl für Biophysik, Am Hubland, 97074 Würzburg, Germany

Introduction: Measurement of xylem water flow velocity is an important tool in the investigation of long-distance water transport in plants. We present a new method for the investigation of this parameter based on the reduction of T_1 relaxation times of Gd-DTPA doped nutrient solution.

Materials and Methods: For the experiments young maize plants (*Zea mays*, 14 - 16 days old) were used, which were grown in hydroponics and kept in hydroponics for the NMR measurements. The experiments were performed on a Bruker AMX500 NMR microscope with a field strength of 11.75 Tesla. During the experiments the plants were placed in a climate chamber which allows the simultaneous measurement of the transpiration of the plants. Both flow and transpiration were measured while changing the illumination.

The plants were cut above the corn and the excised plant was placed in a tube with nutrient solution. The plant was positioned in the probehead adjusting an image slice 57 mm above the cutting plane. The nutrient solution was exchanged by a Gd-DTPA doped nutrient solution (concentration 5mM, $T_1 \approx 50$ ms). The flow velocities were determined by measuring the uptake of the contrast agent indicated by a signal enhancement with time. The ascent of the solution in the plant was imaged by a rapid series (48 images) of spin echo images with a temporal distance of 8.53 s. Further experimental parameters were:

FOV = 4x4 mm^2, 128 x 32 pixel (zerofilled to 128 x 128 pixel),

slice = 1.5 mm, TR = 133 ms, 2 averages

acquisition time for one image 8.53 s.

The velocities were calculated by measuring the duration of sap ascent and the distance between cut and measuring point.

After each experiment the undoped solution was reexchanged and the flow velocities were measured now by the time course of signal loss. Furthermore this allows several experiments on the same plant.

Results: The measured xylem flow velocities are in the range of 200 µm/s (lower limit of the experiment) to 2500 µm/s depending on the illumination. The change in water flow velocity with changing illumination is in agreement with transpiration changes although there are significant deviations in the behaviour of different vessels.

The velocities measured by Gd-DTPA inflow are for nearly all vessels higher than the velocities determined by Gd-DTPA outflow.

Conclusion: With this contrast agent method an easy method is available to determine xylem water flow velocities. The reversibility of Gd-DTPA uptake also allows functional measurements on a single plant. In comparison to PGSE methods for flow determination the method is fast and its analysis is straightforward. The significant difference in flow velocities for the inflow and outflow experiment is still not completely understood. A disadvantage is clearly that the experiments are invasive as they are performed on excised plants since the contrast agent cannot penetrate the plant roots.

Investigation of water transport in intact plants with direct and indirect deuterium NMR imaging

E. Kahler, E. Kuchenbrod, A. Haase
Physikalisches Institut, Lehrstuhl für Biophysik, 97074 Würzburg, Germany

Introduction

Deuterium has been widely used as a tracer for water transport in plants in biological research (1). The purpose of our study is to apply this tracer in NMR microimaging for investigation of water transport in intact plants. We concentrate on horizontal water transport in plants out of the vascular bundles into surrounding parenchyma tissue which is not accessible by conventional NMR flow or diffusion measurements (2,3).

Theory

Assuming diffusion–like processes as the major contribution for horizontal water transport in parenchyma tissue, the time course of deuterium enrichment in a horizontal slice of a plant can be described by an exponential function (4). To approximate this transport process we developed two models for a plant leaf. These two models simulate the structure and form of a plant leaf and its surrounding vascular bundles in two different ways. The time evolution of deuterium enrichment in plants as an exponential function in these models. By their application upper and lower limit of a propagation constant for this transport process can be calculated.

Materials and Methods

For the NMR experiments we used young maize plants (*Zea mays*, 8-10 days old), which were grown in hydroponics. The experiments were performed on a Bruker AMX500 NMR microscope with a field strength of 11.75 Tesla, a bore size of 89 mm and maximum gradient strength of 700 mT/m. A homebuild 5 mm Helmholtz shaped RF coil was used. During the experiments the plants were placed in a climate chamber which allows the simultaneous measurement of the transpiration of the plants. The plants were supplied with nutrient solution with a concentration of 50% deuteriumoxid. The uptake and distribution of deuterium in plants were imaged by a series of spin echo experiments for about 5 - 6 hours. These experiments were performed both with proton and deuterium NMR imaging. The images show a horizontal slice of the plant about 4 - 5 cm above the corn. The images were acquired with following parameters:
^{1}H–imaging: TR = 2 s, TE = 3.58 ms, 2 averages, slice = 500 μm, FOV = (5×5) mm^2, 128^2 pixels.
^{2}D–imaging: TR = 1 s, TE = 15.0 ms, 8 averages, slice = 3000 μm, FOV = (8×8) mm^2, 128^2 pixels.
For each model the time evolution of deuterium enrichment was approximated in a three parameter fit by an exponential function leading to the propagation constants.

Results and Discussion

Both deuterium and proton NMR imaging are reflecting the deuterium distribution in plants and both methods are leading to the same results. The uptake of deuterium in the plants is a slow process. Depending on the size of the leaves, deuterium can be detected not before 1 - 2 hours in the NMR images. After 4 - 5 hours the uptake of deuterium reaches a steady state which depends on the concentration of deuterium in the nutrient solution. The signal enhancement in deuterium imaging (or the signal loss of proton imaging) is uniform troughout single leafs, though the dynamics of deuterium enrichment is different in each leaf. No harmfull effects on transpiration can be detected due to the administered deuterium. The calculated limits of the propagation constant for deuterium for horizontal transport processes in plants are found to be:

$$D_{lower} = 7.00 \cdot 10^{-9} m^2/s \qquad D_{upper} = 65.45 \cdot 10^{-9} m^2/s \tag{1}$$

Conclusion

With exogenously administered deuterium the horizontal propagation of water out of the vascular bundles into the surrounding parenchyma tissue can be visualized. Since the results are the same the investigations can be done by both deuterium NMR imaging or by the easier method of proton NMR imaging. For this transport process the limits of a propagation constant could be calculated which is roughly ten times higher than the free self–diffusion constant of deuterium ($2.272 \cdot 10^{-9}$ m^2/s). It is obvious that besides diffusion other processes must cause this transport process in plants.

References:

(1) J. Link, J. Seelig: *Comparison of Deuterium NMR Imaging Methods and Application to Plants*, J. Mag. Res 89, 310 - 330 (1990)
(2) E. Kuchenbrod, E. Kahler, F. Thürmer, A. Haase, U. Zimmermann: *Investigation of plant water flow under different environmental conditions using NMR imaging*, 3rd Meeting of the SMR, Book of Abstracts 478, August 1995
(3) E. Kuchenbrod, R. Benkert, H. Schneider, A. Haase, U. Zimmermann: *Quantitative NMR microscopy on Intact Plants*, MRI 13(3), 1995.
(4) J. Crank: *The mathematics of Diffusion*. Clarendon Press, Oxford, 1964

In Vivo Quantification of Sucrose in the Phloem Region of Ricinus Communis Seedlings by ^{1}H Spectroscopic Imaging

B. Kalusche *, J. Verscht +, A. Metzler *, W. Köckenberger +, E. Komor +, A. Haase *

* Physikalisches Institut, Universität Würzburg, 97074 Würzburg, Germany, + Pflanzenphysiologie, Universität Bayreuth, 95440 Bayreuth, Germany

Introduction

In most plants sucrose is the major form in which assimilated carbon is transported from the source organs to the sink organs. The concentration of sucrose in different parts of the plant is a point of high interest for the understanding of plant metabolism.
We investigated the phloem region of Ricinus communis as a model for the application of ^{1}H spectroscopic imaging (SI) to in vivo quantification of sucrose in plants. This method provides advantages over the conventional destructive measurements because it is non invasive and different parts of the same plant can be examined successively. We present data from two parts of the hypocotyl of Ricinus communis seedlings.

Methods

The experiments were performed on a BRUKER AMX 500 wide bore spectrometer with actively shielded gradients. We used 6 days old Ricinus communis seedlings grown in a special glass tube which fits into a micro imaging probe. For quantification we added a capillary tube with a solution of 200mM sucrose in 95% D_2O, 5% H_2O.
On the same plant two SI experiments were carried out. For the first experiment at the cell division zone 0.5cm behind the cotyledons (apical hypocotyl) we used a 5mm saddle coil. A 32x32x512 SI data set with a field of view (FOV) of 4mm was acquired. The total acquisition time was 1h 10m (repetition time TR 1s, 4 averages). For the second experiment at a site 1cm above the roots (basal hypocotyl) we used a 8mm saddle coil [1]. A 64x64x512 SI data set with a FOV of 6mm was acquired. The total acquisition time was 4h 30m (TR 1s, 4 averages). Both experiments were performed with a sweep width of 5000Hz and an echo time of 7ms. The slice thickness was 2mm.
The quantification was done by integration over the g_6 f_6 sucrose resonances (3.72 to 3.65 ppm).

Results

In the phloem region of the apical hypocotyl we found sucrose concentrations between 130mM and 160mM. In the phloem region of the basal hypocotyl the sucrose concentration was between 160mM and 230 mM. These values must be corrected with the dry weight share in the phloem tissue which is 28% for the apical hypocotyl and 12.2% for the basal hypocotyl [2].
This leads to sucrose concentrations in the phloem regions of 180-220mM for the apical hypocotyl and 180-260mM for the basal hypocotyl.

Discussion

The sucrose concentration of extracts of whole hypocotyl slices from different parts of the plant was examined photometrically. It was found to be 2-3 times lower in the apical hypocotyl than in the basal hypocotyl [2].
This behavior is not found in our NMR results from the phloem regions. The sucrose concentrations in the apical hypocotyl and in the basal hypocotyl are in good agreement. Photometrically examinations of phloem exudat from these parts of the hypocotyl showed the same behavior.
This leads to the conclusion that the sucrose gradient in the plant is not caused by the phloem region.

Conclusion

We applied ^{1}H spectroscopic imaging to the quantification of sucrose in the hypocotyl of Ricinus communis seedlings. In two different parts of the hypocotyl we measured sucrose concentrations of 180-260mM in the phloem region.
The total experimental time can be reduced by a decrease of the repetition time (T_1 of sucrose in the Ricinus communis seedlings ≈700ms). This will give the possibility of monitoring dynamic changes in plant metabolism while changing environmental parameters.

References

[1] Metzler, A., Köckenberger, W., von Kienlin, M., Komor, E., Haase, A., Book of Abstracts, Twelfth Annual Meeting, Society of Magnetic Resonance in Medicine, p. 298, 1993

[2] Köckenberger, W., PhD thesis, Bayreuther Forum Ökologie, BITÖK, Bd.14, 1995

AN APPLICATION OF NMR MICROIMAGING TO INVESTIGATE NITROGEN-FIXING ROOT NODULES

JOHN A. CHUDEK*, GEOFFREY HUNTER*, JANET I. SPRENT#, and GERALD WURZ*

Departments of Chemistry* and Biological Sciences#
University of Dundee
Dundee DD1 4HN,
Scotland

Various techniques to obtain high resolution NMR images (voxel sizes down to 39 x 39 x 250 mm) of nitrogen fixing root nodules from soybean (*Glycine max* (Merr.)) and peanut (*Arachis hypogaea L.*) are compared. Artefacts arose from variation in magnetic susceptibility and techniques for their minimisation are described. A series of T_1 (TR = 220 to 3020 ms) and T_2 (TE = 9.3 to 33.6 ms) weighted images are presented and possible interpretations in terms of nodule biochemistry and physiology are given.

The data and parameters presented are shown to serve as a basis for more extensive investigations of root nodules (e.g. the oxygen diffusion barrier or the mechanisms driving the regulation of the oxygen concentration in the infected zone by leghaemoglobin) by NMR microimaging.

Determination of 3-Dimensional Histology of Grape Seeds using NMR Microscopic Techniques

S.M. Glidewell[1], B. Williamson[1], J.A. Chudek[2], G. Hunter[2], R.J. McNicol[1] and B.A. Goodman[1]

[1] Scottish Crop Research Institute, Invergowrie, Dundee DD2 5DA, Scotland
[2] Department of Chemistry, University of Dundee, Dundee DD1 4HN, Scotland

Standard spin and gradient echo imaging techniques from the Bruker sequence library have been used to study seeds of grape berries in intact fruit and as separate entities in either Bruker AM300/WB or AMX300/SWB FT spectrometers with Bruker microimaging accessories. Both 2- and 3-dimensional images were generated under chemical shift selective, T_1-, or T_2-weighted conditions. By combining 3-dimensional imaging with surface rendering techniques it was possible to determine the internal histology of separated seeds, including visualisation of the endosperm, the embryo and the chalaza under appropriate experimental conditions, the features in the NMR images being related to structural components revealed by conventional histological techniques. Variations in the relaxation characteristics of tissues between different specimens may be the consequence of the high free radical contents of grape seeds, which may also be responsible, at least in part, for magnetic susceptibility enhanced image intensity associated with the seed surface.

3rd International Conference on Magnetic Resonance Microscopy, Wurzburg, August 1995

MR MICROSCOPY OF THE PLANT *Dactylis Glomerata*

S.Kwieciński, B.Tomanek, A.Jasiński, A.Krzyżak, P.Kulinowski, T.Skórka, Z.Sułek
H.Niewodniczański Institute of Nuclear Physics, Radzikowskiego 152, 31-342 Kraków, Poland

Introduction:
Plants are an excellent model for MR research, since they are immobile and rich of water, which consequently leads to the strong NMR signal. Our experiments were focused on the obtaining high quality MR images in normal conditions, supporting all physiological functions of the plant. As a case study, we chose a plant *Dactylis Glomerata.*

Materials and Methods:
Plant's stem was cut and placed immediately afterwards into the cylindrical probe, filled out with water. The whole set was put into the home made MRI System, based on the superconducting magnet 6.4 T, made by Oxford Instruments. The diameter of the typical stem varied from 3 to 8 mm.

The conventional Spin-Echo (T_1 &T_2 weighted) imaging sequence was used. The diffusion weighted MR imaging sequence, where an extra diffusion gradient (250mT/m) is applied in the direction perpendicular to the plant's stem symmetry axis and the direction of the magnetic field B_o, was also introduced. The images were recorded in form of a matrix 256x256 with in plane resolution from 15μm x 15μm up to 40μm x 40μm with slice thickness 300μm - 500μm.

Results:
Number of MR Images of the plant *Dactylis Glomerata* were obtained in the longitudinal and transversal directions. The thorough analysis together with histological comparative studies of the same samples was performed. By introducing diffusion gradient different details of the inner structure could be seen. A noticeable difference in contrast as to compare with T_1 and T_2 weighted one is observed. This is a method which possibly could lead to the exact measurement of the diffusion coefficient and distribution of velocities of vascular flow. Attempts to the imaging of the diffusion tensor were made.

Conclusions:
The images obtained are of outstanding quality with the reasonable signal to noise ratio. It proves to be a promising tool for research upon water dynamics in plants. MR Microscopy can be invaluable in measurement of water quality, diffusion and flow in any direction in plant tissue.

NMR Microimaging of Healthy and Diseased Potato Tubers

A.J. Snijder, S.M. Glidewell and B.A. Goodman

Scottish Crop Research Institute, Invergowrie, Dundee DD2 5DA, Scotland, UK

Procedures for discrimination of the different types of tissue in potato tubers have been investigated by NMR imaging at 7 T using a probe of "birdcage" design in a Bruker AMX300/SWB spectrometer with a 150 mm internal bore. 2- and 3-dimensional spin and gradient echo imaging sequences were used to determine the distribution of the vasculature, cortex, outer medulla and pith in healthy tubers of cvs Pentland Crown and Maris Piper. In tubers inoculated with the pathogens *Phytophthora infestans* (late blight), *Phoma foveata* (gangrene), *Fusarium sulphureum*, and *Fusarium coeruleum* (both of which cause dry rots), diseased and uninfected tissue were readily distinguished. Furthermore, tissue infected by different pathogens showed different imaging characteristics, although the decrease in NMR signal did not correlate with the decrease in water content of blight-infected tissue. EPR measurements on healthy and infected tissue revealed disease-induced changes in contents of paramagnetic species, the most significant being the Fe(III) component with $g = 4.3$ and we suggest that changes in relaxation times caused by variations in the contents of paramagnetic species represent the main sources of the contrast observed in these tissues. Examples are also presented of the development of blight-infected tissue using surface-rendering techniques for defining the boundaries between healthy and diseased tissues.

3rd International Conference on Magnetic Resonance Microscopy, Wurzburg, August 1995

Identification of the Sites of Frost Damage to Flower and Leaf Buds of Woody Perennial Fruit Crop Genera using NMR Microimaging

R.M. Brennan[1], J.A. Chudek[2], G. Hunter[2] and B.A. Goodman[1]

[1] Scottish Crop Research Institute, Invergowrie, Dundee DD2 5DA, Scotland
[2] Department of Chemistry, University of Dundee, Dundee DD1 4HN, Scotland

Low temperature stress is a major factor limiting the production of many temperate fruit crop species, including blackcurrant (*Ribes nigrum* L.) and raspberry (*Rubus ideaus* L.). Winter damage to buds of non-acclimatised raspberry plants results in cane death, whereas freezing injury during the flowering period is the principal abiotic factor limiting blackcurrant yields. The production of cultivars with improved low temperature tolerance at crucial stages of development is being aided by the use of NMR microimaging as an *in vivo* screening method in combination with a breeding programme using existing later flowering genotypes with other genotypes showing good physiological resistance to freezing. This paper reports the use of 3-dimensional NMR imaging procedures to identify the sites of freezing damage in leaf buds of raspberry and floral tissues of blackcurrant through the increase in signal intensity in T_2-weighted images of damaged tissue, where membrane disruption results in leakage of cellular contents into intercellular spaces.

3rd International Conference on Magnetic Resonance Microscopy, Wurzburg, August 1995

A NEW APPROACH TO STUDY FUNGAL INFECTIONS IN BIOLOGICAL MATERIALS.

H. Van As[1], D. van Dusschoten[1], C.P.A.M. Kloks [1,2] S. Nagarajan[1], and R. Sierra-Alvarez[2].

Wageningen Agricultural University
Dept. of Molecular Physics, Wageningen Agricultural NMR Centre[1] and Department of Forestry[2]
Dreijenlaan 3, 6703 HA Wageningen, The Netherlands.

There is much interest in prevention of fungal infections in biological materials and products such as plants, fruits and wood. Therefore, knowledge of the biochemical and biophysical properties of the infection process is of considerable interest. Since fungal infections affect water content and cell structures MRI is a sensitive technique to study these processes. However, imaging sequences that result in contrast from a combination of paramaters (proton density, T_1, T_2, T_2^*) can hardly be used for a correct and unique interpretation of the results. In contrast, quantitative relaxation time imaging results in pure proton density, T_2 and T_1 images (1). This approach has been applied to study fungal infection in strawberry, in an intact tomato plant and in (preserved) wood.

In selected wood pieces of pine proton density and relaxation times strongly depend on the wood anatomy and heterogeneity of these samples. Anatomy indepent information is obtained by taking the ratio between T_1 and T_2, since these are highly correlated. Doing so, differences in spring and summer wood no longer obscure the measurements. These results can be explained by the model of Brownstein and Tarr (2). On the basis of the effect on proton density, T_1 and T_2 and the correlation between these parameters for each voxel, infection of white and brown rot in (preserved) pine, oak, beech and birch has been studied. These studies reveal differences between untreated and preserved wood and between white and brown rot, which are related to the mechanism of the fungal infection.

In the strawberry, the effect of a bruise and of infection with botritus could clearly be discriminated on the basis of the ratio T_1 over T_2 and T_1 vs. T_2.

These examples demonstrate that the multi parameter approach is very powerful to study the mechanism of fungal infection in biological materials.

This research was supported, in part, by the European Union, grant no. CI1-CT93-0187 and contract no. CHGE-CT94-0061.

References:

1. H.T. Edzes, D. van Dusschoten, H. Van As. Quantitative imaging of NMR relaxation in plants. Book of abstracts 2nd International Conf. on Magnetic Resonance Microscopy, Heidelberg, Germany, September 6-9, 1993, p. 129.

2. K.R. Brownstein and C.E. Tarr, Phys. Rev. A 19, 2446-2453 (1979).

VISUALISATION OF FAT MIGRATION INTO CHOCOLATE BY MAGNETIC RESONANCE IMAGING MICROSCOPY

Thierry M. Guiheneuf†, Patrick J. Couzens‡, Hans-J. Wille§, Laurance D. Hall†

† *Herchel Smith Laboratory for Medicinal Chemistry, Cambridge University School of Clinical Medicine, Robinson Way, Cambridge CB2 2PZ, U.K.*

‡ *Nestlé Research & Development Centre, York, Po Box 204, York YO1 1XY, U.K.*

§ *Nestec Ltd, Research Centre, Vers-Chez-les-Blanc, Po Box 44, CH-1000 Lausanne 26 (Switzerland)*

NMR micro-imaging (MRI) has been used to visualise the migration of fat between a layer of hazelnut oil filling (oil + icing sugar) and a layer of chocolate, which was prepared as a model of composite confectionery products.

Fat bloom [1] is an undesirable surface defect described as a *'white or greyish haze'* [2] which can occur during storage of chocolate products. In composite products (cream filling + chocolate coating), *fat bloom* is sometimes associated with the migration of foreign fats into the chocolate coating. The liquid fats that are present in the filling tend to migrate easily into the chocolate structure where they form an *eutectic* mixture with cocoa butter [2]. This leads to an undesirable softening of the chocolate and, occasionally, fat recrystallizes on the surface of the chocolate in the form of the *fat bloom* defined earlier. It is well-known that the signal intensity of the protons of lipids in chocolate confectionery is sufficiently high to support high resolution MRI [3]. Furthermore, the image contrast is sensitive to the morphology of the chocolate matrix, and more precisely to the crystalline polymorphic form of cocoa butter.

A study of fat migration was undertaken both at room temperature (19 °C) and 28 °C. Substantial differences were observed between the one-dimensional migration rates at those temperatures and in the distribution of liquid fat across the chocolate layer after migration. The MRI data for fat migration were compared with independent measurements of the solid fat content (%) in chocolate-hazelnut oil mixtures, in addition to bulk relaxation time measurements [4]. It is suggested that the mechanism of fat migration involves both diffusion and capillary action of the hazelnut oil into the porous matrix of the chocolate.

1 - Vaeck, S.V. *Man. Confect.*, **40**, pp 35-73, (1960).

2 - Jana, A.H. Thakar, P.N. *Indian Food Ind.*, **12**, pp 33-39, (1993).

3 - Duce, S.L. Carpenter, T.A. Hall, L.D. *Lebensm. -Wiss. u. -Technol.*, **23**, pp 545-549, (1990).

4 - Lambelet, P. Desarzens, C. Raemy, A. *Lebensm.-Wiss. u. -Technol.*, **19**, pp 77-81, (1986).

The Change of Moisture Distribution in a Grain of Rice During Cooking Observed by T2 Imaging Methods

Sigeki Takeuchi*, Mitsuo Maeda*,
Yu-Ichiro Gomi#, Mika Fukuoka# and Hisahiko Watanabe#@

* Mitsubishi Electric Co. Ltd., Central Research Laboratory
Tsukaguchi Honmachi 8, Amagasaki, Hyogo 661 Japan.
Tokyo University of Fisheries, Food Engineering Laboratory
Konan 4, Minato, Tokyo 108 Japan.
@ To whom correspondence should be addressed.

Japanese rice has a short grain which is rich in amylopectine. It is boiled with an appropriate amount of water all of which is absorbed into the rice grain when cooking is completed. The deep understanding of the cooking process is helpful for the design of an electric rice cooker,which can cook rice more tasty with shorter time.

For analyzing the cooking process of rice the change of moisture distribution in a grain of polished rice during cooking was observed using transverse relaxation time (T2) imaging methods. In the first half of this paper, partly cooked sample were taken at various times and the two-dimensional spin echo images of moisture in a slice perpendicular to the long axis of the grain was observed at 25 C. In the second half, real time measurement of the change of moisture content in a rice grain during cooking at 98 C was performed using a one-dimensional imaging method associated with CPMG. We separately measured T2 of water in rice starch/water system to obtain a relationship between T2, moisture content and temperature. This enabled us to convert T2 map into a moisture population map.

We used rice grains treated by cellulase which is expected to damage the cell walls, as well as cellulase untreated rice grains. The moisture images in a cellulase untreated rice grain was rather rough than in a cellulase treated grain. However, no remarkable difference between a cellulase treated rice grain and an untreated rice grain, was observed in the change of the moisture profile during cooking. This suggests that the cell wall has little effect on suppressing moisture migration.

The moisture population map in a cellulase treated rice grain after 10, 12, 14 minutes cooking clearly showed the progress in the rise of moisture content from outside to inside of the grain; this progress was found not symmetrical, i.e., the uncooked core tended to shift to the dorsal side of the grain. The reason of this asymmetry could be attributed to the obstruction of water diffusion caused by a protein layer located at the outermost shell in the dorsal side of the grain. Picking up the moisture population data along a lateral line from the dorsal to the ventral side in the two-dimensional moisture map, a one-dimensional moisture profile is obtained, which exhibited a parallel upward movement in the ventral side.

The experimentally obtained moisture profile in a cellulase treated grain of rice during cooking was compared with that of predicted using a simple mathematical model. The process of cooking rice is governed by two rate processes; moisture diffusion and starch gelatinization. An infinite cylinder consisting of rice starch with equilibrium moisture content at room temperature is assumed to be boiled in excess water. The rate of gelatinization of rice starch was measured in a gravimetric method separately. Using literature data and our data collected by PFG-NMR, an empirical formulae for moisture diffusion coefficient in the rice starch/water system was obtained as a function of temperature and moisture content . With all these data and using a finite difference method to solve the moisture diffusion equation, the increment of moisture content at each node in the cylinder of the starch was calculated. The increment was managed to be confined to the value which the rate of gelatinization allowed. The predicted moisture profile using the model calculation was compared with experimental values. A reasonably good agreement existed between experimental and predicted values.

In a real time monitoring experiment, a grain of rice with water in a test tube was heated from outside of the tube by hot air generated using a ceramic heater located just above the transmitter coil in the magnet. The result of the experiment will be also shown in the conference.

Characterization of Starch Gels by NMR Microscopy

Jutta Pauli, Waltraut Vorwerg*), Clemens Mügge

Humboldt Universität Berlin
Institut für Chemie
Hessische Str. 1-2
D-10115 Berlin
Germany

*) Fraunhofer Institut für Angewandte Polymerforschung
Kantstr. 55
D-14513 Teltow-Seehof
Germany

The properties of aqueous starch polysaccharide solutions are determined by molecular ordering and subsequent aggregation and crystallization. The size distribution, density, interaction and lifetime of formed structures are seen as important parameters for resulting thermal and mechanical properties as well as industrial applications. The physical nature of starch polysaccharide interactions in aqueous dispersions and gels demands a characterization method without influence on the investigating system. In this respect the NMR microscopy posses the advantage to establish true structures and structural changes.

Gels of waxy maize starch, wheat starch, wrinkled pea starch and pure amylose were studied by NMR microscopy. The spin echo multislice technique was used at a Bruker spectrometer AM300 with the following parameters: TE 16,8 ms; TR 8 s; pixel resolution 18,4 µm; slice thickness: 250 µm; image matrix: 256 x 256 points. Eight images per gel were analyzed. Image processing and image analyzing were done using the software programmes AdOculos and Optimas.

The results of our studies let us assume a correlation between the amount of amylose and particle quantity in starch gels. With higher amount of amylose the number of particles is increased. The formed particles are stable over a period of 20 days, but show a high mobility in the gels.

The contrast in the starch images is determined in first order by the differences in the water content of particles as compared with the surroundings.

CHARACTERIZATION OF THE OIL-BEARING ROCK SAMPLES BY NMR IMAGING AT LOW FREQUENCY

V. Frolov

Research Institute of Physics, The University of Sanct-Petersburg,
198904 Petrodvoretz, Sanct Petersburg, Russia

To estimate oil-deposit productivity of the oil seams the investigations of rock cores brought to the surface is important for prognosis of oil recovery efficiency. The NMR signal amplitude and relaxation time mesurements of water-filled porous rock samples provide the information on total and open porosities. A new important information like size pore distribution and fractal dimension data are accessible using NMR imaging at very high magnetic field [1]. Here is repoted NMR imaging investigation of series of oil-bearing rock core samples got from different petroliferous regions. The samples was cleaned from nativ fillers (oil or/and phreatic water) and impregnated with water. The ^1H images have been received using home built non-expensive NMR mini-imagers for technical applications one with Strontium ferrite permanent magnet [2] and another with air-coil solenoid. The unlike appearance of the images obtained at high and low magnetic fields is explained by the different sensitivity to local magnetic field gradients due to a difference between magnetic susceptibilities of the pore fluid and grain material or to paleomagnetic centres. The result is that T_2 contrasted low frequency field images characterize fluid-pore surface interaction more adequately than high field images. A deficiency of low frequency imaging is that an imaging of single small pore is impossible. Nevertheless the distribution function for filled fluid and other statistic parameters are available and may be used as characterization of the rock.

[1] G.V.Romanov, A.V.Iliasov, R.Ch.Muslimov et al. NMR imaging application to complex study of oil-bearing rock. International Symposium "Non-traditional hydrocarbon raw material sources and problems of their use". October 12-16, 1992 St Petersburg, Russia. Abstracts, part 1, p.124 (in Russian).

[2] V.Frolov, B.A.Bazarov, A.V.Podolsky, G.B.Zhevna Yu.V.Bogachev, V.Z.Drapkin, V.P.Zelenin. NMR mini imager using ferrite magnet for technological applications. 12th European Experimental NMR Conference. June 5-10, 1994 Oulu, Finland. Abstracts p.290.

OPTICAL-DETECTION EPR-IMAGING OF SHORT-LIVED ION-RADICAL PAIRS

Boris M.Odintsov
Zavoysky Physical-Technical Institute Russian Academy of Sciences,
Sibirsky trakt, 10/7, Kazan 420029, Tatarstan, Russian Federation

The new method for detecting the irregularities in the spatial distribution of short-lived radical pairs has been developed. The fundamental importance of short-lived intermediate ion-radical states produced during chemical reactions or by any kind of ionizing radiation in solids determines the necessity of their detailed and comprehensive studies, including investigation of their spatial distribution. Such data may be also important for estimating the penetrating power and geometry of ionizing radiation, etc. The conventional EPR and EPR-imaging methods can not be used for these purposes, because the short-lived paramagnetic centers formed are presented at an extremely low concentration, and they recombine too rapidly, in nanoseconds.

The effectiveness of EPR-imaging is primarily determined by the technical possibilities for creating magnetic field gradients and by the sensitivity of the receiver. Improving the sensitivity of the method is particularly desirable since EPR-imaging is based on the detection of EPR lines which are broadened in a nonuniform magnetic field. Thus the effective sensitivity of the method is lowered in this case, since the signal intensity is inversely proportional to the linewidth. There was accordingly a great deal of interest in the possibility of improving the sensitivity of EPR-imaging by using the optical detection of EPR.

The results of our optical detection EPR experiments in nonuniform magnetic fields are given in this report. The samples of polystyrene with a 10^{-3} M admixture of paraterphenyl-d_{14} were used as models. This study has shown under optical detection increases the sensitivity of conventional EPR-imaging by three or more orders of magnitude. Optical detection expands the capabilities of the method to the research of new classes of compounds. The results show that the method of optical-detection EPR-imaging proposed here makes it possible to carry out studies of the irregularities of short-lived ion-radical states in space. These are crucial to fast solid-state chemical reactions which are of fundamental importance.

INVESTIGATION OF THE STRUCTURE OF POROUS GLASS BIORAN BY PFG-NMR

R. Valiullin, V. Skirda
Dept. of Molecular Physics, Kazan State University, Lenina St. 18, Kazan 420008, Russia
R. Kimmich, S. Stapf
Sektion Kernresonanzspektroskopie, Universität Ulm, D-89069 Ulm, Germany

MRI techniques are successfully employed for obtaining unique informations about the structure of objects under study. However, in some cases this method is restricted by a shortage of resolution (10-20 $\cdot 10^{-6}$ m). The present work is devoted to the investigation of the structure of BIORAN porous glass.
According to the data of the manufacturer (Schott Glaswerke, Mainz, Germany), this glass is defined as porous particles of 80-130 μm in size with a very sharp pore size distribution around a mean value of 40 nm.

The measurements habe been carried out by the PFG-NMR method with strong field gradients (G_{max}=100 T/m). This method allows to register directly a mean-square displacement $< r^2 >^{\frac{1}{2}}$ of molecules that are a function of the self-diffusion coefficient and the diffusion time t_d. The range of experimentally accessible diffusion times is restricted by technical possibilities of the device and the longitudinal relaxation time T_1. In our experiments, the t_d-intervals have been varied in the interval 3-5000 ms. As diffusing liquids, we used linear Polydimethylsiloxane (PDMS, M_w= 37500, M_w/M_n= 1.09) and decane. The large discrepancy in the diffusion coefficients of these liquids permitted us to register the $< r^2 >^{\frac{1}{2}}$ in the range of 0.1-300 μm (0.1-1 μm for PDMS, 5-300 μm for decane). The pore filling factor was equal to 1 for both cases.

The diffusional decays of the stimulated spin echo have been studied over a dynamical range of three decades. No influence of the porous structure on the shape of the diffusional decay has been observed for the scale $< r^2 >^{\frac{1}{2}} \leq 1$ μm. On larger scales, changes of the diffusional decay shapes were indicative of the restricted diffusion at distances from 5 to 100 μm, and of exchange processes at larger scales. The average value of the self-diffusion coefficient depended on t_d as $[\mathcal{D}(t_d) - \mathcal{D}_{eff}] \propto t_d^{-0.5}$, where $\mathcal{D}_{eff}$ is the self-diffusion coefficient for $< r^2 >^{\frac{1}{2}}$ of more than 1 μm.

Analysis of the experimental results points to the following facts:

1. The spatial distributions of the paths of percolation obey a Gaussian statistics with a radius of the percolation cycle of about 0.8 μm. On a large spatial scale the macroheterogeneities of the porous material with typical dimensions of $\approx$ 100 μm show themselves.
2. The matrix of the porous material does not influence the mechanism of polymer translational mobility.

Acknowledgments: Volkswagen-Stiftung N1/68675 and RFFI N94-03-09346A

POLYSULFIDE OLIGOMERS AND VULCANIZATES STRUCTURE AND VULCANIZATION NMR - CONTROL

P.P.Sukhanov, V.S.Minkin, A.V.Kostochko
State Technological University,K.Marx str.,68,
Kazan 420015,Tatarstan,Russian Federation

The results of polysulfide olygomers(thiokols) and vulcanizates NMR - investigations are reported. It is found that polysulfide olygomer structure and olygomer vulcanizate nets and kinetic parameters correlate to the NMR spectra and/or relaxation characteristics. The possibility of industrial thiokols and their vulcanizates quality NMR express-control organization is shown.

The control includes:

- olygomers analysis of copolymers and free sulfur content by means of NMR-^{1}H and ^{13}C- spectroscopy;
- determination of minimum vulcanization time, oxidation agents activities and vulcanizates polymer nets characteristics by means of NMR relaxation parameters.

There are no principal restrictions for working out analogous industrial control NMR - systems for all proton-containing rubber materials.

LOW-MOLECULAR RUBBERS STRUCTURE-FORMATION PROCESSES NMR - ANALYSIS

P.P.Sukhanov, V.I.Kimelblat, A.V.Kostochko
State Technological University, K.Marx str., 68,
Kazan 420015, Tatarstan, Russian Federation

The procedure of NMR-analysis and continuous study of branching and network-formation based on correlation of spectroscopic and relaxation NMR - parameters with modified branching characteristics is suggested. The use of introduced universal polymer chain discreteness measure both for theoretical analysis and experimental estimation of structural-topological phenomena in macromolecular assembly is proved for polyurethane and polysulfide olygomers structure-formation processes.

L.V. Boyland et al. Chem. Phys. Lett. 1991 (5) p. 450

Local Nongradient NMR of Cross-Linked Polymer Surface

K.V. Ermolaev, V.A. Dubovitskij, N.N. Volkova, and L.N. Erofeev
Institute of Chemical Physics in Chernogolovka
Chernogolovka, Moscow Region, Russia

A narrow peak was found to emerge on the broad NMR spectrum of ^{1}Hcross-linked m-phenyldiamine epoxy polymer at 350 K. The peak was ascribed to non-cross-linked residuals present in the network while calorimetry indicated that the network formation had been completed. The residuals concentration was studied vs separation from the polymer surface by an ingenious NMR slice selection technique which enabled the measurement of an undistorted broadline NMR spectrum (the width was about 30 kHz) from a slice of less than 0.2 mm thickness (the slice thickness was limited by instrumental imperfections but not by the NMR linewidth). The slice selection assumed sample position near the edge of an RF coil and required no gradient facilities. So the technique can be applied at any commercial NMR spectrometer.

The signal from the slice can be spatially resolved by using a surface RF coil translated along the sample surface [1]. The resolution of such an imaging is limited by the coil size but can be significantly improved by 2D version of the histogram method used earlier for 1D image restoring [2, 3]. Simulations of the experiment, in which NMR signal was measured by scanning a surface coil over the surface of the sample, showed that 2D histogram made it possible to restore noisy (signal/noise) perfectly unresolved patterns.

The significant feature of the reported imaging techniques is their independence (or very slight dependence for slice selection) of spectral linewidth that makes them useful for broadline solid NMR imaging.

REFERENCES

1. B. Blümich, C. Fülber, F. Weigand, and H.W. Spiess, Extended Abstracts of the XXVII Congress AMPERE, Kazan, August 1994, p.111.
2. K. Ermolaev, V. Dubovitskij, and L. Erofeev, Extended Abstracts of the XXVII Congress AMPERE, Kazan, August 1994, p.703.
3. V. Dubovitskij and K. Ermolaev, Zh. Khim. Fiz., 1994, vol.13, no. 12, p. 64.

LIST OF AUTHORS

T

U

V

W

X

Y

Z

LIST OF KEYWORDS

T

U

V

W

X

LIST OF PARTICIPANTS

Mr Abbott, Richard

University of Dundee, Chemistry Department
.
Dundee DD1 4HN
Scotland
Phone: 0044-1382-344334
Fax: 0044-1382 395517
E-Mail:

Prof. Dr. Andrew, E.R.

Dept. of Physics, University of Florida
P.O.Box 118440
Gainesville, FL 32611
USA
Phone: 001-904 392 6691
Fax: 001-904 392 8863
E-Mail:

Mr Artemov, Dimitri

Johns Hopkins University
720 Rutland Avenue, 217 Traylor Bldg.
Baltimore MD 21205
USA
Phone: 001-410 955 4221
Fax: 001-410 614 1948
E-Mail:

Mr Balcom, Bruce J.

Physics Department, University of New Brunswick
Fredericton Campus, Box 4400
Fredericton, N.B., E3B 5A3
Canada
Phone: 001-506-453-4723
Fax: 001-506-453-4581
E-Mail: bjb@unb.ca

Mr Behr, Wolfgang

Physikalisches Institut EPV, Uni Würzburg
Am Hubland
97074 Würzburg
Germany
Phone: 0049-931-888-5109
Fax: 0049-931-706297
E-Mail:

Dr. Bertora, Franco

Esaote
.
Genova, 16153
Italia
Phone: 0039 10 6547236
Fax: 0039 10 6547275
E-Mail:

Mr Adriaensens, Peter

Limburg University
Universitaire Campus
Diepenbeek B-3590
Belgium
Phone: 0032-11-268352
Fax: 0032-11-268301
E-Mail:

Prof. Dr. Armstrong, Robin L.

University of New Brunswick
Fredericton Campus, Box 4400
Fredericton, N.B., E3B 5A3
Canada
Phone: 001-506-453-4567
Fax: 001-506-453-4599
E-Mail: rla@unb.ca

Mr Assaf, Yaniv

Tel Aviv University
Ramat Aviv
Tel Aviv, 69978
Israel
Phone: 00972-3-640-7232
Fax: 00972-3-640-9293
E-Mail:

Mr Bartusek, Karel

Institute of Scientific Instruments
Kralovopolska
Brno, 61265
Czech Republic
Phone:
Fax:
E-Mail:

Prof. Dr. Berliner, Lawrence

Ohio State University, Chemistry Dept.
120 W 18th Ave.
Columbus, OH 43210-1106
USA
Phone: 001-614-292-0134
Fax: 001-614-292-1532
E-Mail: berliner@livers.mps.ohio-state.e

Mr. Beuls, Emile

Limburg Universitaire Centrum
Universitaire Campus
3590 Diepenbeek
Belgium
Phone: 0032 11 26 85 02
Fax: 0032 11 26 85 99
E-Mail:

Mr Black, S.

University of Surrey, Dept. of Physics
.
Gildford, Surrey GU2 5XH
UK
Phone:
Fax:
E-Mail:

Prof. Dr. Blümich, Bernhard

Lehrstuhl für Makromolekulare Chemie
RWTH Aachen
52056 Aachen
Germany
Phone: 0049-241-806421
Fax: 0049-241-8888-185
E-Mail: bluemich@rwth-aachen.de

Dr. Botto, Robert E.

Argonne National Laboratory, Chemistry Division,
Bldg. 200
9700 South Cass Avenue
Argonne, Illinois 60439
USA
Phone: 001-708-252-3524
Fax: 001-708-252-9288
E-Mail:

Mr Brandl, Matthias

Physikalisches Institut EPV, Uni Würzburg
Am Hubland
97074 Würzburg
Germany
Phone: 0049-931-888-5110
Fax: 0049-931-8885851
E-Mail:

Bruker Analytische Messtechnik GmbH,

Silberstreifen
76287 Rheinstetten
Germany
Phone: 0049-721-5161-0
Fax:
E-Mail:

Mr Casieri, Cinzia

Univ. la Sapienza
P. le Aldo Moro 2
00185 Roma
Italia
Phone: 0039-6-49913471
Fax: 0039-6-49913484
E-Mail:

Blazek, Almira

University of British Columbia
2036 Main Mall
Vancouver B.C., V6T1Z1
Canada
Phone: 001-604-822-2293
Fax: 001-604-822-2847
E-Mail:

Dr. Blümler, Peter

Inst. für Makromolekulare Chemie, RWTH Aachen
Worringer Weg 1
52056 Aachen
Germany
Phone: 0049-241-806971
Fax: 0049-241-8888-185
E-Mail:

Dr. Dr. Bowtell, Richard

MR Center, Department of Physics
University of Nottingham
Nottingham NG7 2R15
UK
Phone: 0044-115-951-4737
Fax: 0044-115-951-5166
E-Mail:

Dr. Brown, J.S. Robert

.
515 W. 11th Street
Claremont, CA 91711-3721
USA
Phone: 909 626 7595
Fax:
E-Mail: rjsbmeb@aol.com

Prof. Dr. Callaghan, Paul T.

Massey University
.
Palmerston North
New Zealand
Phone: 0064-6-3505164
Fax: 0064-6-3540207
E-Mail:

Dr. Chudek, John A.

University of Dundee, Chemistry Department
.
Dundee, DD1 4HN
Scotland
Phone: 0044-1382 344334
Fax: 0044-1382 395517
E-Mail:

Mr. Cieslikowski,

Cryophysics GmbH
Landwehrstr. 48
64293 Darmstadt
Germany
Phone: 0049-6151-86281
Fax: 0049-6151-815799
E-Mail:

Mr Cohen, Yoram

Tel Aviv University
Ramat Aviv
Tel Aviv, 69978
Israel
Phone: 00972-3-640-7232
Fax: 00972-3-640-9293
E-Mail:

Mr Commodari, Fernando

NIH/NIA/GRC/LCMB/room 4D10
4940 Eastern Ave.
Baltimore, MD 21224
USA
Phone: 001-410-558-8176
Fax: 001-410-558-8173
E-Mail: fern@vax.grc.nia.nih.gov

Dr. Crozier, Stuart

Centre For Magnetic Resonance, Queensland University
St. Lucia
Brisbane, QLD 4072
Australia
Phone: 0061-7-365-4100
Fax: 0061-7-365-3833
E-Mail:

Prof. Dr. Dawson, Joan M.

University of Illinois
1307 West Park Street
Urbana IL 61801
USA
Phone: 001-217 244 1295
Fax: 001-217 244 1330
E-Mail:

Dr. Denner, P.

Hochschule Erfurt, Institut für Physik
.
66089 Erfurt
Germany
Phone: 0049-361-737-1643
Fax: 0049-361-737-1918
E-Mail:

Miss Codd, S.C.

University of Kent, Physics Department
.
Canterbury CT2 7NR
UK
Phone: 0044-1227 764000 3763
Fax: 0044-1227 475423
E-Mail:

Mr. Colet, Jean-Marie

.
Avenue du Champ de Mars, 24
7000 Mons
Belgium
Phone: 0032 65 37 35 19
Fax: 0032 65 37 35 20
E-Mail:

Mr Coy, Andrew

Royal Institute Technology, Physical Chemistry
.
10044 Stockholm
Sweden
Phone:
Fax: 0046 8 790 8207
E-Mail:

Cryophysics GmbH,

Landwehrstr. 48
64293 Darmstadt
Germany
Phone: 0049-6151-86281
Fax: 0049-6151-815799
E-Mail:

Mr Deichmann, Ralf

Physikalisches Institut EPV, Uni Würzburg
Am Hubland
97074 Würzburg
Germany
Phone: 0049-931-888-5883
Fax: 0049-931-8885851
E-Mail:

Mr Depauw, Mark

Konignkijke Musea Kunst-Geschiet
Jubelpark 10
B-1040 Brussel
Belgium
Phone:
Fax:
E-Mail:

Prof. Dereppe, J.M.

University Louvain
Pl. L. Pasteur, 1,3a
Louvain La Neuve, B1348
Belgium
Phone: 0032-10-472775
Fax: 0032-10472774
E-Mail:

Mr Dorn, Tobias

Physikalisches Institut EPV, Uni Würzburg
Am Hubland
97074 Würzburg
Germany
Phone: 0049-931-888-5113
Fax: 0049-931-888-5851
E-Mail:

Mr Doty, F. David

Doty Scientific
700 Clenson Road
Columbia, SC 29223
USA
Phone: 001-803-788-6497
Fax: 001-803-731-5495
E-Mail:

Doty,

Doty Scientific
700 Clenson Road
Columbia, SC 29223
USA
Phone: 001-803-788-6497
Fax: 001-803-731-5495
E-Mail:

Mr Dunn, Keh-Jim

Chevron
1300 Beach Blvd
LeHabra, CA 90631-6374
USA
Phone: 001-310-694-7051
Fax: 001-310-694-7228
E-Mail:

Dr. Elgert, K.-F.

Dt. Institute für Textil- und Faserforschung
DITF Stuttgart
Körschtalstr.26,
73770 Denkendorf
Germany
Phone: 0049-711- 9340-185
Fax: 0049-711-9340-185
E-Mail:

Mr. Devauchelle, Didier

.
31, Rue du Chemin Vert
75011 Paris
France
Phone:
Fax:
E-Mail:

Mrs. Dörr, Lydia

Varian GmbH
Alsfelder Str. 3
64289 Darmstadt
Germany
Phone: 0049-6151-703-233
Fax: 0049-6151-703-200
E-Mail:

Mrs. Doty, Judy M.

Doty Scientific
700 Clenson Road
Columbia, SC 29223
USA
Phone: 001-803-788-6497
Fax: 001-803-731-5495
E-Mail:

Dr. Dubovitskij, V.A.

Mathematical dept., Institute of Chemical Physics
Chernogolvka
Moscow Region, 142432
Russia
Phone:
Fax: 007-96-57-53-588
E-Mail:

Mr Eidmann, Gunnar

Inst. für Makromolekulare Chemie, RWTH Aachen
Worringer Weg 1
52056 Aachen
Germany
Phone: 0049-241-806425
Fax: 0049-241-8888-185
E-Mail:

Mr Engelhardt, Robert Thomas

Duke University Medical Center
DUMC Box 3302
Durham, NC 27710
USA
Phone: 001-919-684-7677
Fax: 001-919-681-7122
E-Mail:

Mrs. Ercken, Monique

Limburg University
Universitaire Campus
Diepenbeek B-3590
Belgium
Phone: 0032-11-268387
Fax: 0032-11-268301
E-Mail:

Dr. Fichtner, Klaus-Peter

Dt. Krebsforschungszentrum, Zentrale Spektroskopie
Im Neuenheimer Feld 280
69120 Heidelberg
Germany
Phone: 0049-6221-42-4514
Fax: 0049-6221-42-4554
E-Mail:

Prof. Dr. Freed, Jack H.

Dept of Chemistry, Baker Laboratory, Cornell University
.
Ithaca, NY 14853-1301
USA
Phone: 001-607-255-3647
Fax: 001-607-255-4137
E-Mail:

Prof. Dr. Fukushima, Eiichi

The Lovelace Institutes
2425 Ridgecrest Dr. SE
Albuquerque, NM 87108
USA
Phone: 001-505-262-7155
Fax: 001-505-262-7043
E-Mail:

Mr Gelbert, Martin

Universität Karlsruhe, Inst. f. Mech. Verfahrenstechnik u. Mech.
Am Fasanengarten
76131 Karlsruhe
Germany
Phone: 0049-721-608-3758
Fax: 0049-721-608-3758
E-Mail:

Dr. Glidewell, Sheila

Scottish Crop Research Institute
Invergowrie
Dundee DD2 5DA
Scotland
Phone: 0044-1382-562431
Fax: 0044-1382-562426
E-Mail: specsg@scri.sari.ac.uk

Prof. Dr. Fiat, Daniel

Dept. of Physiology and Biophysics,
University of Illinois
901 S Wolcott Avenue
Chigaco, Il 60612-7342
USA
Phone: 001-312 996 7609
Fax: 001-312-996-1414
E-Mail:

Mr Frantz, Stefan

Med. Klinik, Universität Würzburg
Josef-Schneider-Str. 2
97080 Würzburg
Germany
Phone: 0049-931 201-3455
Fax: 0049-931 201 2664
E-Mail:

Dr. Frolov, V.V.

Res. Institute of Physics, St. Petersburg University
1 Ulianovskaya, Petrodvoretz
198904 Sanct Petersburg
Russia
Phone:
Fax: 007-812-428-7042 o. 4679
E-Mail:

Prof. Dr. Gelan, Jan.

Limburg University
Universitaire Campus
Diepenbeek B-3590
Belgium
Phone: 0032-1126-8312
Fax: 0032-1126-8301
E-Mail: jgelan@luc.ac.be

Dr. Gewiese, Bernd

Bruker Medizintechnik GmbH
Rudolph Planck Straße 23
76275 Ettlingen
Germany
Phone: 0049-7243-504-560
Fax: 0049-7243-504-539
E-Mail:

Mrs. Görke, Ute

Universität Ulm, Sektion Kernresonanzspektroskopie
Albert-Einstein-Allee 11
89069 Ulm
Germany
Phone: 0049-731-502-3130
Fax: 0049-731-502 3150
E-Mail:

Mr Götz, J.

Uni Karlsruhe, Institut für Mechanische
Verfahrenstechnik
Am Fasanengarten
76131 Karlsruhe
Germany
Phone:
Fax:
E-Mail:

Dr. Gross, Dieter

Bruker Analytische Meßtechnik GmbH
Silberstreifen
76287 Rheinstetten
Germany
Phone: 0049-721-5161-167
Fax: 0049-721-5161-297
E-Mail:

Mr. Guiheneuf, T.M.

University of Cambridge, Medicinal Chemistry
Robinson Way
Cambridge, CB2 2PZ
UK
Phone: 0044 1223 336805
Fax: 0044 1223 336748
E-Mail:

Dr. Gyngell, M.L.

Max-Planck-Institut f. neurologische Forschung
Gleueler Str. 50
510931 Köln
Germany
Phone: 0049-221-4726315
Fax: 0049-221-4726298
E-Mail:

Prof. Dr. Haase, Axel

Physikalisches Institut EPV, Uni Würzburg
Am Hubland
97074 Würzburg
Germany
Phone: 0049-931-888-5868
Fax: 0049-931-8885851
E-Mail:

Prof. Hall, L.D.

University of Cambridge, Medicinal Chemistry
Robinson Way
Cambridge CB2 2PZ
UK
Phone: 0044-1223-33805
Fax: 0044-1223-336748
E-Mail: ldh11@hslmc.cam.ac.uk

Dr. Grondey, Hiltrud

Dept. of Chemistry, UBC
2036 Main Mall
Vancouver B.C., V6T1Z1
Canada
Phone: 001-604-822-2293
Fax: 001-604-822-2847
E-Mail:

Dr. Gründer, Wilfried

Inst.für Med. Physik und Biophysik
Liebigstr. 27
04103 Leipzig
Germany
Phone: 0049-341-9715707
Fax: 0049-341-9715709
E-Mail:

Mr Gulani, Vikas

University of Illinois, Urbana-Champaign
1307 W. Park St.
Urbana, IL 61801
USA
Phone: 001-717-384-5349
Fax: 001-217-244-1330
E-Mail:

Prof. Dr. Haacke, Mark

Malinckrodt Inst. of Radiology- Washington University
510 S. Kingshighway
St. Louis, MO 63110
USA
Phone: 001-314-362-2737
Fax: 001-314-362-2350
E-Mail:

Mrs. Hahn, Susanne

Med. Klinik, Universität Würzburg
Josef-Schneider-Str. 2
97080 Würzburg
Germany
Phone: 0049-931 201-3455
Fax: 0049-931 201 2664
E-Mail:

Dr. Halse, M.R.

University of Kent, Physics Department
.
Canterbury CT2 7NR
UK
Phone: 0044-1227 764000 3763
Fax: 0044-1227 475423
E-Mail:

Mrs. Hauck, Daniela

Inst. für Makromolekulare Chemie, RWTH Aachen
Worringer Weg 1
52056 Aachen
Germany
Phone: 0049-241-806425
Fax: 0049-241-8888-185
E-Mail:

Dr. Hedlund, Laurence

Dept. of Radiology, Duke Univ. Medical Center
.
Durham, NC 27710
USA
Phone: 001-919-684-7767
Fax: 001-919-681-8648
E-Mail:

Mr Heshiki, Atsuko

Saitama Medical School
Iruma-Gun
Saitama, 350-04
Japan
Phone: 0081-492-76-1265
Fax: 0081-492-95-8003
E-Mail:

Mr Heuert, Uwe

Uni Halle
Friedemann-Bach Pl. 6
06108 Halle
Germany
Phone: 0049-345-37761
Fax: 0049-345-832580
E-Mail:

Mr Hiller, Karl-Heinz

Physikalisches Institut EPV, Uni Würzburg
Am Hubland
97074 Würzburg
Germany
Phone: 0049-931-888-5861
Fax: 0049-931-888-5851
E-Mail:

Dr. Hoehn-Berlage, M.

Max-Planck-Institut f. neurologische Forschung
Gleueler Str. 50
510931 Köln
Germany
Phone: 0049-221-4726315
Fax: 0049-221-4726298
E-Mail:

Dr. Hausmann, Richard

Siemens B Med, Dept. MRA
Henkestraße 127
91052 Erlangen
Germany
Phone: 0049-9131-84-5684
Fax: 0049-9131-84-2724
E-Mail:

Mr Henkelmann, Rainer

Siemens AG, Medizinische Technik
Henkestr. 127
91052 Erlangen
Germany
Phone: 0049-9131-84-7572
Fax: 0049-9131-842724
E-Mail:

Mrs. Hesse, Kathrin

Universität Dortmund, Physikalische Chemie II
Otto-Hahn-Str. 6
44227 Dortmund
Germany
Phone: 0049-231-755-3932
Fax: 0049-231-755-3771
E-Mail:

Mrs. Hillenbrand, Claudia

Physikalisches Institut EPV, Uni Würzburg
Am Hubland
97074 Würzburg
Germany
Phone: 0049-931-888-5861
Fax: 0049-931-888-5851
E-Mail:

Dr. Hilton, Bruce

.
PO Box B NCI- FCRDC
Frederick, Maryland
USA
Phone: 001-301-846-1226
Fax: 001-301-846-5866
E-Mail:

Dr. Horn, Michael

Med. Klinik, Universität Würzburg
Josef-Schneider-Str. 2
97080 Würzburg
Germany
Phone: 0049-931-201-3455
Fax: 0049-931-201-2664
E-Mail:

Prof. Dr. Hull, William E.

German Cancer Research Center,
Central Spectroscopy Dept.
Neuenheimer Feld 280
69120 Heidelberg
Germany
Phone: 0049-6221-424515
Fax: 06221-424554
E-Mail:

Mrs. Illing, Barbara

Med. Klinik, Universität Würzburg
Josef-Schneider-Str. 2
97080 Würzburg
Germany
Phone: 0049-931 2013455
Fax: 0049-931 201 2664
E-Mail:

Dr. Jakob, Peter

Physikalisches Institut EPV, Uni Würzburg
Am Hubland
97074 Würzburg
Germany
Phone: 0049-931-888-5871
Fax: 0049-931-888-5851
E-Mail:

Prof. Dr. Jelinski, Lynn W.

Cornell University,
New York State Center for Advanced Techn.
130 Biotechnology Building
Ithaca, NY14853
USA
Phone: 001-607-255-2300
Fax: 001-607-255-6249
E-Mail:

Dr. Jonsen, Paul

Chemagnetics
7 Claro Court Business Centre, Claro R
Harrogate HG1 2QP
UK
Phone: 0044-1423-531-645
Fax: 0044-1423-531-647
E-Mail:

Mr Kalusche, Bernhard

Physikalisches Institut EPV, Uni Würzburg
Am Hubland
97074 Würzburg
Germany
Phone: 0049-931-888-5861
Fax: 0049-931-888-5851
E-Mail:

Prof. Hunter, Geoffrey

University of Dundee, Chemistry Department
.
Dundee DD1 4HN
Scotland
Phone: 0044-1382 344305
Fax: 0044-1382 225163
E-Mail:

Mr Ishida, Nobuaki

National Food Research Institute
Tsukuba Science City,
Ibaraki 305
Japan
Phone: 0081-298-38-8035
Fax: 0081-298-38-7996
E-Mail:

Mr Jasinski, Andrzev

MRI Laboratory, Inst of Nuclear Physics
Ul Zadzikowskiedo 152
31-342 Krakov
Poland
Phone: 004812- 370-222
Fax: 004812-375-441
E-Mail:

Prof. Dr. Johnson, G. Allan

Duke Univ. Med. Center
PO. Box 3808
Durham, NC 27710
USA
Phone: 001-919-660-2711-4355
Fax: 001-919-681-8648
E-Mail:

Mrs. Kahler, Elke

Physikalisches Institut EPV, Uni Würzburg
Am Hubland,
97074 Würzburg
Germany
Phone: 0049-931-888-5871
Fax: 0049-931-888-5851
E-Mail:

Dr. Kanazawa-Kamei, Yoko

Kyushu University, Faculty of Pharmaceutical Sciences
Higashi-ku
Fukuoka, 812-21
Japan
Phone: 0081-92-641-1151
Fax: 0081-92-641-8154
E-Mail:

Prof. Dr. Kimmich, Rainer

Universität Ulm,Sektion Kernresonanzspektroskopie
Albert-Einstein-Allee 11
89069 Ulm
Germany
Phone: 0049-731 502 3140
Fax: 0049-731-502 3150
E-Mail:

Mr Klinkenberg, Maurice

Inst. für Makromolekulare Chemie, RWTH Aachen
Worringer Weg 1
52056 Aachen
Germany
Phone: 0049-241-806430
Fax: 0049-241-8888-185
E-Mail:

Mr Knörgen, Manfred

Uni Halle
Friedemann-Bach Pl. 6
06108 Halle
Germany
Phone: 0049-345-37761
Fax: 0049-345/832580
E-Mail:

Mr Kober, Frank

Physikalisches Institut EPV, Uni Würzburg
Am Hubland
97074 Würzburg
Germany
Phone: 0049-931-888-5864
Fax: 0049-931-888-5851
E-Mail:

Mr Kose, Katsumi

Institute of Applied Physics, University of Tsukuba
.
Tsukuba 305
Japan
Phone: 0081-298-53-5335
Fax: 0081-298-53-5205
E-Mail:

Mr Krishnan, Bala S.

Bristol-Myers Squibb Company
(Dept.: Analytical Research)
5 Research Parkway
Wallingford, CT 06492
USA
Phone: 001-203-284-6343
Fax: 001-203-284-6137
E-Mail:

Dr. Kleinberg, Robert

Schlumberger-Doll Research
Old Quarry Road,
Ridgefield, CT 06877
USA
Phone: 001-203-431-5410
Fax: 001-203-438-3819
E-Mail:

Mr Kmiecik, Joseph A.

University of Illinois
524 Burrill Hall, 407 S. Goodwin
Urbana, IL 61801
USA
Phone: 001-217 244 4234
Fax: 001-217-333-4133
E-Mail:

Mr. Knüttel, B.

Bruker Medizintechnik GmbH
Rudolph Planck Straße 23
76275 Ettlingen
Germany
Phone: 0049-7243-504-530
Fax: 0049-7243-504-539
E-Mail:

Dr. Köckenberger, W.

Centre d'Etudes Nucleaire DBMS RMBM
15, Rue des Martyrs
38054 Grenoble, Cedex
France
Phone: 0033- 76- 885181
Fax: 0033-76-885483
E-Mail:

Mr Kreibich, W.

Bruker Medizintechnik GmbH
Rudolph Planck Straße 23
76275 Ettlingen
Germany
Phone: 0049-7243-504-565
Fax: 0049-7243-504-539
E-Mail:

Mr Kuchenbrod, Erwin

Physikalisches Institut EPV, Uni Würzburg
Am Hubland
97074 Würzburg
Germany
Phone: 0049-931-888-5883
Fax: 0049-931-888-5851
E-Mail:

Dr. Kuhn, W.P.

Fraunhofer-Insitut für Biomedizinische Technik
.
St. Ingbert
Germany
Phone: 0049-6894-980-250
Fax: 0049-6894-980-400
E-Mail: wpk@ibmt.fhg.de

Mr Kwiecinski, Stanislaw

MRI Laboratory, Inst of Nuclear Physics
.
31-342 Krakov
Poland
Phone: 004812- 370-222
Fax: 004812-375-441
E-Mail:

Mr Lasarov, Harri

University of Joensuu, Department of Chemistry
P.O. Box 111
Fin-80101 Joensuu
Finnland
Phone: 00358-73-1514650
Fax: 00358-73-1513390
E-Mail:

Mrs. Laukemper, Simone

Inst. für Makromolekulare Chemie, RWTH Aachen
Worringer Weg 1
52056 Aachen
Germany
Phone: 0049-241-806421
Fax: 0049-241-8888-185
E-Mail:

Prof. Dr. Lauterbur, Paul C.

University of Illinois
1307 West Park Street
Urbana IL 61801
USA
Phone: 001-217 244 0600
Fax: 001-217-244 1330
E-Mail:

Mr Lehmann, Volker

Bruker Analytische Meßtechnik GmbH
Silberstreifen
76287 Rheinstetten
Germany
Phone: 0049-721-5161-167
Fax: 0049-721-5161 297
E-Mail:

Dr. Kulagina, T.P.

Institute of Chemical Physics
Chernogolovka
Moscow region 142432
Russia
Phone:
Fax:
E-Mail:

Mr Landschütz, Wilfried

Physikalisches Institut EPV, Uni Würzburg
Am Hubland,
97074 Würzburg
Germany
Phone: 0049-931-888-5766
Fax: 0049-931-888-5851
E-Mail:

Mr Lauenstein, Asa

Uppsala University, Institute of Chemistry
Box 531
75121 Uppsala
Sweden
Phone: 0046 18 3759
Fax: 0046 18 50 8542
E-Mail:

Prof. Dr. Laukien, Günther

Bruker Analytische Meßtechnik GmbH
Silberstreifen
76287 Rheinstetten
Germany
Phone: 0049-721-5161-238
Fax: 0049-721-5161-297
E-Mail:

Prof. Dr. Le Bihan, Denis

Service Hospitalitaire F. Joliot
Place Le Clerc
91406 Orsay
France
Phone: 0033-169-867700
Fax: 0033-169-867768
E-Mail:

Mr Lloyd, Charles

University of Dundee, Dept. of Dental Prosthetics
.
Dundee DD1 4HN
Scotland
Phone: 0044-1382 6358979
Fax: 0044-1382 225163
E-Mail:

Dr. Lohman, Joost A.B.

Bruker Spektrospin Ltd.
Banner Lane
Coventry CV4 9GH
UK
Phone: 0044-1203-855200
Fax: 0044-1203-465317
E-Mail:

Dr. Lurie, David J.

University of Aberdeen, Dept. of Bio-Medical Physics
Foresterhill
Aberdeen AB9 2ZD
UK
Phone: 0044-1224 681818 o. 54061
Fax: 0044-1224 685645
E-Mail: lurie@aberdeen.ac.uk

Mr Maddinelli, G.

Eniricerche SPA
Via F. Maritano 27, S. Donato
20097 Milano
Italia
Phone:
Fax: 00392520-24611
E-Mail:

Dr. Mallet, M.

University of Kent, Physics Department
.
Canterbury CT2 7NR
UK
Phone: 0044-1227 764000 3763
Fax: 0044-1227 475423
E-Mail:

Mr Mastikhin, Igor V.

International Tomography Center
Institutskaya 3a
Nobosibirsk 630090
Russia
Phone:
Fax: 007382 350827
E-Mail: mast@tomosoft.nsk.su

Prof. Dr. McCarthy, Michael J.

University of California, Dept. of Food Science a. Technol.
.
Davis, CA 95616-8598
USA
Phone: 001-916-752-8421
Fax: 001-916-752-4759
E-Mail:

Mr Lugeri, Nicola

Univ. la Sapienza
P. le Aldo Moro 2
00185 Roma
Italia
Phone: 0039-6-49913928
Fax: 0039-6-49913484
E-Mail:

Prof. Dr. Lutz, Otto

Physikalisches Institut
Morgenstelle
72076 Tübingen
Germany
Phone: 0049-7071 296265
Fax: 0049-7071 296296
E-Mail:

Dr. Maier, Walter

BASF AG CHU/5-B9
.
67056 Ludwigshafen
Germany
Phone: 0049-621-6045209
Fax: 0049-621-6020914
E-Mail:

Mr Martin-Landrove, Miguel

Centro de Resonancia Magnetica, Facultad de Ciencias, UCV
Apartado Postal 47586
Caracas 1041- A
Venezuela
Phone: 00582-619811
Fax: 0058-2928903,000582-6930855
E-Mail: landrove@dino.conicit.ve

Prof. Dr. Mateescu, G.D.

Case Western Reserve University, Dept of Chemistry
.
Cleveland, OH 44106
USA
Phone: 001-216 368 2589
Fax: 001-216 368 3006
E-Mail: gdm2@po.cwru.edu

Mr Meininger, Martin

Physikalisches Institut EPV, Uni Würzburg
Am Hubland
97074 Würzburg
Germany
Phone: 0049-931-888-5864
Fax: 0049-931-888-5851
E-Mail:

Dr. Miller, Joel B.

Naval Research Laboratory,
Chemistry Division, Code 6120
.
Washington D.C. 20375
USA
Phone: 001-202 767 2337
Fax: 001-202 767 0594
E-Mail:

Dr. Moreaux, Claudette

Univ. Louvain
Pl. L. Pasteur 1.3a
Louvain La Neuve1348
Belgium
Phone: 0032-10472775
Fax: 0032-10-472774
E-Mail:

Mr Moscicki, J.K.

Baker Laboratory of Chemistry, Cornell University
.
Ithaka, NY 14853
USA
Phone:
Fax:
E-Mail:

Prof. Dr. Muller, R.N.

Laboratoire de RMN, Université de Mons-Hainaut
Avenue du Champ de Mars 24
Mons 7000
Belgium
Phone:
Fax: 0032-65-373520
E-Mail:

Prof. Dr. Navon, G.

School of Chemistry, Tel Aviv University
.
Tel Aviv, 69978
Israel
Phone: 00972-3-6408156
Fax: 00972-3-6410665
E-Mail:

Mr Nestle, Nikolaus

Sektion NMR, Uni Ulm
Albert-Einstein-Allee 11
89069 Ulm
Germany
Phone: 0049-731-502-3135
Fax: 0049-731-502 3150
E-Mail:

Mr Mohd Som, Fauzi

University of Dundee, Chemistry Department
.
Dundee DD1 4HN
Scotland
Phone: 0044-1382 344334
Fax: 0044-1382 225163
E-Mail:

Mr Morris, Herman D.

University of Illinois
1307 West Park St.
Urbana IL 61801
USA
Phone: 001-217-244-0290
Fax: 001-217-244-1330
E-Mail:

Dr. Mould, Richard F.

.
41,Ewhurst Avenue, Sanderstead
South Croydon, Surrey, CR2 ODH
USA
Phone:
Fax:
E-Mail:

Mr Müller, Hans-Peter

Universität Ulm, Sektion Kernresonanzspektroskopie
Albert-Einstein-Allee 11
89069 Ulm
Germany
Phone: 0049-731-502 3133
Fax: 0049-731-502 3150
E-Mail:

Dr. Nesbitt, G.

Shell Research
Badhuisweg 3
1031 CM Amsterdam
Niederlande
Phone:
Fax: 0031-206-304-037
E-Mail:

Dr. Neubauer, Stefan

Med. Klinik, Universität Würzburg
Josef-Schneider-Str. 2
97080 WÜrzburg
Germany
Phone: 0049-931-201-3158
Fax: 0049-931-201-2664
E-Mail:

Dr. Neue, Günther

Universität Dortmund, Physikalische Chemie II
Otto-Hahn-Str. 6
44221 Dortmund
Germany
Phone: 0049-231-755-3932
Fax: 0049-231-755-3771
E-Mail:

Prof. Dr. Odintsov, B.M.

Zavoisky Phys.-Techn. Inst.
Sibirsky tract, 1017
420029 Kazan
Russia
Phone:
Fax: 007-8432-765075
E-Mail:

Dr. Pakkanen, Tuula

Univ. of Joensuu, P.O.Box 111
.
Fin-80101, Joensuu
Finland
Phone: 00358-73-1513340
Fax: 00358-73-1513344
E-Mail:

Mr Paulsen, Kim

Royal Institute Technology, Physical Chemistry
.
10044 Stockholm
Sweden
Phone:
Fax: 0046 8 790 8207
E-Mail:

Mr Pilatus, Ulrich

Johns Hopkins University
720 Rutland Avenue, 217 Traylor Bldg.
Baltimore MD 21205
USA
Phone: 001-410-955-4221
Fax: 001-410-614-1948
E-Mail:

Prof. Dr. Pope, J.M.

Queensland University of Technology,
School of Physics
GPO Box 2434
Brisbane 4001
Australia
Phone: 00617-864-2328
Fax: 00617-864-1521
E-Mail: jmp@newt.phys.unsw.edu.au

Mrs. Nöth, Ulrike

Physikalisches Institut EPV, Uni Würzburg
Am Hubland
97074 Würzburg
Germany
Phone: 0049-931-888-5883
Fax: 0049-931-888-5851
E-Mail:

Mr Odoj, Florian

Physikalisches Institut EPV, Uni Würzburg
Am Hubland
97074 Würzburg
Germany
Phone: 0049-931-888-5110
Fax: 0049-931-888-5851
E-Mail:

Mrs. Pauli, Jutta

HUB Institut für Chemie
Hessische Str. 1-2
10115 Berlin
Germany
Phone: 0049-30-28468-387
Fax: 0049-30-28468343
E-Mail:

Prof. Dr. Peck, Timothy

University of Illinois
1406 W. Green St.
Urbana IL 61801
USA
Phone: 001-217-244-2382
Fax: 001-217-244-0105
E-Mail: tpeck@mrel.brl.uiuc.edu

Mr Pohmann, Rolf

Physikalisches Institut EPV, Uni Würzburg
Am Hubland
97074 Würzburg
Germany
Phone: 0049-931-888-5862
Fax: 0049-931-888-5851
E-Mail:

Mrs. Preibisch, Christine

Physikalisches Institut EPV, Uni Würzburg
Am Hubland
97074 Würzburg
Germany
Phone: 0049-931-888-5864
Fax: 0049-931-888-5851
E-Mail:

Dr.Dr. Pschorn, Uwe

Dept. of Biological Research - Neuropharmacology -
Boehringer Ingelheim KG
55216 Ingelheim
Germany
Phone:
Fax: 0049-6132-77-3758
E-Mail:

Prof. Randall, E. W.

Queen Mary and Westfield College
Mile End Road
London E1 4NS
UK
Phone: 0044-171 775 3258
Fax: 0044-181 981 8745
E-Mail:

Dr. Rommel, Eberhard

Physikalisches Institut EPV, Uni Würzburg
Am Hubland
97074 Würzburg
Germany
Phone: 0049-931-888-5113
Fax: 0049-931-888-5851
E-Mail:

Dr. Sarkar, Susanta K.

Smithkline Beecham Pharmaceuticals
709 Swedeland Road
King of Prussia, PA 19406
USA
Phone: 001-610-270-6652
Fax: 001-610-270-6608
E-Mail:

Mr Schick, Fritz

Physikal. Institut, Uni Tübingen
Auf der Morgenstelle 18
71076 Tübingen
Germany
Phone: 0049-7071-292425
Fax: 0049-7071-296296
E-Mail:

Mr Schneider, Horst

Uni Halle
Friedemann-Bach Pl. 6
06108 Halle
Germany
Phone: 0049-345-37761
Fax: 0049-345-832580
E-Mail:

Mr Pusiol, Daniel J.

National University of Cordoba - FAMBF
Ciudad Universitaria
5000 Cordoba
Argentina
Phone: 0054-51-680069
Fax: 0054-51-681862
E-Mail: pusiol@fis.uncor.edu

Mr Roder, Fridtjof

Physikalisches Institut EPV, Uni Würzburg
Am Hubland
97074 Würzburg
Germany
Phone: 0049-931-888-5861
Fax: 0049-931-888-5851
E-Mail:

Mr Ruff, Jan

Physikalisches Institut EPV, Uni Würzburg
Am Hubland
97074 Würzburg
Germany
Phone: 0049-931-888-5111
Fax: 0049-931-888-5851
E-Mail:

Mr. Schaff, A.

Uni Duisburg, FB 6
.
47048 Duisburg
Germany
Phone: 0049-203-379-3102
Fax: 0049-203-379-3522
E-Mail:

Dr. Schnackerz, Klaus D.

Physiol. Chemie I Biozentrum der Uni.Würzburg
Am Hubland
97074 Würzburg
Germany
Phone: 0049-931-888-4142
Fax: 0049-931-8884150
E-Mail:

Dr. Scrimgeour, S.N.

University of Dundee, Dept. of Dental Prosthetics
.
Dundee DD1 4HN
Scotland
Phone: 0044-1382 035877
Fax: 0044-1382 225163
E-Mail:

Prof. Dr. Seelig, Joachim

Biozentrum der Uni Basel, Biophysikalische Chemie
Klingelbergstr. 70
4056 Basel
Schweiz
Phone: 0041-61-267-2190
Fax: 0041-61-267-2189
E-Mail:

Mr Shattuck, Mark

Duke University Radiology
DUMC 3302
Durham, NC 27710
USA
Phone: 001-919-684-7757
Fax: 001-919-681-8648
E-Mail:

Dr. Simon, Gerald

VARIAN GmbH Darmstadt
Alsfelder Str. 3
64289 Darmstadt
Germany
Phone: 0049-6151-703-253
Fax: 0049-6151-703-200
E-Mail:

Prof. Dr. Skirda, V.

Dept.of Molecular Physics, Kazan State University
Lenina St. 18
420008 Kazan
Russia
Phone:
Fax:
E-Mail:

Dr. Spohn, Karl-Heinz

Universität Ulm, Sektion Kernresonanzspektroskopie
Albert-Einstein-Allee 11
89069 Ulm
Germany
Phone: 0049-731 502 3145
Fax: 0049-731 502 3150
E-Mail:

Prof. Dr. Strange, John H.

Physics Laboratory, University of Kent at Canterbury
Canterbury, Kent CT2 7NR
UK
Phone: 0044-1227-823321
Fax: 0044-1227-475423
E-Mail: j.-h.strange@ukc.ac.uk

Dr. Seo, Yoshitero

National Institute for Physiological Sciences
38 Myodaiji
Okazaki 444
Japan
Phone: 0081-564-55-7812
Fax: 0081-564-52-7913
E-Mail: yseo@nips.ac.jp

Dr. Shaw, Derek

GE Medical Research
352 Buckingham Avenue
Slough SL1 4ER
UK
Phone: 0044-753-874495
Fax: 0044-75-387-4573
E-Mail:

Dr. Skibbe, Ute

.
Alte Märsch 27
44319 Dortmund
Germany
Phone: 0049-231-215925
Fax: 0049-231-215925
E-Mail:

SMIS ltd.,

69 High Street, Corsham
Wiltshire SN13 OEZ
England
Phone: 0044 1249 701641
Fax: 0044 1249 701642
E-Mail:

Dr. Stilbs, Peter

Royal Inst. Technology, Physical Chemistry
.
S-10044 Stockholm,
Sweden
Phone: 0046 8 790 8201
Fax: 0046 8 790 8207
E-Mail: peter@physchem.kth.se

Dr. Sukhanov, P.P.

Kazan State Technological University
K. Marx Str. 68
720015 Kazan
Russia
Phone:
Fax: 007-8432-38-08-96 o. 76-54-03
E-Mail:

Prof. Dr. Sukumar, Subramaniam

Bruker Instruments Inc.
47697 Westinghouse Dr.
Fremont, CA 94587,
USA
Phone: 001-510-683-4399
Fax: 001-510-490-6586
E-Mail:

Mr Szimtenings, Michael

Physikalisches Institut EPV, Uni Würzburg
Am Hubland
97074 Würzburg
Germany
Phone: 0049-931-888-5864
Fax: 0049-931-888-5851
E-Mail:

Mr Takeuchi, Shigeki

Mitsubishi Electric Co.
Tsukaguchi Honmachi 8-1-1
Amagasaki, Hyogo 661
Japan
Phone: 0081 6 497 7067
Fax: 0081 6 497 7294
E-Mail:

Mr Toffanin, Renato

Poly-tech
Area Science Park, Padriciano 99
Trieste 34012
Italia
Phone: 039 40 3756606
Fax: 0039 40 7797091
E-Mail: toffanin@poly01.tbs.trieste.it

Mr Uyemura, Osamu

Dept. of Orthop. Surg., Kyoto Pref.Univ. of Med.
Kawaramachi-Hirokoji, Kamigyo-ku
Kyoto 602
Japan
Phone: 0081-75-251- 5549
Fax: 0081-75-251-5841
E-Mail:

Dr. Van As, H.

Wageningen Agricultural University,
Dept. of Molekular Physics
Dreijenlaan 3
6703 HA Wageningen
Niederlande
Phone: 0031-8370-82034
Fax: 0031-8370-82725
E-Mail: henk.vanas@water.mf.wau.nl

Dr. Szeles, J. Constantin

Chirurgische Universitätsklinik Wien
Währinger Gürtel 18-20
A-1090 Vienna
Austria
Phone: 00431-407-58-95 o. 40400-696
Fax: 00431-587-71-56-33
E-Mail:

Mrs. Taivainen, Jaana

University of Joensuu
P.O. Box 111
Fin-80101 Joensuu
Finnland
Phone: 00358-73-1513317
Fax: 00358-73-1513390
E-Mail:

Mr Tallarek, Ulrich

Inst. für Organ. Chemie, Uni Tübingen
Auf der Morgenstelle 18
72076 Tübingen
Germany
Phone: 0049-7071-296240
Fax: 0049-7071-296 296
E-Mail:

Mr Urban, Bert

Med. Klinik, Universität Würzburg
Josef-Schneider-Str. 2
97080 Würzburg
Germany
Phone: 0049-931-201-3455
Fax: 0049-931 201 2664
E-Mail:

Dr. Valiullin, R.

Dept.of Molecular Physics, Kazan State University
Lenina St. 18
420008 Kazan
Russia
Phone:
Fax:
E-Mail:

Mrs. Van der Toorn, Annette

Dept. of Molecular Physics
Dreijenlaan 3 Tranistorium
6703 HA Wageningen
Niederlande
Phone: 0031-8370-82047
Fax: 0031-8370-82725
E-Mail:

Dr. van Dusschoten, D.

Agricultural University, Dept. of Molekular Physics
Dreijenlaan 3
6703 HA Wageningen
Niederlande
Phone:
Fax: 0031-8370-82725
E-Mail:

Mrs. Vandersteen, Marjan

LUC Universitaire Campus
.
B-3590 Diepenbeek
Belgium
Phone: 0032-11-26 8512
Fax: 0032-11-26-8599
E-Mail:

VCH Verlagsgesellschaft,

Messereferat, Postfach 101161
69451 Weinheim
Germany
Phone:
Fax:
E-Mail:

Mrs. Verscht, Jutta

Universität Bayreuth, Lehrstuhl für Pflanzenphysiologie
Universitätsstr. 30
95440 Bayreuth
Germany
Phone: 0049-921-552638
Fax: 0049-921-552642
E-Mail: jutta.verscht@uni-bayreuth.de

Dr. Voelkl, Rüdiger

BASF
Abt. ZKM - Bau G 201
67056 Ludwigshafen
Germany
Phone: 0049-621-6041949
Fax: 0049-621-6021863
E-Mail:

Mr Wachsmut,

Höchst AG, Werk Kalle-Albert,TD Rheumatologie
Rheingaustr. 190-196
65203 Wiesbaden
Germany
Phone:
Fax:
E-Mail:

Prof. Dr. Van Tri, Nguyen

Institute of Technical Physics,
Hanoi National Univ. of Technol.
P. CHT, Vien Vat ly Ky thuat
Dai hoc Bach khoa Hanoi
Vietnam
Phone: 0084-4-691671
Fax: 0084-4-692006
E-Mail:

Mrs. Vanormelingen, Linda

LUC Universitaire Campus
.
B-3590 Diepenbeek
Belgium
Phone: 0032-11-26 8512
Fax: 0032-11-26-8599
E-Mail:

Mr Veeman, S.W.

Uni Duisburg, FB 6, Physikal. Chemie
.
47048 Duisburg
Germany
Phone: 0049-203- 3793102
Fax: 0049-203-3793522
E-Mail:

Prof. Dr. Vieth, Hans-Martin

Freie Universität Berlin, Institut für
Experimentalphysik
Arnimallee 14
14195 Berlin
Germany
Phone:
Fax: 0049-30-838-6081
E-Mail:

Dr. von Kienlin, Markus

Physikalisches Institut EPV, Uni Würzburg
Am Hubland
97074 Würzburg
Germany
Phone: 0049-931-888-5109
Fax: 0049-931-888-5851
E-Mail:

Mr Watanabe, Hisahiko

Tokyo University Fisheries
Konan 4, Minato
Tokyo 108
Japan
Phone: 0081-3 5463 0618
Fax: 0081-3 5463 0497
E-Mail:

Mr Waterton, J.C.

Zeneca Pharmaceuticals
Alderley Park
Macclesfield SK10 4TG
UK
Phone: 0044-1625 513633
Fax: 0044-1625 583074
E-Mail:

Dr. Wells, Terry

SMIS ltd.
69 High Street, Corsham
Wiltshire SN13 OEZ
England
Phone: 0044 1249 701641
Fax: 0044 1249 701642
E-Mail:

Dr. Williams, J. L.

SMIS ltd.
10 Alan Turing Road, Surrey Research P
Guildford, Surrey GU2 5YF
UK
Phone: 0044 1483 506236
Fax: 0044 1483 63114
E-Mail:

Dr. Xia, Yang

Oakland University, Dept. of Physics
.
Rochester, MI 48309
USA
Phone: 001-810-370-3420
Fax: 001-810-370-3408
E-Mail:

Dr. Zick, Klaus

Bruker Analytische Meßtechnik GmbH
Silberstreifen
76287 Rheinstetten
Germany
Phone: 0049-721-5161-124
Fax: 0049-721-5161-297
E-Mail:

Mr Webb, Andrew

University of Illinois
405 N. Methews
Urbana IL 61861
USA
Phone: 001-217-333-7480
Fax: 001-217-244-0105
E-Mail:

Mrs. Willanowski, Silke

Universität Dortmund, Physikalische Chemie II
Otto-Hahn-Str. 6
44221 Dortmund
Germany
Phone: 0049-231-755-3932
Fax: 0049-231-755-3771
E-Mail:

Dr. Wurz, Gerald

Inst. For Organic Chemistry, Univ. of Vienna
Wöhringerstr. 38
A-1090 Vienna
Austria
Phone: 0043-1 31367-2253
Fax: 0043-1 31367-2280
E-Mail:

Mr Yap, Markus

California Institute of Technology/Conductus Inc.
969 West Maude Avenue
Sunnyvale, CA 94086
USA
Phone: 001-408-523-9418
Fax: 001-408-523-9999
E-Mail: myap@conductus.com